THE UNIVERSITY
of EDINBURGH

Fear behaviour and its underlying physiology in the *Nlgn3*$^{-/y}$ rat model of autism

Natasha Anstey B.Sc. (Hons)

THE UNIVERSITY *of* EDINBURGH

A thesis submitted for the degree of Doctor of Philosophy

Biomedical Sciences

School of Medicine and Veterinary Medicine

University of Edinburgh

May 2020

Abstract

Neurodevelopmental disorders, including autism spectrum disorder (ASD) and intellectual disabilities (IDs), are a heterogeneous range of disorders thought to affect approximately 3-5 % of the population. There are currently no effective pharmacological treatments for ASD or ID, due in part to a lack of understanding of the pathophysiology of these disorders. Single-gene mutations account for a large proportion of cases where individuals present with ASD and co-occurring moderate to severe ID; and of these, mutations in synaptic proteins have been repeatedly implicated.

Mutations in the gene encoding the postsynaptic transmembrane protein neuroligin-3 (*Nlgn3*) are highly correlative with autism spectrum disorders (ASDs) and intellectual disabilities (IDs) in humans. Some of the most debilitating aspects of ASD/ID are anxiety and altered emotional responses, and although these cannot be examined directly using rodent models, we can gain insight on these aspects of the disorders by investigating behavioural tasks that involve similar brain circuitry. Previous work on *Nlgn3*$^{-/y}$ rats carried out by my colleagues examined behavioural tasks, such as fear conditioning and conditioned place avoidance, which rely on several brain areas involved in fear, anxiety and emotion. *Nlgn3*$^{-/y}$ rats show abnormal fear responses during these tasks, displaying a greater propensity to exhibit escape responses in contrast to the classic freezing behaviour seen in their wild-type littermates.

In this thesis, I examine the electrophysiology of the periaqueductal grey (PAG), a midbrain area involved in the execution of flight-freeze responses. I firstly provide an electrophysiological and morphological characterisation of neuronal populations in the PAG using whole-cell patch clamp recordings in acute slices, highlighting the heterogeneity of cells in this brain area. Secondly, I identify hyperexcitability of neurons in the dorsal, but not ventral, PAG of *Nlgn3*$^{-/y}$ rats, which may promote activation of circuits eliciting flight behaviour. Furthermore, electrical stimulation of the PAG *in vivo* resulted in a higher proportion of *Nlgn3*$^{-/y}$ rats exhibiting flight behaviours in comparison to wild-types, suggesting the threshold for eliciting an escape response is lower in these rats. However, local field potential recordings in the PAG during fear recall following auditory fear conditioning revealed no differences between wild-type and *Nlgn3*$^{-/y}$ rats. Overall, these physiological changes in the PAG of *Nlgn3*$^{-/y}$ rats may underly the imbalance of flight-freeze behaviours they display in response to fearful stimuli.

In the final chapter of this thesis, I investigate the effect of *Nlgn3* loss on the physiology of two other brain areas involved in fear learning: the hippocampus and medial pre-frontal cortex. Additionally, I present a direct comparison of the electrophysiology in these brain areas with another model of ASD/ID; the *Nrxn1*$^{+/-}$ rat. *Nrxn1* encodes the neurexin-1 protein, a presynaptic cell adhesion molecule that binds to neuroligin-3, mutations in which are highly correlated with ASD and ID. I find that, although both models display reduced hippocampal long-term potentiation, the majority of pathophysiologies identified in either model do not show convergence. This chapter highlights the importance of studying genetically diverse models of ASD to gain better insight into the pathophysiologies of these disorders.

In summary, this thesis provides evidence that *Nlgn3*$^{-/y}$ rats display physiological deficits in brain areas involved in the 'fear circuit' that may underlie the abnormal fear responses seen in the behaviour of these animals. This work highlights novel avenues for ASD/ID research and treatment, particularly in the context of understanding the anxiety disorders and emotional behaviours often seen in individuals with autism and ID.

Lay Summary

Autism spectrum disorder (ASD) is a complex neurological disorder that is diagnosed in individuals that present with social difficulties, communication problems and exhibit repetitive behaviours. There is a vast amount of variation between individuals with ASD, making the disorder difficult to understand, and therefore difficult to treat. For this reason, there are no cures or effective treatments for ASD. Individuals with ASD have a high risk of also presenting with other neurological disorders. These include intellectual disability (ID), epilepsy, and anxiety disorders. The work presented in this thesis aims to develop our understanding of anxiety disorders in ASD, by investigating a rat model of ASD/ID. This rat model lacks a protein called neuroligin-3 (henceforth called the *Nlgn3* knock-out (KO) rat) which is known to be involved in forming and maintaining neural connections. Mutations in the gene encoding neuroligin-3 have been found in individuals with ASD/ID.

Fear is a crucial part of typical neural development, however in individuals with ASD/ID, the development of typical fear learning, as well as the functioning of many brain areas involved in fear are disrupted. Dysfunction of these brain areas may result in specific phobias, generalised anxiety, separation anxiety and inappropriate emotional responses often seen in individuals with ASD/ID. It is impossible to directly study emotions such as fear and anxiety in a rat. However, fear responses such as fight-flight-freeze, as well as fear learning, can be observed in rodents and involve many of the same brain regions as in humans. Therefore, study of these behaviours and brain regions in rodents may provide significant insight into the neural mechanisms contributing to anxiety disorders. Previous work on the *Nlgn3* KO rat model has revealed that they display inappropriate responses to fearful stimuli that are heavily biased towards flight behaviour.

In this thesis, I investigate the function of the three key brain regions mediating fear learning and responses in the *Nlgn3* KO rat model of ASD/ID: the periaqueductal grey (PAG), hippocampus (HC) and prefrontal cortex (PFC). The PAG is crucial for executing responses to fearful stimuli, which can be broadly categorised into fight, flight, or freeze. I find physiological changes in neurons within the PAG of *Nlgn3* KO rats that are likely to promote flight behaviour, rather than freezing.

In addition to an external fearful stimulus, flight responses can be elicited in rats directly by stimulating the PAG. I show that *Nlgn3* KO rats display flight responses

at much lower stimulation than control rats, suggesting that the neurons in the PAG require less input to promote a flight response in the neuroligin-3 rats in comparison to controls.

Furthermore, I investigate the function of the HC, a brain area involved in the formation of memories, and the PFC, which is thought to be important for relaying contextual information to the HC and PAG. I find that connections between neurons within the HC of *Nlgn3* KO rats are less able to change their strength in response to activity, however this was not the case for the PFC of *Nlgn3* KO rats.

Lastly, I compare the neurons of the HC and PFC of *Nlgn3* KO rats to those of another model of ASD/ID, the *Nrxn1* Het rat. I find few similar features between the two models, reflecting the diversity of genetically distinct causes of ASD/ID.

Overall, this thesis provides evidence that brain areas involved in the 'fear-circuit' are disrupted in rat models of ASD/ID. This work highlights new avenues for research and treatment development for anxiety disorders in ASD.

Acknowledgement

There are so many people I would like to thank for their support throughout my PhD. Firstly to my many supervisors, Prof. Peter Kind, Prof. David Wyllie, Prof. Emma Wood and Dr Sam Booker, thank you all for your academic support and guidance over the last four years. I am very grateful to all of you. Also thank you to Prof. Sumantra Chattarji for welcoming me to his lab in Bangalore, I had a fantastic time there.

Secondly, I would like to thank those who have helped me technically throughout my PhD, in particular Dr Tom Watson, for his excellent mentorship and teaching me *in vivo* electrophysiology, for running experiments with me, and for many useful discussions regarding the periaqueductal grey. Also Dr Adam Jackson, thank you for teaching me how to patch, how to troubleshoot field recordings, for many insightful conversations about my work, and for always being patient with me. Thank you to Dr Nicola Romanò and Dr Claudius Degro for their help with data clustering, Dr Owen Dando and Zrinko Kozic for their help with generalised linear mixed modelling, Tiago Marcos for his help with R and FISH, Dr Felicity Inkpen for writing and editing the LFP script, and Dr Emma Perkins and Dr Ali Thomson for their help proofreading this thesis.

I would also like to thank all the wonderful people I have met throughout my PhD both in Hugh Robson Building and at NCBS. A special thanks to my PhD buddies Laura Oliveira and Joanna Smith for their unwavering support, and to Anna Toft for her help and friendship throughout everything (be it at work or up a mountain). Thank you to Teresa Spanò for being a great lab partner, and making late night experiments almost fun. Thank you to Jini Basu and Katherine Bonnycastle for all our adventures in India. Thank you to my friends in Bangalore, particularly Vaibhhav Sinha and Shivona Bhojwani, for the endless fun we had, and Dr Shashank Tiwari and Vijay Kapgal for all your help and guidance.

To Kyle Harris who, despite knowing nothing about neuroscience, proofread this entire PhD thesis during the coronavirus pandemic, thank you so much. Also to Katie, Becky, Steph, Jim, Carlota, Ryan, Niall, Matty, Pascal, Kevin, and of course my family, thank you for always being there and supporting me.

Finally to Tom Bolland, for absolutely everything, thank you. This would have been so much harder without you.

Declaration

I declare that this thesis was composed by myself and that the work contained herein is my own, unless otherwise states and with exception of the following:

- The surgeries and behavioural experiments in Chapter 4 were carried out in conjunction with Dr Thomas Watson, who supervised me with these experiments and performed many of the surgeries.
- The extracellular field recordings in Chapter 5 were collected with assistance from Teresa Spanò.
- Generalised linear mixed modelling of data in Chapter 5 was carried out by Zrinko Kozic and Dr Owen Dando.

No part of the work contained in the results chapters of this thesis has been submitted for any other degree or professional qualification.

Signed: Date: 01/05/2020

Contents

List of Abbreviations

A-P	Anterior-posterior
ADP	After-depolarisation potential
AMPA	α-amino-3-hydroxy-5-methyl-4-isoxazolepropionic acid
AP	Action potential
ASD	Autism spectrum disorder
BLA	Basolateral amygdala
cACSF	Cutting artificial cerebrospinal fluid
CBDS	Centre for Brain Development and Repair
CDBS	Centre for Discovery Brain Sciences
CeA	Central amygdala
CNQX	Cyanquixaline
CS	Conditioned stimulus
DG	Dentate gyrus
DHPG	Dihydroxyphenylglycine
EIB	Electronic interface board
ERP	Event-related potential
fAHP	Fast after-hyperpolarisation potential
fEPSP	Field excitatory post synaptic potential
fMRI	Functional magnetic resonance imaging
GABA	γ-aminobutyric acid
GM	Genetically modified
HC	Hippocampus
HCN	Hyperpolarization-activated cyclic nucleotide–gated
Het	Heterozygote
HFS	High-frequency stimulation
ID	Intellectual disability
IL	Infralimbic
ITI	Inter-tone interval
KO	Knock-out
LFP	Local field potential
LFS	Low-frequency stimulation
LTD	Long-term depression

LTP	Long-term potentiation
mAHP	Medium after-hyperpolarisation potential
mEPSC	Miniature excitatory post-synaptic currents
mGluR	Metabotropic glutamate receptor
mIPSC	Miniature inhibitory post-synaptic currents
mPFC	Medial prefrontal cortex
NDDs	Neurodevelopmental disorders
NGS	Normal goat serum
NMDA	N-methyl-*D*-aspartate
PAG	Periaqueductal grey
PBS	Phosphate-buffered saline
PC	Pyramidal cell
PCR	Polymerase chain reaction
PFA	Paraformaldehyde
PL	Prelimbic
PPF	Paired-pulse facilitation
PTP	Post-tetanic potentiation
PTX	Picrotoxin
rACSF	Recording artificial cerebrospinal fluid
RMP	Resting membrane potential
RRP	Readily-releasable pool
SC	Schaffer collaterals
SD	Sprague-Dawley
sEPSC	Spontaneous excitatory post-synaptic current
TBE	Tris-borate-EDTA
TBS	Tris-bufferred saline
TBST	Tris-buffered saline Tween 20
TD	Typically developing
TTX	Tetrodotoxin
US	Unconditioned stimulus
WT	Wild-type

List of Figures

List of Tables

Chapter 1

Introduction

1.1 Autism spectrum disorder and intellectual disability

Neurodevelopmental disorders (NDDs), including autism spectrum disorder (ASD) and intellectual disabilities (IDs), are a heterogeneous range of disorders thought to affect approximately 3-5% of the population (Srivastava and Schwartz, 2014). ASD is diagnosed on the basis of symptoms which can be categorised into two groups: social and communication deficits, and restricted, repetitive patterns of behaviour. Due to its phenotypic variability, autism is defined now as a "spectrum disorder", whereas in the past diagnoses were split into autism, Asperger's syndrome, and pervasive developmental disorder not otherwise specified (PDD-NOS). ID is defined as an IQ of less than 70 at the age of 18 and can be classified as mild (IQ 50-69), moderate (IQ 35-49), or severe (IQ 20-34). ASD and ID have high heritability; early twin studies suggested as high as 90% (Bailey et al., 1995; Steffenburg et al., 1989). However, more recent studies show slightly lower rates (Hallmayer et al., 2011) (38%), (Sandin et al., 2017) (83%). The low heritability rates in the Hallmayer et al. (2011) study are likely due to firstly the small sample size of patients (192 pairs, in comparison to 37,570 pairs in Sandin et al. (2017)), and secondly due to the treatment of "strict autism" and "ASD" as two separate disorders. It is therefore likely that the percentages reported in Sandin et al. (2017) are more reflective of reality.

ASD and ID are often co-occurring; ID has been reported to be observed in 30–50% of ASD patients, and 10–30% of individuals with ID have also received a diagnosis of ASD (Srivastava and Schwartz, 2014). Furthermore, both ASD and ID show significant co-occurence with childhood epilepsies; 20% of ASD/ID patients also present with

epilepsy (Besag, 2018). Severe neurodevelopmental disorder occurs when two or more of these three disorders overlap in a single person, and often have a monogenic cause (Fig. 1.1).

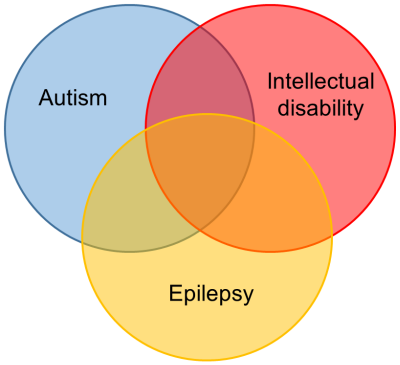

Figure 1.1: Autism, intellectual disabilities and epilepsy. ASD, ID and epilepsy are often co-occurring, and where these disorders overlap the most severe cases are seen.

These disorders present very early in development, and create consistent issues throughout the individuals' lives, often interfering with ability to function in social and employment settings. Severity of the core symptoms of ASD varies greatly, making this disorder difficult to diagnose and treat. Social and communication deficits, for example, may manifest as either withdrawal from social situations or increased inappropriate sociability. Individuals with ASD may also present with a hyper- or hypo-sensitivity to sensory stimuli, show perseveration behaviours, or rigidity in their routines and mannerisms.

Furthermore, in addition to the high co-occurrence of ID, ASD often presents with many other additional psychiatric disorders. Leyfer et al. (2006) reported 72% of individuals with autism met the criteria for at least one more psychiatric diagnosis (not including ID). 30% of these individuals met critera for a further two diagnoses in addition to ASD. Moreover, these results are likely to be an underestimation of the true co-occurrence rates, due to diagnostic overshadowing (Mason and Scior, 2004). Of these co-occurring psychiatric disorders, mood disorders (such as depression), anxiety disorders (such as separation anxiety) and disruptive disorders (such as ADHD) are the most prevalent (Leyfer et al., 2006).

1.1.1 Anxiety and emotional responses in ASD/ID

Co-occurrence of anxiety in individuals with ASD ranges from rates of 11-84% depending on the severity of ASD (White et al., 2009; Leyfer et al., 2006; van Steensel et al., 2012). Clinically, the presentation of anxiety disorders, phobias, and emotional dysregulation are so prevalent in individuals with ASD that they are considered an auxiliary feature of the autism spectrum, and often used as part of diagnosis (Kerns and Kendall, 2014). Accordingly, whether anxiety and fear-related symptoms are contained with the core features of ASD or reflective of a co-occurring separate anxiety disorder remains difficult to discern. For example, social deficits are a key diagnostic feature of ASD, and many behaviours presented by individuals struggling with ASD-related social dysfunction overlap with those seen in social anxiety (Bellini, 2004, 2006). Furthermore, repetitive behaviours, another core diagnostic criteria for ASD, occur predominantly during stressful or frightening situations (reviewed in Sinha et al. (2014)), and positively correlate in severity with generalised anxiety disorder and separation anxiety disorder diagnoses (Gadow et al., 2005; Guttmann-Steinmetz et al., 2010). Generalised anxiety, social anxiety, separation anxiety, specific phobias, and panic disorders are therefore commonly diagnosed alongside ASD/ID (Leyfer et al., 2006; van Steensel et al., 2012). These 'fear-disorders' are one of the most debilitating aspects of ASD, making it difficult for individuals to carry out typical lifestyles and routines.

In typically developing (TD) children, the development of fear is relatively well characterised, and reflective of cognitive development (Gullone, 2000; Ollendick et al., 2004). Gullone (2000) describes the stages of fear development in TD children; in infancy fear is mostly limited to stimuli in the immediate environment, with fears of the unknown increasing throughout the first few years of life. Fear of pain and social fears develop between ages of 4-12. Finally, cognitively abstract fears (eg. fear of dying) develop in adolescence. Growth and understanding of these fears are vital for typical development. The onset of 'fear development' is delayed in children with ASD (Davis et al., 2011) as well as the distortion of many of these fears into what would be diagnosed as anxiety, panic disorder or phobia.

Fear has been described to have three main components (Davis and Ollendick, 2014):

- Physiological; for example changes in heart rate, increases in cortisol, and activation of brain regions involved in fear.

- Behavioural; for example fight, flight or freeze responses.
- Cognitive; such as thoughts of panic, confusion and alarm.

To understand the pathophysiology of ASD and ID, and identify potential treatment options, rodent models containing genetic mutations known to be associated with these disorders have been used extensively (see section 1.2). Yet it is impossible, when working with rodent models, to directly assess the cognitive aspect of fear; instead it must be inferred from experimentation. Both behavioural and physiological fear responses, and the brain circuitry that contributes to them, are well characterised and require many of the same brain regions in rodents as they do in humans. For example, the amygdala is known to be cruicial for formation of fear memories and execution of fear responses in both rodents and humans (Janak and Tye, 2015; Tovote et al., 2015). The brain regions involved in fear are further described in section 1.6. Investigation of these brain regions in rodents, in addition to the use of behavioural paradigms that tap into this brain circuitry, can provide significant insight into the underlying pathophysiologies leading to anxiety disorders and abnormal emotional responses in individuals with ASD/ID.

1.2 Modelling ASD/ID

Modelling neurodevelopmental disorders such as ASD and ID is challenging given the heterogenetity and complexity of their symptoms and causes. Nevertheless, understanding the pathophysiology of these disorders is crucial for developing effective treatments, and the use of animal models provides the opportunity to study this. Recent advances in genetic manipulation have made the creation of animal models easier to accomplish. Whilst there are several external factors thought to cause autism, such as maternal infection (Zerbo et al., 2016), premature birth, and intrauterine hypoxia (Getahun et al., 2017), the genetic causes of ASD and ID are far more prevalent (Bailey et al., 1995; Steffenburg et al., 1989; Hallmayer et al., 2011; Sandin et al., 2017).

Large scale genetic studies have identified hundreds of genes correlated with ASD/ID (Deciphering Developmental Disorders, 2015, 2017; Krumm et al., 2013; Poultney et al., 2013; Willsey et al., 2014; Devlin et al., 2012; Iossifov et al., 2012; De Rubeis et al., 2014; O ' Roak et al., 2012). Furthermore, a large proportion of genetic causes of ASD and ID are accounted for by single-gene mutations. Recent studies by Deciphering Developmental Disorders (2017) (DDD) found that 42% of NDD cases examined

were caused by *de novo* single gene mutations using whole-exome sequencing, and a further ∼3% caused by *de novo* mutations in regulatory elements using whole-genome sequencing (Short et al., 2018). Moreover, if you consider that these studies filtered out patients with known monogenic causes of autism such as Fragile-X syndrome, Rett Syndrome, and Phelan-McDermid syndrome, this could increase estimates even further. Monogenic causes therefore contribute to a large proportion of moderate to severe cases of ASD; those that often co-occur with ID, epilepsy and other psychiatric disorders, shown in the overlapping region of Figure 1.1. Accordingly, studying monogenic causes of ASD and ID allows insight into the pathophysiology of these disorders. Genetically engineered animal models of specific genetic causes of ASD/ID provide a research tool with which behavioural and physiological phenotypes can be studied and potential therapeutic targets identified.

Genetically modified mice have been invaluable to research investigating the mutations leading to neurological disorders. The short gestational periods and large litter sizes of mice make them an useful preclinical model; in addition to the large genetic toolbox available and advantages of smaller brains for precise optogenetic stimulation. However, advances in genetic manipulation, along with the need to study inter-species translation of phenotypes, have led to the development of genetically modified rat models. Mice and rats are evolutionarily separated by 12 million years (Gibbs et al., 2004). Researching translational phenotypes between mice and rats is therefore vital for understanding conserved pathophysiologies across mammalian species. The use of rat models has several advantages over mice when considering research of neurological disorders. Firstly, the more complex social behaviours and cognition of rats (Kummer et al., 2014; Whishaw and Tomie, 1996; Colacicco et al., 2002) and lower experimenter-induced anxiety (Meijer et al., 2007; Ellenbroek and Youn, 2016) allows for more intricate examination of ASD and ID related phenotypes. Secondly, the larger brain size possessed by rats makes for more efficient and accurate surgical experimentation, increased spatial resolution of imaging studies, as well as for experiments studying anatomically distinct regions (Ellenbroek and Youn, 2016). Thirdly, although not utilised in the work presented in this thesis, the metabolic physiology and biochemistry of rats is closer to that of humans (Goutianos et al., 2015), making the rat a better model for studying drug pharmacodynamics when considering potential treatments. Lastly, laboratory rat strains are often outbred, unlike mice, leading to greater genetic diversity between individual

animals that is more representative of a natural population.

1.3 The synapse

In order to create relevant genetically modified models of neurological disorders, the genetic mutations leading to human disorders must be identified. Hundreds of genetic mutations have been identified as risk factors for autism and ID, and of these, genes encoding synaptic proteins have been repeatedly implicated (Yuen et al., 2017; De Rubeis et al., 2014). These include cell adhesion molecules such as neuroligins and neurexins, ion channels and receptors such as the N-methyl-*D*-aspartate receptor (NMDAR), scaffolding proteins such as shanks, and synaptic signalling proteins including SynGAP and PTEN (Yuen et al., 2017; De Rubeis et al., 2014). This cluster of synaptic proteins implicated in autism suggests that, although diverse in their structures and functions, synaptic dysfunction is a common feature between genetically distinct causes of ASD/ID. Studying synaptic function in monogenic causes of ASD/ID could therefore provide important insights into these disorders. The following sections are brief overviews of synaptic development and function that are necessary to contextualise how mutations in synaptic proteins lead to the manifestation of ASD/ID.

1.3.1 Synapse formation

Synapses are highly specialised asymmetric structures that, once formed, are dynamic in nature and underlie the plasticity and complexity of neural transmission. Synapses comprise of three compartments: the presynaptic terminal (or 'synaptic bouton'), which contains an active zone and is the site of synaptic vesicle fusion; the postsynaptic terminal, which includes the electron-dense postsynaptic density; and the synaptic cleft, a 20-25 μm gap between the pre- and post-synapse (Fig. 1.2). Pre- and postsynaptic proteins are already expressed in the axon growth cone and dendrite respectively prior to synapse formation (Rao et al., 1998). Initial contacts between synaptic partners are often established through filopodial protrusions from an axon or dendrite that go on to stabilise and form synapses (the filopodial model of synapse formation). The formation of synapses requires a host of signalling and adhesion molecules to form complexes spanning the synaptic cleft, and to recruit pre- and postsynaptic proteins to their appropriate compartment. Two such adhesion molecules are the postsynaptic neuroligins,

and their presynaptic binding partners, neurexins. These proteins bridge the synaptic cleft during synapse formation; the extracellular domain of β-neurexin interacts with the cholinesterase-like extracellular domain of neuroligins. Furthermore, both neuroligins and neurexins have intracellular domains including PDZ binding motifs capable of binding multiple proteins (Hata et al., 1993; Biederer and Südhof, 2000; Irie et al., 1997; Meyer et al., 2004; Chih et al., 2005) (Fig. 1.2). The expression of neuroligins 1 and 2 in cultured non-neuronal cells is sufficient to trigger neurexin accumulation and the development of a presynapse in contacting axons (Scheiffele et al., 2000).

Neuroligin-neurexin binding has been shown to be dependent on both Ca^{2+} binding to a high-affinity site on neurexin, and alternative splicing of neurexins (see section 5.1.1) (Ichtchenko et al., 1995; Nguyen and Südhof, 1997). This initiates synaptogenesis and determines synapse specificity. Following this, scaffolding proteins are recruited, which allows the formation of protein complexes. These include CASK, mints, and synaptotagmin, which bind presynaptically to neurexins and allow recruitment of synaptic vesicles along with further scaffolding proteins (Biederer and Südhof, 2000; Hata et al., 1993, 1996), in addition to PSD-95 and shank which bind postsynaptically to neuroligins and recruit signalling molecules and neurotransmitter receptors (Chih et al., 2005; Irie et al., 1997; Meyer et al., 2004) (Fig. 1.2).

Once formed, synaptic pruning or withdrawal is thought to take place relatively early in development in an activity dependent manner. Rodent cortical synapses have been shown to decrease by 36% after post-natal day 30 (p30) (Markus and Petit, 1987), and a similar drop of approximately 31% was reported between the ages of 10-15 in human cortex (Huttenlocher, 1979). However, it is important to note that these studies did not normalise to neuron number. Changes in brain growth and cell death would also lead to a reduction in total synapses without affecting synapses per neuron. These percentages therefore may be an overestimate of the true scale of synaptic pruning. Furthermore, the study by Huttenlocher (1979) also reported only a single sample between the ages of 15 and 30. A more recent study found that cortical spine density (also normalised to area not neuron number) continues to decrease past adolescence and was seen in humans up until the age of around 30 (Petanjek et al., 2011). Synaptic pruning is reported to be altered in models of ASD, ID and schizophrenia (reviewed in de Silva (2018)), however changes in the initial development and stabilisation of synapses may also account for many reported synaptic pruning phenotypes.

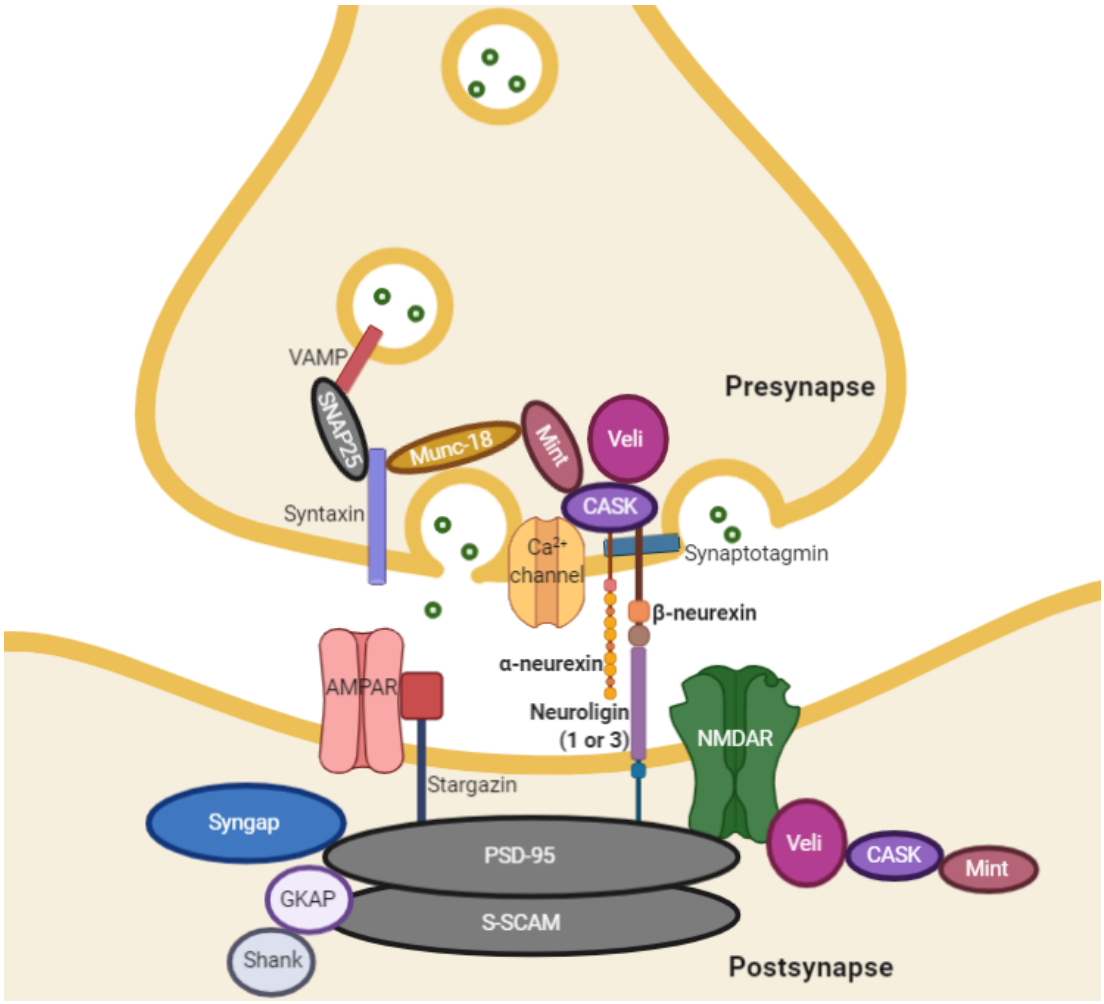

Figure 1.2: Known pre- and postsynaptic protein interactions at glutamatergic synapses. Adapted from Craig and Kang (2007).

The synapses that remain into adulthood are still not always stable; the development and withdrawal of synapses can happen throughout an organism's life span and is induced during learning, such as the formation of fearful memories (Dalzell et al., 2011). The mechanisms underlying synaptic plasticity are described in section 1.4.

1.3.2 Measuring synaptic function

The majority of the work presented in this thesis utilises *ex vivo* electrophysiology in acute brain slices to investigate synaptic function and neural transmission. Several crucial stages of synaptic transmission can be measured using electrophysiological techniques, described in Box 1. These include the recording of miniature excitatory or inhibitory postsynaptic currents, evoked release, and neuronal intrinsic properties. Extracellular electrophysiology recording techniques, such as field potentials, can provide information regarding local circuits but have relatively poor spatial resolution. By contrast, whole-cell patch-clamp electrophysiology provides the high spatial resolution of recording of single neurons, but is limited for understanding network-level connectivity. However, the temporal acuity of electrophysiological recordings is high in comparison to, for example, immunocytochemistry. Utilisation of a combination of these techniques can therefore provide multiple lines of evidence to generate meaningful insight into circuit connectivity and function.

Measuring synaptic function allows important insight into the pathophysiology of ASD, as many of the genetic causes of ASD/ID result in altered synaptic transmission, synaptic plasticity, and neuronal excitability (see section 1.5.4). Understanding the nature of if/how synapses and neurons are dysfunctional in a model of ASD/ID will result in a better grasp of the disorder, and may allow identification of potential treatment targets.

Box 1: Measuring synaptic function

Size and number of neurotransmitter vesicles

The number of vesicles being exocytosed at the presynaptic membrane, and the amount of neurotransmitter they contain, can be determined by intracellularly recording *miniature excitatory or inhibitory postsynaptic currents* (mEPSCs/ mIPSCs) in the presence of a pharmacological action potential blocker (such as tetrodotoxin). The frequency of mEPSCs/ mIPSCs reflects the number of vesicles binding (which in turn is dependent on the presynaptic release probability (see below), and the number of functional synapses), and the amplitude of mEPSCs/ mIPSCs reflects the amount of neurotransmitter contained by the vesicles and number of neurotransmitter-gated receptors on the postsynapse (reflecting the synaptic strength). In the absence of an action potential blocker, *spontaneous excitatory or inhibitory postsynaptic currents*, sEPSCs/ sIPSCs will be recorded, which reflect not only the subthreshold events but also those that are initiated by action potentials.

Neurotransmitter release probability

The release probability of synaptic vesicles at the presynapse depends predominantly on the size and replenishment rate of the readily-releasable pool (RRP). This reflects synaptic efficacy and can be measured using *minimal stimulation* of a putative single axon, which allows the intracellular recording of all-or-nothing responses in the postsynapse. Information about the RRP can also be gleaned from the frequency of mEPSCs/ mIPSCs. The presynaptic release probability can also be measured for all of the synapses contacting a postsynaptic neuron by measuring the *paired-pulse facilitation or depression* (PPF/ PPD) of a postsynaptic potential in response to stimulations with short intervals (discussed further in section 1.4.1). The change in response amplitude during PPF or PPD reflects the Ca^{2+}-evoked release of presynaptic vesicles.

Neurotransmitter receptor activity

Electrical currents through postsynaptic receptors (such as AMPA, NMDA or GABA receptors) initiated by neurotransmitter binding (glutamate, glycine, GABA) can be measured by either pharmacological or electrical isolation of the synaptic current of interest. Pharamacological block of glutamate receptors will allow GABA receptor currents to be recorded and vice versa. Alternatively (or additionally), voltage clamping the cell at reversal potentials of unwanted currents allows synaptic currents of interest to be measured. Investigating the $GABA_AR/AMPAR$ *ratios* allows examination of excitation:inhibition balance of synaptic input to a neuron.

Population-level synaptic conductance

The subthreshold synaptic activity of neurons on a population level can be measured extracellularly using *field excitatory or inhibitory postsynaptic potentials* (fEPSP/ fIPSPs).

Box 1 (continued): Measuring synaptic function

(continued)

The amplitude and rising phase slope of an fEPSP/ fIPSP can be used to determine synaptic conductance. fEPSP/ fIPSP amplitude has a non-linear relationship with synaptic conductance as it can be contaminated by population spikes; however, the slope has a linear relationship with synaptic conductance (Johnston and Wu, 1994).

Action potential generation

The threshold of synaptic input required to elicit an action potential depends predominantly on Na^+ channel density, however it is also influenced by the total conductance of the membrane (including voltage-gated, leak, and synaptic conductances) (Platkiewicz and Brette, 2010). *Threshold potential* can be determined by artificially injecting current into the cell, and simultaneously recording the response potential in the neuron intracellularly.

Action potential propagation

The speed of an action potential depends on cell membrane resistance (which in turn depends predominantly on the size of the axon and the number of channels it contains). The depolarisation phase of an action potential is predominantly due to the influx Na^+ across the cell membrane, and the repolarisation phase is due to efflux of K^+ ions. Upon artificially eliciting an action potential in a neuron, the *depolarisation and repolarisation rates* can be measured.

Action potential recovery

Immediately following the repolarisation phase of an action potential, there is an after-hyperpolarisation phase in which Ca^{2+}-activated K^+ channels transiently increase the membrane permeability to K^+ and result in an overshoot of the repolarisation. The *amplitude and decay curve of fast after-hyperpolarisations* can be measured following the elicitation of an artificial action potential. Medium and slow after-hyperpolarisations, involving M-channels and hyperpolarisation-activated cyclic nucleotide–gated (HCN) channels, can also occur on longer time scales.

1.4 Synaptic plasticity

Activity-dependent synaptic plasticity, the ability for a synapse to strengthen and weaken in response to neuronal activity, has been proposed as the cellular basis for learning and memory for many years (Bliss and Collingridge, 1993). This theory was first postulated by Hebb (1949) and Stent (1973), and is often summarised as "cells that fire together, wire together" (Hebb) and "cells that fire out of sync lose their link" (Stent).

The mechanisms of synaptic plasticity are, however, more complex then these phrases suggest. Early studies on synaptic plasticity examined perforant path synapses in the dentate gyrus and found that tetanic stimulation of presynaptic neurons resulted in a potentiated response recorded from postsynaptic neurons that lasted for several hours. This potentiation was also input-specific and did not occur in a control pathway (Bliss and Gardner-Medwin, 1973; Bliss and Lømo, 1973). Synaptic plasticity is bidirectional (long-term potentiation, LTP; long-term depression, LTD), and can be short or long-lasting. Bidirectional plasticity is vital for experience-dependent refinement of neural networks; both the loss of unused synapses and the strengthening of required synapses results in a network that is defined, efficient, and effective, and allows for learning, forgetting, and reversal learning. There is a considerable body of work on both the mechanisms of synaptic plasticity, and its role in neurological disorders such as ASD and ID.

1.4.1 Mechanisms of synaptic plasticity

Synaptic plasticity can occur presynaptically through changes in neurotransmitter release, or postsynaptically through alterations in receptor number or biophysical properties. Short term plasticity is usually the outcome of presynaptic changes, and long term plasticity dependent on postsynaptic changes, however this is not always the case; long lasting changes in presynaptic function have also been shown to be required for some forms of LTP/LTD (reviewed in Yang and Calakos (2013)).

Short term plasticity is a form of plasticity that lasts up to a maximum of a few minutes. On the shortest timescale, there is paired-pulse facilitation or depression; when two stimuli are delivered to a presynaptic neuron with a short interval, the second response observed in the postsynaptic neuron can be increased or decreased relative to the first. Paired-pulse depression can be induced by delivering two stimuli within approximately 20 ms of each other (although this can be longer depending on the type of neurons and size of the RRP), and is thought to be caused by depletion of the RRP or transient inactivation of voltage-gated Na^+ or Ca^{2+} channels at the presynapse (Kirischuk et al., 2002). Paired-pulse facilitation, on the other hand, requires a slightly longer inter-stimulus interval (of around 50-500 ms) and is thought to be due to a combination of residual Ca^{2+} present in the presynaptic bouton, in addition to the activation presynaptic phosphoproteins and protein kinases (Rosahl et al., 1993).

Facilitation or depression of a synaptic response depends on initial release probability; synapses displaying an initial high release probability are more likely to depress given paired-pulse stimulation and vice versa (Dobrunz and Stevens, 1997).

Short term plasticity can also be observed on the scale of minutes following tetanic or low frequency stimulation. During tetanic stimulation, Ca^{2+} builds up in the presynapse, causing increased neurotransmitter release in response to action potentials following the tetanic stimulation (Regehr et al., 1994). This is often referred to as post-tetanic potentiation, PTP. During prolonged low frequency stimulation, short term depression is due in part to depletion of presynaptic Ca^{2+} and the RRP, in addition to changes in release probability at presynaptic terminals (Varela et al., 1997). Long-lasting changes in presynaptic function are thought to involve increased expression of proteins involved in exocytosis of synaptic vesicles, resulting in more efficient exocytosis and increased neurotransmitter release (reviewed in Yang and Calakos (2013)).

At the postsynapse, the trafficking of AMPARs (α-amino-3-hydroxy-5-methyl-4-isoxazolepropionic acid receptors) plays a large role in synaptic strengthening and weakening. The first evidence of this was provided by Lledo et al. (1998), demonstrating the role of postsynaptic exocytosis of AMPARs in LTP. The number of AMPARs at the postsynapse is important for determining synaptic strength, and therefore addition/removal of these receptors allows long-lasting changes in synaptic efficacy to occur. AMPARs are hetero-oligomeric proteins consisting of subunits GluR1, GluR2, GluR3, GluR4 (Hollmann and Heinemann, 1994). Following LTP induction, Ca^{2+} influx to the postsynapse causes CaMKII activation and binding to NMDARs (Zhou et al., 2007). In addition, AMPARs are inserted into extrasynaptic or perisynaptic sites through exocytosis of AMPAR-containing vesicles. The receptors then laterally diffuse to the postsynapse and are trapped in the PSD by CaMKII-triggered phosphorylation events (Opazo and Choquet, 2011). This increases the number of functional AMPARs at the postsynaptic membrane, therefore increasing synaptic strength (Andrásfalvy and Magee, 2004). During LTD the opposite occurs, AMPARs are endocytosed in a dynamin and clathrin-dependent manner resulting in reduced density at the postsynaptic membrane (Carroll et al., 1999a,b; Man et al., 2000). AMPAR trafficking during LTD initially allows desensitised receptors to be quickly exchanged for functional ones, resulting in fast recovery. As repeated stimulation progresses, AMPAR trafficking is slowed through rises in intracellular calcium or stargazin-induced stabilisation at the postsynaptic membrane,

resulting in reduced synaptic efficacy (Heine et al., 2002; Constals et al., 2015).

The insertion or removal of additional receptors to the postsynaptic membrane also causes ultrastructural changes to the synapse that affect synaptic efficacy. Spines associated with synapses that have undergone LTP have been shown to increase in size (Matsuzaki et al., 2004) and have larger PSDs (Toni et al., 2001). By contrast, spines that have undergone LTD have been reported to decrease in size and have smaller PSDs (Zhou et al., 2004; Nägerl et al., 2004). However, there are some discrepancies in the literature on the relationship between spine size and synaptic strength; Araya et al. (2014) reported that LTP can occur without overall changes in spine head size, but with changes in spine neck width, and Meyer et al. (2014) reported a delay of ∼80 minutes in the increase of PSD size following LTP induction, suggesting that the relationship between synaptic strength and PSD size is not linear. Furthermore, previous research from our lab has demonstrated a lack of correlation between spine size and synaptic strength (Wijetunge et al., 2014). Spine density and the number of multi-innervated spines has also been shown to increase during LTP (Toni et al., 1999; Giese et al., 2015). These studies imply a more complex relationship between spine morphology and synaptic strength than was initially speculated.

LTP and LTD can also be protein synthesis dependent; first described by Krug et al. (1984) and Stanton and Sarvey (1984). During LTP or LTD induction, local dendritic translation results in the synthesis of new proteins that allow the expression of potentiation or depression of synapses (Kang and Schuman, 1996; Huber et al., 2000; Cracco et al., 2005). Changes in levels of local protein synthesis at a synapse also allows both the insertion of new AMPARs (Sutton et al., 2006) and long-lasting changes in presynaptic neurotransmitter release (Johnstone and Raymond, 2013). The involvement of new protein synthesis during LTP has also led to the 'synaptic tagging' hypothesis (Frey and Morris, 1997). Synaptic tagging occurs when weak stimulation of a presynaptic neuron activates a small number of synapses, priming them for potentiation with a synaptic 'tag'. Strong stimulation to another set of synapses that terminate on the same postsynaptic neuron causes dendritic protein synthesis (Kang and Schuman, 1996) of LTP proteins that are delivered to synapses that have been 'tagged'. This results in the weakly stimulated synapses also exhibiting LTP. This form of LTP is called associative LTP, and is crucial for the formation of fear memories (Rogan et al., 1997) as it allows the strengthening of synaptic responses to non-fearful stimuli when

paired with fearful ones (discussed further in section 1.6).

1.4.2 Induction of synaptic plasticity

LTP and LTD can be induced via many different mechanisms; chemically, electrically, and using many different protocols. Each induction method has advantages and disadvantages, allowing examination of different aspects of synaptic plasticity, including the function of contributing receptors. The most extensively studied synapses in terms of plasticity are the hippocampal CA3-CA1 synapses, also named the Schaffer collaterals (SCs). The SC synapses carry incoming information from the dentate gyrus and entorhinal cortex to CA1, which then allows output from CA1 to the subiculum. These synapses have been described to undergo several different forms of plasticity, including forms dependent on NMDARs and metabotropic glutamate receptors (mGluRs).

NMDAR-dependent plasticity

NMDARs are ionotropic glutamate receptors heavily involved in controlling synaptic plasticity (Collingridge et al., 1983; Coan et al., 1987). They are heterotetramers, consisting of two NR1 and two NR2 subunits. The NR2 subunits can be a combination of NR2A, NR2B, NR2C and NR2D; however, in the hippocampus NR2A and NR2B are thought to be most common (Monyer et al., 1994). NMDARs are non-specific cation channels, highly permeable to Ca^{2+}, but are blocked at rest by endogenous Mg^{2+} (Mayer et al., 1984). NMDAR-dependent LTP and LTD can be induced by specific patterns of stimulation at SC synapses (Malenka, 1994). NMDARs act as coincidence detectors, as their activation relies on the voltage-dependent release of the Mg^{2+} block through postsynaptic depolarisation, in addition to glutamate binding. NMDAR-dependent LTP and LTD are therefore input-specific, as they are dependent on stimulation-induced glutamate release from synapses; meaning high or low-frequency stimulation can be given to a certain pathway without affecting neighbouring synapses (Harvey and Svoboda, 2007).

Tetanic stimulation of presynaptic neurons leads to strong temporal summation of EPSPs causing postsynaptic depolarisation. This co-activation of pre- and postsynaptic neurons allows the coincident depolarisation and glutamate binding required to activate NMDARs. Following this, NMDARs are able to allow maximal Ca^{2+} influx to the postynapse, which activates intracellular signalling cascades that provoke LTP. By

contrast, low frequency stimulation of the presynaptic neuron without co-activation of the postsynaptic neuron causes smaller Ca^{2+} influxes over a longer period of time that run down synaptic Ca^{2+} and induce LTD (reviewed in Lüscher and Malenka (2012)).

mGluR-dependent plasticity

Group 1 mGluRs are seven transmembrane domain receptors that have been shown to be heavily involved in the expression of NMDAR-dependent and NMDAR-independent forms of synaptic plasticity (Bashir et al., 1993a,b; Schoepp and Conn, 1993). Group 1 mGluRs comprise of mGluR1 and mGluR5 subtypes, which localise to the postsynapse in the perisynaptic zone surrounding ionotropic receptors (Luján et al., 1996). mGluRs are canonically linked to $G\alpha_{q/11}$ hetereotrimeric G-proteins, which activate downstream signalling pathways involved in protein translation. mGluR-dependent LTD can be induced by paired-pulse low frequency stimulation (Huber et al., 2000) (although this is also mediated by M1 mAChRs (Volk et al., 2006)) or brief application of the group 1 mGluR agonist dihydroxyphenylglycine (DHPG) (Palmer et al., 1997). mGluR-dependent LTP is less well described, and often either additionally dependent on NMDARs or occluded by NMDAR-dependent mechanisms (Fidzinski et al., 2008; Anwyl, 1999). However, mGluR-dependent LTP is thought to occur following faster frequency and longer duration tetanic stimulation than that required to elicit NMDAR-dependent LTP (Grover and Teyler, 1990; Wang et al., 2016).

During chemical or low frequency stimulation, activation of group 1 mGluRs results in the activation of protein tyrosine phosphatase inhibitors, which in turn cause dephosphorylation of AMPARs. This dephosphorylation induces the removal of AMPARs from the postsynaptic membrane, resulting in LTD (Moult et al., 2006). mGluR activation during both LTD and LTP induction also stimulates protein synthesis through Arc signalling and FMRP activation (Huber et al., 2002; Nosyreva and Huber, 2006; Park et al., 2008; Wang et al., 2016). The differentiation between translation of proteins leading to LTP or LTD is thought to depend on Ca^{2+} influx to the postsynapse via voltage-gated calcium channels (Wang et al., 2016; Kim et al., 2015). It is important to note that mechanisms of mGluR-dependent LTD at hippocampus SC synapses are not consistent throughout development; younger animals (>p15) display mGluR-dependent presynaptic LTD with no change in postsynaptic AMPARs, whilst older animals display postsynaptic AMPAR expression alterations (Nosyreva and Huber, 2005).

1.4.3 Cortical synaptic plasticity

Synaptic plasticity also plays a major role in shaping circuitry outside of the hippocampus. In the cortex, synaptic plasticity is crucial for refining developing networks in an experience-dependent manner. For example, Hubel and Wiesel (1970) demonstrated plasticity of the cat visual system in response to visual deprivation during a critical period of the cats' development. Critical periods are developmental time windows in which synapses are particularly plastic and susceptible to influence by experience and activity. Some brain regions, however, such as the prefrontal cortex (PFC), remain plastic throughout development and into adulthood (reviewed in Kolb et al. (2012)).

The induction of LTP and LTD at cortical synapses requires protocols often dissimilar to those utilised for the hippocampus, due to the more distributed spatial organisation of synapses within the cortical layers. Nonetheless, LTP and LTD can be induced, for example, at layer 2/3 to layer 5 synapses of the PFC. High frequency stimulation of layer 2/3 neurons results in LTP of responses recorded from layer 5 in the PFC, and is dependent on NMDARs and dopamine receptors (D1 receptors) (Huang et al., 2004). Furthermore, low frequency stimulation of this pathway results in a transient depression that can be converted to LTD by bath application of dopamine, suggesting depressive plasticity in this pathway is also dependent on D1 receptors (Huang et al., 2004).

1.5 The molecular basis of ASD

The high incidence of synaptic proteins that are causally linked to ASD/ID (Yuen et al., 2017; De Rubeis et al., 2014) implicates synaptic dysfunction as a core feature of ASD/ID. Whilst the genetic contribution of ASD/ID is well established, there is a continuing need to understand how genetic mutations leading to ASD/ID affect brain structure and function. The main focus of this thesis is on neuroligin-3, mutations in which have been linked to ASD, ID and epilepsy (Table 1.1). Chapter 5 also addresses the function of neurexin-1, mutations in which have been associated with a range of neurodevelopmental disorders including ASD, ID schizophrenia, epilepsy, ADHD, Tourette's syndrome and borderline personality disorder (see section 5.1.1 for further details). Mutations in the same gene can lead to distinct diagnoses of psychological disorders due to a number of reasons: firstly different mutations within the same gene may have differential effects on the resulting protein (i.e. loss-of-function or gain-of-

function), secondly the different experiences of each individual will shape the behavioural manifestation of the genetic mutations, and lastly the overlapping diagnostic criteria of many of these disorders makes categorising them difficult.

As described above, neuroligin is a postsynaptic cell adhesion protein that binds to presynaptic neurexin in a Ca^{2+}-dependent manner (Ichtchenko et al., 1995; Nguyen and Südhof, 1997). Neuroligins and neurexins are sufficient for synapse formation (Scheiffele et al., 2000; Graf et al., 2004), but not necessary (Missler et al., 2003; Varoqueaux et al., 2006). However, they are necessary for synapse maturation and maintenance. Mice containing triple knock-out mutations of all neuroligin proteins (Varoqueaux et al., 2006) or all α-neurexin proteins (Missler et al., 2003) die shortly after birth due to respiratory problems. These mice also have near-complete depletion of all synaptic transmission, despite electron microscopy experiments showing overall synaptic density was unaffected.

Several mouse models of ASD/ID containing mutations in *Nlgn3* and *Nrxn1* have previously been described, however the work presented in this thesis utilises *Nlgn3*$^{-/y}$ and *Nrxn1*$^{+/-}$ rats. Two studies have been published to date (Hamilton et al., 2014; Thomas et al., 2017) describing the *Nlgn3*$^{-/y}$ rat, and none describing the *Nrxn1*$^{+/-}$ rat. However, behavioural characterisations of a *Nrxn1*$^{-/-}$ rat have been carried out by Esclassan et al. (2015) and Twining et al. (2017). Further details of previous work carried out on *Nlgn3*$^{-/y}$ mice and rats are described in section 1.5.4.

1.5.1 Neuroligin-3 and ASD

Neuroligin-3 (gene: *NLGN3*) was originally linked to ASD by Jamain et al. (2003), who described two brothers with point mutations within *NLGN3* (*R451C*). Both brothers presented with non-syndromic ASD, ID and one also with epilepsy (Table 1.1). This mutation was maternally inherited from an unaffected mother, as *NLGN3* is located on the X chromosome. The *R451C* mutation is within the highly conserved esterase domain of *NLGN3*, and results in 90% reduction of neuroligin-3 protein in mice with equivalent mutations (Tabuchi et al., 2007). However, the small fraction of the protein that is not degraded is correctly trafficked to the cell surface (De Jaco et al., 2010). The protein fraction that does reach the synapse has compromised binding ability to β-neurexin-1 (Comoletti et al., 2004). It has been suggested that the *NLGN3 R451C* mutation results in a gain of function (Tabuchi et al., 2007).

NLGN3 mutations have since been shown to be associated with ASD/ID by several studies (Table 1.1). Yet, it is important to note that many studies have also found no evidence of *NLGN3* mutations in screens of ASD/ID probands, as shown in Table 1.2. Mutations in *NLGN3* therefore likely account for a very small proportion of ASD cases. Nonetheless, mutations in this gene appear to be highly penetrant. Identified ASD-associated *NLGN3* mutations are diverse in nature; single-nucleotide polymorphism (SNP), duplication, indel, and truncation mutations have all been shown to present in individuals with ASD (Table 1.1), in addition to occurring in both exons and introns.

Several of these mutations result in a complete or near-complete loss of the neuroligin-3 protein (Tabuchi et al., 2007; Chih et al., 2004; Talebizadeh et al., 2006; Kenny et al., 2014; Redin et al., 2014; Quartier et al., 2019), but the effect of many of the *NLGN3* mutations listed in Table 1.1 are unknown. From the variability in expected protein function these mutations cause, it is likely that any disruption of *NLGN3* (whether that be complete loss, partial loss, dominant negative, or gain of function) results in increased risk of ASD. Thus, the study of a *Nlgn3* knock-out (KO) rat model is a useful tool for ASD/ID research, allowing insight into the specific function of neuroligin-3 during development, and the effects of its loss on cellular physiology, circuitry and behaviour. Furthermore, drawing comparisons between the previous work published on *Nlgn3*$^{-/y}$ mice will allow further understanding of translational phenotypes between the two species.

Table 1.1: Summary of *NLGN3* mutations in individuals with ASD. AA: amino acid, LOF: loss-of-function, SNP: single-nucleotide polymorphism. NB. Yu et al. (2011) reports a common variant in *NLGN3* associated with increased risk of ASD.

Study	Patient description	Individuals	Mutation	AA change (if reported)	Effect on *NLGN3* protein
Jamain et al. (2003)	ASD, ID, epilepsy	2	SNP in exon 6	R451C	90% reduction, reduced NRXN binding
Ylisaukko-oja et al. (2005)	ASD	1	SNP in exon 1	Y74Y	Silent, non-pathogenic
Talebizadeh et al. (2006)	ASD	9	Truncation in exon 4	-	Premature stop codon, loss of exons 7 & 8
Levy et al. (2011)	ASD	1	33 kb deletion in exon 1	-	Predicted LOF
Yu et al. (2011)	ASD	N/A	Intronic SNP	-	Unknown
Steinberg et al. (2012)	ASD	2	SNP in 3'UTR	-	9% reduction
Steinberg et al. (2012)	ASD	1	Indel in 3'UTR	-	9% reduction
Steinberg et al. (2012)	ASD	4	Intronic SNP	-	Affects transcription factor binding
Steinberg et al. (2012)	ASD	1	Intronic SNP	-	Unknown
Yanagi et al. (2012)	ASD	12	Intronic SNP	-	Unknown
Yanagi et al. (2012)	ASD	1	Intronic SNP	-	Unknown
Yanagi et al. (2012)	ASD	1	SNP in exon 7	K566K	Silent, predicted non-pathogenic
Volaki et al. (2013)	ASD	3	SNP in exon 7	G758S	Predicted pathogenic
Yu et al. (2013)	ASD, ID, ADHD	1	SNP in exon 5	V321A	Unknown
Iossifov et al. (2014)	ASD	1	SNP in exon 6	-	Unknown
Iossifov et al. (2014)	ASD	1	SNP in exon 6	-	Unknown
Kenny et al. (2014)	ASD	1	Indel in exon 2	-	Premature stop codon, predicted LOF
Kenny et al. (2014)	ASD	2	SNP in exon 5	A199A	Predicted premature stop codon
Kenny et al. (2014)	ASD	1	SNP in exon 8	H825H	Predicted premature stop codon
Mikhailov et al. (2014)	ASD	1	SNP in exon 7	K566K	Silent, predicted non-pathogenic
Mikhailov et al. (2014)	ASD	1	Intronic SNP	-	Unknown
Mikhailov et al. (2014)	ASD	1	Intronic SNP	-	Unknown
Redin et al. (2014)	ASD, ID	1	SNP in exon 1	R617W	90-100% reduction
Redin et al. (2014)	ASD, ID	1	SNP in exon 8	R471C	90-100% reduction
Xu et al. (2014)	ASD, epilepsy	1	SNP in exon 2	G426S	Non-pathogenic
Yuen et al. (2017)	ASD, OCD	1	Duplication in exon 6	T469	Predicted LOF
Yuen et al. (2017)	ID, ADHD	1	Duplication in exon 7	T429	Predicted LOF
Quartier et al. (2019)	ASD, ID, sleep disorder	3	SNP in exon 6	P514S	90-100% reduction

Table 1.2: Summary of studies finding no correlation of *NLGN3* mutations in individuals with ASD.

Study	Individuals tested
Vincent et al. (2004)	196
Gauthier et al. (2005)	96
Blasi et al. (2006)	124
Wermter et al. (2008)	107
Liu et al. (2013)	285
Pampanos et al. (2009)	169
Avdjieva-Tzavella et al. (2012)	20
Yan et al. (2005)	148

1.5.2 Expression of neuroligins

In rodents, the neuroligins are expressed specifically in the brain (Ichtchenko et al., 1995, 1996; Scheiffele et al., 2000), however some evidence suggests neuroligin-3 is more widely expressed in humans; including in the heart, skeletal muscles, placenta and pancreas (Philibert et al., 2000). Low levels of neuroligin expression can be detected in the first few days after birth corresponding with synapse formation, and increase during development (Song et al., 1999; Scheiffele et al., 2000; Varoqueaux et al., 2006). Neuroligin-3 is expressed in almost all brain areas including the hippocampus, cortex and midbrain (Varoqueaux et al., 2006; Uhlén et al., 2015; Uchigashima et al., 2020). Neuroligin-1 localises to excitatory synapses (Song et al., 1999), whereas neuroligin-2 localises to inhibitory synapses (Varoqueaux et al., 2004). Unlike the other two neuroligins, neuroligin-3 is found at both excitatory and inhibitory synapses (Budreck and Scheiffele, 2007), and is also expressed in glial cells (Gilbert et al., 2001).

1.5.3 Structure and binding of neuroligins

The genes encoding the neuroligins are located on the X chromosome, rendering male rats with one null copy completely deficient of that neuroligin. Neuroligins have a relatively conserved structure and amino acid sequence between them. They have a structure similar to cholinesterases and belong to the cholinesterase-like adhesion molecule family, however, they are enzymatically inactive due to lacking a residue in the catalytic triad within the cholinesterase-like domain (Hoffman et al., 2004). There are five genes encoding neuroligins in humans (*NLGN1, NLGN2, NLGN3, NLGN4 NLGN4Y*), but only three of these are conserved in rodents (*NLGN1, NLGN2, NLGN3*)

(Ichtchenko et al., 1996). *NLGN4Y* is not a true neuroligin, rather a functional homolog located on the Y chromosome. A distant variant of *NLGN4* has been identified in mice that displays the core properties of a neuroligin protein, however, this variant displays sequence variation between different strains of mice (Bolliger et al., 2008).

All neuroligins bind to both α-neurexin and β-neurexins (Boucard et al., 2005; Chih et al., 2006; Comoletti et al., 2006; Lee et al., 2010), with the binding of neuroligin-3 to α-neurexins still being explored (Uchigashima et al., 2020). A third neurexin, γ-neurexin, was relatively recently identified in mice (Sterky et al., 2017; Yan et al., 2015). The binding and function of γ-neurexin is yet to be fully elucidated (Kurshan et al., 2018). There are two alternative splice sites within *NLGNs* (A and B), allowing up to 4 isoforms (Ichtchenko et al., 1996). *NLGN1* is spliced at both A and B sites, whilst the other *NLGNs* are spliced at the A site only (Ichtchenko et al., 1996). This alternative splicing is thought to contribute to synapse specificity; the extracellular splice insertion at the B site restricts neuroligin activity to certain synapses. This results in the localisation of neuroligin-1 (containing the B splice site) to glutamatergic, and neuroligin-2 to GABAergic synapses (Chih et al., 2004). The alternative splicing of neuroligins also alters their interactions with neurexins, and which further promotes appropriate synapse formation (Chih et al., 2004). In addition to neurexin binding, neuroligin-1 was shown to recruit NMDA receptors through extracellular domain binding (Budreck et al., 2013). The cytoplasmic tail of neuroligins contains a PDZ binding sequence at the C-terminal which allows binding to PDZ-containing proteins such as PSD-95 (Irie et al., 1997).

1.5.4 Models of neuroligin-3 deficiency

Several animal and cellular models of ASD/ID with mutations in *Nlgn3* have been described. The vast majority of work on these models has been on mice, with either complete deletions of *Nlgn3* or with the *R451C* mutation described in the original study linking neuroligin-3 to autism (Jamain et al., 2003). An additional model that is often utilised is the *Nlgn3 R704C* mouse, which contains a mutation identified within *NLGN4* in individuals with ASD/ID (Yan et al., 2005) introduced into the *Nlgn3* gene of the mouse. These three models appear to show diverging phenotypes to each other, even when directly compared (Tabuchi et al., 2007; Zhang et al., 2017), and additionally between brain areas within the same model (Etherton et al., 2011). Furthermore, behavioural studies carried out on the $Nlgn3^{-/y}$ rat reported both converging and diverging

phenotypes from its mouse counterpart (Hamilton et al., 2014; Thomas et al., 2017), suggesting that many behavioural deficits are species-specific.

As neuroligin-3 indirectly associates with NMDARs through interactions with PSD-95, Etherton et al. (2011) investigated NMDAR/AMPAR ratios in the forebrain of *Nlgn3 R451C* mice. They found increased NMDAR-mediated synaptic transmission and increased NMDA-dependent LTP in CA1 of the hippocampus in *Nlgn3 R451C* mice, but no equivalent change was observed in *Nlgn3*$^{-/y}$ mice. This change in NMDAR function in *Nlgn3 R451C* mice was accompanied by an increase in NR2B subunit expression. These results suggest that the *R451C* is a gain-of-function mutation, and additionally provides evidence that, in mice, this mutation is more pathogenic than full *Nlgn3* deletion. The phenotype reported in this study, however, was specific to the hippocampus as NMDAR-mediated synaptic transmission was not altered in the cortex of *Nlgn3 R451C* mice.

The *Nlgn3 R704C* mutation appears to cause distinct phenotypes to both the *Nlgn3 R451C* and *Nlgn3* full deletions. Chanda et al. (2016) reported no change to NMDAR-mediated synaptic transmission, or inhibitory synaptic function, but instead a large decrease in AMPAR-mediated synaptic currents. However, this study was examining cultured hippocampal neurons, not using mouse acute brain slices. Differential effects of *Nlgn3* mutations were also reported by Zhang et al. (2017) in the Calyx of Held. This study showed that *Nlgn3 R451C* and *R704C* decreased or increased AMPAR-mediated excitatory synaptic transmission, respectively. Full deletion of *Nlgn3* was again reported to have no effect on synaptic transmission at Calyx of Held synapses, however when *Nlgn3* was deleted after P6, the phenotype mimicked that seen in *Nlgn3 R451C* mice; AMPAR-mediated synaptic transmission was decreased. This suggests that full deletions of *Nlgn3* provoke compensation, perhaps by other neuroligins, however this compensation is only possible early in development. However, AMPAR-mediated synaptic transmission was reported to be decreased in Purkinje neurons of *Nlgn3*$^{-/y}$ mice (Baudouin et al., 2012), providing further evidence that *Nlgn3* mutations result in brain-region specific phenotypes.

Nlgn3 R451C mice were also described to have increased inhibitory synaptic function in CA1 (Tabuchi et al., 2007). Vesicular inhibitory amino acid transporter (VGAT) puncta and sIPSC frequency were increased in CA1 pyramidal neurons in *Nlgn3 R451C* mice, suggesting an increase in inhibitory synapse number. Again, Tabuchi et al. (2007)

reported no equivalent changes in *Nlgn3*$^{-/y}$ mice. This phenotype was also described for CA3 pyramidal neurons by Pizzarelli and Cherubini (2013); mIPSC frequency recorded from CA3 pyramidal neurons was increased throughout development in *Nlgn3 R451C* mice, with no corresponding change in $GABA_A$ channel conductance. This suggests the change in mIPSC frequency is driven by increased number of GABAergic synapses. Furthermore, Földy et al. (2013) reported differential effects of the *Nlgn3 R451C* mutation on cholecystokinin-positive (CCK^+) and parvalbumin-positive (PV^+) interneurons in CA1. CCK^+ synapses exhibited an increase in inhibitory synaptic strength in *Nlgn3 R451C* mice, driven by an increase in presynaptic GABA release probability. Conversely, GABAergic synaptic transmission was reduced at PV^+ cell synapses. This latter phenotype affecting PV^+ neurons was also conserved in *Nlgn3*$^{-/y}$ mice. Interestingly, conditional complete deletion of *Nlgn3* in PV^+ interneurons caused selective effects on glutamatergic synapses onto interneurons (Polepalli et al., 2017). This study reported increased presynaptic release probability of glutamate and increased NMDAR-mediated postsynaptic currents, suggesting the change in NMDAR function reported in Etherton et al. (2011) may be due to changes in inhibitory synapses.

Nlgn3 mutations have also been reported to affect endocannabinoid signalling. Földy et al. (2013) demonstrated that the increased GABAergic transmission at CCK^+ interneurons in *Nlgn3 R451C* mice can be explained by a loss of tonic activation of presynaptic CB1 receptors. This effect was exclusively seen at inhibitory synapses, and interestingly was also observed in *Nlgn3*$^{-/y}$ mice. Endocannabinoid signalling was also disrupted in triple β-neurexin KO mice (Anderson et al., 2015). Together, these studies suggest a crucial role for the neuroligins and neurexins in endocannabinoid signalling.

In addition to physiology, *Nlgn3* mutations appear to have a significant effect on mouse behaviour. Behavioural characterisations of *Nlgn3 R451C* mice have reported reduced sociability during the three chamber task, hyperexcitability in an open field, and enhanced spatial navigation learning in the Morris water maze in comparison to WT littermates (Tabuchi et al., 2007; Jaramillo et al., 2014). However, these phenotypes appear to be dependent on the background strain of the mice as when these experiments (originally on a hybrid C57BL6J/129S2/SvPasCrl background) were repeated by the same lab and others using pure C57BL6J mice harbouring the *Nlgn3 R451C* mutation, all phenotypes observed by Tabuchi et al. (2007) and Jaramillo et al. (2014) were occluded (Chadman et al., 2008; Jaramillo et al., 2018). This is

further supported by Hosie et al. (2018) and Burrows et al. (2015), who reported no changes in social behaviour in *Nlgn3 R451C* mice that were originally B6;129 strain bred onto the C57BL6J background. Hosie et al. (2018) and Burrows et al. (2015) both reported increased aggression of *Nlgn3 R451C* mice during social interactions, despite the lack of change in social memory, and Hosie et al. (2018) also reported increased jumping behaviour in this mouse model; both of these phenotypes suggest potential changes in fight-flight-freeze responses in these rats. Interestingly, almost all physiology experiments described above were carried out on hybrid C57BL6J/129S2/SvPasCrl mice, mostly by the same laboratory, so it is unknown if these reported phenotypes are also dependent on background strain. This is with the exception of Baudouin et al. (2012), who utilise C57BL6J *Nlgn3*$^{-/y}$ mice, in addition to Hosie et al. (2018) and Burrows et al. (2015). It is therefore difficult to discern whether the distinct effects (or lack of effects) on AMPARs reported by Zhang et al. (2017), Etherton et al. (2011) and Baudouin et al. (2012) in *Nlgn3*$^{-/y}$ mice are due to the brain region or mouse strain investigated.

Both Chadman et al. (2008) and Jaramillo et al. (2018) reported normal freezing behaviour of *Nlgn3 R451C* mice during both cued and contextual fear conditioning tasks, despite differences in mouse background strain. Conversely, full deletion of neuroligin-3 does appear to decrease freezing behaviour of mice during both cued and contextual fear recall (Radyushkin et al., 2009). Interestingly, the opposite phenotype (increased freezing during fear recall) was observed when *Nlgn3* is deleted conditionally from PV^+ interneurons (Polepalli et al., 2017). Radyushkin et al. (2009) also reported decreases in sociability behaviour of *Nlgn3*$^{-/y}$ mice during the three chamber task, similar to the phenotype observed in *Nlgn3 R451C* mice (Tabuchi et al., 2007; Jaramillo et al., 2014), however this study goes on to provide evidence that this altered sociability is driven by an olfactory deficit. Other converging phenotypes between the two models of neuroligin-3 deficiency include reduced cognitive flexibility (Norris et al., 2019), increased rotarod performance (Rothwell et al., 2014; Chadman et al., 2008), and hyperactivity in open field arenas (Radyushkin et al., 2009; Jaramillo et al., 2014), suggesting that motor coordination is affected by both types of *Nlgn3* mutation.

There are also discrepancies between studies published investigating the behaviour of *Nlgn3*$^{-/y}$ rats. Similar to *Nlgn3*$^{-/y}$ mice, *Nlgn3*$^{-/y}$ rats were observed to have reduced sociability during the three chamber task, and display increased distance travelled in

open field arenas (Thomas et al., 2017). However, in *Nlgn3*$^{-/y}$ rats with the same mutation and background strain, these phenotypes were not seen by Hamilton et al. (2014). Hamilton et al. (2014) also reported a trend towards reduced freezing behaviour during cued fear recall in *Nlgn3*$^{-/y}$ rats, however this was not significantly different. Though, this result may be confounded by the use of white noise as the conditioned stimulus, which has been shown to be innately fearful to rats (Taylor, 1981).

In summary, the work carried out so far investigating the effect of *Nlgn3* mutations on synaptic function and animal behaviour highlights several key points of consideration:

1. Although modelling the same disorder, *Nlgn3 R451C* and *R704C* mutations do not result in the same physiological or behavioural phenotypes as each other, or as in the full deletion of *Nlgn3*. However, as most of these experiments were carried out on the hybrid background strain shown to affect mouse behaviour, verification of these phenotypes on another background strain of mice would provide a more complete understanding.

2. Full deletions of *Nlgn3* appear to be less detrimental to synaptic function and behaviour than either point mutation. A likely explanation for this is compensation by neuroligins-1 and 2; nonsense mediated decay of all *Nlgn3* mRNA may trigger upregulation of the other neuroligins, whilst gain-of-function point mutations *R451C* and *R704C* may result in less nonsense mediated decay and therefore fewer compensatory changes.

3. Mutations in *Nlgn3* result in cell-type specific phenotypes, despite being expressed at both glutamatergic and GABAergic synapses (Budreck and Scheiffele, 2007). This implies that, whilst present at both, neuroligin-3 has differential roles in synaptic maintenance at glutamatergic and GABAergic synapses.

4. Mutations in *Nlgn3* appear to result in phenotypes that are brain-area specific, despite relatively similar levels of expression across the brain (Varoqueaux et al., 2006). The role of neuroligin-3 at synapses may therefore not be entirely consistent throughout different brain regions, or different areas do not compensate for neuroligin-3 loss in a uniform manner.

5. Standardising behavioural testing is crucial for understanding phenotypes that are a true result of genetic mutations, especially when investigating the relatively

subtle phenotypes expected in models of ASD/ID.

1.6 The 'fear circuit'

This thesis focuses on understanding fear responses and learning in ASD/ID, utilising the *Nlgn3*$^{-/y}$ rat to model these disorders. Defensive responses elicited by fear are vital survival mechanisms, and are highly conserved across many species. These defensive responses can be broadly categorised into fight (i.e. aggressive or confrontational behaviour towards the threat), flight (i.e. jumping, running), or freeze (complete immobility except for respiration) (Fig. 1.3). Fight or flight behaviours are often termed active responses, whilst freezing behaviour is termed a passive response. These fear responses can be evoked upon encounter of an inherently fearful stimulus, or following presentation of a learned fearful stimulus. Associative fear learning (also called Pavlovian fear conditioning) is the association of a previously neutral stimulus with a fearful one. It is a highly conserved form of learning that has been well described in many species, including humans, rats and mice. Associative fear learning forms the basis of many typical and atypical forms of fear in humans; associative fear learning is a crucial part of development (i.e. learning fire is hot), however it can be distorted in children with ASD/ID, resulting in specific phobias, generalised anxiety, separation anxiety and inappropriate responses to fearful situations.

Investigation of associative fear learning tasks in rodent models of ASD/ID provides valuable information about firstly the animal's ability to form, maintain, and overwrite associative fearful memories, and secondly their response behaviour in reaction to fearful stimuli. Although the emotion of fear cannot directly be studied in rodents, the brain areas responsible for fear learning and responses are overlapping between rodents and humans (Janak and Tye, 2015). The involvement of different brain regions in a certain behaviour can be examined using lesioning, chemical or electrical stimulation, or (more recently) optogenetic and chemogenetic modulation. Studies utilising these methods allow identification of brain regions recruited for the different aspects of fear, and in combination with behavioural assessment and the study of neuronal and synaptic function *ex vivo*, can be used to understand the fear circuit and how it may be disrupted in models of ASD/ID. Investigation of these brain areas in rodent models of ASD/ID may provide significant insight into the pathophysiology of anxiety disorders

in individuals with ASD/ID. This following section is not a comprehensive description of all of the brain areas involved in fear response behaviour, fear memory acquisition, and fear extinction, but focuses on several key brain regions in the fear circuit relevant to the work in this thesis.

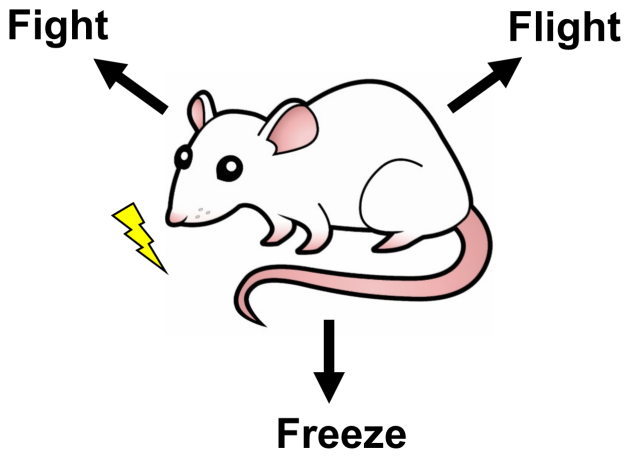

Figure 1.3: Fight, flight, or freeze in response to fearful stimuli. Clip art image from: Clip arts

1.6.1 Fear response behaviour; the expression of fear

Whether active or passive behaviours are exhibited in response to fear depends on predator-prey dynamics, salience of the fearful stimuli, and context of the situation in which it is presented. The integration of fearful sensory inputs crucial for the expression of appropriate response behaviour is dependent on the amygdala (reviewed in Kim and Jung (2006)). The amygdala can be broadly subdivided into the basolateral amygdala (BLA, which can be further split into basal amygdala, BA, and lateral amygdala, LA) and central amygdala (CeA), which contain comparable ratios of glutamatergic and GABAergic neurons to the cortex and striatum, respectively. The majority of long-range output projections from the amygdala complex originate in the CeA and target downstream brain areas involved in executing fear response behaviour. Within the CeA, competitive local inhibition between corticotropin-releasing factor positive (CRF^+) and somatostatin-positive (SOM^+) interneurons determines the promotion of flight or freeze responses respectively (Fadok et al., 2017). These responses occur through disinhibitory connections terminating in the ventral periaqueductal grey (vPAG) (Tovote et al., 2016) and hypothalamus (Wang et al., 2015).

The PAG has been viewed for many years as the final common path for the execution of defensive responses, and can be subdivided into dorsal and ventral PAG (dPAG, vPAG). Stimulation of the dPAG can evoke differing responses depending on the intensity of the stimulation; low intensity results in freezing behaviour (Vianna et al., 2001; Schenberg et al., 1990; Fanselow, 1991), whilst higher intensity results in flight behaviour (Bandler and Depaulis, 1988; Bandler and Carrive, 1988; Tomaz et al., 1988; Zhang et al., 1990; Bandler et al., 1985; Deng et al., 2016; Assareh et al., 2017). In addition, fight responses have been linked to activation of anterior dPAG sites (reviewed in Keay and Bandler (2004)), however this is less well studied. Conversely, activation of the vPAG promotes freezing (Bandler and Depaulis, 1988; Bandler and Carrive, 1988; Carrive, 1993; Depaulis et al., 1992; Keay and Bandler, 2001; Tovote et al., 2016; Deng et al., 2016). The PAG has been shown to be active during freezing behaviour exhibited by rats in fear conditioning and recall (see Table 1.3), and CS-evoked responses in the PAG attenuate with freezing behaviour during extinction (Watson et al., 2016). It is important to note, however, that Watson et al. (2016) also identified 'extinction resistant cells'; the firing of which did not correlate with extinction. Within the PAG itself, connections from flight-promoting dPAG glutamateric neurons onto interneurons in the vPAG cause local inhibition of freeze-promoting glutamatergic neurons in the vPAG (Tovote et al., 2016), allowing the drive for exhibiting flight responses to override passive freezing behaviour.

Furthermore, activation of PAG-projecting medial pre-frontal cortex (mPFC) neurons is required for the discrimination of fearful and non-fearful contexts (Rozeske et al., 2018), suggesting the PAG receives contextual information regarding the fearful stimulus via the mPFC. In addition, distinct subpopulations of mPFC neurons exhibited an increase in their tonic activity before active or passive fear responses were exhibited by the animal, with very few mPFC neurons responding nonselectively to the onset of the CS (Halladay and Blair, 2015). Therefore, this mPFC-PAG projection may underpin context-dependent alterations in fight-flight-freeze expression. Supporting this, freezing behaviour can be triggered by 4 Hz oscillations in the mPFC, which are relayed to the BLA. These 4 Hz oscillations were shown to be distinct from hippocampal theta oscillations, and further implicate the role of the mPFC in driving distinct fear response behaviours (Karalis et al., 2016).

In addition to the PAG, the hypothalamus is critical for the expression of fear

response behaviour. Electrical or chemical stimulation of the medial hypothalamus elicits defensive responses (Fernandez De Molina and Hunsperger, 1962, Lammers et al., 1988, Lipp and Hunsperger, 1978, Schmitt et al., 1985, Silveira and Graeff, 1988, Wilent et al., 2010), and inactivation of the ventromedial hypothalamus (VMH) decreases freezing behaviour in response to innately fearful stimuli (Silva et al., 2013). Furthermore, neurons within the VMH have collateral projections to both the anterior hypothalamic nucleus (AHN) and dPAG (Wang et al., 2015). Wang et al. (2015) demonstrated activation of the VMH to AHN pathway results in active fear responses such as jumping and running, whereas VMH to dPAG projection activation results in freezing behaviour.

There are many behavioural paradigms that have been designed to investigate fear in rodents, and the design of each encourages a certain fear response behaviour to be expressed. Classic fear conditioning paradigms (described in more detail in section 1.6.2) have no escape route, hiding places, or visible aggressor, and therefore typically evoke freezing behaviour in rodents. Fight responses to fear are less well studied in rodents as they are predominantly prey species, however confrontational responses can be observed in some paradigms where the aggressor is present (eg. Calvo et al. (2019)). Avoidance or flight behaviour is a defensive strategy employed by rodents to decrease the likelihood of a dangerous encounter. Active avoidance can be tested using behavioural paradigms that combine fear conditioning with an escape route (eg. Lesburguères et al. (2016)), further described in section 1.6.5.

1.6.2 Fear learning

The fear responses described in section 1.6.1 can occur in response to intrinsically fearful stimuli (eg. pain) or in response to a stimuli that is not inherently fearful but has become associated with a stimulus that is. Fear conditioning is a well-established, robust paradigm that utilises Pavlovian-style conditioning methods in order to create a fearful memory. Paradigms usually involve the paring of conditioned and unconditioned stimuli (CS and US) in a novel environment, followed by presentation of the CS alone to observe "fear memory". The CS can be any stimulus not inherently fearful to the animal, such as a noise, light, or environment. Conversely, inherently fearful stimuli such as foot-shocks, predator odours, loud noises or air puffs can be used as the US for rodent fear conditioning paradigms. The animal will exhibit fear responses following US

presentation, and these behaviours will increase given repeated CS-US pairings. The pairing of CS and US is termed fear conditioning, and allows investigation of "fear learning"; the acquisition of a fearful memory (Table 1.3).

Table 1.3: Studying fear learning and responses.

Experiment	Aspect investigated	Expected response
Fear conditioning	Fear learning Fear response behaviour	Increasing fear response behaviours
Fear recall	Fear memory strength Fear response behaviour	Presence of fear response behaviours
Fear extinction	Re-learning	Decreasing fear response behaviours

Fear learning is highly dependent on the amygdala. The amygdala receives sensory inputs from diverse brain areas, including the thalamus, cortex and hippocampus (reviewed in Kim and Jung (2006)). Incoming sensory information regarding the fearful stimulus (US) is integrated in the BLA, where the association of the US and previously neutral stimulus (CS) is thought to take place. This association requires activity-dependent plasticity of sensory afferents to LA neurons (Rogan et al., 1997; Quirk et al., 1995). Depolarisation of LA neurons in response to an aversive US causes strengthening of the CS inputs, resulting in defensive responses to the CS that were previously not observed (reviewed in Maren and Quirk (2004)). In addition to the LA, fear learning (but not response behaviour) is also dependent on the hippocampus (Kim et al., 1993), and CS-evoked responses in the hippocampus have been shown to potentiate during fear conditioning (Tang et al., 2003). The plasticity of LA synapses is dependent on local disinhibition by PV^+ and SOM^+ interneurons, which act differentially on CS and US inputs to promote associative plasticity (Wolff et al., 2014).

Furthermore, a subpopulation of LA neurons has been shown to respond preferentially to unpredictable stimulus (Belova et al., 2007), suggesting that large prediction errors drive synaptic plasticity in the LA. The plasticity of sensory afferents to LA neurons is thought to be predominantly NMDAR-dependent (Bauer et al., 2002; Kim et al., 1991; Miserendino et al., 1990; Goosens and Maren, 2004), although NMDAR-independent mechanisms are also present (Shaban et al., 2006).

Potentiated CS inputs into LA neurons are then relayed to the BA and CeA. The CeA can be further split into the central lateral (CeL) and central medial (CeM) amygdala. Glutamatergic projections from the LA synapse onto SOM^+ neurons in the CeL, and potentiation of these synapses is also necessary for fear learning (Li et al.,

2013). Furthermore, LA neurons target the intercalated cell masses (ICMs) which relay feedforward inhibition to CeL interneurons and, together with LA-to-SOM$^+$, release tonic inhibition of CeM output neurons (Sah et al., 2003). ICMs are a dense bundle of predominantly GABAergic neurons located between the BLA and CeA that serve to regulate the information flow through the amygdala. In addition to direct connections with CeL GABAergic neurons, LA glutamatergic neurons also target BA glutamatergic neurons, which in turn excite CeM interneurons. These BA-CeM connections promote fear response behaviour (Paré et al., 1995). Amygdala microcircuits are tightly regulated by GABAergic inhibition (Szinyei et al., 2007; Shaban et al., 2006; Li et al., 1996; Polepalli et al., 2010; Wolff et al., 2014; Miserendino et al., 1990), allowing the appropriate output response (fight, flight, freeze) to be exhibited. Whilst activation of the CeM is required for the expression of fight-flight-freeze behaviour (Ciocchi et al., 2010) (section 1.6.1), the CeL is necessary for fear learning.

Prediction error

The effectiveness of fear conditioning (how strongly the CS and US become associated) increases when the CS is paired with an unexpected, rather than expected, US (Sutton and Barto, 1981). LA neurons also preferentially respond to unexpected stimuli during fear conditioning (Belova et al., 2007; Johansen et al., 2010). The PAG has been implicated in relaying prediction errors to the LA, notably by Johansen et al. (2010), who demonstrated that inactivation of the PAG prevented fear learning, and US-evoked responses in both the PAG and LA were diminished with increasing US predictability. The cerebellum has also been suggested to be involved in encoding prediction error. A recent functional magnetic resonance imaging (FMRI) study in humans described increased BOLD signal in the cerebellum during CS presentation, including when the usually-paired US was unexpectedly omitted (Ernst et al., 2019). Together, these results suggest that midbrain and hindbrain areas are not simply involved in the execution of fear response behaviours, but also relay prediction error information back to forebrain regions in order to modulate their responses.

This section describes the circuitry required for form a CS-US association in which a previously neutral stimulus transitions to become a fearful stimulus. The strength of this association can be tested by investigating fear responses to the CS alone, which is detailed in the following section.

1.6.3 Fear memory recall

After fear conditioning and a period of memory consolidation, presentation of the CS alone induces robust recall of fear; displayed as a high percentage of time expressing fear response behaviours. The expression of fear behaviours in response to learned fear involves some distinct brain regions in addition to those described in section 1.6.1, as it requires both recall of the fearful memory and expression of fear response behaviours. Neuronal responses to the CS in the LA that underwent potentiation during fear learning are sufficient to induce a fear response in an animal during this recall phase (Li et al., 2013). In addition to the amygdala, the contextual input required for the retrieval of fear memories is dependent on the hippocampus. Inactivation of the ventral hippocampus abolishes contextual fear recall (Hobin et al., 2006), however the ventral hippocampus has been shown not to be required for the recall of cued fear memories (Phillips and LeDoux, 1992). Blocking protein synthesis in the dorsal hippocampus following CS-US pairings has been shown to significantly reduce fear response behaviour during cued fear recall (Yang et al., 2011). Reciprocal connections between the hippocampus and BA are thought to encode sensory and contextual information vital for driving appropriate fear responses (Herry et al., 2008).

Fear recall is also dependent on activation of the mPFC (reviewed in Courtin et al. (2013)). The necessity of prelimbic mPFC activation is specific to learned fear and is not required for innate fear responses (Corcoran and Quirk, 2007). Courtin et al. (2014) provided evidence that during fear recall, inhibition of PV^+ interneurons in the mPFC causes disinhibition of long-range prelimbic mPFC to BLA projections and synchronisation of neuronal firing to theta oscillations that result in fear responses. Furthermore, optogenetic activation of specific cell populations in the LA (Kwon et al., 2014), dorsal hippocampus (Liu et al., 2012b) or dorsal-medial mPFC (Courtin et al., 2014) are sufficient to induce fear response behaviour in novel contexts not previously associated with US presentations. These studies support the idea that fear memory formation recruits specific neuronal populations to a 'fear memory engram', activation of which subsequently results in recall of fear.

Fear memory recall is cue- or context-specific, an aspect of fear thought to be dependent on the infralimbic mPFC. Sangha et al. (2014) demonstrated that in rats that usually exhibited fear response discrimination between fear conditioned stimuli and safety stimuli, inactivation of the infralimbic mPFC caused generalised fear responses

that spanned the presentation of both stimuli. The discrimination of fearful stimuli is also thought to involve PAG-projecting mPFC neurons, which have been shown to be activated during transition periods between fearful and non-fearful contexts. Optogenetic inhibition of these connections also resulted in generalised fear responses (Rozeske et al., 2018).

1.6.4 Fear memory extinction

Further CS-only presentations can be given to extinguish the fearful memory; seen as reduction in fear response behaviour which occurs during repeated presentations of the CS without reinforcement of the US. The encoding of fear extinction, which is a form of learning in itself, involves many of the same brain regions as fear conditioning and fear recall, however the circuitry controlling this learning is different. Sierra-Mercado et al. (2011) suggests distinct roles of the mPFC, BLA and hippocampus in the different aspects of fear extinction; whilst the prelimbic mPFC was required for fear responses, infralimbic mPFC was essential for fear extinction. Moreover, the BLA and ventral hippocampus were required for both the execution of fear response behaviours and extinction of cued fear memories.

Plasticity of the BLA is also required for fear extinction (Sotres-Bayon et al., 2007; Herry et al., 2006). In addition, as extinction takes place, a different population of neurons within the BA become active to those active during fear conditioning (Herry et al., 2008). These different populations of BA neurons project to discrete subregions of the mPFC; BA neurons targeting the prelimbic mPFC are active during high fear states in fear recall and acquisition, whereas BA neurons targeting the infralimbic mPFC are recruited and undergo plasticity during fear extinction (Senn et al., 2014). In addition, inactivation of the infralimbic, but not the prelimbic, mPFC inhibits fear extinction (Laurent and Westbrook, 2009), and neurons from the infralimbic mPFC have been shown to be active during fear extinction but not during fear conditioning or recall (Milad and Quirk, 2002). The activation of these 'extinction neurons' in the BA are important for inhibiting fear response-promoting output from the CeM to the PAG and hypothalamus, as stimulation of the infralimbic mPFC leads to inhibition of the CeM (Quirk et al., 2003). Furthermore, Amano et al. (2010) reported increased inhibition in the CeM during fear extinction, mediated by potentiation of BLA-ICM synapses which relay feedforward inhibition to the CeM. In addition to ICMs, Trouche

et al. (2013) reported perisomatic synapses of PV^+ and CCK^+ interneurons targeting a subpopulation of pyramidal neurons in the BA that promote fear response behaviour. These perisomatic synapses increased during fear extinction, silencing the fear-promoting output of these BA neurons.

The extinction of fear is not the same as forgetting the CS-US association, but rather re-learning the association is no longer valid (Quirk, 2002). This idea is supported by Herry et al. (2008) who identified a subpopulation of BLA neurons that display CS-evoked responses similar to during fear recall even after complete extinction of fear behaviours has taken place. The profile of extinction depends on both the strength of the initial CS-US association and the prediction error.

1.6.5 Active avoidance learning

The fear learning, fear memory recall, and fear memory extinction as described above has predominantly been defined in the context of Pavlovian-style fear conditioning. When fear learning is investigated in paradigms where fear response behaviours other than freezing are permitted or enforced, distinct brain circuity is required. One such paradigm is the active place avoidance task, developed by Lesburguères et al. (2016), which requires rats to associate an unconditioned stimulus with a stationary spatial location within a moving arena, and use external cues to navigate and avoid this zone. As well as providing information about fear learning, this task allows examination of active fear responses not often seen in fear conditioning paradigms. It also allows investigation of spatial navigation techniques and learning.

Increased activity in the mPFC, BLA, and ventral striatum have all been correlated with the expression of active avoidance (Diehl et al., 2018; Bravo-Rivera et al., 2015), and furthermore, projections from the prelimbic mPFC to BLA have been shown to be involved in the retrieval of avoidance behaviour (Diehl et al., 2018). Long-term (but not short-term) NMDAR-dependent plasticity of reciprocal connections from BLA to prelimbic mPFC are thought to be required for the extinction of avoidance learning (Fragale et al., 2016) and (similar to the extinction of classical fear conditioning) extinction of active avoidance learning has been linked to BLA-infralimbic mPFC connections (Diehl et al., 2018), and activation of ventral hippocampus (Rosas-Vidal et al., 2014).

A recent study suggested the role of inhibition within the rostral prelimbic mPFC that was specific to active avoidance, and not required for fear conditioning, suggesting

these neurons signal the avoidable nature of this task (Diehl et al., 2018). Overall, circuitry involved in the expression of active avoidance behaviour is similar to fear conditioning and recall, however, the two behaviours may employ different neuronal activation patterns to signal the appropriate defensive strategy.

1.6.6 Summary of fear circuitry

Overall, the acquisition, recall and extinction of fearful memories, as well as the expression of fear responses, involve many distributed brain areas and highly organised circuitry. The connectivity of the brain areas relevant to the work presented in this thesis is shown in Figure 1.4, although this is not an exhaustive summary. Understanding the physiology of the brain areas involved in this circuit and the nature of the connections between them will provide valuable insight into how this circuit is disrupted in anxiety disorders.

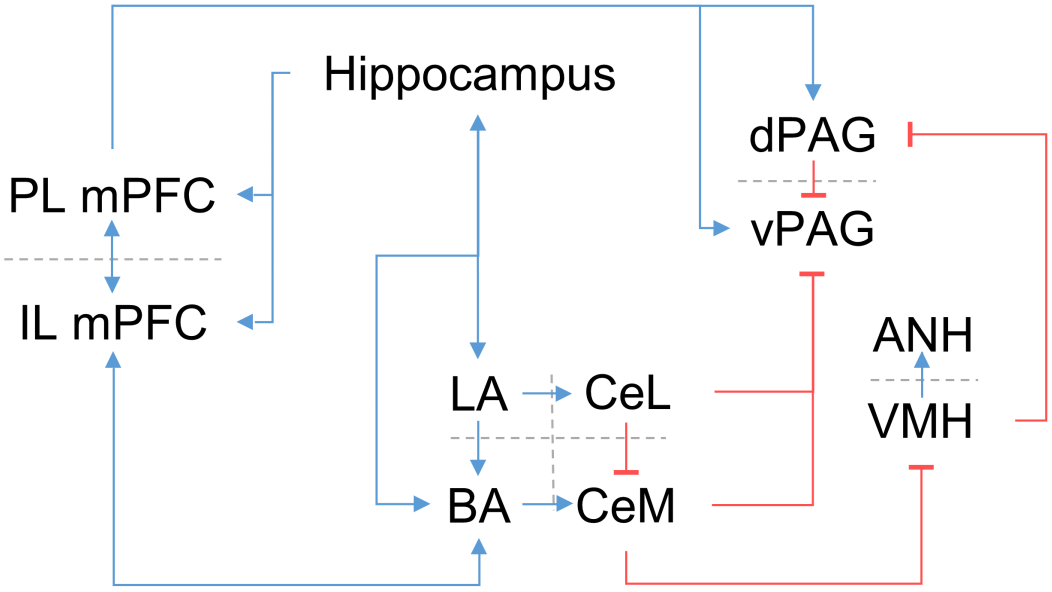

Figure 1.4: The fear circuit. A simplified schematic of fear circuitry identified in the rodent brain. Red arrows denote inhibitory connections, blue arrows denote excitatory connections. PL: prelimbic, IL: infralimbic, mPFC: medial prefrontal cortex, LA: lateral amygdala, BA: basal amygdala, CeL: centrolateral amygdala, CeM: centromedial amygdala, VMH: ventromedial hypothalamus, ANH: anterior hypothalamic nucleus, dPAG: dorsal periaqueductal grey, vPAG: ventral periaqueductal grey.

1.7 Imbalance of flight-freeze responses in *Nlgn3$^{-/y}$* rats

This section provides a brief overview of unpublished research into the behaviour of *Nlgn3$^{-/y}$* rats carried out by myself and colleagues (V. Kapgal and S. Tiwari, with guidance from Professors P. Kind, O. Hardt, E. Wood and S. Chattarji) at the Centre for Brain Development and Repair (CBDR) in Bangalore, India. This work is being submitted as part of another thesis (Vijayakumar Kapgal, CDBR), however serves as the basis of many hypotheses explored in this thesis, and therefore is summarised below. The methodologies for these behavioural paradigms are described in Appendix A.1.

Anxiety and disrupted emotional responses are some of the most debilitating aspects of ASD/ID (see section 1.1.1), and the brain circuitry underlying these are relatively well characterised (see section 1.6). One way to investigate anxiety and emotion in a laboratory setting is to use behavioural paradigms that tap into similar circuits. Fear conditioning is a well-characterised and robust behavioural task that is known to require the hippocampus, medial-prefrontal cortex, amygdala and periaqueductal grey (see section 1.6). Therefore, we trained WT and *Nlgn3$^{-/y}$* rats in an auditory fear conditioning paradigm (Fig. 1.5A) in which they receive three pairings of conditioned (tone) and unconditioned (0.9 mA foot shocks) stimuli. The rats were then placed in a different context and presented with the conditioned stimulus alone. We found that *Nlgn3$^{-/y}$* rats display significantly reduced freezing behaviour (defined as no movement except for respiration) during both the conditioning and recall phases of this task (Fig. 1.5B-C).

Reduced freezing behaviour in response to CS presentation following fear conditioning could be interpreted as a fear learning deficit. However, reviewing the videos for this task indicated that animals were responding to the CS, but not with full-body freezing. Instead, *Nlgn3$^{-/y}$* rats displayed cessation of exploratory behaviour and a lack of limb movement in response to the tone, yet moved the head and neck in observation of their environment. Reanalysis of these videos revealed that 80% of this freezing deficit could be attributed to head movements alone, whilst the paws of the rat remained stationary (Fig. 1.5D). This suggested that *Nlgn3$^{-/y}$* rats were still forming the association between tone and shock but expressing their fear in a different manner. Furthermore, no difference was observed in the basal activity levels of the same *Nlgn3$^{-/y}$* rats; tested in

an open field arena before fear conditioning (Fig. 1.6). This suggests that any changes to motor behaviour during fear recall was specific to fearful situations.

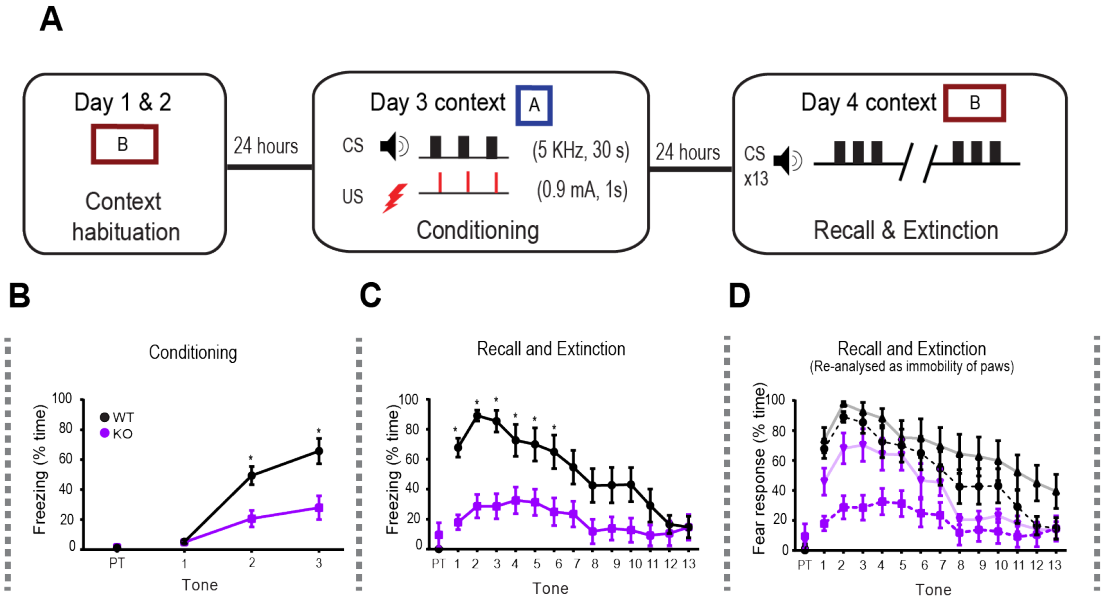

Figure 1.5: *Nlgn3*$^{-/y}$ rats display reduced classic freezing behaviour in an auditory fear conditioning paradigm. (A) Schematic of the auditory fear conditioning protocol. (B) *Nlgn3*$^{-/y}$ rats show less classic freezing behaviours during the conditioning phase ($p = 0.015$, $F = 6.61$, repeated measures two-way ANOVA; WT n = 12, KO n = 12). (C) *Nlgn3*$^{-/y}$ rats show less classic freezing behaviours during the recall and extinction phase ($p = 0.0011$, $F = 13.96$, repeated measures two-way ANOVA; WT n = 12, KO n = 12). (D) When analysed as "immobility response" (i.e all four paws unmoving but allowing for movement of head and neck, shown in light purple/grey) *Nlgn3*$^{-/y}$ rats show significantly increased response to CS in comparison to classic freezing scoring ($p = 0.029$, $F = 5.39$, repeated measures two-way ANOVA; KO n = 12, KO n = 12).

To further explore the fear learning and responses in *Nlgn3*$^{-/y}$ rats, we employed the active place avoidance (APA) task. The APA task is a circular rotating platform in which rats use external cues to learn the position of a fixed (relative to the external environment), low-ampere shock-zone (Lesburguères et al., 2016) (Fig. 1.9A). When rats initially began training in this task, after receiving one or more shocks, 8/9 *Nlgn3*$^{-/y}$ rats and 1/9 WT rats tested jumped out of the arena altogether (Fig. 1.7), suggesting an alternative flight-based strategy for avoiding the shock.

One possible explanation for altered fear responses is that *Nlgn3*$^{-/y}$ rats are hypersensitive to electrical shocks. We tested this hypothesis by performing a "shock-ramp" test, in which we gave WT and *Nlgn3*$^{-/y}$ rats increasing intensities of foot shocks (0.06 to 1 mA) at fixed intervals and scored and categorised their response behaviour (Fig. 1.8A). We found that the minimum shock required to elicit any response was not different between *Nlgn3*$^{-/y}$ and WT rats (Fig. 1.8B-C), implying they are not hypersensitive.

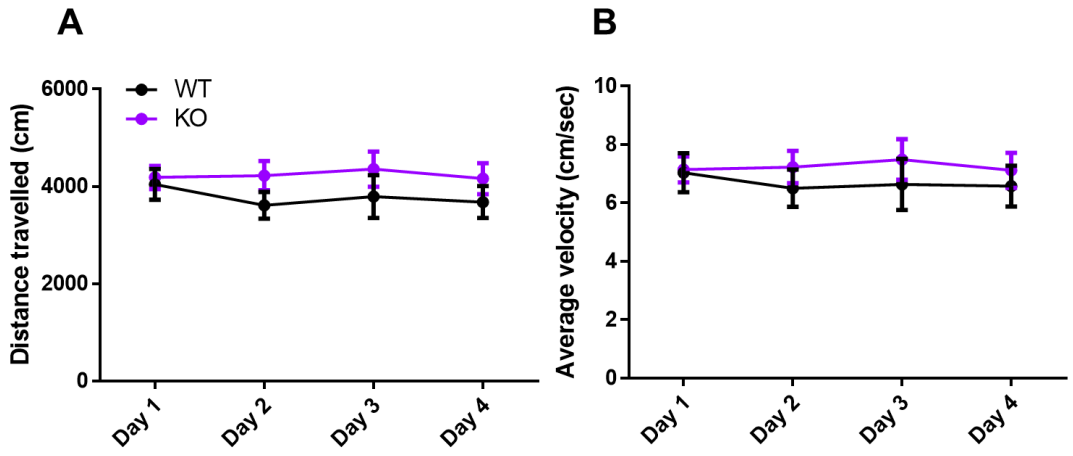

Figure 1.6: No change in basal activity of *Nlgn3*$^{-/y}$ rats during an open field task. (A) No change in average distance travelled of *Nlgn3*$^{-/y}$ rats on any of the four days tested (WT n = 12, KO n = 12, p = 0.29, F = 1.18, repeated measures two-way ANOVA). (B) No change in average velocity of *Nlgn3*$^{-/y}$ rats on any of the four days tested (WT n = 12, KO n = 12, p = 0.52, F = 0.43, repeated measures two-way ANOVA).

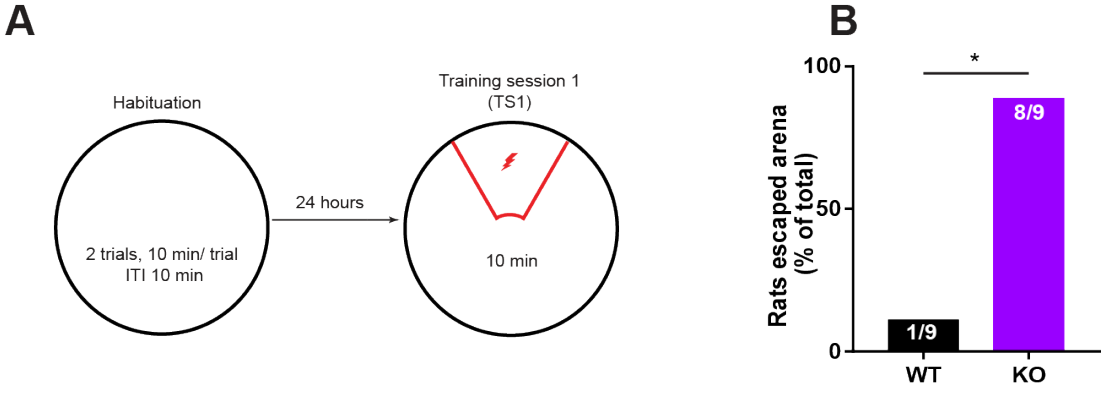

Figure 1.7: *Nlgn3*$^{-/y}$ rats escaped entire arena when given training foot shock.(A) Schematic depicting habituation day and first training session of active place avoidance task. There was no lid on this arena. (B) 88.9 % *Nlgn3*$^{-/y}$ and 11.1 % WT rats jumped out of the arena following 0.2 mA foot shocks given during training ($p < 0.00001$; Fisher's exact test; WT n = 9, KO n = 9).

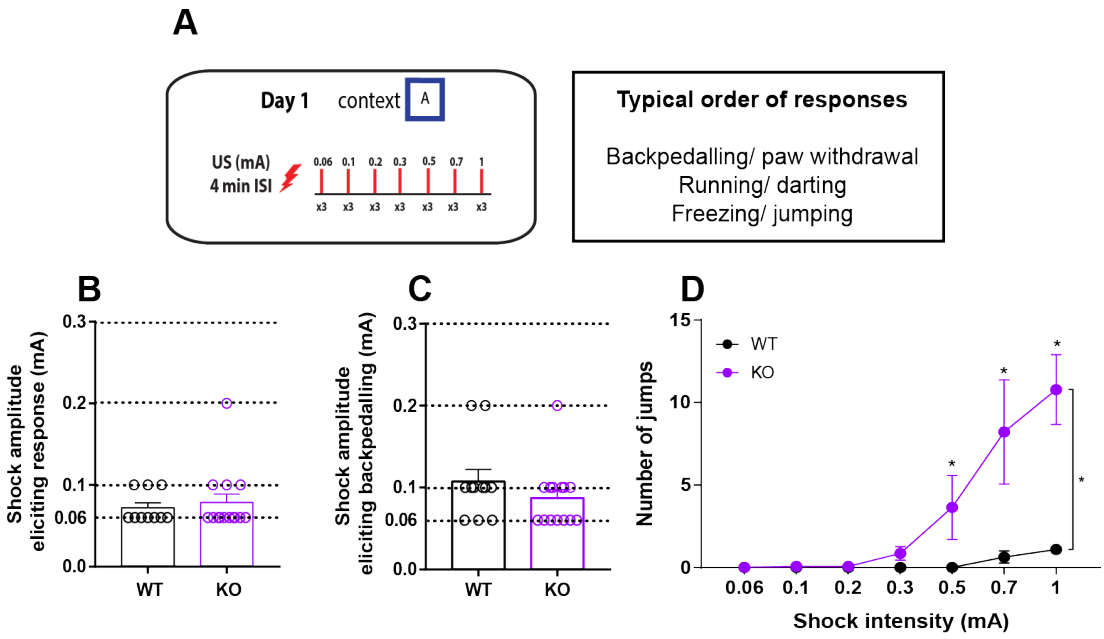

Figure 1.8: *Nlgn3*$^{-/y}$ rats display increased jumping behaviour in response to electrical shocks. (A) Schematic of the shock-ramp test protocol and typical order of responses seen. (B) Shock amplitude required to elicit a response of any kind was not different between WT and *Nlgn3*$^{-/y}$ rats ($p = 0.13$; unpaired t-test; WT n = 11, KO n = 14). (C) Shock amplitude required to elicit backpedalling response was not different between WT and *Nlgn3*$^{-/y}$ rats ($p = 0.26$; unpaired t-test; WT n = 11, KO n = 14). (D) *Nlgn3*$^{-/y}$ rats display significantly more jumps in response to increasing intensity electrical foot shocks ($p = 0.0081$, $F = 8.39$, repeated measures two-way ANOVA; WT n = 11, KO n = 14).

However, we again saw that *Nlgn3*$^{-/y}$ rats displayed significantly increased jumping behaviour in response to the shocks (Fig. 1.8D). Intriguingly, an increase in jumping behaviour has also been reported in *Nlgn3 R451C* mice during social interaction (Hosie et al., 2018).

Due to this increased jumping behaviour, to be able to assess learning in *Nlgn3*$^{-/y}$ rats we had to adapt the APA arena to include a lid for all subsequent cohorts to ensure rats could not escape the arena. When tested with a lid on the arena, both WT and *Nlgn3*$^{-/y}$ rats learned the location of the shock zone, and could successfully avoid it by actively navigating to the safe zone by the end of the training sessions (Fig. 1.9A-G), suggesting associative and spatial learning abilities are not impaired in *Nlgn3*$^{-/y}$ rats. Indeed, *Nlgn3*$^{-/y}$ rats displayed faster learning in comparison to WT rats, as indicated by reduced shock zone entries (Fig. 1.9C), increased maximum time avoided (Fig. 1.9E), and increased time to second shock zone entry (Fig. 1.9G). However, *Nlgn3*$^{-/y}$ rats showed prolonged avoidance of the zone once the shock had been removed, perhaps indicating a decrease in cognitive flexibility in these rats (Fig. 1.9H-L).

Together, these results suggest that *Nlgn3*$^{-/y}$ rats display an imbalance of flight-freeze responses that is heavily biased towards flight. Additionally, they suggest that *Nlgn3*$^{-/y}$ rats do not show a deficit in fear learning, and instead display faster learning in comparison to WT rats. However, *Nlgn3*$^{-/y}$ rats may have reduced cognitive flexibility. This work also highlights the importance of in-depth behavioural characterisation of a model, as a change in fear expression as oppose to fear learning may have been overlooked or misinterpreted without further investigation. These findings led to the experiments undertaken in this thesis and the aims and hypotheses summarised below.

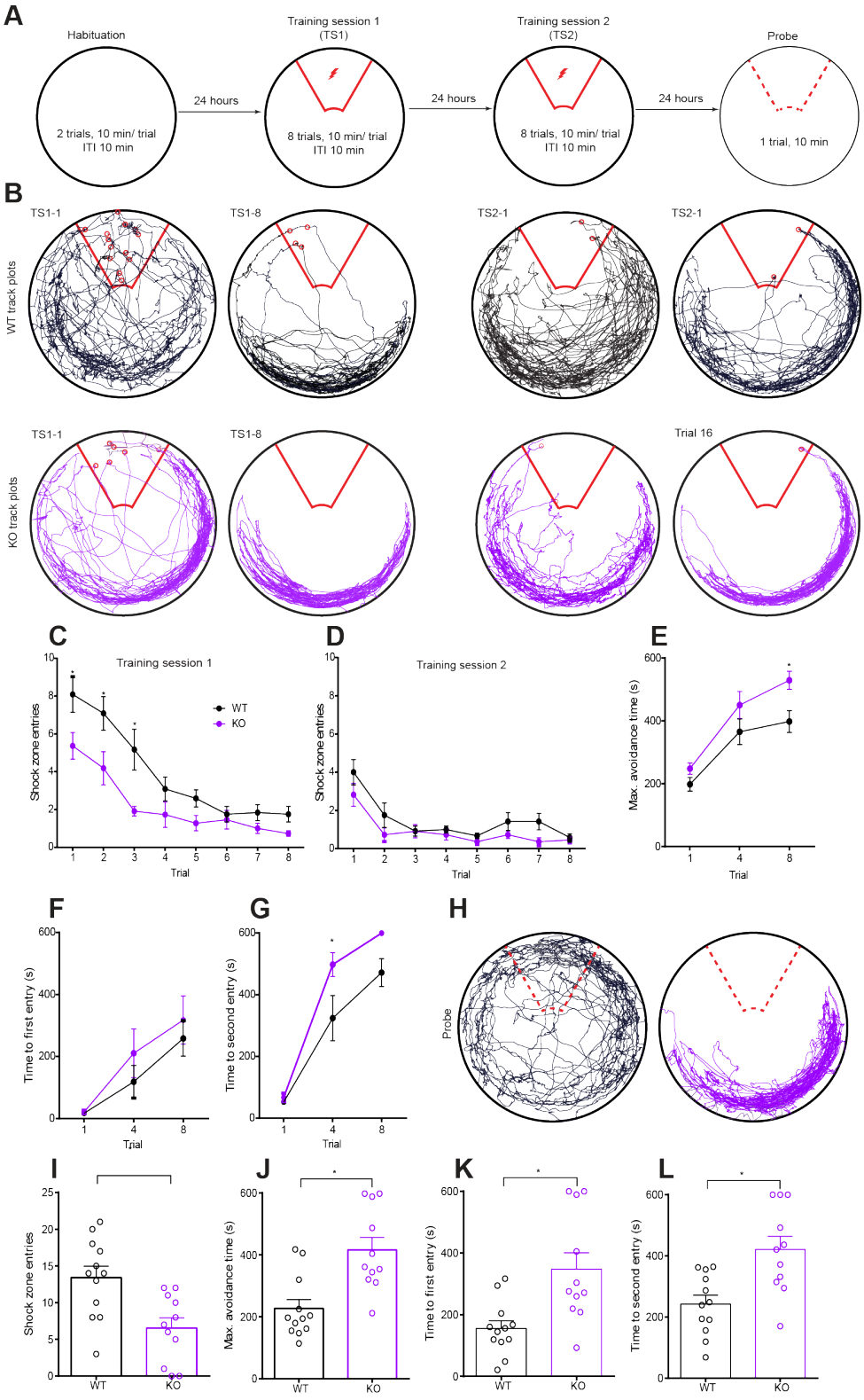

Figure 1.9: *Nlgn3*$^{-/y}$ rats show faster learning and prolonged avoidance of the shock zone in an active place avoidance task.

Figure 1.9 ***(previous page)*****: *Nlgn3*$^{-/y}$ rats show faster learning and prolonged avoidance of the shock zone in an active place avoidance task.** (A) Schematic of the active place avoidance task. (B) Representative track plots for WT and *Nlgn3*$^{-/y}$ rats in trials 1 and 8 of both training sessions. (C) *Nlgn3*$^{-/y}$ rats enter the shock zone significantly fewer times during training session 1 ($p = 0.0045$, $F = 10.09$, repeated measures two-way ANOVA; WT n = 12, KO n = 11), but show comparable entries to WTs in training session 2 ($p = 0.044$; repeated measures two-way ANOVA; WT n = 12, KO n = 11). (D) *Nlgn3*$^{-/y}$ rats show significantly fewer shock zone entries to WT rats during training session 2 ($p = 0.044$, $F = 4.60$, WT n = 12, KO n = 12). (E, F, G) *Nlgn3*$^{-/y}$ rats show increased maximum time avoided and time to second entry, but comparable time to first entry in training session 1 ((E) $p = 0.0044$, $F = 10.18$, (F) $p = 0.33$, $F = 0.98$, (G) $p = 0.012$, $F = 7.62$; repeated measures two-way ANOVAs; WT n = 12, KO n = 11.). (G) Representative track plots for WT and *Nlgn3*$^{-/y}$ rats in the probe trial. (H) Representative track plots for WT and *Nlgn3*$^{-/y}$ rats during the probe session. (I) *Nlgn3*$^{-/y}$ rats enter the shock zone significantly fewer times during the probe trial ($p = 0.0036$; unpaired t-test). (J, K, L) *Nlgn3*$^{-/y}$ rats show increased maximum time avoided, time to first entry and time to second entry in training session 1 ($p = 0.0008$ (J), 0.0029 (K), 0.002 (L); unpaired t-tests, WT n = 12, KO n = 11).

1.8 Aims of this thesis

The overarching aim of this thesis is to determine physiological mechanisms by which autism-associated mutations in *NLGN3* and *NRXN1* lead to altered fear, anxiety and emotional responses. The first two chapters of this thesis address the behavioural finding that *Nlgn3*$^{-/y}$ rats display increased flight and decreased freezing behaviours in response to fearful stimuli (Figs. 1.5, 1.7, 1.8). The physiology of the PAG was therefore investigated, as this is the main integration and output centre for executing flight or freeze responses. To address this, firstly a detailed characterisation of PAG neurons in wild-type rats was carried out, as relatively little is known about the electrophysiological properties of cells in this brain region. I then tested the hypothesis that altered physiological properties of PAG neurons underlies the bias towards flight behaviours in *Nlgn3*$^{-/y}$ rats (Chapters 3 and 4). In the final experimental chapter, I tested the hypothesis that there would be convergence of physiological phenotypes between *Nlgn3*$^{-/y}$ and *Nrxn1*$^{+/-}$ rats.

Chapter 3: I hypothesised that in WT rats, neurons of the PAG could be subdivided based on their electrophysiological properties, and these properties would be reflective of neuronal morphology. Furthermore, I hypothesised that in *Nlgn3*$^{-/y}$ rats, neurons in the flight-promoting dPAG region would be hyperexcitable. My findings supported both of these hypotheses; I define four electrophysiologically distinct neuronal subpopulations in the PAG, and I provide evidence of increased intrinsic excitability in dPAG neurons of *Nlgn3*$^{-/y}$ rats which may underpin the increased flight responses observed.

Chapter 4: I hypothesised that this hyperexcitability of the dPAG in *Nlgn3*$^{-/y}$ rats would lead to altered local field potentials in the PAG during auditory fear recall and a reduced threshold required to elicit flight responses in animals receiving *in vivo* dPAG stimulation. I found that local field potentials were largely unaffected in *Nlgn3*$^{-/y}$ rats, however threshold to elicit dPAG-induced flight responses was reduced in *Nlgn3*$^{-/y}$ rats.

Chapter 5: Previous work on models of ASD/ID has suggested that genetically distinct causes of these disorders may converge on common cellular pathophysiologies (Krumm et al., 2014; Pinto et al., 2014; Barnes et al., 2015; Baudouin et al., 2012). I therefore hypothesised that there would be convergence of physiological phenotypes

between *Nlgn3*$^{-/y}$ and *Nrxn1*$^{+/-}$ rats. My findings provide evidence for both convergent and divergent phenotypes whilst investigating neuronal and synaptic properties, as well as synaptic plasticity, in the hippocampus and medial pre-frontal cortex of *Nlgn3*$^{-/y}$ and *Nrxn1*$^{+/-}$ rats.

Chapter 2

Materials and Methods

2.1 Animals and ethical statement

Work shown in this thesis was carried out at either the Centre for Discovery Brain Sciences (CDBS, at the University of Edinburgh) or at the Centre for Brain Development and Repair (CBDR, at the National Centre for Biological Sciences, Bangalore). Experimental set-up and protocols were kept as similar as possible between the two sites. Any differences in experiments between sites are noted in the relevant section.

All experiments and analyses were done blind to genotype. All procedures (including those carried out at CBDR) were conducted in accordance with University of Edinburgh Animal Welfare Committee and Home Office guidelines under the 1986 Animals (Scientific Procedures) Act. Procedures carried out at CBDR were also performed in line with the CPCSEA guidelines and approved by the Institutional Animal Ethics Committee.

Rats were housed on either a 14/10 hr (Bangalore) or 12/12 hr (Edinburgh) light/dark cycle with food and water *ad libitum*. For electrophysiology experiments, rats were housed with littermates post-weaning. For behaviour experiments rats were housed with 2 wild-type (WT) and 2 genetically modified (GM) animals per cage, littermate pairs where possible. For animals undergoing surgery, animals were housed with littermates post-weaning, then single-housed after surgery had taken place.

2.1.1 *Nlgn3*$^{-/y}$ rats

The rat model referred to as *Nlgn3*$^{-/y}$ in this thesis is a genetically modified rat line bred onto the Sprague-Dawley (SD) background, in which there is a knock-out

(KO) mutation of the *Nlgn3* gene. This rat model was designed and engineered by Horizon Discovery, and utilises a zinc-finger nuclease to target exon 5 of *Nlgn3* (Fig. 2.1A), leading to a 58 bp deletion and complete loss of the neuroligin-3 protein (Fig. 2.1C). RNA sequencing of this model revealed the possible presence of a truncated form of neuroligin-3 in the KO rats (predicted size 289 amino acids) due to non-standard splicing around the deletion. We therefore ran Western blotting using an antibody for the N-terminus of neuroligin-3 (Fig. 2.1D), however no bands were present at either the expected size for neuroligin-3 (∼120 kDa) or the truncated version (∼32 kDa).

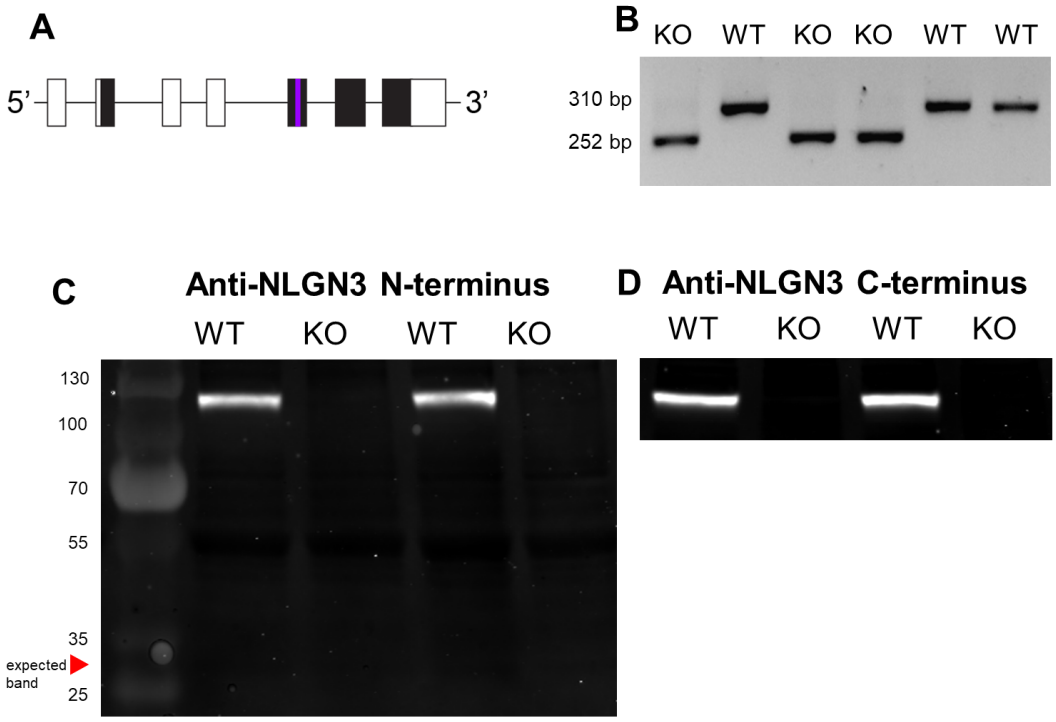

Figure 2.1: Validation of the *Nlgn3*$^{-/y}$ rat model. (A) Schematic of zinc finger target within exon 5 of *Nlgn3*. (B) PCR from *Nlgn3*$^{-/y}$ and WT rats showing the presence of WT band (310 bp) in WT and homozygote band (252 bp) in *Nlgn3*$^{-/y}$ rats. (C) Western blot from WT and *Nlgn3*$^{-/y}$ homogenates showing the absence of neuroligin-3 protein in the KO rat using an antibody specific to NLGN3 N-terminus. There is also no band present at 32 kDa (red arrow), indicating a truncated form of the protein is also not present. (D) Western blot from WT and *Nlgn3*$^{-/y}$ homogenates showing the absence of neuroligin-3 protein in the KO rat using an antibody specific to NLGN3 C-terminus.

2.1.2 *Nrxn1*$^{+/-}$ rats

The rat model referred to as *Nrxn1*$^{+/-}$ in this thesis is a genetically modified rat line bred onto the Sprague-Dawley (SD) background, in which there is a heterozygous (Het) mutation affecting the the *Nrxn1* gene. This rat model was designed and engineered

by Horizon Discovery, and utilises a zinc-finger nuclease to target exon 1 of *Nrxn1* (Fig. 2.2A), leading to a 16 bp deletion and loss of *Nrxn1* in one allele. This causes a haploinsufficiency of neurexin-1 protein.

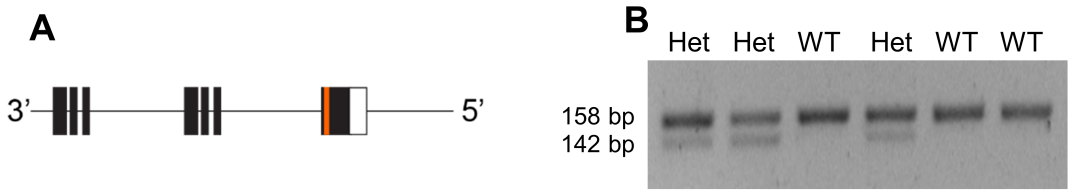

Figure 2.2: Genotyping of the *Nrxn1*$^{+/-}$ rat model. (A) Schematic of zinc finger target on exon 1 of *Nrxn1*. (B) PCR from *Nrxn1*$^{+/-}$ and WT rats showing the presence of WT band (310 bp) in WT, and both the WT (310 bp) and homozygote bands (252 bp)in *Nrxn1*$^{+/-}$ rats.

2.2 Genotyping

Genotyping was carried out either by Transnetyx Inc., or using the protocols described below.

2.2.1 Tissue collection and DNA extraction

Ear punches were collected either at weaning for routine animal identification markers or post-mortem after experimental culling. DNA was extracted from the tissue using a DNeasy Blood and Tissue kit (QUIAGEN) as per their provided protocol.

2.2.2 Primers

Single assays were used for *Nlgn3*$^{-/y}$ and *Nrxn1*$^{+/-}$ genotyping using the primers shown in Table 2.1.

Table 2.1: *Nlgn3*$^{-/y}$ and *Nrxn1*$^{+/-}$ forward and reverse primers for PCR.

	Forward	Reverse
***Nlgn3*$^{-/y}$**	CATCCGAGACAGTGGTGCTA	AGAAAGCCCTTGGTATTCGG
***Nrxn1*$^{+/-}$**	GCAGCTCAGCTTCTCCATCT	ACTTGACCTCCACCCACTTG

2.2.3 Polymerase Chain Reaction (PCR)

Polymerase chain reaction (PCR) mixes were composed as shown in Table 2.2. The thermocycling conditions for *Nlgn3*$^{-/y}$ primers are described in Table 2.3. The PCR products were run on a 2% agarose gel made in Tris-borate-EDTA (TBE) buffer containing EtBr at 140 V for 30 minutes. A GeneRuler 100 bp DNA ladder (Thermo Fisher) was used. Figure 2.1B provides an example of *Nlgn3* PCR genotyping.

Wild-type band: 310 bp

Homozygote band: 252 bp

The thermocycling conditions for *Nrxn1*$^{+/-}$ primers are described in Table 2.3. The PCR products were run on a 4% agarose gel made in TBE buffer containing EtBr at 100 V for 30 minutes and then 200 V for a further 30 minutes. A GeneRuler 100 bp DNA ladder was again used. Figure 2.2B provides an example of *Nrxn1* PCR genotyping.

Wild-type band: 158 bp

Homozygote band: 142 bp

Table 2.2: PCR reaction mixes. 12 μl reaction.

	μl per sample
DreamTaq Green (Thermo Fisher)	6
Nuclease-free water	3
10 μM forward primer	1
10 μM reverse primer	1
DNA	1

Table 2.3: PCR thermocycling conditions

Cycle Step	**Temp** (°C)	**Time**	
1	95	5 min	
2	95	30 s	x 35 cycles
3	60	30 s	
4	68	45 s	
5	68	5 min	

2.3 Western blotting

2.3.1 Solutions

Solutions used for Western blotting are shown in Table 2.4.

Table 2.4: Solutions and buffers for Western blotting

Solution	Recipe	Company
Lysis buffer	150 mM NaCl	Sigma Aldrich
	1% Triton-X 100	Sigma Aldrich
	0.5% Sodium deoxycholate	Sigma Aldrich
	0.1% SDS	Bio-rad
	50 mM Tris, pH 8.0	Sigma Aldrich
	Protease inhibitors	Sigma Aldrich
	Phosphatase inhibitor cocktail sets II and III	Sigma Aldrich
Laemmli loading buffer	0.004% Bromophenol blue	Sigma Aldrich
	10% β-mercaptoethanol	Sigma Aldrich
	10% Glycerol	Sigma Aldrich
	4% SDS	Sigma Aldrich
	0.125M Tris-HCl	Sigma Aldrich
Tris-buffered saline (TBS)		Bio-rad
Tris-buffered saline tween-20 (TBST)	TBS	Bio-rad
	20% Tween 20	Sigma Aldrich
Running buffer	Tris-glycine SDS	Bio-rad
Transfer buffer	Tris-glycine	Bio-rad
Blocking buffer (in TBS)		Li-Cor

2.3.2 Tissue preparation and homogenisation

P60-90 male *Nlgn3*$^{-/y}$ and WT rats were anaesthetised with isoflourane and decapitated. The brain was quickly extracted and cooled in ice-cold (> 4°C) carbogenated (bubbled with 95% O_2/ 5% CO_2) cutting artificial cerebrospinal fluid (cACSF , Table 2.5). Tissue was dissected, snap frozen on dry ice and weighed. Tissue was then transferred to Bead Mill tubes (Fisher Scientific) containing ice-cold lysis buffer (Table 2.4) (1-5 mg tissue per ml of lysis buffer). Tissue was homogenised using a Bead Mill (Fisher Scientific) and 30 μl reserved for the protein concentration assay. Laemmli buffer (Table 2.4) was added to reach a 1 x concentration with the volume of cell lysate present. The β-mercaptoethanol in Laemmli buffer breaks disulphide bonds and coats the proteins in a negative charge to allow Western blotting. Samples were then denatured by boiling at 95°C for 5 minutes, before centrifuging for 5 minutes at 16000 G to pull down condensation, and finally vortexed.

2.3.3 Protein concentration assay

The protein concentration assay was carried out using a Pierce^{TM} BCA Protein Assay Kit (Fisher Scientific) as per their provided protocol. Bovine serum albumin (BSA) standards were made by preparing 2 mg/ml BSA stock and serially diluting this in double-distilled H_20 to create a logarithmic scale of BSA standards from 2 - 0.625 mg/ml. 5 μl of each standard and sample were pipetted in triplicate into a 96-well plate before incubating under agitation for 15 minutes at room temperature. Protein concentrations were then measured using a CLARIOstar plate reader (BMG Labtech), and sample concentrations calculated based on the BSA standard curve.

2.3.4 Gel electrophoresis and membrane transfer

10% Mini-PROTEAN TGX Precast Protein Gels (Bio-rad) were allowed to equilibrate to room temperature before loading to encourage equal migration of the samples. A gel electrophoresis tank (Bio-rad) was filled with running buffer (Table 2.4), and 20 μl of sample or protein ladder (PageRuler Plus Prestained Protein Ladder, Fisher Scientific, diluted in Laemmli buffer) was loaded into each well. The gels were run at a 50 V constant voltage for 30 minutes or until the samples had migrated through the stacking gel. Voltage was then increased to 150 V for 1 hour.

The gel was removed from the tank and case, stacking gel trimmed, and washed in transfer buffer (Table 2.4) for 15 minutes. Filter paper, nitrocellulose membrane (Bio-rad), sponges and cassettes were washed in water and soaked in transfer buffer prior to transfer. A transfer tank (Bio-rad) was then filled with transfer buffer, and samples transferred to the nitrocellulose membrane by running at 85 V for 2 hours.

2.3.5 Total protein measurement

Nitrocellulose membrane was washed in several changes of H_20, MemCode stain (Pierce Reversible Protein Stain Kit, Fisher Scientific) for 5 minutes, Wash Solution (Pierce Reversible Protein Stain Kit, Fisher Scientific) for 5 minutes, and then again in several changes of H_20. Total protein was imaged using an Odyssey infrared imaging system (Li-COR Bioscience). Total protein stain was removed using a Stain Eraser (Pierce Reversible Protein Stain Kit, Fisher Scientific), and washed in several changes of H_20, followed by TBST (Table 2.4).

2.3.6 Immunodetection

The membrane was blocked using blocking buffer (Table 2.4) for 1 hour at room temperature. Primary antibodies (Table 2.10) and 0.01% sodium azide were added to fresh blocking buffer, and the membrane incubated in this overnight at 4°C. The membrane was then washed several times in TBST (Table 2.4) for 10 minutes each and incubated in appropriate secondary antibody (Table 2.11) in blocking buffer for 2 hours at room temperature. Membrane was then washed in several changes of TBST (Table 2.4) for 10 minutes each and subsequently in several changes of TBS (Table 2.4) before imaging using an Odyssey infrared imaging system (Li-COR Bioscience).

2.4 *Ex vivo* electrophysiology

2.4.1 Solutions

Solutions for *ex vivo* electrophysiology recordings are described below. All slices were prepared in high magnesium cutting artificial cerebrospinal fluid (cACSF, Table 2.5) and recordings took place while the slices were bathed in recording artificial cerebrospinal fluid (rACSF) (Table 2.5). Potassium gluconate based internal solutions were used for whole-cell patch-clamp recordings that took place in current clamp configuration, and caesium based internal solutions were used for recordings in voltage-clamp configuration to allow blockage of K^+ channels and improve space-clamp (Tables 2.6, 2.7, 2.8). 24 mM Cl^- internal was used in all experiments requiring a potassium gluconate based internal solution in Chapter 5, in order to match as closely as possible with similar recordings obtained from other rat models of ASD/ID. Internal with 8 mM Cl^- is more physiological, and was used for all other recordings requiring a potassium gluconate based internal in this thesis.

2.4.2 Acute slice preparation

Male WT and transgenic rats (p13-15 or p25-35, specified in appropriate results section) were anaesthetised with isoflourane or halothane before decapitation. The brain was quickly extracted and cooled in ice-cold (> 4°C) carbogenated cACSF (Table 2.5) to reduce cell excitotoxicity and preserve slice health. The cerebellum was removed, and the brain cut coronally in half before slicing the hippocampus (HC) horizontally,

Table 2.5: External solutions for *ex vivo* electrophysiology. External solutions were continuously carbogenated with 95% O_2/5% CO_2

	Cutting ACSF	**Recording ACSF**
	Concentration (mM)	**Concentration (mM)**
NaCl	86	124
NaH_2PO_4	1.2	1.2
KCl	2.5	2.5
$NaHCO_3$	25	25
D-glucose	25	20
Sucrose	75	0
$CaCl_2$	0.5	2
$MgCl_2$	7	1

Table 2.6: Potassium gluconate based internal solutions. Solution was adjusted to pH 7.30 with KOH and osmolarity determined to be ∼280-300 mOsm.L^{-1}.

	8 mM Cl^-	**24 mM Cl^-**
	Concentration (mM)	**Concentration (mM)**
K-gluconate	142	120
KCl	4	20
EGTA	0.5	0
HEPES	10	10
$MgCl_2$	2	0
Na_2ATP	2	0
MgATP	0	4
Na_2GTP	0.3	0.3
Phosphocreatine	10	10

Table 2.7: Caesium gluconate based internal solutions. Solution was adjusted to pH 7.30 with CsOH and osmolarity determined to be ∼280-300 mOsm.L^{-1}.

	8 mM Cl^-	**24 mM Cl^-**
	Concentration (mM)	**Concentration (mM)**
Cs-gluconate	140	0
CsOH	0	110
CsCl	3	20
D-gluconic acid	0	110
HEPES	10	10
EGTA	0.2	0.2
QX-314 chloride	5	5
MgATP	2	4
Na_2GTP	0.3	0.3
NaATP	2	0
Phosphocreatine	10	10

Table 2.8: Caesium chloride based internal solutions. 140 mM Cl^- internal was used for recording mIPSCs. Solution was adjusted to pH 7.30 with CsOH and osmolarity determined to be ∼280-300 mOsm.L^{-1}.

	140 mM Cl^-
	Concentration (mM)
CsCl	140
HEPES	10
EGTA	0.5
QX-314 chloride	5
$MgCl_2$	2
Na_2GTP	1
MgATP	5
Phosphocreatine	10

medial pre-frontal cortex (mPFC) coronally or periaqueductal grey (PAG) coronally into 400μm slices on a Leica VT 1200S vibratome. Slicing speeds of 0.12-0.14 mm/s were used for hippocampal and mPFC slices, and 0.05 mm/s was used to create PAG slices, as these were particularly sensitive to slicing speed. Slices used for extracellular field recordings were allowed to recover in carbogenated rACSF (Table 2.5) at 35 ± 1°C for 30 minutes, then at room temperature for a minimum of 10 minutes before recording. Slices used for whole-cell patch clamp recordings were allowed to recover in carbogenated cACSF at 35 ± 1°C for 30 minutes, then at room temperature for a minimum of 10 minutes before recording.

2.4.3 Extracellular field recordings

Slices were transferred to a recording chamber and perfused with pre-warmed carbogenated rACSF at 31 ± 1°C at a rate of 3-4 ml/min. Electrodes with 1-3 MΩ tip resistance were pulled from borosilicate glass capillaries with filaments (inner/outer diameters 0.86/1.5 mm respectively) and backfilled with rACSF. Electrodes were placed into the *stratum radiatum* layer of CA1 (Fig. 2.3A) or in L2/3 and L5 of mPFC (Fig. 2.3B). Synaptic responses were evoked by applying single current pulses (DS3 isolated constant current stimulator, Digitimer Ltd.) to the Schaffer collaterals using a bipolar stimulating electrode made of twisted nickel/chromium wire (80%/20% respectively). Stimuli (3 - 300 μA, 200 μs, delivered at a frequency of 0.033 Hz) were set to produce 50% of the maximal response amplitude. Field extracellular post-synaptic potentials (fEPSPs) were able to reach 1 mV in size before population spiking (pop-spiking) of cells

occurred. After a stable 20 min baseline, LTP/LTD induction protocol was initiated. For Figures 5.2 and 5.13, 50 μM D-AP5 was present in ACSF throughout recordings.

Synaptically-induced hippocampal LTP

Long-term potentiation (LTP) was induced by 2 trains of 100 Hz stimulation for 1 second each with an inter-train interval of 20 seconds (Komiyama et al., 2002).

Synaptically-induced mPFC LTP

LTP was induced using 5 trains of 300 Hz stimulation for 0.5 seconds, each with an inter-train interval of 3 mins (Huang et al., 2004).

Synaptically-induced NMDAR-dependent LTD

Long-term depression (LTD) was induced by 900 pulses of 1 Hz stimulation for 15 minutes (Dudek and Bear, 1992; Mulkey and Malenka, 1992).

Chemically-induced mGluR-dependent LTD

LTD was induced by acute application of group 1 metabotropic glutamate receptor (mGluR) agonist S-DHPG (50 μM; Tocris) for 5 minutes (Huang et al., 1999; Overstreet et al., 1997; Fitzjohn et al., 1999; Palmer et al., 1997).

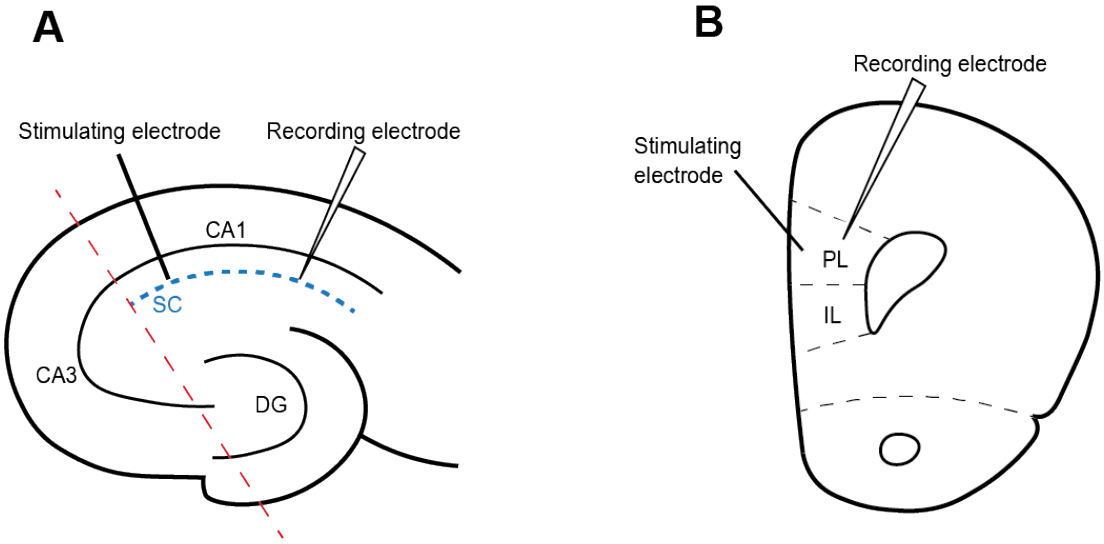

Figure 2.3: Schematics of areas recorded from in extracellular field recording experiments. (A) Schematic illustrating positions of stimulating and recording electrodes for field recordings from CA1 Schaffer collaterals (blue) in an acute horizontal hippocampal slice. Red line indicates where CA3 is removed for LTD experiments. SC: Schaffer collaterals, DG: dentate gyrus. (B) Schematic illustrating positions of stimulating and recording electrodes for field recordings from L2/3 (stimulating electrode) to L5 (recording electrode) in an acute coronal mPFC slice. PL: prelimbic, IL: infralimbic.

Analysis

WinLTP software was used for extracellular field recordings and analysis (University of Bristol, UK). For all protocols magnitude of LTP or LTD was calculated as the average 10-90% field excitatory post synaptic potential (fEPSP) slope 50-60 minutes after induction divided by the average 10-90% fEPSP slope during the 20 min baseline period. Custom-written Matlab scripts were used to create representative traces (Dr Adam Jackson, University of Edinburgh, unpublished).

2.4.4 Whole-cell patch clamp recordings

Slices were transferred to a recording chamber and perfused with carbogenated rACSF at 31 ± 1°C at a rate of 5-7 ml/min. Slices were visualized using a 40x (1.0 NA) water immersion objective mounted on a Scientifica slicescope, using infrared differential interference contrast (IR-DIC) video on a digital camera (DAGE-MTI). These were paired with Patchstar micromanipulators and heater units, and controlled using LinLab 2 (Scientifica). Electrodes with 2-6 MΩ tip resistance were pulled from borosilicate glass capillaries with filaments (inner/outer diameters 0.86/1.5 mm respectively). These were backfilled with appropriate internal solution (Tables 2.6, 2.7, 2.8). Internal solutions included 2 mg/ml biocytin where required.

Cells of interest in the HC and mPFC were identified by area (Fig. 2.4), visual morphology, capacitance and firing properties. Cells in the PAG were identified by area, and sampled pseudo-randomly within that. For all cells, a +10 mV, 1 ms seal test was used to identify when a >1 GΩ seal was achieved. A -70 mV holding potential was applied following the creation of a >1 GΩ seal. The fast and slow membrane capacitances were neutralised before breaking through the cell membrane into the whole-cell configuration. Recordings were made using a Multiclamp 770B amplifier and signals were digitised with a Digidata 1550A or 1550B (Molecular Devices). Signals were sampled at 20 kHz and filtered at 10 kHz (current clamp) or 2 kHz (voltage clamp). Clampex 10 software (pCLAMP 10, Molecular Devices) was used for data acquisition and generation of stimulus protocols. Liquid junction potential is not corrected for in the data shown in this thesis.

Inclusion criteria for cells:

- Access resistance must be <30 MΩ.

- Change in access resistance must be <20%.
- Cell resting membrane potential (RMP) must be less depolarised than -50 mV for pyramidal cells in the HC and mPFC, and less depolarised than -40 mV for cells in the PAG.
- Cells must fire ≥ 2 action potentials when +400 pA injected.

Recording protocols and conditions

Passive membrane properties The passive membrane properties of cells were examined in current clamp during whole-cell configuration, using potassium gluconate based internal solution (Table 2.6). The RMP of cells was determined by a 60 s gap-free recording with no current injection. Following this protocol, appropriate current was injected to hold the cell at -70 mV and maintained for all other passive and active intrinsic property recordings. Input resistance (R_{in}), membrane time constant (τ), and cell capacitance (C_M) were determined using sweeps of -10 pA current injections for 500 ms. R_{in} was calculated using Ohm's law:

$$V = IR$$

where,
V= mean steady state voltage response to the current injection
I= current step, 10 pA

Membrane time constant was calculated by fitting a monoexponential curve to the initial decay phase of the current step. C_M was calculated using the following equation:

$$C_M = \frac{\tau}{R_{i_n}}$$

where,
τ = membrane time constant
R_{in} = input resistance

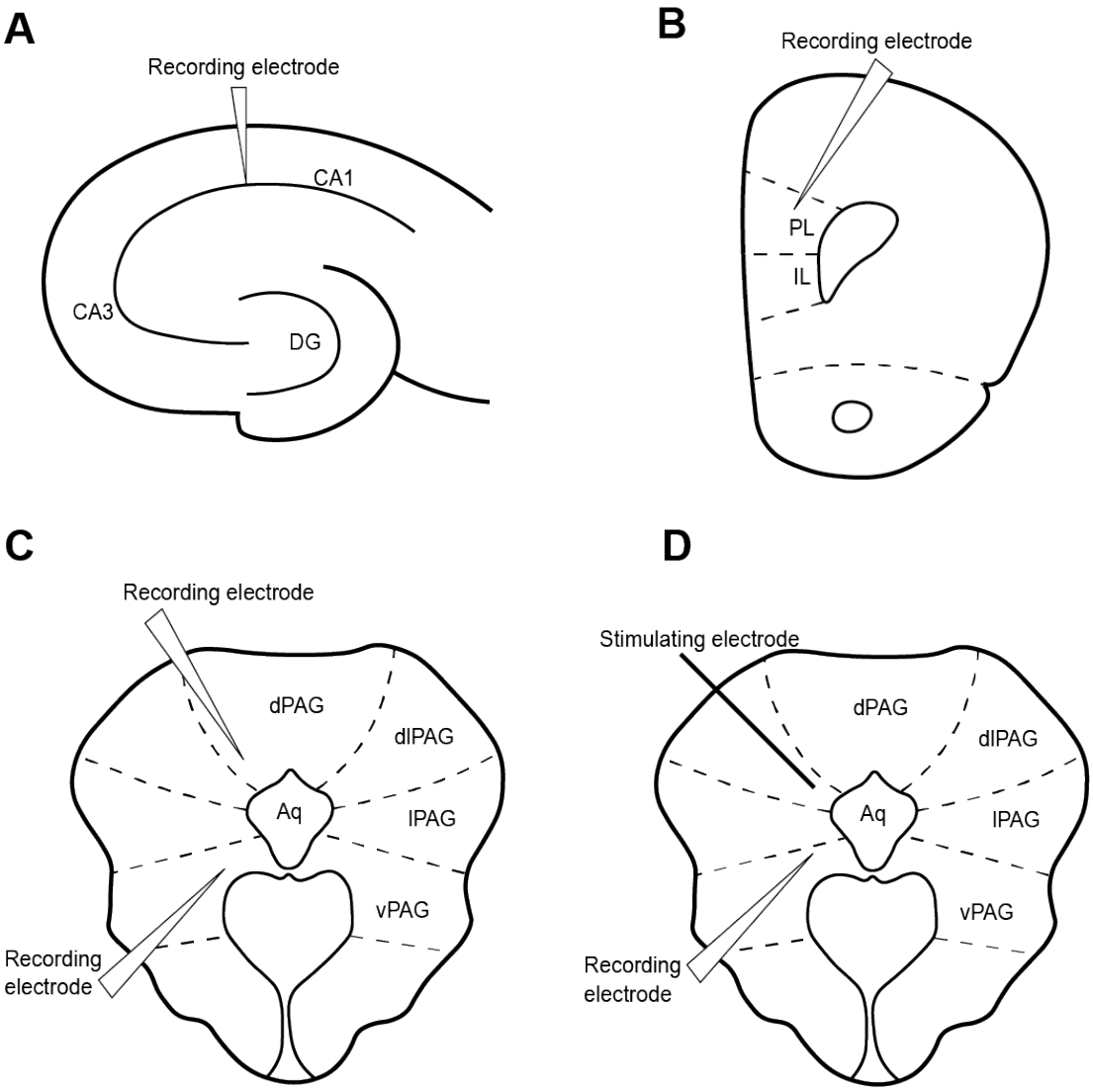

Figure 2.4: Schematics of areas recorded from in whole-cell patch clamp experiments. (A) Schematic illustrating approximate position of recording electrode for recordings from CA1 pyramidal cell layer in an acute horizontal hippocampal slices. DG: dentate gyrus. (B) Schematic illustrating approximate position of recording electrodes for recordings from L5 in an acute coronal mPFC slice. PL: prelimbic, IL: infralimbic. (C) Schematic illustrating approximate position of recording electrodes for intrinsic property and mEPSC recordings from dPAG and vPAG. dPAG: dorsal periaqueductal grey, dlPAG: dorsolateral periaqueductal grey, vlPAG: ventrolateral periaqueductal grey, vPAG: ventral periaqueductal grey, Aq: aqueduct. (D) Schematic illustrating approximate position of stimulating and recording electrodes for $GABA^AR$/ AMPAR and minimal stimulation recordings from vPAG. dPAG: dorsal periaqueductal grey, dlPAG: dorsolateral periaqueductal grey, lPAG: lateral periaqueductal grey, vPAG: ventral periaqueductal grey, Aq: aqueduct.

'Sag' potential is seen at hyperpolarising currents due to the opening of hyperpolarisation - activated cyclic nucleotide–gated (HCN) channels. Accordingly, 500 ms sweeps of -250 pA current steps were injected to hyperpolarise the membrane and peak sag potential was measured in comparison to steady state voltage response.

Active membrane properties To determine the active intrinsic properties of a cell, a series of 500 ms current steps were injected. Distinct brain regions required different step sizes in order to obtain optimal information about the input-frequency curve of that cell and avoid depolarising block. These were as follows:

- -100 $\rightarrow$ +400 pA, 25 pA steps for HC or mPFC pyramidal cells
- -100 $\rightarrow$ +100 pA, 10 pA steps for PAG cells

Rheobase current was defined as the current step required to first elicit action potential firing. All action potential (AP) waveform measurements (peak, threshold and half-height width, depolarisation speed, repolarisation speed, fAHP) in this thesis are obtained from the first action potential elicited during rheobase current injection to avoid preceding action potentials affecting measurements (see Fig. 2.5 for details).

The after-depolarisation potential (ADP) was examined by injecting 2 nA of current for 2 ms to elicit a single action potential, and the maximal peak following the AP was measured. Trains of five 2 nA pulses (20, 40, 60, 80 and 100 Hz) were used to measure medium afterhyperpolarisation potentials (mAHP). mAHP was taken to be the maximal peak in the 200 ms following the final AP. For the characterisation of PAG cells shown in Chapter 3, fast afterhyperpolarisation potential (fAHP) and ADP were measured from rheobase, as well as the recovery τ from maximal fAHP. fAHP was taken to be mV between AP threshold and maximal hyperpolarisation immediately following the AP. τ was calculated in this case by fitting a biexponential curve to the repolarisation following the fAHP.

Synaptic events To investigate miniature excitatory post-synaptic currents (mEPSCs) and miniature inhibitory post-synaptic currents (mIPSCs), recordings were made using either Cs-gluconate (Table 2.7) or Cs-Cl (Table 2.8) based internal solutions respectively, to increase stability and improve space-clamp. Following membrane breakthrough, cells were voltage clamped at -70 mV and allowed to stabilise for $\geq$5 minutes, in which time 300 nM tetrodotoxin (TTX) and either 50 μM picrotoxin (PTX, to isolate excitatory

currents) or 10μM cyanquixaline (CNQX, to isolate inhibitory currents) were washed in. mEPSCs/mIPSCs were recorded for 5 minutes following drug wash-in, and access resistance was monitored every minute with a +10 mV voltage step.

Spontaneous EPSCs (sEPSCs) were also recorded in some cells using K-gluconate based internal solution, after recording intrinsic properties. sEPSCs were recorded in voltage clamp configuration, holding the cell at -70 mV. In these cases, no drugs were present in the rACSF and sEPSCs were recorded for 1 minute only.

Synaptic currents To investigate $GABA_AR$/ AMPAR ratios of vPAG cells, evoked EPSCs were recorded at -70 mV (to isolate AMPAR responses) and 0 mV (to isolate $GABA_AR$ responses). The stimulating electrode was placed in the dPAG (Fig. 2.4C), and vPAG cells were recorded from until a clean monosynaptic response of ∼100-200 pA could be observed. 8 mM Cl^- Cs-gluconate internal solution (Table 2.7) was used for these recordings. The stimulating electrode and constant current stimulator were the same as used for extracellular field recordings (see above). Access resistance was monitored throughout using a +10 mV step. The average of 15 sweeps (10 s inter-stimulus interval, ISI) at -70 mV and 0 mV were taken as the AMPAR and $GABA_AR$ responses for that cell. Pharmacological elimination of these responses using 10 μM CNQX or 50 μM PTX was performed in a subset of cells to confirm synaptic currents responsible.

Single-afferent strength To investigate the strength of single afferents projecting from dPAG-vPAG, stimulating and recording electrodes were positioned as shown in Fig. 2.4D. 8 mM Cl^- Cs-gluconate internal solution (Table 2.7) was used for these recordings, and 50 μM PTX was present in the rACSF throughout. Cells were held at -70 mV in voltage clamp configuration, and once a cell exhibiting a response had been identified, stimulation was decreased in increments of 1 μA or smaller until the threshold of quantal release was approached and response failures were seen at a rate of between 5% and 95%. Cells were allowed to stabilise for 2 minutes before beginning to record responses. 50 sweeps (5 s ISI) were recorded, and access resistance was monitored throughout using a +10 mV step. Due to the sensitivity of these recordings to changes in access resistance, cells with >10% change in access were excluded. Failure rate was calculated by tallying the total number of successful and failed responses. Amplitude of successfully evoked responses was also calculated (excluding failures). Paired-pulse

facilitation (PPF) of these responses was calculated as amplitude of second response (50 ms paired-pulse interval) divided by amplitude of first response (excluding failures).

Analysis

Either Stimfit software (Guzman et al., 2014) or custom-written MATLAB scripts (A. Jackson) were used for whole-cell patch-clamp data analysis. Action potential waveform was analysed as shown in Figure 2.5A. For mEPSC/mIPSCs, the final 2-3 minutes of the 10 minute recording was analysed. Events were detected using template-matching (Fig. 2.5B) and filtered at 3 x standard deviation of baseline (Clements and Bekkers, 1997). As recordings of mEPSCs/mIPSCs, $GABA_AR$/ AMPAR currents, and minimally stimulated responses are particularly sensitive to changes in access resistance, the access resistance was plotted for these recordings to ensure any changes between genotypes were not as a result of differences in access (Figs. S1, S2). No difference in access resistance was observed between genotypes for any dataset.

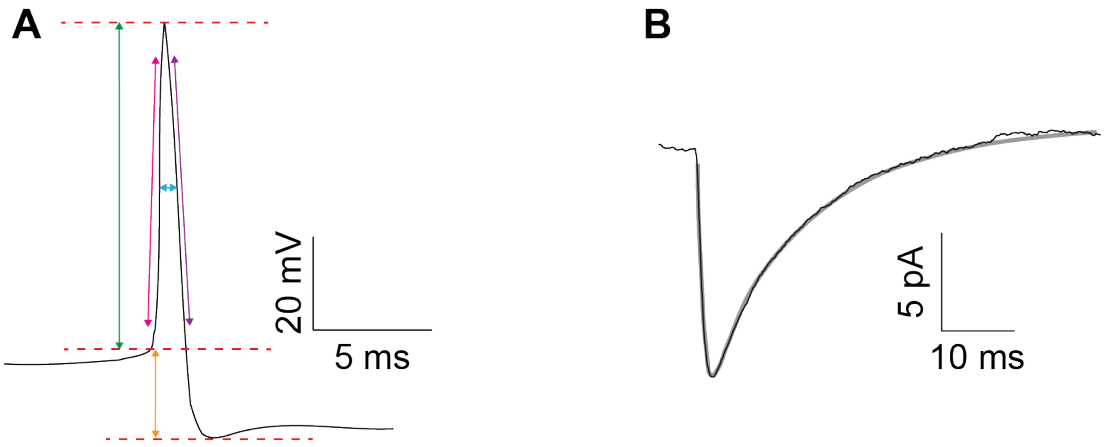

Figure 2.5: Measuments of action potentials and miniature events. (A) Measurements of waveform on an example rheobase AP. Green arrows denote measurements for peak height (top) and AP threshold (bottom). Blue arrows show measurements for AP width at half AP height. Pink and purple arrows denote 10-90 % of the AP rise and decay phases, where repolarisation rate and depolarisation rate are measured. Orange arrow shows fAHP measurement. (B) Example trace (black) of template matching (grey) to an average miniature event waveform (Guzman et al., 2014; Clements and Bekkers, 1997).

Cell morphology

Cells were filled with 1% biocytin during patch-clamp recordings. Cells were re-sealed after recordings had finished by slowly pulling the pipette away from the cell and reducing voltage-clamp back to 0 mV. Slices were then post-fixed for ∼24 hours

in 4% paraformaldehyde (PFA) (Table 2.9) at 4°C before being transferred to 1x phosphate-buffered saline (PBS) (Table 2.9). If slices were being kept >2 weeks they were transferred to cryopreserve solution (Table 2.9), allowed to sink overnight, then stored at -20°C. Cells were visualised using a fluorescent conjugates of streptavidin to detect biotinylated biomolecules (see 2.5).

2.5 Immunocytochemistry

2.5.1 Solutions

Table 2.9: Solutions used for fixation and processing of fixed tissue. All solutions adjusted to pH 7.4 with NaOH.

	4% PFA	**0.1 M PB**	**1x PBS**	**Cryopreserve**
	mM	**mM**	**mM**	**mM**
NaH_2PO_4	25.84	25.84	6.46	6.46
Na_2HPO_4	77.49	77.49	19.37	19.37
NaCl	0	0	137	137
Paraformaldehyde	1.33	0	0	0
Sucrose	0	0	0	876.42
Glycerol	0	0	0	3257.7

2.5.2 Immunodetection

Sections were washed in PBS, then non-specific labelling blocked with 10% normal goat serum (NGS) in solution with 0.3% Triton-X for cell permeabilisation, 0.05% sodium azide to avoid microbial growth and PBS for 1 hour. Sections were then incubated in primary antibodies (Table 2.10) in a solution containing 5% NGS, 0.3% triton-X, 0.05% sodium azide and PBS for ∼48 hours at 4°C. Sections were washed in PBS again before incubating in secondary antibodies (Table 2.11) in solution with 3% NGS, 0.1% Triton-X, 0.05% sodium azide and PBS overnight at 4°C. Sections were washed in PBS then desalted in PB to prevent NaCl crystallisation, and mounted in Vectashield hard-set mounting medium (Vector Labs).

Anti-GAD65/67 and anti-GABA labelling was unsuccessful on 400 μm thick post-fixed PAG slices, due to sensitivity of these antibodies on fixation in midbrain sections.

Table 2.10: Primary antibodies. Details of primary antibodies used in this thesis.

Antibody	Host	Mono/polyclonal	Concentration	Supplier
Anti-NeuN	Mouse	Mono	1:1000	Abcam
Anti-NLGN3 C-terminus	Rabbit	Poly	1:1000	Synaptic Systems
Anti-NLGN3 N-terminus	Rabbit	Poly	1:1000	Invitrogen
Anti-GAD65/67	Rabbit	Poly	1:500	Abcam
Anti-GABA	Rabbit	Poly	1:2000	Sigma Aldrich

Table 2.11: Secondary antibodies. Details of secondary antibodies used in this thesis.

Antibody	Concentration	Supplier
Streptavidin 488	1:500	Fisher Scientific
Goat anti-mouse 568	1:500	Life technologies
Goat ant-rabbit 488	1:500	Life technologies
Goat anti-rabbit 800	1:500	Li-COR

2.5.3 Imaging and analysis

Sections were visualised on a LS800 (Zeiss) upright confocal microscope with built-in Zen Sytem software. 512 x 512 resolution images were taken at x20 magnification. Z-stacks with 1 μm steps were taken of the entire cell and dendritic arbour were imaged and stitched. Cells were viewed and reconstructed offline using FIJI (ImageJ) software with the Simple Neurite Tracer plugin. Cell classification of PAG neurons was performed qualitatively, based on soma shape, soma size, number of proximal dendrites and length of dendritic processes (based on classifications carried out by Mantyh (1982); Beitz and Shepard (1985); Meller and Dennis (1990); Liu and Hamilton (1980); Gioia et al. (1985); Chieng and Christie (1994)).

Pyramidal cells were assumed to be similar to Beitz and Shepard (1985); Mantyh (1982); Meller and Dennis (1990)'s "pyramidal cells", Chieng and Christie (1994)'s "triangular cells", and Gioia et al. (1985); Liu and Hamilton (1980)'s "type II" cells. Pyramidal cells were identified based on triangular shaped soma of 15-20 μm in size, and the presence of one thick apical dendrite with many branch points dividing from it. They also possessed two or more basal dendrites also emerging from the soma. Pyramidal cells has the most branch points and furthest reaching dendrites in comparison to other defined PAG cell types.

Multipolar cells were assumed to be similar to Beitz and Shepard (1985); Mantyh (1982); Chieng and Christie (1994)'s "multipolar cells", Meller and Dennis (1990)'s "polygonal cells", Gioia et al. (1985)'s "type II" and "type V" cells, and Liu and Hamilton (1980)'s "type III cells".
Multipolar cells were identified based on a small, round soma of 10-15 μm in size, with three or more dendrites emerging from the soma. These dendrites were far-reaching and branched multiple times. The majority of recovered neurons were multipolar.

Fusiform cells were assumed to be similar to Mantyh (1982); Chieng and Christie (1994)'s "fusiform cells", Beitz and Shepard (1985)'s "bipolar cells", Meller and Dennis (1990)'s "spindle" and "ovoid" cells, Gioia et al. (1985)'s "type IV" cells, and Liu and Hamilton (1980)'s "type I cells".
Fusiform cells were defined based on a long, oval-shaped soma of 20-30 μm in length, with one process emerging from each end. They had few dendritic bifurcations and were more numerous closer to the aqueduct.

Pseudounipolar cells were assumed to be similar to Meller and Dennis (1990)'s "round cells".
Pseudounipolar cells had round somas with one dendrite that immediately split into two. They had few branch points, and only accounted for a small number of recovered neurons.

Not recovered cells refers to those that were either damaged during the removal of the patch pipette, unsucessfully filled with biocytin, or the morphology of the cell could not be distinguished.

To create representative cell images, contrast and brightness was adjusted using FIJI/ ImageJ, then reconstructed 3D image smoothened, flattened and colour-inverted. Anterior-posterior axis position was estimated based on slice number taken and size and shape of the aqueduct in comparison to Paxinos and Watson (2007) Rat Brain Atlas.

2.6 *In vivo* electrophysiology

2.6.1 Electrode construction

Local field potential electrodes Local field potential (LFP) electrodes were made in-house by inserting annealed PFA-coated stainless steel wire (50.8 μm diameter, 63.5 μm insulation, A-M Systems) in to a cannula (inner/outer diameters 0.32/0.64 respectively, Bilaney Consultants Ltd. C317GS-5/SPC) glued to an electronic interface board (EIB; Neuralynx). The insulation was removed from either end of the electrode wire, and one end secured to the EIB using a gold pin. Teflon coated silver wire (30 AWG, 4 μm thick insulation, World Precision Instruments) was soldered to the ground and reference vias of the EIB, ready to be attached to the ground screws during surgery.

Stimulation electrodes Twisted stainless steel stimulation electrodes were purchased from Bilaney Consultants Ltd.

2.6.2 Surgical procedures for stimulating and recording electrode implantation

Stimulating or recording electrodes were surgically implanted as per the following protocol. Stimulating electrodes were implanted bilaterally, recording electrodes were implanted unilaterally.

P60-90 male WT or transgenic rats were anaesthatised using gaseous isofluorane (4% isofluorane and 700-800 ml/ min O_2), weighed and the surgical area shaved. They were then placed in a stereotaxic frame and stabilised using atraumatic ear bars, nose clamp and tooth bar. Gaseous anaesthetic (1.5-2.5% isofluorane and 400-500 ml/ min O_2) was administered throughout the surgery via the nose clamp. Breathing rate and paw withdrawal reflexes were checked regularly throughout the surgery and level of isofluorane adjusted accordingly. Viscotears^{TM} was applied to eyes to prevent drying and 4 mg/kg Rimadyl^{TM} was injected subcutaneously. A rectal probe was inserted to allow temperature monitoring and heat-pad adjustments. Iodine was applied to the shaved head and the rat's body draped.

The following steps were performed using aseptic technique. A midline scalp incision was made and the skull cleaned before 1 mm holes were drilled above the cortex and cerebellum, and either unilateral or bilateral craniotomy/ies drilled over the PAG. Skull

screws and ground screws (Screws and More, DIN84A2M1X3) were inserted into the holes over the cortex and cerebellum. Bregma and lambda were measured to confirm <0.01 mm offset. The dura was pierced in the craniotomy/ies and appropriate electrodes (see above) stereotaxically lowered through the craniotomy to the PAG. The coordinates defined were (in mm relative to bregma): -7.08 (stimulation) or -7.56 (LFP) anterior-posterior, -4.2 dorsal-ventral, 2.0 medial-lateral, at an angle of 18°. Dental cement was used to cover and secure electrodes, skull screws, electrode and EIB (if present). The incision was closed using nylon surgical suture and sterelised with iodine. Gaseous anaesthetic was reduced to 0%, and rats were given 1 ml of warm saline by subcutaneous injection. Rats were left to recover for a minimum of 1 week post-surgery, individually housed.

2.6.3 Local field potential recordings

Auditory fear conditioning

Animals were handled for approximately 10-15 minutes per day for 3 days prior to behavioural testing.

Habituation: days 1 & 2 Each animal was tethered to an Open Ephys electrophysiology recording system, and placed individually in the centre of context B (Fig. 4.1); an arena (length 40 cm, width 25 cm, height 30 cm) with white (bottom 15 cm) and transparent (top 15 cm) walls, a lid, and $\sim$ 2cm bedding. This was inside a sound-proofed box, with 20 lux and yellow-tinted lighting. Toothpaste mixed with water was used to create a peppermint odour in the arena. Behaviour was recorded for 20 mins (Freeze Frame software, Actimetrics). Each rat was returned to their home cage following habituation and the arena cleaned with disinfectant.

Tone habituation and fear conditioning: day 3 Each animal was tethered and placed individually in the centre of context A (Fig. 4.1), arena with metal walls and lid, metal grated floor, and one wall baring a black and white striped cue. This was inside a sound-proofed box, and lighting was 5 lux and blue-tinted. No peppermint odour was present, and arena was cleaned with 70% ethanol immediately before each animal enters. Rats were given 2 minutes to explore the arena, then presented with 3 tones (5 kHz; 75 dB) for 30 seconds each, and 1 minute inter-tone interval (ITI). Behaviour and LFPs

were recorded throughout. Recordings were made via a 16-channel digitising headstage (C3334, Intan Technologies, USA) connected to a flexible tether cable (12-pin RHD SPI, Intan Technologies, USA), custom built commutator and OpenEphys acquisition board (OEPS, Portugal). LFP signals were sampled at 2 kHz and bandpass-filtered from 0.1-600 Hz and in OpenEphys software. Rat headstages were then disconnected, and the same protocol repeated. However, during this conditioning phase, tones co-terminated with scrambled foot shock of 0.9 mA for a duration of 1 second. Behaviour was recorded throughout the protocol. Each rat was returned to their home cage following conditioning and the arena cleaned with 70% ethanol.

Recall and extinction: day 4 Each animal was placed individually in the centre of context B as described on habituation days. Rats were given 2 mins to explore the arena, then were presented with 13 tones of 5 kHz for 30 seconds each, with 30 seconds ITI. Behaviour and LFPs were recorded throughout the protocol. Each rat was returned to their home cage following extinction and the arena cleaned with disinfectant.

2.6.4 dPAG stimulation

Animals were handled for approximately 10-15 minutes per day for 3 days prior to behavioural testing.

Habituation: days 1 & 2 Each animal was tethered to a current stimulator (DS3 isolated constant current stimulators, Digitimer Ltd.) and placed individually in the centre of context B as described above, however no bedding or peppermint odour were present. Rats were given 20 minutes to explore the arena, recorded using Freeze Frame software (Actimetrics). Each rat was then returned to their home cage and the arena cleaned with disinfectant.

Increasing stimulations: day 3 Rats bilaterally implanted with stimulating electrodes were placed individually in the centre of context B and tethered to the current stimulators. Rats were allowed to explore the arena for 2 minutes, then given a 30 μA (1 second) bilateral stimulation and behavioural response assessed. Rats were then allowed 3 minutes to recover before a 35 μA stimulation was given. This was repeated with the stimulation current increasing in 5 μA increments up to 75 μA. Behaviour was recorded throughout the protocol using Freeze Frame software (Actimetrics). Each

rat was returned to their home cage following stimulation and the arena cleaned with disinfectant.

Single stimulation: day 10 Rats were placed individually in the centre of context B and tethered to the current stimulators. Rats were allowed to explore the arena for 2 minutes, then given a single 60 μA stimulation followed by a 3 minute recovery period. Behaviour was recorded throughout the protocol using Freeze Frame software (Actimetrics). Each rat was returned to their home cage and the arena cleaned with disinfectant.

2.6.5 Analysis of behaviour

Behaviour of the rats was manually scored using Z-Score software built by our collaborator (Prof. Oliver Hardt, McGill University). Classic freezing behaviour was defined as no movement at all except for respiration, and must last >1 second. Z-chop (O. Hardt) software was used to divide scored behaviours into relevant sections of time (eg. during tone). Response behaviours to *in vivo* stimulation were classified manually, based on criteria from Coimbra et al. (2017).

Escape was classified as complete and successful departure of the arena via jumping and climbing.
Jumping behaviour was classified as a dynamic vertical movement in which all four paws temporarily leave the floor of the arena.
Startle was classified as a sudden, involuntary movement of the head and upper torso.
Attention was classified as interruption of ongoing behavior and adoption of a stiff posture with small head movements observing and smelling the surrounding environment.

2.6.6 Analysis of local field potentials

Tone-evoked potentials were identified and analysed using custom-written Matlab scripts (Dr Felicity Inkpen, University of Edinburgh). The peak and trough of each LFP was manually checked, and each event was z-scored according to a baseline period of 200 ms pre-tone.

$$z = \frac{x - mean}{\delta}$$

where,

x = raw value

δ = standard deviation of baseline

Peak to trough values were then calculated from the z-scored data. Duration of LFP was taken to be the time between first peak/trough and second peak/trough, irrelevant of polarity.

2.6.7 Histology

Perfusions and tissue collection

In order to lesion the site of the electrodes, rats that had undergone surgeries for electrode implantation and behavioural assessment were anaesthatised with gaseous isofluorane followed by IP injection of sodium pentobarbitol (28 g/kg) until hindpaw reflexes could not be seen. A wire (positive) was then attached to the appropriate channels on the headstage of the rat, and another wire (negative) through the tip of the rat's tail. A current pulse of 150 μA for 2 seconds (DS3 isolated constant current stimulator, Digitimer Ltd.) was applied. Rats were then transcardially perfused with ∼50 ml filtered PBS, and then ∼50 ml filtered 4% PFA (Table 2.9). Headstages were taken out, and brains were removed and post-fixed overnight in 4% PFA (Table 2.9). Brains were then sectioned into 80 μm thick sections on a freezing microtome (ThermoScientific Microm HM450). Sections were then mounted on Superfrost Plus adhesion microscope slides (Fisher Scientific) and left to dry overnight.

Nissl staining

The mounted sections were washed in distilled water then dehydrated in rising concentrations of ethanol (70, 90, 100%) before being immersed in xylene for 10 minutes. Sections were then rehydrated in decreasing concentrations of ethanol (100, 90 70%) then again washed in distilled water. Sections were then immersed in cresyl violet stain solution (Sigma-Aldrich) for 2-3 seconds. Sections were again washed in water, then rising concentrations of ethanol (70, 90, 100%) before being immersed briefly in xylene.

Slides were covered in DPX mounting medium (Sigma-Aldrich) and coverslipped. DPX was allowed to harden overnight before imaging on a bright field microscope (Leica) at 5x magnification.

2.7 Statistics

Statistical analysis was carried out using GraphPad Prism software (t-tests, one-way ANOVAs, two-way ANOVAs, generalised linear model, post-hoc multiple comparisons testing, Pearson's R correlations), R Studio (Ward's method clustering, Fisher's exact test, Cramer's V correlations) or by Zrinko Kozic and Owen Dando (generalised linear mixed modelling). Data is presented throughout as mean ± SEM. Dots on bar charts represent individual cells or animals, depending on statistical test used (defined in figure legends). When performing t-tests or two-way ANOVAs, animal averages were used to avoid pseudoreplication. In Chapter 3 and Chapter 5, generalised linear models were applied in order to avoid pseudoreplication, take into account cell and animal variability, and reduce false-positive results from performing too many individual statistical tests. Statistical tests and n numbers used are reported in figure legends throughout. P values < 0.05 were considered statistically significant, and any values less than 0.05 are represented as a single star (*) throughout. Sample sizes used are consistent with those normally found in the literature, however on small datasets power analyses have been performed where appropriate.

Generalised linear mixed modelling Chapters 3 and 5 utilise generalised linear (mixed) modelling (GLMM) in the place of multiple t-tests for statistical analysis of cell intrinsic property data. GLMM takes into account variability in the data produced by a number of random effects not considered by a t-test; such as animal, litter, breeding pair, or time of day the recording took place. It also allows consideration that many of these variables will be hierarchical (i.e. animal and litter) and assigns variability in the data appropriately. GLMMs can also cope with data that is not normally distributed, where a t-test would not be appropriate. Pseudoreplication can be avoided by using animal, rather than cell, averages. However, GLMMs provide a method of statistically analysing data that avoids pseudoreplication and additionally does not discard the information provided by measuring many cells from a single animal.

Ward's clustering method (Chapter 3) is an agglomerative hierarchical, unsupervised clustering method which was chosen for its capability of clustering data into an undefined number of groups based on the relationship of multiple parameters. Parameters were normalised using the following equation so that all values lay between 0 and 1, and contributed to the clustering equally.

$$Normalised\, x = \frac{x - mean}{range}$$

Parameters used for Ward's clustering in Chapter 3 were: RMP, input resistance, membrane time constant, capacitance, sag, action potentials fired at 100 pA, action potentials fired at 200 pA, rheobase, threshold, adaptation ratio, action potential height, action potential width, depolarisation speed, repolarisation speed, afterdepolarisation potential, fast afterhyperpolarisation, τ of afterhyperpolarisation recovery, sEPSC amplitude, and sEPSC frequency.

Chapter 3

Physiology of the periaqueductal grey

3.1 Introduction

The periaqueductal grey (PAG) is a midbrain region known for its involvement in a host of survival behaviours including fear responsiveness, vocalisation, sleep, autonomic functions, analgesia, reproduction and maternal behaviour. As these behaviours are all essential for survival, it is unsurprising that the PAG is a highly conserved structure, with evidence of its existence defined in fish (Fiebig, 1988; Kittelberger et al., 2006), birds (Kingsbury et al., 2011), amphibians (Pezalla, 1983), lizards (Pezalla, 1983), rabbits (Meller and Dennis, 1986) and cats (Bandler and Depaulis, 1988), as well as rodents, monkeys and humans (studies from which are discussed throughout this introduction). Although the PAG is a key brain region in mediating many behaviours, this thesis will focus on the role of the PAG in fear responses. As outlined in section 1.6, fear responses, at the most basic level, consist of a decision to fight, flee or freeze. The PAG is important for expressing these responses both to innately fearful situations and in learned fear (DeOca et al., 1998; Kim et al., 2013).

The PAG (or central grey) has been studied as far back as Magoun et al. (1937), who identified the involvement of the PAG in fear-related vocalisations and faciovocal reactions in monkeys and cats. During the 1980s and 1990s, seminal studies demonstrated firstly that electrical and chemical stimulation of the PAG in rats and cats reliably evoked behavioural responses similar to those seen in fearful situations (Bandler and Depaulis, 1988; Bandler and Carrive, 1988; Tomaz et al., 1988; Zhang et al., 1990; Bandler et al., 1985; Carrive, 1993; Depaulis et al., 1992; Fanselow, 1991; Fanselow et al., 1995), and secondly identified a clear functional divide between the dorsal and ventral

parts of the PAG. Stimulation of the dorsal PAG (dPAG) results in flight responses (Bandler and Depaulis, 1988; Bandler and Carrive, 1988; Tomaz et al., 1988; Zhang et al., 1990; Bandler et al., 1985; Deng et al., 2016; Assareh et al., 2017), and therefore is thought to be responsible for active responses to perceived threats. Conversely, ventral PAG (vPAG) stimulation has been shown to elicit immobility or freezing behaviour (Zhang et al., 1990; Fanselow, 1991; Fanselow et al., 1995; Carrive and Bandler, 1991; Depaulis et al., 1992; Keay et al., 1997; Tovote et al., 2016; Assareh et al., 2017), and activity of this area is thought to underlie passive fear responses. There is also evidence indicating a functional divide between the anterior and posterior parts of the dPAG, both of which are responsible for active fear responses. Stimulation of more anterior dPAG sites tended to result in confrontational aggressive responses, whereas stimulation of more posterior sites tended to evoke flight responses (Keay and Bandler, 2004).

Functional magnetic resonance imaging (fMRI) studies demonstrated decreased activity of the PAG during painful/emotional experiences in individuals with ASD (Schneider et al., 2013; Fan et al., 2014). Despite these findings, there has been no research investigating the function or dysfunction of the PAG in the context of ASD or ID. This may be because previous research examining fear conditioning paradigms in ASD/ID rodent models, including in *Nlgn3* deficiency models (Hamilton et al., 2014; Jaramillo et al., 2018; Radyushkin et al., 2009; Chadman et al., 2008; Polepalli et al., 2017), focus on freezing behaviour as the primary readout of fear. Decreases in freezing responses exhibited by rodents during this task are generally interpreted as deficits in fear learning, whereas an alternative explanation is there may be a difference in the expression of fear (Fig. 1.5). Altered fear expression may indicate a dysfunction in the physiology of the PAG.

3.1.1 Connectivity and cytoarchitecture of the PAG

In accordance with the functional divides along the dorsal-ventral and anterior-posterior axes of the PAG, these sub-regions show differences in how they are connected to the wider 'fear circuitry' in the brain.

The PAG receives efferents from multiple forebrain regions that are involved in processing and regulating responses to fearful situations, notably the prefrontal cortex (PFC) (Floyd et al., 2000; An et al., 2006; Beitz, 1982), hypothalamus (Veening et al., 1987, 1991; Canteras, 2002; Semenenko and Lumb, 1992), and central amygdala (Price

and Amaral, 1981; LeDoux et al., 1988; Rizvi et al., 1991; Oka et al., 2008; Tovote et al., 2016). Distinct PFC subregions have been shown to project exclusively to specific regions of the PAG (Floyd et al., 2000). Additionally, the ventral and lateral PAG alone receive significant central amygdala input (Oka et al., 2008; Rizvi et al., 1991; LeDoux et al., 1988; Tovote et al., 2016; Price and Amaral, 1981), whilst the dorsal PAG receives the majority of hypothalamic projections (de Git et al., 2018; Wang et al., 2015; Vianna and Brandão, 2003).

Furthermore, descending projections from the PAG also tend to respect the dorsal/ ventral boundaries. Medullary afferents are localised to the vPAG (Carrive et al., 1988; Hamilton, 1973; Hamilton and Skultety, 1970; van Bockstaele et al., 1991; Tovote et al., 2016), and have been shown to be vital for mediating freezing behaviour in mice (Tovote et al., 2016). Conversely, the predominant output of the dPAG is to the cuneiform nucleus (which, in turn, projects to the ventrolateral medulla) (Redgrave et al., 1988). There is also functional (Kim et al., 2013; Johansen et al., 2010) and modelled (Nicholson et al., 2017) evidence suggesting that the dPAG projects back to the amygdala, and not only to hindbrain and brainstem areas for directing motor output, suggesting a more complex role for the PAG in the wider fear circuitry. The input and output connectivity of the PAG place it ideal position for coordinating and integrating fear responses.

As described in section 1.6, the central amygdala integrates information from BLA and sensory cortices (reviewed in Gross and Canteras (2012)), and therefore passes on a level of threat to the PAG where a response can be coordinated. Central amygdala to vPAG projections mediate freezing behaviour via a disinhibitory mechanism; inhibitory central amygdala efferents target vPAG GABAergic neurons, which in turn release inhibition of local vPAG glutamatergic neurons and allow excitatory output to downstream pre-motor targets in the medulla (Tovote et al., 2016). Additionally, the ventromedial hypothalamic to dPAG pathway is also suspected to be inhibitory in nature (Sandner et al., 1981; Wang et al., 2015), suppressing flight-promoting dorsal PAG output and eliciting freezing behaviour (Wang et al., 2015). More locally, a recent study demonstrated the importance of excitatory superior colliculus to dPAG connections in determining threat level and initiation of escape responses (Evans et al., 2018). However, whether to flee or freeze is not only dependent on the salience of the threat itself; it is also context dependent. Accordingly, direct connectivity between the PFC and PAG is thought to convey contextual information relating to the fearful situation

that allows the appropriate response to be executed (Rozeske et al., 2018). A simplified diagram of PAG connectivity is depicted in Figure 3.1, however it is important to note that this diagram does not contain all known or suspected projections to/from the PAG; only those relevant to executing fear responses. A more detailed connectivity map of the PAG can be found in Faull et al. (2019).

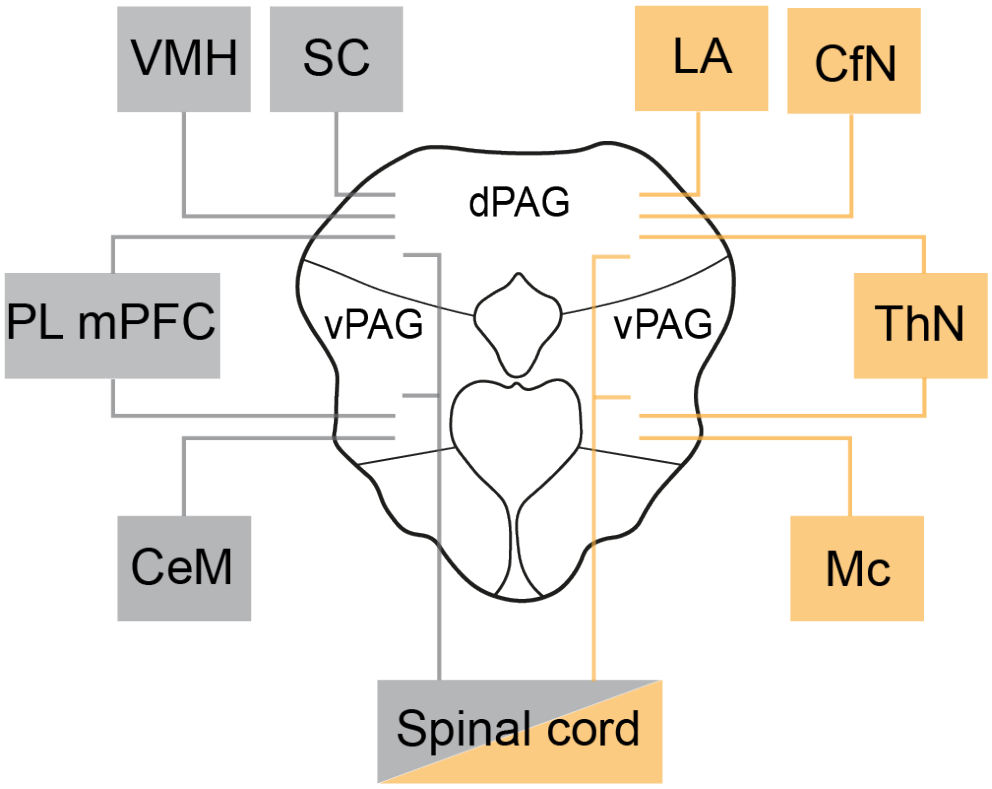

Figure 3.1: Connectivity of the dorsal and ventral subregions of the PAG. Projections targeting the PAG are shown in grey, projections originating in the PAG and targeting downstream brain regions are shown in yellow. VMH: ventromedial hypothalamus, SC: superior colliculus, LA: lateral amygdala, CfN: cuniform nucleus, ThN: thalamic nuclei, Mc: magnocellular nucleus of the medulla, CeM: central amygdala, PL mPFC: prelimbic mPFC, dPAG: dorsal periaqueductal grey, vPAG: ventral periaqueductal grey.

Despite receiving largely differing inputs, the cytoarchitechture of the dorsal and ventral subregions of the PAG are similar. Both the dorsal and ventral PAG are composed of heterogeneous bodies of neurons that differ drastically from their surrounding brain structures, the dorsal raphe nucleus and superior colliculus. GABAergic cells account for ∼50 % PAG neurons, with no notable differences across the anterior-posterior axis of the structure (Sandner et al., 1981). Early cell morphology studies consistently identified a minimum of three distinct neuronal morphology types in the PAG: pyramidal/triangular, fusiform/bipolar and multipolar/stellate (Mantyh, 1982; Beitz and

Shepard, 1985; Meller and Dennis, 1990; Liu and Hamilton, 1980; Gioia et al., 1985; Chieng and Christie, 1994). However, the immunoreactivity and electrophysiology of these morphologically identified cell types is unknown.

3.1.2 Electrophysiology of PAG neurons

There is a vast body of work describing the morphology, electrophysiology, and spatial distribution of cells in many forebrain areas, notably the cortex and hippocampus. However, the same body of work does not exist for the midbrain. This is perhaps because the cells are more heterogeneous and varied in their properties. There is also considerable heterogeneity in cortical interneurons (Cauli et al., 2000; Pelkey et al., 2017; Booker and Vida, 2018), however they can be visually and quantitatively distinguished from cortical pyramidal neurons based on their intrinsic properties (eg. see Cauli et al. (1997), Fig. 3.2).

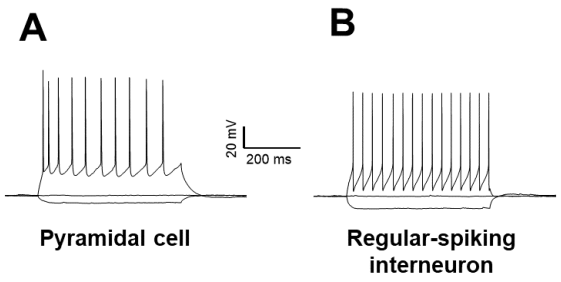

Figure 3.2: Firing properties of cortical pyramidal neuron and interneuron (A) Example of an excitatory pyramidal cell from layer 5 mPFC showing broader and fewer action potentials with lower fast after-hyperpolarisation potential (fAHP). (B) Example of a inhibitory regular-spiking interneuron from layer 5 mPFC showing faster and higher frequency action potentials with high fAHP.

In order to study electrophysiology of the PAG in *Nlgn3*$^{-/y}$ rats, a comprehensive literature search was carried out to determine what is already known about the electrophysiological properties of cells in the PAG. Relatively few studies have ever reported whole-cell patch clamp recordings in the PAG, and surprisingly little is known about the electrophysiology of cells in this brain area. Unlike most forebrain areas, there are a small number of studies to date that have looked at intrinsic properties of cells in the PAG, and all studies limited their recordings to specific cell types or sub-regions of interest (eg. vGluT2^{+} neurons, (Evans et al., 2018), opioid-sensitive neurons (Chieng and Christie, 1994; Heinisch et al., 2011; Osborne et al., 1996; Chiou et al., 2002), CCK-sensitive neurons (Liu et al., 1994), RVM-projecting GABAergic neurons (Park

et al., 2010), dorsal-posterior PAG cells (Lovick and Stezhka, 1999), and ventro-medial PAG cells (Sánchez et al., 1988; Sánchez and Ribas, 1991; Ho et al., 2018)).

3.1.3 Hypotheses and aims

In order to better understand the physiology of the PAG, I aimed to carry out a characterisation of PAG neurons in WT rats. I hypothesised that the morphology of PAG neurons would be reflective of their electrophysiological properties.

Furthermore, this chapter aims to discern PAG involvement in behavioural deficits exhibited by the *Nlgn3*$^{-/y}$ model of ASD/ID. Behavioural studies carried out by myself, V. Kapgal and S. Tiwari described in section 1.7 show that *Nlgn3*$^{-/y}$ rats display increased flight and decreased freezing behaviour in response to fearful stimuli. Given the vital role of the PAG in fear expression, I hypothesised that this imbalance of flight-freeze responses may be underpinned by physiological changes in the PAG, such as hyperfunction of the flight-promoting dorsal PAG, or hypofunction of the freeze-promoting ventral PAG. This behavioural phenotype makes the *Nlgn3*$^{-/y}$ rat a useful model for studying the function of the PAG in ASD/ID.

In this chapter, I use a combination of whole-cell patch-clamp electrophysiology and imaging techniques to assess synaptic physiology, cellular excitability and neuronal morphology in dorsal and ventral PAG neurons to address this question.

3.2 Results

An electrophysiological and morphological characterisation of PAG neurons in WT rats

3.2.1 Intrinsic properties of WT PAG cells

I carried out an electrophysiological and morphological characterisation of rat PAG neurons spanning the dorsal-ventral and anterior-posterior axes of the brain region. In acute PAG slices taken from WT Sprague-Dawley rats, I recorded and calculated passive intrinsic properties (resting membrane potential (RMP), input resistance, membrane time constant, capacitance, and I_h-mediated sag) and active intrinsic properties (including input-frequency curve, rheobase, action potential (AP) peak, AP width, AP depolarisation speed and AP repolarisation speed, after-depolarisation potential (ADP),

and fast-afterhyperpolarisation potential (fAHP)), as well as spontaneous excitatory postsynaptic currents (sEPSCs) of dorsal and ventral PAG cells from -6.3 to -8.3 mm bregma in 119 cells from 12 WT rats.

Ward's method clustering analysis

There are several studies describing the heterogeneity of cells in the PAG (Lovick and Stezhka, 1999; Beitz and Shepard, 1985; Park et al., 2010; Behbehani, 1995; Sánchez et al., 1988). I therefore performed Ward's method clustering analysis (see Methods section 2.7 for details) using both intrinsic and synaptic properties recorded from PAG cells, and found the cells clustered into two main types; named type 1 (red) and type 2 (blue) henceforth (Fig. 3.3). Additionally, these two main populations clustered further into subpopulations named type 1a (maroon, 6.7 %), type 1b (red, 30.3 %), type 2a (blue, 15.9 %), type 2b (navy, 47.1 %) (Fig. 3.3). Assuming this data is representative of the total population of cells in the PAG, type 2b cells are the most predominant subpopulation (Fig. 3.3A).

Passive properties

Unsupervised clustering of electrophysiological data allows the identification of distinctive features of each group. Examination of the passive membrane properties in each group revealed that RMP varied from -40 mV (cells with an RMP of <-40 mV were discarded) to -73.6 mV, and type 2a cells showed considerably more depolarised RMPs than other cell types (Fig. 3.4A, Table 3.1). Input resistance of these cells varied greatly, similarly to values reported in the literature (Lovick and Stezhka, 1999; Sánchez et al., 1988), and was significantly higher in type 2 cells in comparison to type 1 cells (Fig. 3.4B, Table 3.1). Membrane time constant was significantly faster in type 1b cells in comparison to type 2a and type 2b cells (Fig. 3.4C, Table 3.1). As type 2 cells generally had higher input resistance and slower membrane time constants in comparison to type 1 cells, cell capacitance was also lower (Fig. 3.4D, Table 3.1). Sag (as a percentage of potential) was not different between any cell types, and 41.5% cells showed no sag at all. Together, these passive properties indicate that type 2 cells are perhaps comparable to cortical interneurons, and type 1 cells to cortical pyramidal cells (Greene and Totterdell, 1997).

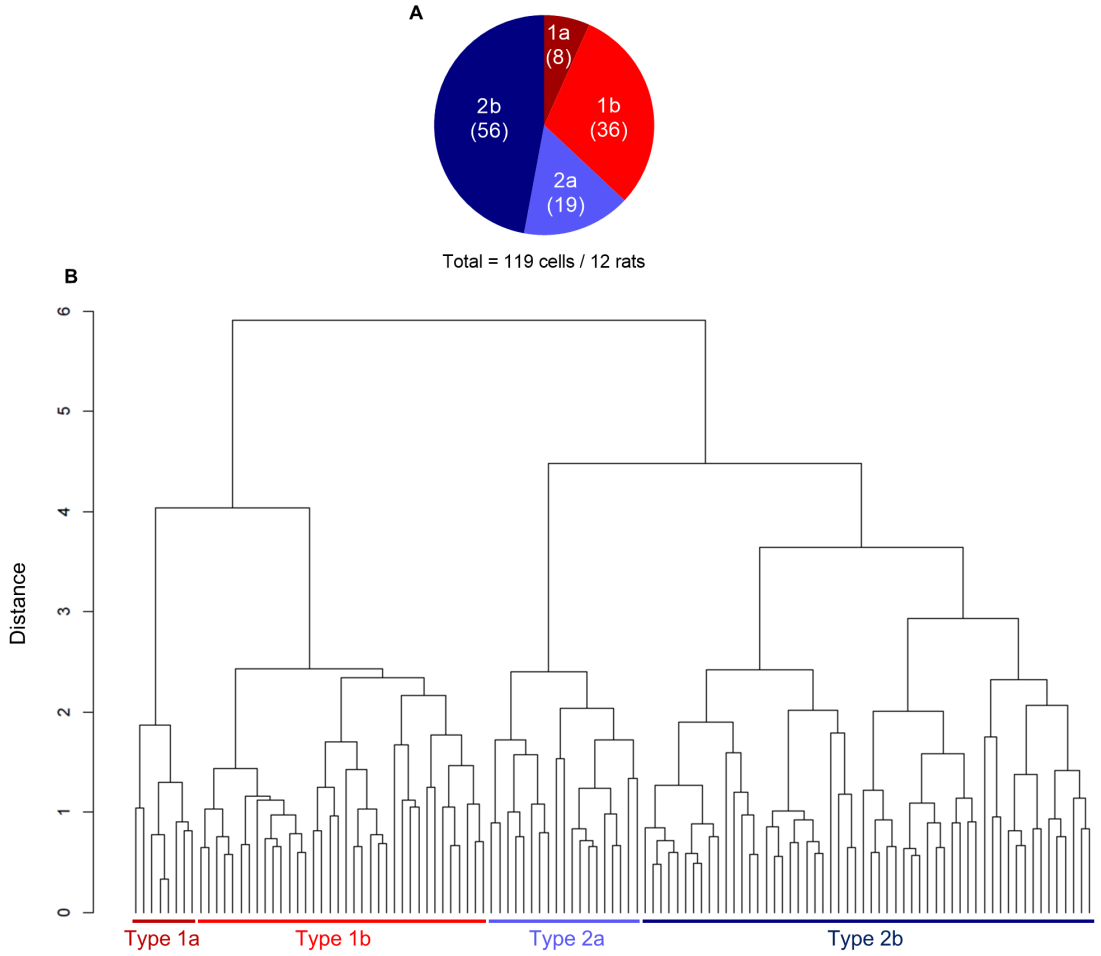

Figure 3.3: Ward's cluster of PAG cell intrinsic and synaptic properties (A) Pie chart representing percentages of each cell type. (B) Clustering of cells plotted against Euclidean distance. 'Type 1a' cells marked in maroon, 'type 1b' cells marked in red, 'type 2a' cells marked in blue, 'type 2b' cell marked in navy.

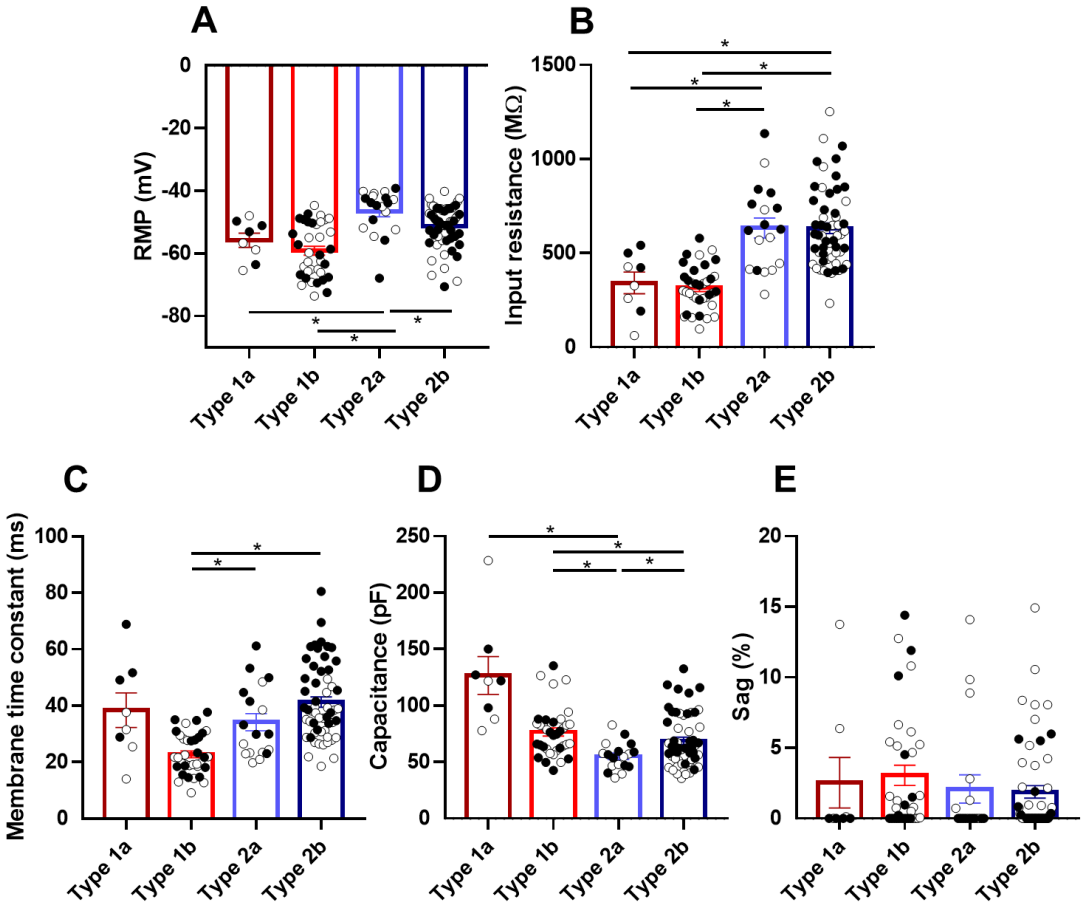

Figure 3.4: Passive properties of WT PAG neurons (A) Type 2a cells have significantly lower RMP (1a vs. 1b p = 0.61, 1a vs. 2a p = 0.02, 1a vs. 2b p = 0.31, 1b vs. 2a p <0.0001, 1b vs. 2b p < 0.0001, 2a vs. 2b p = 0.08, GLM with Geisser Greenhouse correction and Tukey's multiple comparisons). (B) Type 2 cells have significantly higher input resistance than type 1 cells (1a vs. 1b p = 0.97, 1a vs. 2a p = 0.01, 1a vs. 2b p < 0.0001, 1b vs. 2a p <0.0001, 1b vs. 2b p <0.0001, 2a vs. 2b p >0.99, GLM with Geisser Greenhouse correction and Tukey's multiple comparisons). (C) Type 1b cells have significantly faster membrane time constants in comparison to type 2 cells (1a vs. 1b p = 0.14, 1a vs. 2a p = 0.92, 1a vs. 2b p = 0.97, 1b vs. 2a p = 0.01, 1b vs. 2b p <0.0001, 2a vs. 2b p = 0.20, GLM with Geisser Greenhouse correction and Tukey's multiple comparisons). (D) Type 2 cells have significantly lower capacitance than type 1 cells (1a vs. 1b p = 0.08, 1a vs. 2a p = 0.01, 1a vs. 2b p = 0.04, 1b vs. 2a p <0.0001, 1b vs. 2b p = 0.38, 2a vs. 2b p = 0.01, GLM with Geisser Greenhouse correction and Tukey's multiple comparisons). (E) Sag (as a % of input resistance) is not different between clustered cell types (1a vs. 1b p = 0.78, 1a vs. 2a p = 1.00, 1a vs. 2b p = 0.96, 1b vs. 2a p = 0.60, 1b vs. 2b p = 0.95, 2a vs. 2b p = 0.87, GLM with Geisser Greenhouse correction and Tukey's multiple comparisons). Type 1a n = 8 cells/ 6 rats, type 1b n = 36 cells/ 11 rats, type 2a n = 19/ 9 rats cells, type 2b n = 56 cells/ 12 rats.
Clear symbols represent cells in dPAG, filled symbols represent cells in vPAG.

Active properties

Previous work on forebrain neuronal populations has disclosed that cell firing, as well as the shape of the action potential, provides a clear estimate of gross cell type (Greene and Totterdell, 1997). Cells in the PAG, although heterogeneous, are less distinguishable based on these properties (Fig. 3.5A). Nonetheless, cluster analysis revealed that type 2 cells fired significantly more action potentials in response to depolarising current steps than type 1 cells, and had lower rheobase potentials (Fig. 3.5A-C, Table 3.1). AP threshold was only significantly different between type 2a and type 2b cells (Fig. 3.5D, Table 3.1). Most PAG cells were non-adapting, apart from a proportion of type 2 cells which showed adaptation ratios ranging up to 7.1 (Fig. 3.5E, Table 3.1). Depolarising current steps up to 200 pA were used to create the input-frequency plot shown in Figure 3.5B, even though many cells, particularly type 2a, entered into depolarising block after 100 pA. This is reflected by the curve flattening out at higher current injections.

Furthermore, PAG cells also showed great variability in their AP kinetics (Fig. 3.6A). Type 1a cells were identified as having tall, narrow APs with large ADP (Fig. 3.6B-F, Table 3.1). Type 2a cells had similar AP kinetics to type 1a cells, except they were significantly broader and fewer cells showed ADP (Fig. 3.6B-F, Table 3.1). Type 2a cells were predominantly shorter and broader than other types, with very few cells exhibiting ADP (Fig. 3.6B-F, Table 3.1). Type 2b cells had APs that were taller and narrower than type 2a, but less so than type 1, and again showed a large range of cells with and without ADP (Fig. 3.6B-F, Table 3.1). Intriguingly, fAHP, a prominent feature of forebrain interneurons, was high in all cells recorded and not significantly different between groups (Fig. 3.6G, Table 3.1).

These results further supports the working hypothesis that type 2 neurons show properties similar to some types of cortical interneurons, whilst type 1 cells show properties more comparable to cortical pyramidal cells. However, as AP waveforms seen in these PAG cells are generally dissimilar to those of the forebrain, direct comparisons between the two regions should be drawn with caution (see Chapter 5 for forebrain pyramidal neuron data).

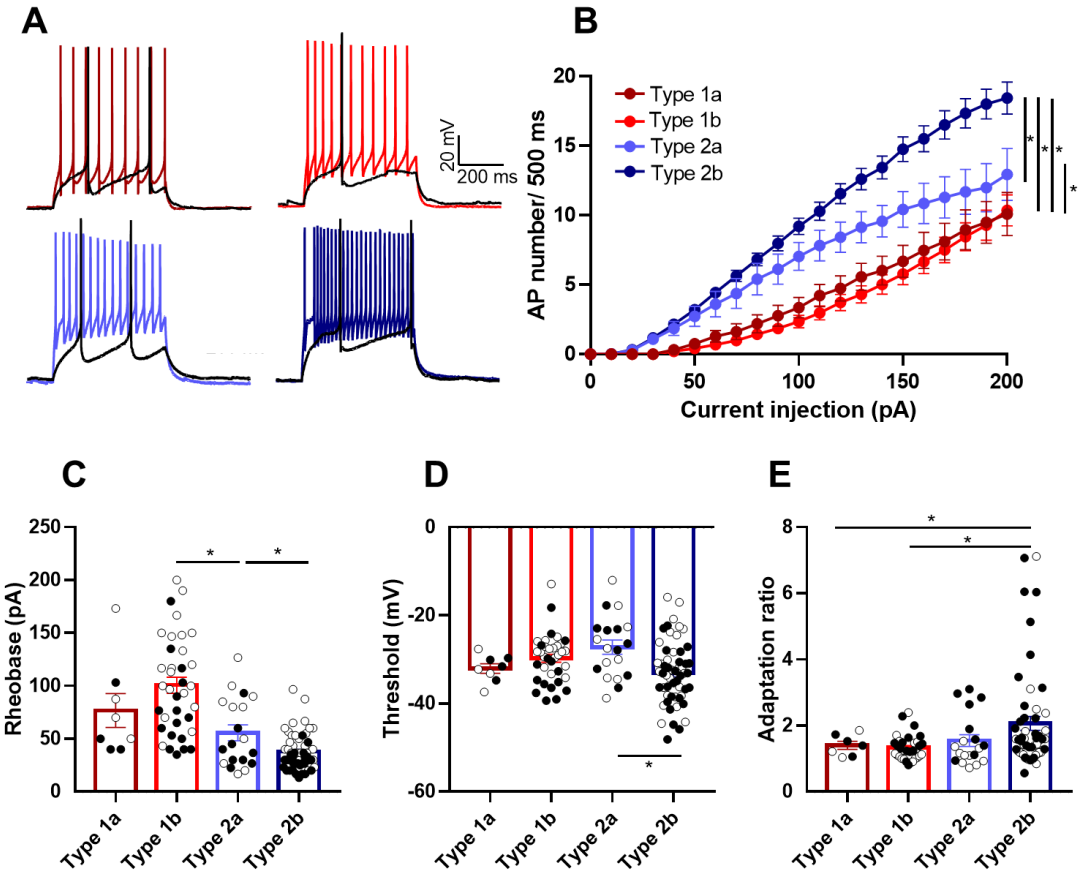

Figure 3.5: Active properties of WT PAG neurons (A) Representative traces of AP firing in response to rheobase and +200 pA current injections for type 1a (maroon), type 1b (red), type 2a (blue) and type 2b (navy). (B) Type 2 cells fire significantly more APs in response to depolarising current steps than type 1 cells (1a vs. 1b p = 0.98, 1a vs. 2a p = 0.30, 1a vs. 2b p = 0.0009, 1b vs. 2a p = 0.0098, 1b vs. 2b p <0.0001, 2a vs. 2b p = 0.032, two-way ANOVA with Tukey's multiple comparisons testing). (C) Rheobase current is significantly higher in type 1b cells in comparison to type 2a cells, and significantly higher in type 2a cells than type 2b (1a vs. 1b p = 0.56, 1a vs. 2a p = 0.65, 1a vs. 2b p = 0.16, 1b vs. 2a p <0.0001, 1b vs. 2b p <0.0001, 2a vs. 2b p = 0.13, GLM with Geisser Greenhouse correction and Tukey's multiple comparisons). (D) AP threshold is significantly more negative in type 2b cells in comparison to type 2a cells (1a vs. 1b p = 0.38, 1a vs. 2a p = 0.09, 1a vs. 2b p = 0.90, 1b vs. 2a p = 0.53, 1b vs. 2b p = 0.06, 2a vs. 2b p = 0.02, GLM with Geisser Greenhouse correction and Tukey's multiple comparisons). (E) Adaptation ratio is significantly higher in type 2b cells in comparison to type 1 cells (1a vs. 1b p = 0.95, 1a vs. 2a p = 0.91, 1a vs. 2b p = 0.04, 1b vs. 2a p = 0.67, 1b vs. 2b p = 0.01, 2a vs. 2b p = 0.24, GLM with Geisser Greenhouse correction and Tukey's multiple comparisons).
Type 1a n = 8 cells/ 6 rats, type 1b n = 36 cells/ 11 rats, type 2a n = 19/ 9 rats cells, type 2b n = 56 cells/ 12 rats.
Clear symbols represent cells in dPAG, filled symbols represent cells in vPAG.

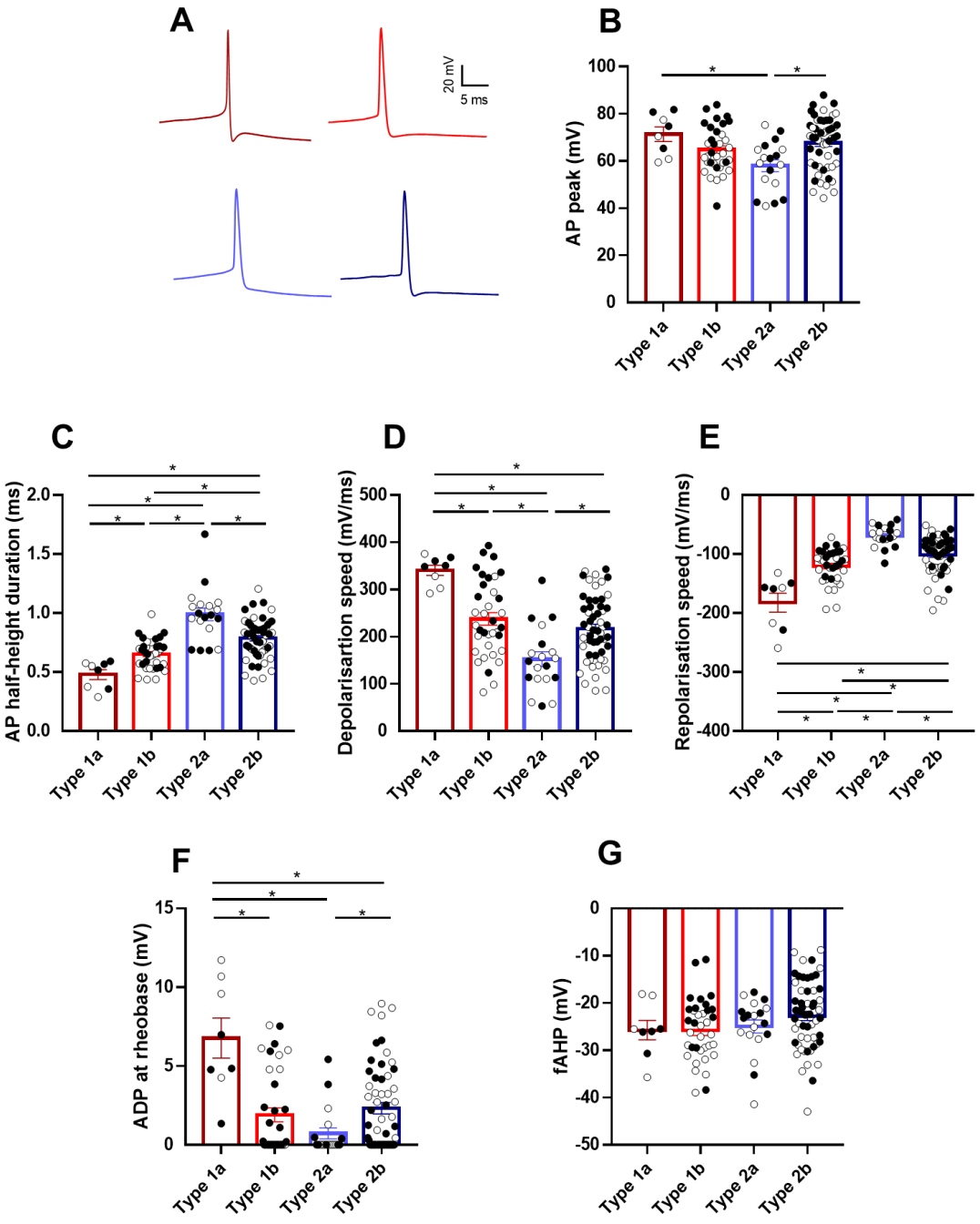

Figure 3.6: Action potential kinetics of WT PAG neurons.

Figure 3.6 ***(previous page)*****: Action potential kinetics of WT PAG neurons** (A) Representative traces of rheobase AP for type 1a (maroon), type 1b (red), type 2a (blue) and type 2b (navy). (B) AP peak is significantly lower in type 2a cells in comparison to types 1a and 2b (1a vs. 1b p = 0.22, 1a vs. 2a p = 0.01, 1a vs. 2b p = 0.62, 1b vs. 2a p = 0.13, 1b vs. 2b p = 0.57, 2a vs. 2b p = 0.01, GLM with Geisser Greenhouse correction and Tukey's multiple comparisons). (C) AP half-height duration was significantly different between all clustered cell types (1a vs. 1b p = 0.02, 1a vs. 2a p <0.0001, 1a vs. 2b p < 0.0001, 1b vs. 2a p <0.0001, 1b vs. 2b <0.0001, 2a vs. 2b p = 0.01, GLM with Geisser Greenhouse correction and Tukey's multiple comparisons). (D) AP depolarisation speed was significantly different between all clustered cell types, except for type 1b and 2b cells, which showed comparable speeds (1a vs. 1b p <0.0001, 1a vs. 2a p <0.0001, 1a vs. 2b p <0.0001, 1b vs. 2a p = 0.0001, 1b vs. 2b p = 0.60, 2a vs. 2b p = 0.01, GLM with Geisser Greenhouse correction and Tukey's multiple comparisons). (E) AP repolarisation speed was significantly different between all clustered cell types (1a vs. 1b p = 0.03, 1a vs. 2a p < 0.0001, 1a vs. 2b p = 0.01, 1b vs. 2a p <0.0001, 1b vs. 2b p = 0.02, 2a vs. 2b p <0.0001, GLM with Geisser Greenhouse correction and Tukey's multiple comparisons). (F) ADP at rheobase was significantly lower in types 1b and 2a cells (1a vs. 1b p = 0.03, 1a vs. 2a p = 0.01, 1a vs. 2b p = 0.04, 1b vs. 2a p = 0.17, 1b vs. 2b p = 0.88, 2a vs. 2b p = 0.01, GLM with Geisser Greenhouse correction and Tukey's multiple comparisons). (G) fAHP was comparable between all cell types (1a vs. 1b p = 0.97, 1a vs. 2a p = 0.99, 1a vs. 2b p = 0.57, 1b vs. 2a p = 1.00, 1b vs. 2b p = 0.77, 2a vs. 2b p = 0.55, GLM with Geisser Greenhouse correction and Tukey's multiple comparisons).
Type 1a n = 8 cells/ 6 rats, type 1b n = 36 cells/ 11 rats, type 2a n = 19/ 9 rats cells, type 2b n = 56 cells/ 12 rats.
Clear symbols represent cells in dPAG, filled symbols represent cells in vPAG.

3.2.2 Synaptic properties of WT PAG cells

Spontaneous EPSCs

As well as recording intrinsic properties of cells, I recorded sEPSCs in the same cells at -70 mV, and these data were included in the clustering analysis. Spontaneous EPSCs (sEPSCs) in the PAG have been reported to be approximately 22 pA and occurring at 4 Hz (Lau et al., 2014). I found that, if the mean of all cells was taken, it was similar to reported values, however clustering allowed different populations to be observed. Type 1a cells were those with high sEPSC amplitudes and frequencies. Type 1b and 2b showed similar sEPSC amplitudes and frequencies, and type 2a cells had significantly lower amplitudes and frequencies (Table 3.1, Fig. 3.7). This suggests that type 1a cells are receiving the most excitatory synaptic input.

3.2.3 Morphology of WT PAG cells

Recorded neurons were filled with biocytin and, following clustering analysis which defined 4 electrophysiologically distinct subtypes of PAG cells, streptavidin labelling and confocal imaging was used to visualise cell morphology. As described in the introduction

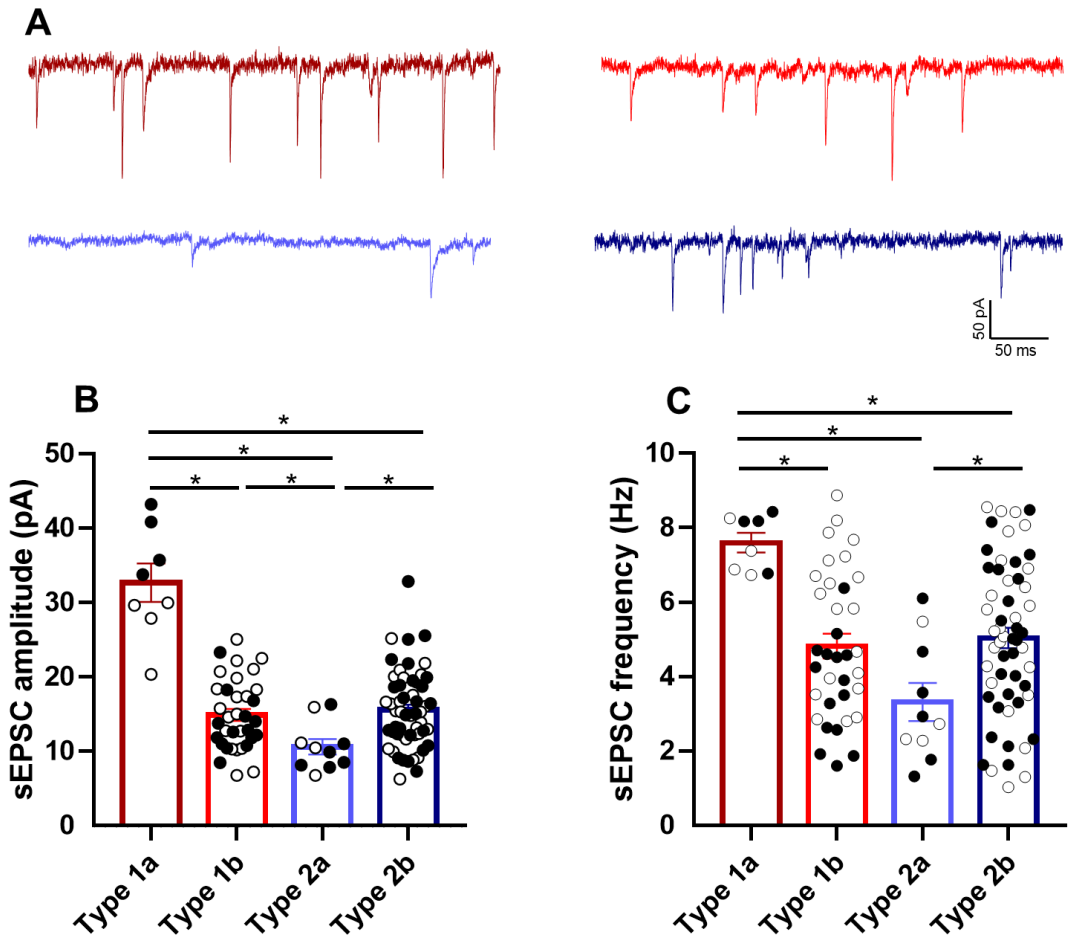

Figure 3.7: sEPSCs in WT PAG neurons (A) Representative sEPSC recordings for type 1a (maroon), type 1b (red), type 2a (blue) and type 2b (navy). (B) sEPSC amplitude was significantly different between all clustered cell types, except for type 1b and 2b cells, which showed comparable amplitudes (1a vs. 1b $p < 0.0001$, 1a vs. 2a $p < 0.0001$, 1a vs. 2b $p < 0.0001$, 1b vs. 2a $p = 0.02$, 1b vs. 2b $p = 0.92$, 2a vs. 2b $p < 0.0001$, GLM with Geisser Greenhouse correction and Tukey's multiple comparisons). (C) sEPSC frequency was significantly different between all clustered cell types, except for type 1b and 2b cells, which showed comparable frequencies (1a vs. 1b $p < 0.0001$, 1a vs. 2a $p < 0.0001$, 1a vs. 2b $p < 0.0001$, 1b vs. 2a $p = 0.10$, 1b vs. 2b $p = 0.96$, 2a vs. 2b $p = 0.04$, GLM with Geisser Greenhouse correction and Tukey's multiple comparisons).
Type 1a n = 8 cells/ 6 rats, type 1b n = 36 cells/ 11 rats, type 2a n = 19/ 9 rats cells, type 2b n = 56 cells/ 12 rats.
Clear symbols represent cells in dPAG, filled symbols represent cells in vPAG.

of this section (section 3.1, also 2.5.3) there are 3-5 discrete cell types in the PAG that have been defined in the literature based on their morphology. I examined cells and, based on a combination of parameters used in these previous classification studies, categorised them into 4 subtypes (see Methods section 2.5.3 for details). These were pyramidal (Fig. 3.8A), multipolar (Fig. 3.8B), fusiform (Fig. 3.8C), and pseudounipolar (Fig. 3.8D). I found a significant correlation between the electrophysiological clusters and morphology using Cramer's V correlation (Fig. 3.9B-C), with a 0.67 probability of predicting morphology from electrophysiological cluster, and a 0.68 probability of predicting electrophysiological cluster from morphology. Type 1a and 1b neurons were predominantly comprised of pyramidal neurons (83 % of pyramidal neurons were type 1), whilst type 2a and 2b cells were mainly fusiform (83.3 % of fusiform neurons were type 2), pseudounipolar (100 % of pseudounipolar cells were type 2, although these accounted for a very small population of neurons), and multipolar (84.2 % multipolar neurons were type 2) (Fig. 3.9B-C). However, although the two major electrophysiologically defined clusters (type 1 and type 2) can be indicative of neuronal morphology, further clustering the data into types a and b did not provide further information about the morphology of the neurons. Nonetheless, these results suggest that intrinsic properties of PAG neurons are indicative of their morphology.

3.2.4 Intrinsic properties along the PAG anterior-posterior axis

The PAG is a relatively long structure, ranging from approximately -5.3 to -8.8 mm bregma (Paxinos and Watson, 2007). There are several tracing studies demonstrating that long range projections terminating in the PAG are spatially localised (Rizvi et al., 1991; de Git et al., 2018). Furthermore, Lovick and Stezhka (1999) illustrated electrophysiologically and morphologically distinct subpopulations of cells within the dPAG, but did not report if these subpopulations were differentially localised along the anterior-posterior (A-P) axis of the PAG. Indeed, the majority of cells reported in this study were located in the posterior dPAG. To understand if there are variations in the cell type or intrinsic properties of neurons across the A-P axis of the PAG, I performed a Pearson's R correlation analysis of A-P axis position and intrinsic properties, sEPSCs and morphology.

I found no significant correlation between any intrinsic property parameter and A-P axis position (Appendix Fig. S3). I also found no correlation between A-P axis position

and sEPSC amplitude (Appendix Fig. S3O), however sEPSC frequency was significantly increased in cells located more anterior (Fig. 3.10B). Furthermore, I examined whether certain cell types, as defined by their morphology, localised to specific subregions along the A-P axis of the PAG. I confirmed that all four identified cell types were found along the entire longitudinal column investigated (Fig. 3.10C). These results suggest that PAG cells, although heterogeneous in nature, are not distributed differently along the A-P axis of the structure. This is with the exception of sEPSC frequency, suggesting that basal synaptic activity (both AP-dependent and independent) or number of synapses is higher in anterior dorsal and ventral PAG neurons.

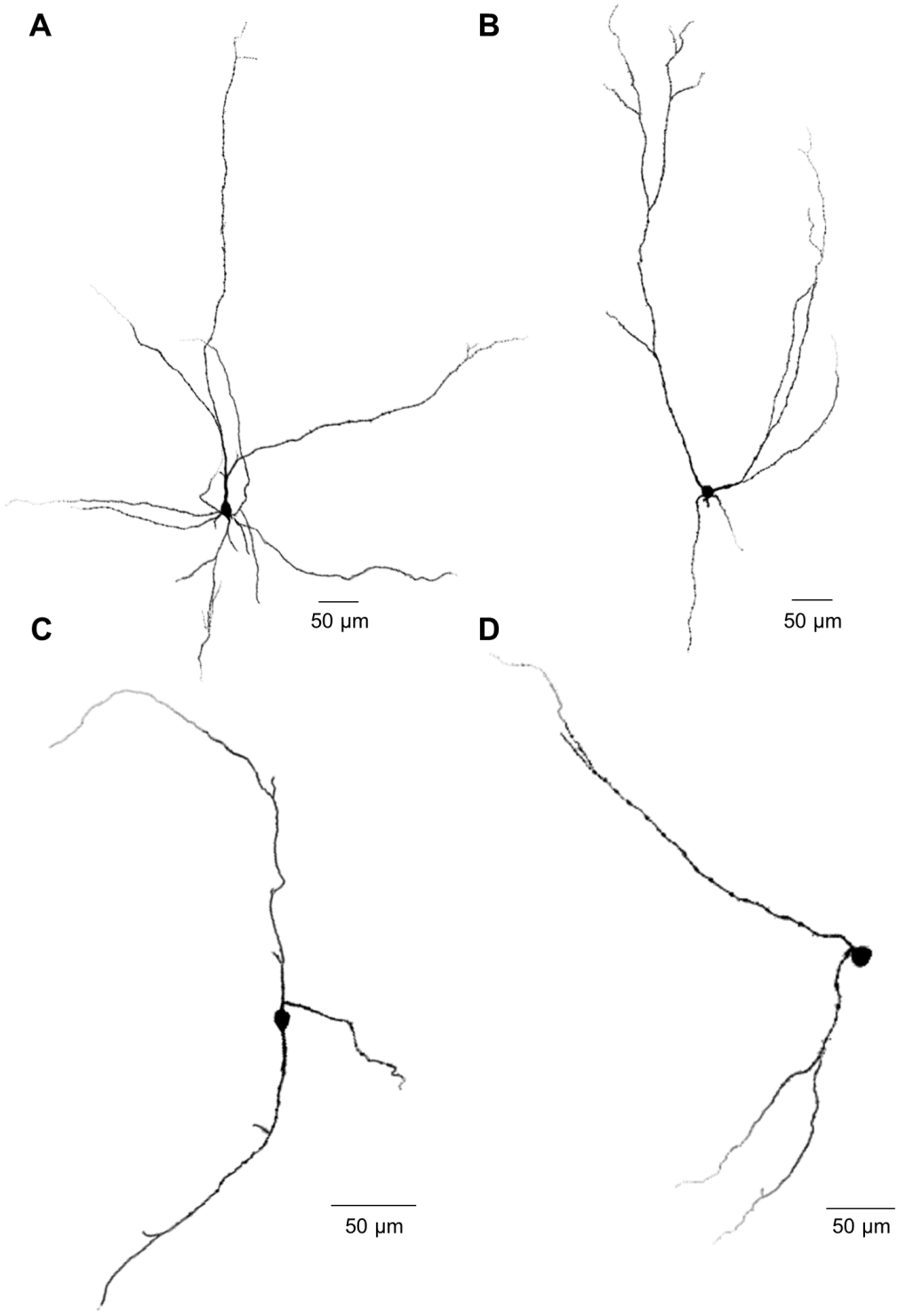

Figure 3.8: Representative filled neurons from WT PAG slices (A) Pyramidal (B) Multipolar (C) Fusiform (D) Pseudounipolar

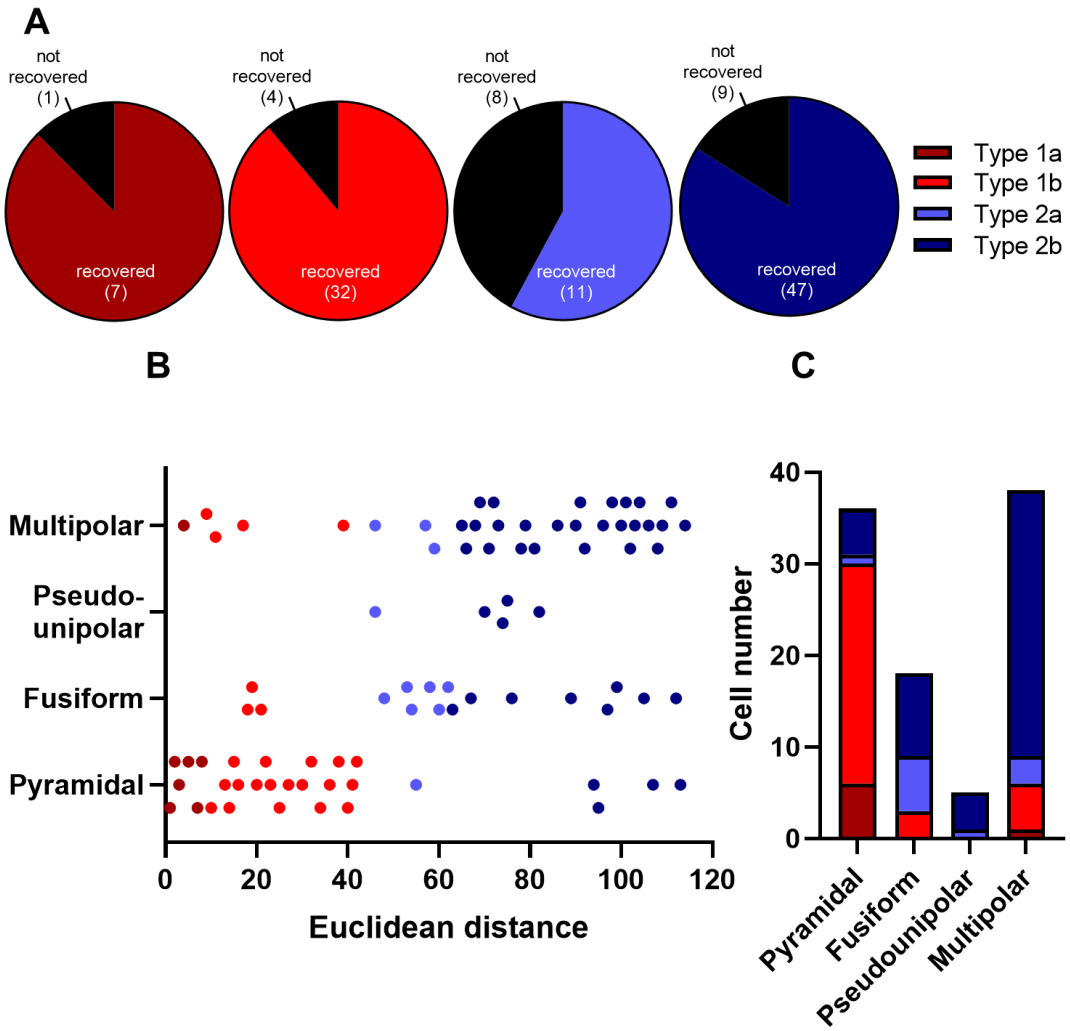

Figure 3.9: Correlation of electrophysiological subtype and neuronal morphology (A) Pie charts illustrating successful cell recovery and identification for type 1a (maroon), type 1b (red), type 2a (blue) and type 2b (navy) (B) Cell morphology plotted against Euclidean distance output from Ward's clustering analysis, cells coloured as per clustered subtype. (C) Summary bar chart showing number of cells identified as each morphological classification and which cluster they belong to based on their morphology ($p < 0.0001$, $V = 0.43$, Cramer's V)

Table 3.1: Means of WT PAG neuron intrinsic properties. Mean values ± SEM for each intrinsic property recorded split into "cell type" as defined by Ward's method clustering analysis. Total n = 119 cells/12 rats, type 1a n = 8 cells/ 6 rats, type 1b n = 36 cells/ 11 rats, type 2a n = 19/ 9 rats cells, type 2b n = 56 cells/ 12 rats.

	Type 1a		**Type 1b**		**Type 2a**		**Type 2b**	
	Mean	± SEM	Mean	± SEM	Mean	± SEM	Mean	± SEM
RMP (mV)	-55.79	2.28	-59.16	1.43	-46.58	1.65	-51.26	0.92
Input resistance (MΩ)	341.8	57.82	315	19.31	634.1	52.9	632	28.07
Membrane time constant (ms)	38.41	6.15	22.76	1.2	34.17	3.02	41.29	1.8
Capacitance pF	126.7	16.72	76.68	3.66	55.04	2.89	68.91	3.11
Sag (%)	2.53	1.79	3.06	0.72	2.09	1	1.88	0.44
APs at 200 pA	10.09	1.46	10.35	1.12	12.93	8.99	18.44	1.15
Rheobase (pA)	76.77	16	100.6	7.62	55.75	7.52	37.86	2.28
Threshold (mV)	-32.05	1.09	-29.72	0.91	-27.21	1.61	-33.04	0.95
Adaptation ratio	1.41	0.12	1.33	0.07	1.55	0.18	2.07	0.21
AP peak (mV)	71.38	3.09	64.86	1.63	58.01	2.52	67.68	1.47
AP width (ms)	0.48	0.042	0.65	0.02	0.99	0.05	0.79	0.02
Depolarisation speed (mV/ms)	340.8	10.81	237.6	13.41	152.4	15.69	217.4	9.08
Repolarisation speed (mV/ms)	-182.3	16.21	-120.5	4.73	-69.57	4.15	-101.4	4.22
ADP at rheobase (mV)	6.77	1.276	1.9	0.44	0.72	0.35	2.32	0.36
fAHP (mV)	-25.76	2.057	-25.83	1.08	-24.99	1.38	-22.75	0.97
sEPSC amplitude (pA)	32.69	2.6	14.9	0.8	10.6	1.03	15.58	0.6
sEPSC frequency (Hz)	7.6	0.26	4.82	0.33	3.32	0.51	5.04	0.28

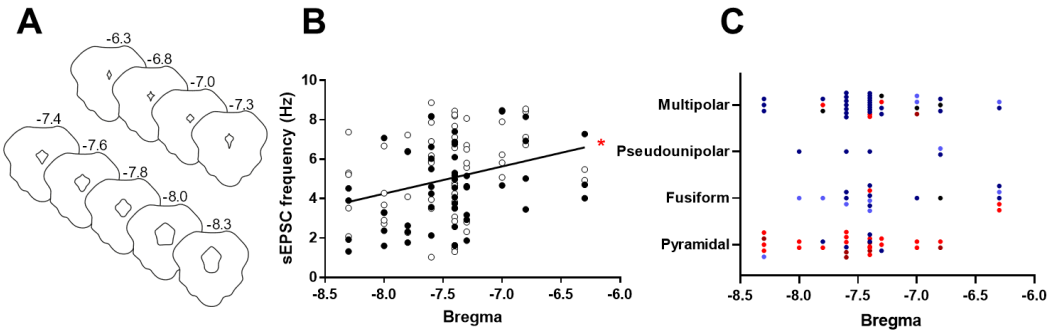

Figure 3.10: Anterior-posterior axis variation of PAG neuron properties (A) Schematics of anterior-posterior axis positions of slices taken for electrophysiology. (B) sEPSC frequency and A-P axis position show significant correlation ($p = 0.0015$, $R^2 = 0.091$, Pearson's R correlation). (C) No significant correlation between cell morphology and A-P axis position ($p = 0.34$, Cramer's V correlation). Clear symbols represent cells in dPAG, filled symbols represent cells in vPAG.

Electrophysiology of *Nlgn3*$^{-/y}$ PAG neurons

3.2.5 Intrinsic properties of *Nlgn3*$^{-/y}$ PAG cells

Intrinsic cellular excitability is an important factor in determining the excitation: inhibition balance within a brain area and therefore for influencing output. Activation of the dorsal or ventral subregions of the PAG elicits flight or freeze responses, respectively (see section 3.1). Increased excitability of dPAG neurons in *Nlgn3*$^{-/y}$ rats may therefore underlie behavioural preferences of flight responses. There is evidence to show that output projections from the vPAG to medulla controlling freezing are glutamatergic (Tovote et al., 2016), but the nature of flight-promoting dPAG projections to downstream motor regions are not known. As *in vivo* stimulation of all neurons in these regions have been shown to elicit flight or freeze responses, an unbiased population of neurons were sampled from dPAG and vPAG regions in WT and *Nlgn3*$^{-/y}$ rats, however, Ward's clustering method was applied post-hoc to the parameters measured in order to give an indication of contributing neuronal subtypes. This data is shown in Appendix B.1 (Fig. S4, Tables B.1, B.2). Proportions of neurons in each cluster were comparable between genotypes (Fig. S4).

No changes in passive membrane properties in the PAG of *Nlgn3*$^{-/y}$ rats

Passive membrane properties of cells can greatly influence excitability. I therefore assessed passive properties in both dorsal and ventral PAG cells in acute slices from

WT and *Nlgn3*$^{-/y}$ rats. Passive intrinsic properties tested were RMP, input resistance, membrane time constant and capacitance. There was no change in RMP, input resistance or capacitance in either dPAG or vPAG between *Nlgn3*$^{-/y}$ and WT (Fig. 3.11, Table 3.2). However, *Nlgn3*$^{-/y}$ vPAG cells showed significantly slower membrane time constants in comparison to WT controls (Fig. 3.11, Table 3.2). This suggests that speed of subthreshold conductance is affected in vPAG cells *Nlgn3*$^{-/y}$ rats.

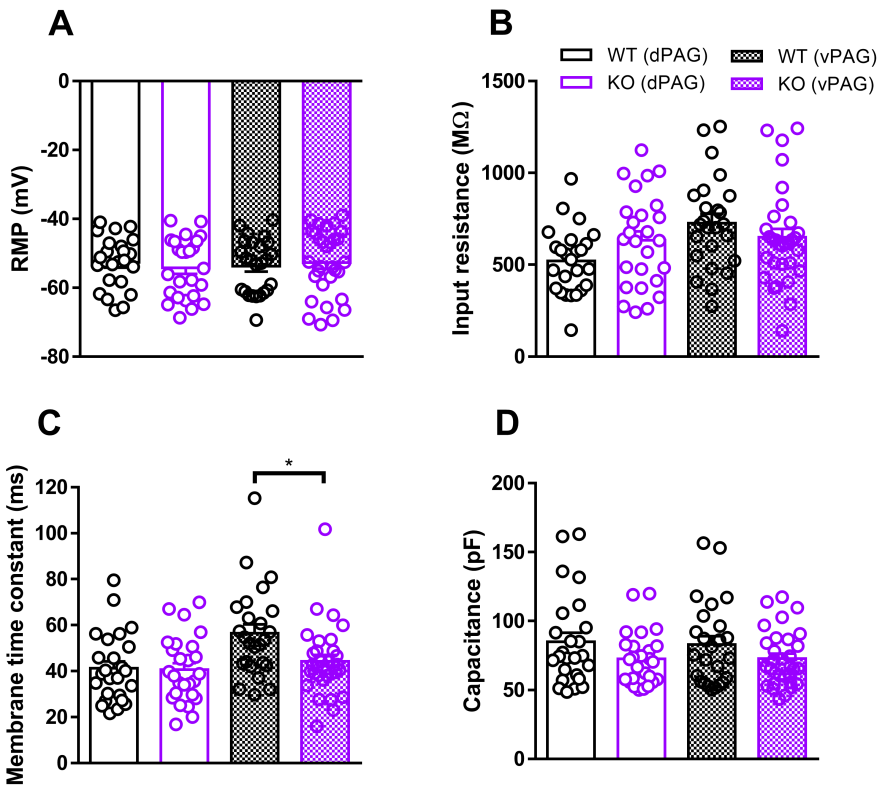

Figure 3.11: Passive membrane properties are affected in vPAG cells but not dPAG cells in *Nlgn3*$^{-/y}$ rats. (A) RMP is comparable between *Nlgn3*$^{-/y}$ and WT rats in both dPAG and vPAG cells (dPAG: WT 25 cells/ 10 rats, KO 26 cells/ 9 rats, p = 0.61; vPAG: WT 24 cells/10 rats, KO 28 cells/ 9 rats, p = 0.75; GLMM). (B) Input resistance is comparable between *Nlgn3*$^{-/y}$ and WT rats in both dPAG and vPAG cells (dPAG: WT 25 cells/ 10 rats, KO 26 cells/ 9 rats, p = 0.09; vPAG: WT 24 cells/10 rats, KO 28 cells/ 9 rats, p = 0.26; GLMM). (C) Membrane time constant is comparable between *Nlgn3*$^{-/y}$ and WT rats in cells recorded from dPAG, however is reduced in vPAG cells of *Nlgn3*$^{-/y}$ compared to WT (dPAG: WT 25 cells/ 10 rats, KO 26 cells/ 9 rats, p = 0.78; vPAG: WT 24 cells/10 rats, KO 28 cells/ 9 rats p = 0.0095; GLMM). (D) Capacitance is comparable between *Nlgn3*$^{-/y}$ and WT rats in both dPAG and vPAG cells (dPAG: WT 25 cells/ 10 rats, KO 26 cells/ 9 rats, p = 0.11; vPAG: 24 cells/10 rats, KO 28 cells/ 9 rats, p = 0.19; GLMM).
Dots represent cells.

Nlgn3$^{-/y}$ dPAG neurons are more likely to be active at RMP

Approximately 30 % of PAG cells have been previously reported to be spontaneously firing at resting membrane potential when recorded in slice (Lovick and Stezhka, 1999). Consistent with this finding, I found spontaneously firing PAG cells in both *Nlgn3*$^{-/y}$ and WT rats. However, a significantly higher proportion of dPAG neurons recorded from *Nlgn3*$^{-/y}$ rats were spontaneously active (46.2 %) in comparison to WT rats (20 %) (Fig. 3.12A), despite there being no change in RMP between genotypes (Fig. 3.11A). Spontaneous firing was not correlated with RMP in either genotype (Fig. 3.12B). This finding indicates there may be a hyperexcitability of neurons in the dPAG of *Nlgn3*$^{-/y}$ rats. In neurons recorded from vPAG, similar numbers of spontaneously active cells were found in both genotypes (WT 45.8 %, KO 37 %, Fig. 3.12C). However, spontaneous activity was weakly correlated with a more depolarised RMP for vPAG cells of WT animals only (Fig. 3.12D), suggesting some of the spontaneous firing neurons in this dataset can be accounted for by their depolarised RMP.

dPAG cells in *Nlgn3*$^{-/y}$ rats are intrinsically hyperexcitable

Cellular excitability was assessed using a series of increasing current injection steps from -100 to +100 pA. Only current injections of up to 100 pA were used as many cells went into depolarising block during higher current injections (see Fig. 3.5B). This revealed that cells in the dPAG of *Nlgn3*$^{-/y}$ rats were hyperexcitable in comparison to WT controls (Fig. 3.13B). Correspondingly, rheobase was decreased in these cells (Fig. 3.13C, Table 3.2). Clustering analysis revealed that this hyperexcitability appears to be driven by type 2 neurons, rather than type 1 (Appendix B.1, Table B.1). By contrast, no changes to excitability were observed in *Nlgn3*$^{-/y}$ vPAG cells in comparison to WT (Fig. 3.13E). Analysis of the rheobase action potential waveform and kinetics, including AP threshold, AP peak, AP width, and AP depolarisation and repolarisation speeds, showed increased AP peak in both dPAG and vPAG *Nlgn3*$^{-/y}$ neurons in comparison to WT (Fig. 3.14B, Table 3.2). Furthermore, vPAG but not dPAG *Nlgn3*$^{-/y}$ neurons displayed increased AP half-height duration (Fig. 3.14C, Table 3.2). No changes in AP threshold, depolarisation speed, or repolarisation speed were detected in either dPAG or vPAG neurons in comparison to WT (Fig. 3.14A, E, F, Table 3.2). fAHP, however, was significantly smaller amplitude in *Nlgn3*$^{-/y}$ dPAG, but not vPAG, neurons (Fig. 3.14D, Table 3.2). These results suggest that dPAG neurons are intrinsically hyperexcitable

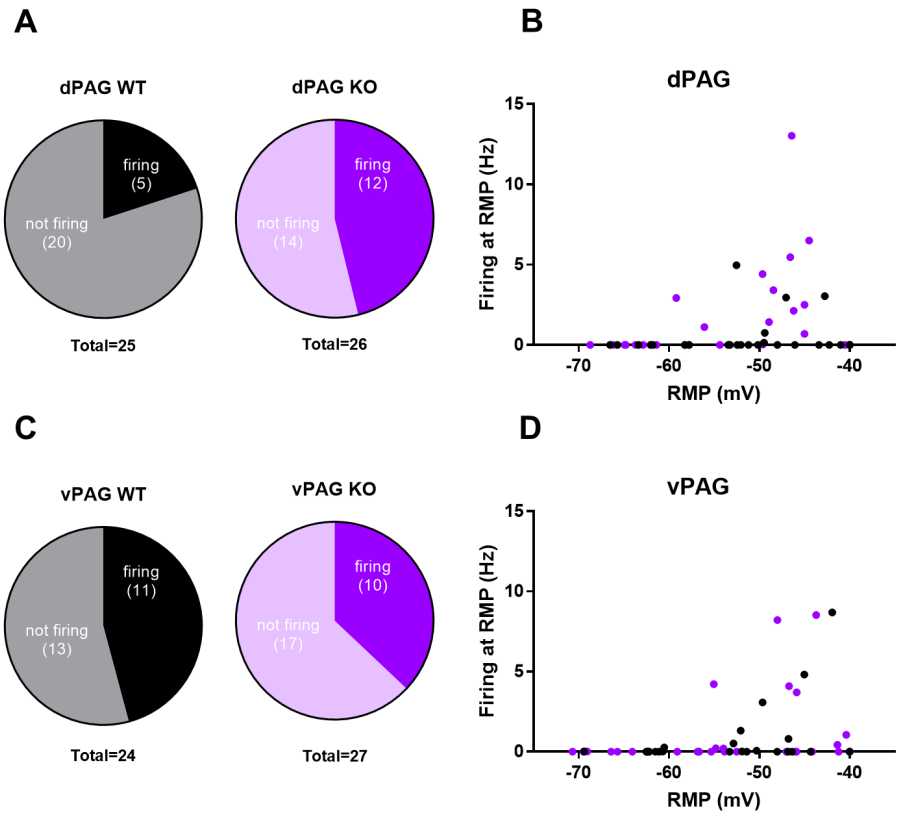

Figure 3.12: Spontaneously active PAG neurons in WT and *Nlgn3*$^{-/y}$ rats. (A) Pie charts depicting significantly higher number of spontaneously active cells recorded in dPAG for *Nlgn3*$^{-/y}$ rats (purple/pink) in comparison to WT (black/grey) (WT n = 25, KO n = 26, p = 0.048, Fisher's exact test). (B) Spontaneous firing frequency is not correlated with RMP in WT dPAG cells (WT n = 25 cells, p = 0.46, r^2 = 0.024, Pearson's R correlation) or KO cells (KO n = 26 cells, p = 0.12, r^2 = 0.098, Pearson's R correlation). (C) Pie charts depicting similar number of spontaneously active cells recorded in vPAG for WT (black/grey) and *Nlgn3*$^{-/y}$ rats (purple/pink) (WT n = 24 cells, KO n = 27 cells, p = 0.52, Fisher's exact test). (D) Spontaneous firing frequency is correlated with RMP in WT vPAG cells (WT n = 24 cells, p = 0.039, r^2 = 0.42, Pearson's R correlation), but not in KO cells (KO n = 27 cells, p = 0.17, r^2 = 0.072, Pearson's R correlation).
Dots represent cells.

in *Nlgn3*$^{-/y}$ rats, potentially due to a decrease in fAHP amplitude. vPAG neurons in *Nlgn3*$^{-/y}$ rats show changes to their intrinsic properties that indicate sodium or potassium channel dysfunctions.

3.2.6 Synaptic properties of *Nlgn3*$^{-/y}$ PAG cells

PAG cells in *Nlgn3*$^{-/y}$ rats show no change in basal synaptic transmission

In addition to intrinsic excitability, the excitability of a neuron depends on the synaptic input it receives. Miniature EPSCs (mEPSCs) recorded from PAG neurons have been reported to be approximately 10-15 pA and occurring at 4 Hz (Hu et al., 2009; Kawahara et al., 2011; Ho et al., 2013). Loss of a synaptic protein such as neuroligin-3 may cause changes in number of synapses or effectiveness of synaptic transmission (Varoqueaux et al., 2006; Fu et al., 2003; Baudouin et al., 2012). I recorded mEPSCs in both dorsal and ventral PAG cells, however I found no changes in mEPSC amplitude or frequency in *Nlgn3*$^{-/y}$ rats in comparison to WT (Table 3.3, Fig. 3.15). Together, these data suggest dPAG cells are intrinsically hyperexcitable, but do not received altered excitatory synaptic input, however, given the hetereogeneity of PAG neurons described in the first part of this chapter and the relatively low number of animals from which mEPSC recordings were performed (dPAG: WT n = 6, KO n = 6, vPAG: WT n = 5, KO n = 6), a higher sample size may be required in order to fully determine if any changes to synaptic input are present.

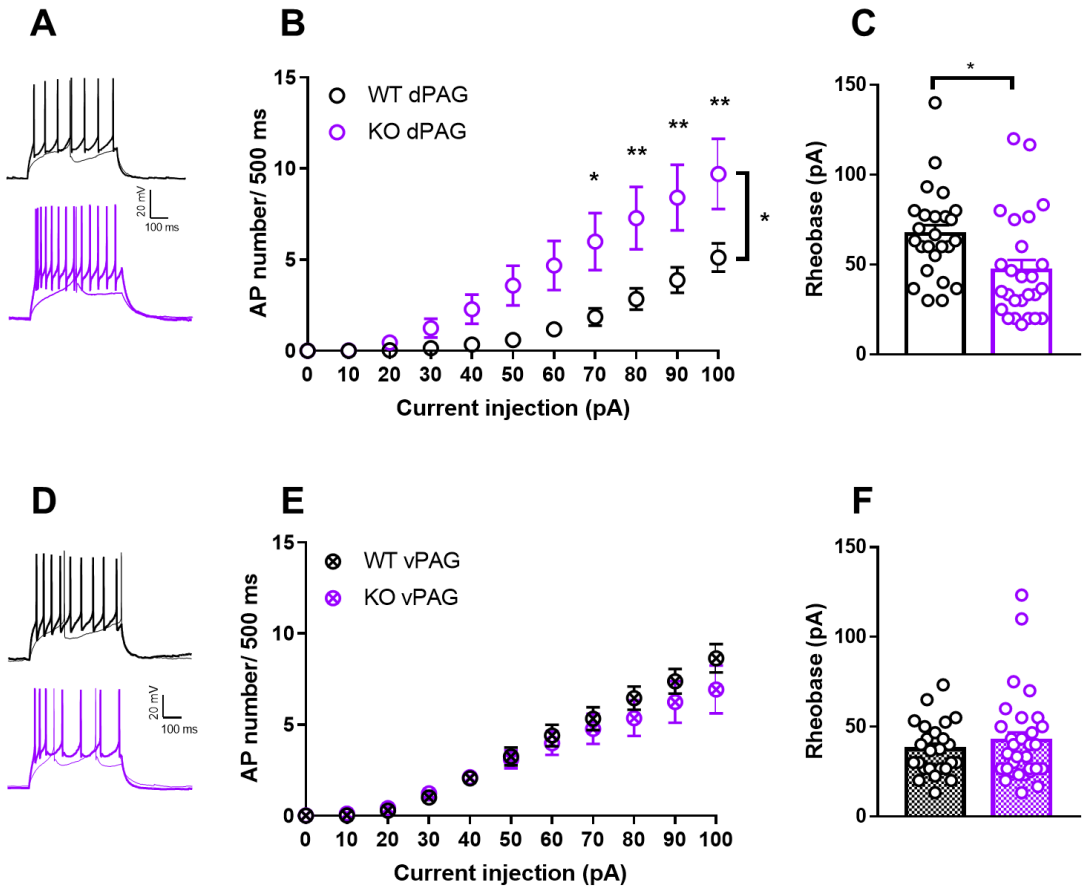

Figure 3.13: Increased firing frequency and decreased rheobase in dPAG but not vPAG cells of *Nlgn3*$^{-/y}$ rats. (A) Representative traces of action potential firing in response to rheobase and +100 pA current steps in WT and *Nlgn3*$^{-/y}$ dPAG cells. (B) Increased firing frequency in dPAG cells of *Nlgn3*$^{-/y}$ rats in response to increasing current injection steps in comparison to WT controls (WT n = 25 cells/ 10 rats, KO: 26 cells/ 9 rats; p = 0.012, F = 5.31, two-way ANOVA (statistics performed on animal averages to avoid pseudoreplication)). (C) Rheobase current is decreased in dPAG cells from *Nlgn3*$^{-/y}$ rats in comparison to WTs (WT 25 cells/ 10 rats; KO 26 cells/ 9 rats; p = 0.015, GLMM). (D) Representative traces of action potential firing in response to -100, 0, rheobase and +100 pA current steps in WT and *Nlgn3*$^{-/y}$ vPAG cells. (E) Comparable firing frequencies seen in *Nlgn3*$^{-/y}$ and WT cells in vPAG (WT n = 24 cells/ 10 rats, KO 28 cells/ 9 rats; p = 0.54, F = 0.00003, two-way ANOVA (statistics performed on animal averages to avoid pseudoreplication)). (F) Rheobase current is comparable between vPAG cells from *Nlgn3*$^{-/y}$ and WT rats (WT 24 cells/ 10 rats; KO 28 cells/ 9 rats; p = 0.40, GLMM).
Dots in rheobase bar charts represent cells.

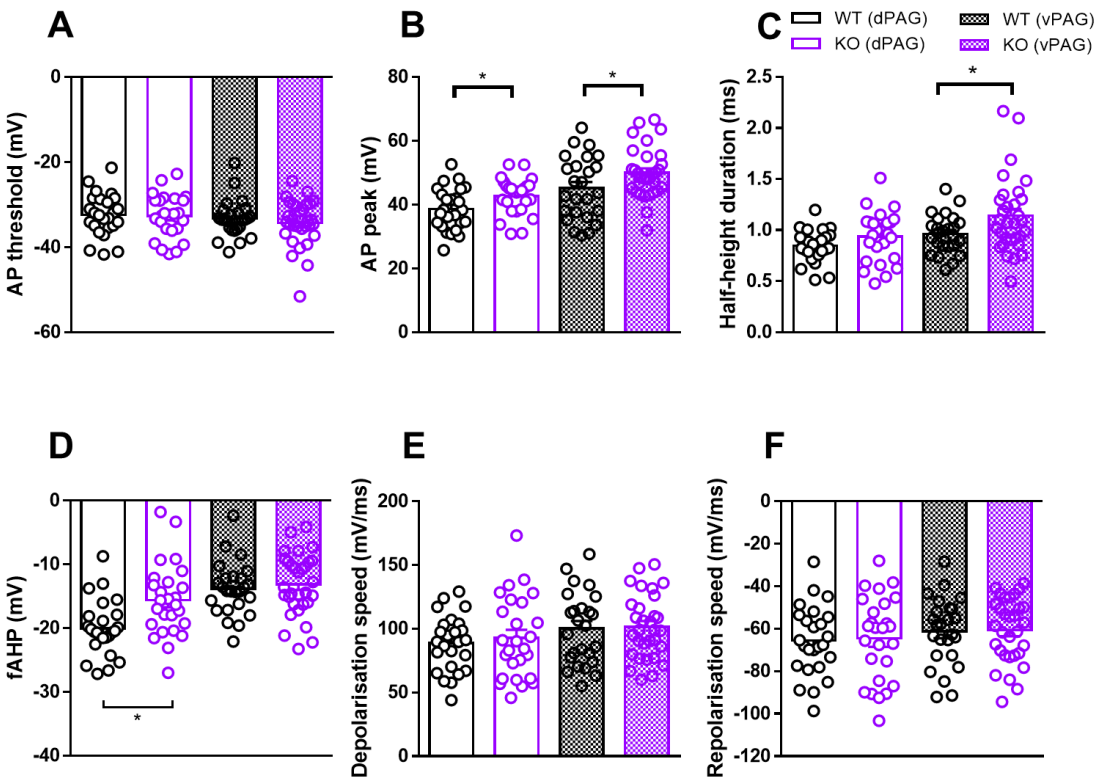

Figure 3.14: No changes in dPAG or vPAG cell action potential threshold or kinetics of *Nlgn3*$^{-/y}$ rats in comparison to WT rats. (A) No difference in AP threshold in dPAG or vPAG of *Nlgn3*$^{-/y}$ rats (dPAG: WT 25 cells/ 10 rats, KO 26 cells/ 9 rats, p = 0.85; vPAG: WT 24 cells/ 10 rats, KO 28 cells/ 9 rats, p = 0.47; GLMM). (B) Increased AP peak height in dPAG and vPAG cells of *Nlgn3*$^{-/y}$ rats (dPAG: WT 25 cells/ 10 rats, KO 26 cells/ 9 rats, p = 0.036; vPAG: WT 24 cells/ 10 rats, KO 28 cells/ 9 rats, p = 0.044; GLMM). (C) No difference in AP width measured at half AP height in dPAG cells of *Nlgn3*$^{-/y}$ rats, increased AP width in vPAG cells (dPAG: WT 25 cells/ 10 rats, KO 26 cells/ 9 rats, p = 0.12; vPAG: WT 24 cells/ 10 rats, KO 28 cells/ 9 rats, p = 0.031; GLMM). (D) Decreased fAHP amplitude of rheobase AP in dPAG, but not vPAG, cells of *Nlgn3*$^{-/y}$ rats (dPAG: WT 25 cells/ 10 rats, KO 26 cells/ 9 rats, p = 0.0047; vPAG: WT 24 cells/ 10 rats, KO 28 cells/ 9 rats, p = 0.58; GLMM). (E) No difference in AP depolarisation speed in dPAG or vPAG of *Nlgn3*$^{-/y}$ rats (dPAG: WT 25 cells/ 10 rats, KO 26 cells/ 9 rats, p = 0.71; vPAG: WT 24 cells/ 10 rats, KO 28 cells/ 9 rats, p = 0.90; GLMM). (F) No difference in AP repolarisation speed in dPAG or vPAG of *Nlgn3*$^{-/y}$ rats (dPAG: WT 25 cells/ 10 rats, KO 26 cells/ 9 rats, p = 0.76; vPAG: WT 24 cells/ 10 rats, KO 28 cells/ 9 rats, p = 0.90; GLMM).
Dots represent cells.

Table 3.2: Means of PAG neuron intrinsic properties for WT and *Nlgn3*$^{-/y}$ rats. Mean values ± SEM for each intrinsic property recorded in cells from WT and *Nlgn3*$^{-/y}$ rats in both dorsal and ventral PAG.

	Dorsal PAG				**Ventral PAG**			
	WT		**KO**		**WT**		**KO**	
	Mean	± SEM	Mean	± SEM	Mean	± SEM	Mean	± SEM
RMP (mV)	-51.41	1.15	-51.92	1.42	-53.36	1.56	-51.6	2.1
Input resistance (MΩ)	517	43.47	631.8	57.1	703	48.56	655.5	52
Membrane time constant (ms)	39.68	3.4	41.7	2.34	56.42	2.99	44.69	3.08
Capacitance (pF)	82.86	7.72	72.95	3.75	84.06	7.59	73.62	3.29
Rheobase (pA)	69.5	6.34	47.82	5.92	36.57	2.89	44.49	3.93
Threshold (mV)	-32.09	1.1	-32.58	0.64	-32.78	0.98	-33.68	0.93
AP peak (mV)	37.95	1.97	42.44	1.34	44.41	1.79	49.00	1.2
AP width (ms)	0.85	0.02	0.92	0.05	0.94	0.04	1.08	0.07
fAHP (mV)	-19.41	0.93	-15.97	0.96	-14.16	0.69	-13.21	0.63
Depolarisation speed (mV/ms)	86.65	4.51	93.52	6.49	100.5	7.51	100.8	4.71
Repolarisation speed (mV/ms)	-64.08	3.63	-65.18	4.31	-62.87	4.14	-62.23	3.94

Table 3.3: Means of PAG neuron mEPSCs in WT and *Nlgn3*$^{-/y}$ rats. Mean values ± SEM for mEPSC amplitude and frequency recorded in cells from WT and *Nlgn3*$^{-/y}$ rats in both dorsal and ventral PAG.

	Dorsal PAG				Ventral PAG			
	WT		KO		WT		KO	
	Mean	± SEM	Mean	± SEM	Mean	± SEM	Mean	± SEM
Amplitude (pA)	15.41	0.91	17.59	1.85	13.94	0.92	15.05	1.59
Frequency (Hz)	6.64	1.27	6.91	1.27	6.64	1.27	6.33	1.01

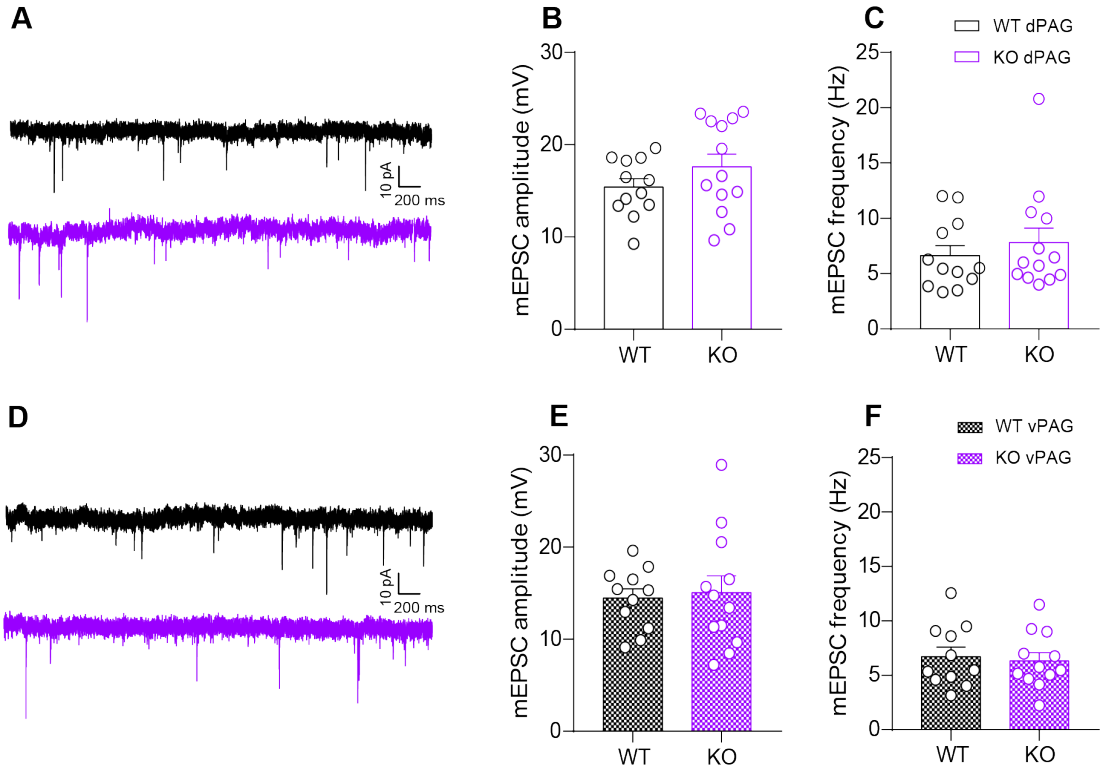

Figure 3.15: No difference in mEPSCs between WT and *Nlgn3*$^{-/y}$ rats in dPAG or vPAG. (A) Representative mEPSC traces for dPAG cells from WT (black) and *Nlgn3*$^{-/y}$ (purple) rats. (B) mEPSC amplitudes in dPAG cells are not different between WT and *Nlgn3*$^{-/y}$ rats (WT n = 12 cells/ 6 rats, KO n = 13 cells/ 6 rats, p = 0.28, GLMM). (C) mEPSC frequencies in dPAG cells are not different between WT and *Nlgn3*$^{-/y}$ rats (WT n = 12 cells/ 6 rats, KO n = 13 cells/ 6 rats, p = 0.61, GLMM). (D) Representative mEPSC traces for vPAG cells from WT (black) and *Nlgn3*$^{-/y}$ (purple) rats. (E) mEPSC amplitudes in vPAG cells are not different between WT and *Nlgn3*$^{-/y}$ rats (WT n = 11 cells/ 5 rats, KO n = 12 cells/ 6 rats, p = 0.78, GLMM). (F) mEPSC amplitudes in vPAG cells are not different between WT and *Nlgn3*$^{-/y}$ rats (WT n = 11 cells/ 5 rats, KO n = 12 cells/ 6 rats, p = 0.88, GLMM).
Dots represent cells.

3.2.7 Synaptic transmission of *Nlgn3*$^{-/y}$ dPAG-vPAG synapses

Tovote et al. (2016) identified the presence of connections between glutamatergic neurons of the dPAG and GABAergic neurons within vlPAG (also theorised in Fanselow

(1991)). In this study, the authors speculate that this local circuit serves as a repressive mechanism for the control of flight-freeze responses. Low-level stimulation of both dorsal and ventral PAG results in freezing responses (Schenberg et al., 1990; Fanselow, 1991; Vianna et al., 2001), however higher-level stimulation of the dorsal PAG switches behavioural output to an active response; fight or flight (Bandler and Depaulis, 1988; Bandler and Carrive, 1988; Tomaz et al., 1988; Schenberg et al., 1990; Zhang et al., 1990; Fanselow, 1991). Given this, activation of glutamatergic dPAG cell terminals on vPAG GABAergic neurons is likely to cause increased local inhibition of vPAG glutamatergic neurons, and therefore decreased freeze-promoting output of the vPAG. Accordingly, Tovote et al. (2016) demonstrated that activation of these glutamatergic dPAG to GABAergic vPAG synapses incites flight behaviour. Therefore, the presentation of active fight or flight responses may be brought about not only directly by increased excitatory output of the dPAG to downstream motor areas, but also by intra-PAG suppression of the freeze-promoting vPAG. I therefore investigated this intra-PAG circuitry in *Nlgn3*$^{-/y}$ rats, hypothesising that this connectivity would be functionally increased in *Nlgn3*$^{-/y}$ rats.

GABA$_A$R/ AMPAR ratios are unchanged in vPAG cells of *Nlgn3*$^{-/y}$ rats

The ratio of GABA$_A$R/ AMPAR EPSCs can be used to assess excitation:inhibition ratio of a cell. I demonstrated that, by stimulating in the dPAG, AMPAR- and GABA$_A$R-mediated EPSCs could be evoked in vPAG cells. Additionally, I pharmacologically confirmed that these responses resulted from activation of AMPA and GABA$_A$ receptors (Fig. 3.16A, B). This provides further evidence of the existence of functional connectivity between dorsal and ventral PAG neurons.

I recorded dPAG-evoked GABA$_A$R/ AMPAR EPSCs in vPAG cells from both WT and *Nlgn3*$^{-/y}$ rats and analysed the ratio of GABA$_A$R/ AMPAR response size. I found that stimulation in dPAG resulted in a GABA$_A$R/ AMPAR ratio in vPAG cells of 1.08 $\pm$ 0.18 in WT rats, and 1.18 $\pm$ 0.22 in *Nlgn3*$^{-/y}$ rats. The ratios were not significantly different (Fig. 3.16C, D). This suggests that, at least on an animal-average level, activation or function of GABA$_A$ and AMPA receptors are unchanged in vPAG cells of *Nlgn3*$^{-/y}$ rats in comparison to WT rats.

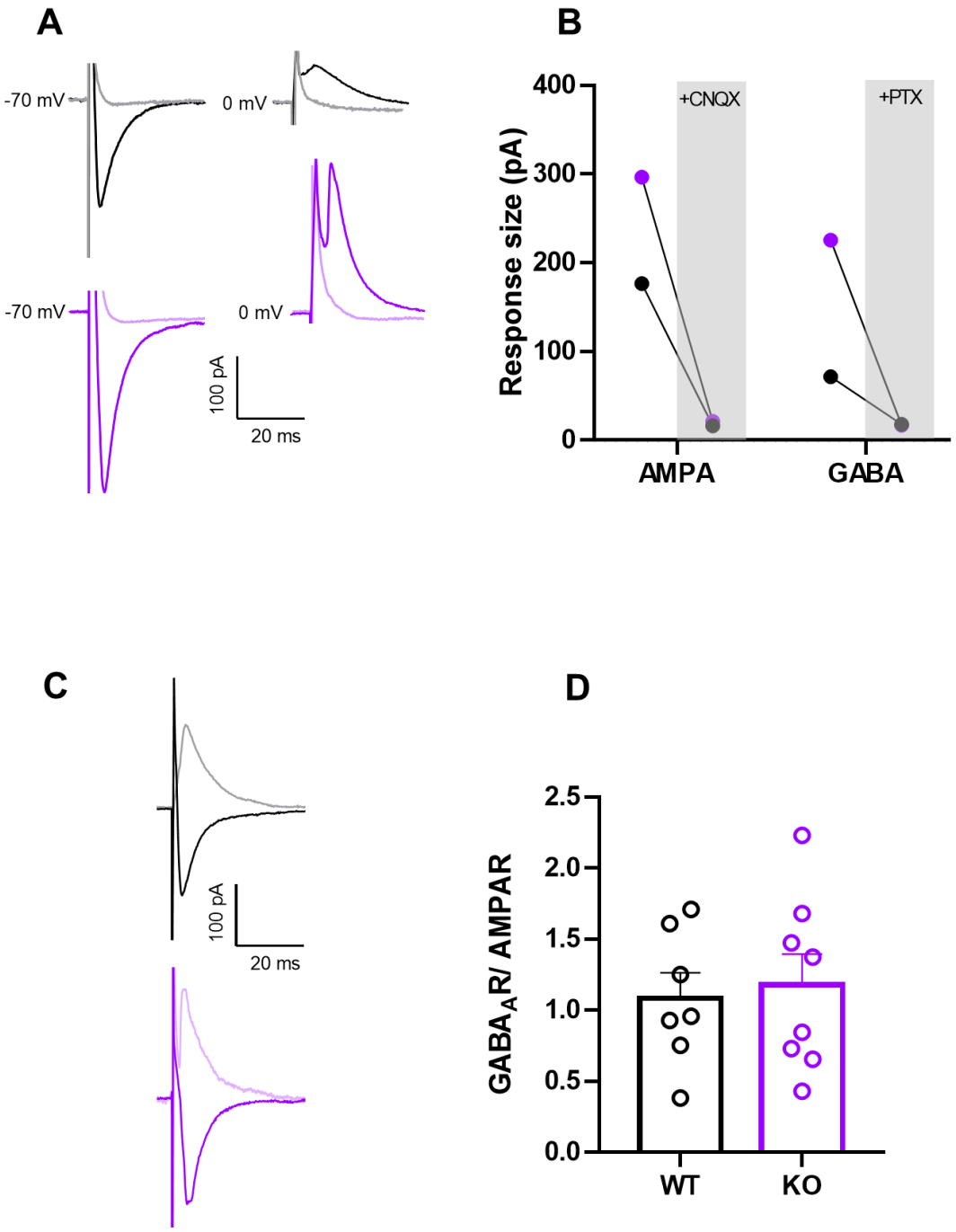

Figure 3.16: No difference in GABA$_A$R/ AMPAR ratios in vPAG cells of WT and *Nlgn3$^{-/y}$* rats. (A) AMPAR (left) and GABA$_A$R (right) responses recorded in vPAG cells whilst stimulating in dPAG. Black/purple traces shows responses in rACSF, grey/pink traces show response following 10 minutes of CNQX or PTX wash in. (B) Summary of EPSC size change in two cells from WT and *Nlgn3$^{-/y}$* rats showing AMPA responses recorded at -70 mV are sensitive to CNQX and GABA responses recorded at 0 mV are sensitive to PTX. Dots represent a single cell in which EPSC was recorded and then pharmacologically inhibited. (C) Representative traces of AMPAR (black/purple) and GABA$_A$R (pink/grey) EPSCs evoked from dPAG stimulation in WT and *Nlgn3$^{-/y}$* rats. (D) GABA$_A$R/ AMPAR ratio of vPAG cells is unchanged between WT and *Nlgn3$^{-/y}$* rats (WT n = 19 cells/ 7 rats, KO n = 32 cells/ 8 rats, p = 0.75, unpaired t-test). Dots represent animal average.

Release probability is increased in a subpopulation of vPAG cells in *Nlgn3*$^{-/y}$ rats

Changes to dPAG-vPAG connections were not observed on a macro level by looking at GABA$_A$R/ AMPAR ratios, however, using this method the absolute amplitude of EPSCs evoked cannot be compared between genotypes as the general range is set by the experimenter (100 - 200 pA, in this case). Therefore, relative stimulation intensity and number of axons activated may differ between animals and slices. Thus, I next investigated dPAG-vPAG connectivity in *Nlgn3*$^{-/y}$ rats at single fibres. I used minimal stimulation to identify putative single synaptic connections between the dorsal and ventral PAG, and examined the release probability of these synapses.

No changes in animal average of dPAG-vPAG minimal stimulated responses in *Nlgn3*$^{-/y}$ rats

I recorded dPAG-evoked EPSCs in the vPAG of WT and *Nlgn3*$^{-/y}$ rats at -70 mV in the presence of picrotoxin to electrically and pharmocologically isolate AMPAR responses. The stimulus strength was then reduced until all-or-nothing synaptic responses were evoked. The stimulation required to evoke threshold-level responses was not different between WT and *Nlgn3*$^{-/y}$ rats (WT 0.94 ± 0.23 pA, KO 0.86 ± 0.10 pA, Fig. 3.17F). When all cells recorded were averaged for each animal (represented as dots in Fig. 3.17), there was no difference in failure rate between WT and *Nlgn3*$^{-/y}$ animals (WT 41.18 ± 7.71 %, KO 34.34 ± 3.17 %, Fig. 3.17C). Average response size was also not different between genotypes (WT -35.7 ± 2.93 pA, KO -30.93 ± 2.09 pA, Fig. 3.17E). This suggests overall synaptic strength at dPAG-vPAG synapses is unchanged between WT and *Nlgn3*$^{-/y}$ rats.

Additionally, I recorded paired-pulse facilitation (PPF) of minimally stimulated synapses by applying another stimulation pulse 50 ms following the first. PPF of minimally stimulated synapses has been shown to be negatively correlated with the success of the initial response (Dobrunz and Stevens, 1997). I found that responses from WT cells showed facilitation of 32.75 ± 9.94 % on average, and responses from *Nlgn3*$^{-/y}$ cells displayed facilitation of 48.47 ± 6.8 %. The percentage facilitation was therefore not significantly different between genotypes (Fig. 3.17E), which was expected given there was no overall change in failure rate.

However, I noted a small change in the distribution of failure rates between *Nlgn3*$^{-/y}$

rats and WT rats (Fig. 3.17B), and whilst inconclusive in itself, this suggests there may be differences that only affect certain populations of cells.

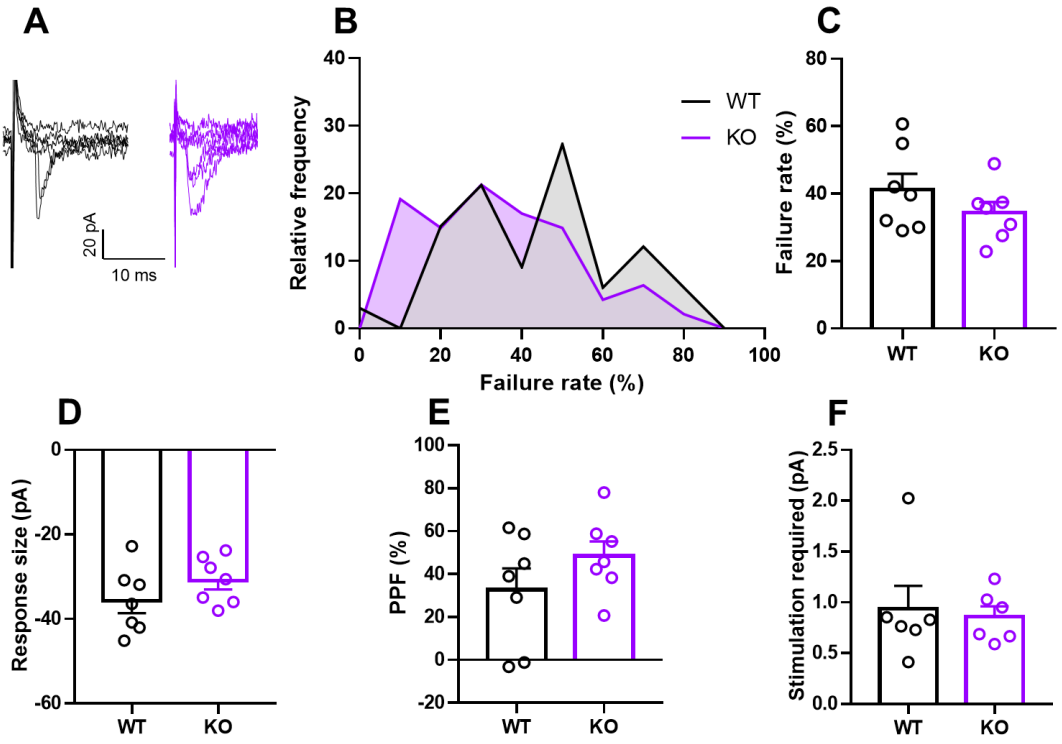

Figure 3.17: dPAG-vPAG stynaptic strength is not different between WT and *Nlgn3*$^{-/y}$ rats. (A) Representative examples of ten sweeps from minimally stimulated dPAG-vPAG synapses in WT and *Nlgn3*$^{-/y}$ rats. (B) Percentage failure rate of vPAG cells plotted as a factor of relative frequency in WT and *Nlgn3*$^{-/y}$ rats. (C) Average failure rats of EPSCs in vPAG neurons at minimal stimulation is not different between WT and *Nlgn3*$^{-/y}$ rats (WT n = 33 cells/ 7 animals, KO n = 47 cells/ 7 animals, p = 0.25, unpaired t-test) (C) Average response size of threshold EPSCs in vPAG cells not different between WT and *Nlgn3*$^{-/y}$ rats (WT n = 33 cells/ 7 animals, KO n = 47 cells/ 7 animals, p = 0.21, unpaired t-test). (E) Paired pulse facilitation of minimally-evoked responses in vPAG cells is not different between WT and *Nlgn3*$^{-/y}$ rats (WT n = 33 cells/ 7 animals, KO n = 47 cells/ 7 animals, p = 0.22, unpaired t-test). (F) Stimulation required to elicit minimal stimulation of dPAG-vPAG synapses is not different between WT and *Nlgn3*$^{-/y}$ rats (WT n = 33 cells/ 7 animals, KO n = 47 cells/ 7 animals, p = 0.76, unpaired t-test).
Dots represent animal averages.

vPAG fusiform cells display lower failure rates for dPAG minimal stimulation in *Nlgn3*$^{-/y}$ rats

In order to determine if the trend towards reduced EPSC failure rate in *Nlgn3*$^{-/y}$ vPAG cells (Fig. 3.17B-C) was driven by an cell-type specific phenotype, I filled recorded cells with biocytin and performed morphological classification as shown in Figures 3.9 and 3.8. Interestingly, I found that cells that responded to dPAG stimulation displayed

different proportions of cell morphologies (Fig. 3.18A) in comparison to pseudo-random sampling of cells for intrinsic properties (Fig. 3.9). Fusiform cells accounted for 53.12 % of WT and 56.10 % of recovered *Nlgn3*$^{-/y}$ cells in this minimal stimulation dataset (which includes only cells exhibiting an evoked response at -70 mV to dPAG stimulation) (Fig. 3.18A), whereas in a pseudorandomly-sampled population of PAG cells, fusiform cells account for only 18.5 % (Fig. 3.3A). This suggests that vPAG-projecting dPAG cells preferentially target fusiform neurons.

Ventral PAG cells of all identified morphologies show threshold-level responses with highly varying failure rates, response sizes and PPF. Individual cell values are plotted in Figure 3.18B-D to illustrate variability, however no statistical analysis has been carried out on this data to avoid pseudoreplication. When fusiform cells only are selected, and an animal average taken, failure rate is significantly lower in *Nlgn3*$^{-/y}$ rats in comparison to WT (WT 43.94 ± 6.68 %, KO 27.15 ± 3.02 %, Fig. 3.18E). EPSC size of fusiform vPAG cells in response to dPAG minimal stimulation was -29.62 ± 4.83 pA in WT and -32.75 ± 3.96 pA in *Nlgn3*$^{-/y}$ rats and showed no significant difference between genotypes (Fig. 3.18F). Additionally, PPF of a second EPSC was not changed between WT (36.61 ± 14.46 %) and *Nlgn3*$^{-/y}$ (49.28 ± 8.06 %, Fig. 3.18G).

This change in minimally stimulated responses was not observed for other morphologically identified cell populations. When taking into consideration only pyramidal cells in the animal average; failure rate, response size, and PPF were all comparable between WT and *Nlgn3*$^{-/y}$ rats (failure rate: WT 54.13 ± 11.89 %, KO 50.06 ± 10.01 %; response size: WT -44.42 ± 17.28 pA, KO -24.19 ± 2.62 pA; PPF: WT 36.61 ± 14.46 %, KO 49.28 ± 8.06 %; Fig. S5A-C). Similarly, when including only multipolar cells in the animal average; failure rate, response size, and PPF were all comparable between WT and *Nlgn3*$^{-/y}$ rats (failure rate: WT 42.17 ± 8.17 %, KO 46.64 ± 5.65 %; response size: WT -33.79 ± 6.83 pA, KO -33.36 ± 5.67 pA; PPF: WT 26.41 ± 13.48 %, KO 39.28 ± 18.08 %; Fig. S5D-F). A comparison was not made of pseudounipolar cells as only one was identified, however the responses of this cell can be seen in Figure 3.18B-D.

These results support the hypothesis that connectivity between glutamatergic dPAG neurons and GABAergic vPAG neurons is strengthened in *Nlgn3*$^{-/y}$ rats, if we presume that fusiform cells are GABAergic in the PAG, as they predominantly are in the cortex (Swanwick et al., 2006; Cauli et al., 2000). These data also suggest the presence of

other dPAG-vPAG synapses which have not yet been identified, such as onto pyramidal cells. However, release probability is not different between WT and *Nlgn3*$^{-/y}$ in these synapses.

3.3 Discussion

The results presented in this chapter provides the first characterisation of the intrinsic properties of WT PAG neurons across the entire dorsal-ventral and anterior-posterior axes and correlates these parameters with known morphological cell types. I also demonstrate differences in the electrophysiology of PAG neurons in *Nlgn3*$^{-/y}$ rats, which may explain the increased flight responses observed in their behaviour. Notably, *Nlgn3*$^{-/y}$ dPAG cells display hyperexcitability, whilst mEPSCs were unchanged. Additionally, release probability was increased at dPAG synapses onto fusiform vPAG cells.

3.3.1 Electrophysiology and morphology of WT PAG neurons

Despite the increasing interest in the PAG in the field of neuroscience, there seems to be a gap in the literature characterising the electrophysiological properties of PAG neurons, and variability of these properties. In this chapter I provide an electrophysiological and morphological characterisation of PAG neurons in WT rats.

My findings confirmed previous reports (Lovick and Stezhka, 1999; Sánchez et al., 1988; Sánchez and Ribas, 1991) that PAG neurons are highly heterogeneous in their passive membrane properties, excitability, and in the spontaneous synaptic input they receive. Lovick and Stezhka (1999) reported cells in the posterior dPAG with RMPs, input resistances, membrane time constants, AP widths and fAHP amplitudes similar to those reported in this chapter. Lovick and Stezhka (1999) also noted two differing AP waveform types, both of which were seen in my recordings, but the authors reported they did not see any clear correlation between AP waveform and morphology.

The very depolarised RMP of PAG neurons in particular has been described in several studies (Lovick and Stezhka, 1999; Evans et al., 2018; Sánchez et al., 1988; Sánchez and Ribas, 1991), despite cells seeming otherwise healthy. As there has been no *in vivo* patch-clamp electrophysiology experiments carried out in the PAG, it is unknown if this depolarised RMP is an artefact of creating acute slices or a true reflection of the neurons' resting state. It should be noted that cells in the PAG have axons and dendritic

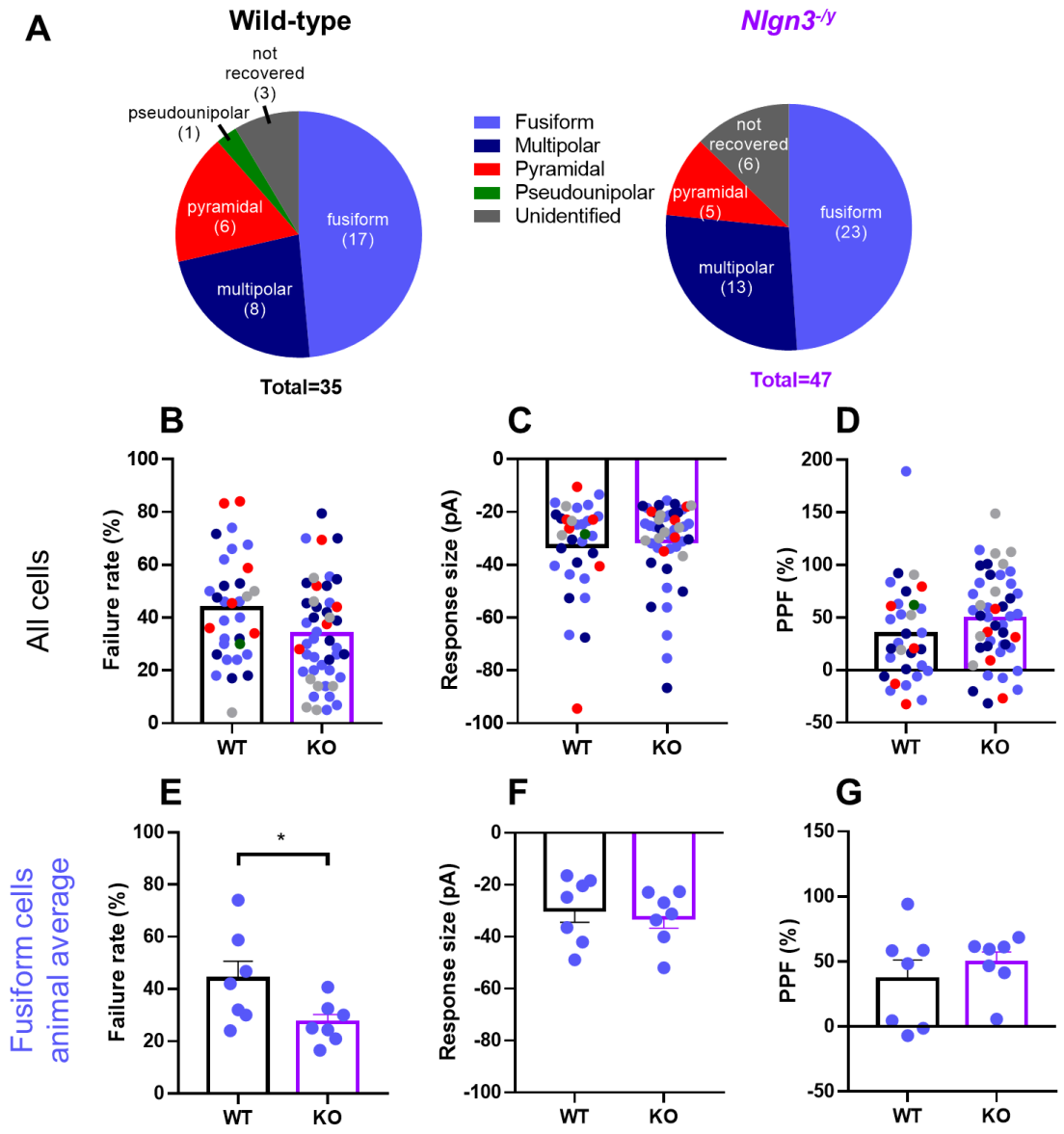

Figure 3.18: vPAG fusiform cells display lower failure rates for dPAG minimal stimulation in *Nlgn3*$^{-/y}$ rats (A) Pie charts of identified morphology of recorded cells responding to dPAG stimulation in WT (left) and *Nlgn3*$^{-/y}$ (right) rats. (B) Failure rate of EPSCs for all vPAG cells recorded in WT (35 cells) and *Nlgn3*$^{-/y}$ (47 cells) rats. Dots represent individual cells, colour coded based on morphology (see legend). (C) Average size of EPSCs for all vPAG cells recorded in WT (35 cells) and *Nlgn3*$^{-/y}$ (47 cells) rats. Dots represent individual cells, colour coded based on morphology (see legend). (D) PPF % of second EPSC (50 ms following first) for all vPAG cells recorded in WT (35 cells) and *Nlgn3*$^{-/y}$ (47 cells) rats. Dots represent individual cells, colour coded based on morphology (see legend). (E) Animal average of WT and *Nlgn3*$^{-/y}$ failure rate when only considering fusiform cells is significantly lower in *Nlgn3*$^{-/y}$ compared to WT rats (WT 17 cells/ 7 rats, KO 23 cells/ 7 rats, p = 0.041, unpaired t-test). (F) Animal average of response size in fusiform cells from WT and *Nlgn3*$^{-/y}$ is comparable between genotypes (WT 17 cells/ 7 rats, KO 23 cells/ 7 rats, p = 0.63, unpaired t-test). (G) Animal average of WT and *Nlgn3*$^{-/y}$ % PPF is comparable for fusiform cells (WT 17 cells/ 7 rats, KO 23 cells/ 7 rats, p = 0.46, unpaired t-test).

arbours that are not limited to one plane. Coronal slices, as taken here and in Lovick and Stezhka (1999); Heinisch et al. (2011); Chiou et al. (2002); Evans et al. (2018) and Ho et al. (2018) optimise the survival of cells as the majority of dendrites run in the dorsal-ventral plane. Preliminary sholl analysis of PAG neurons revealed they had a radius of ∼400-600 μm, and were predominantly contained within the 400 μm thick slices taken for these recordings, however, in particular PAG multipolar neurons were in some cases damaged as their dendritic arbours extend rostro-caudally as well as dorso-ventrally. Slice preparations allow excellent physiological and optical accessibility, as well as the advantage of keeping local circuits intact. However, damage to the tissue as a consequence of the slicing procedure is inevitable, even though preventative measures are taken to reduce this (i.e, ice-cold cACSF, slicing in coronal plane).

Clustering electrophysiological data from the PAG defined two main cell types, that could be further split into two more subtypes (termed type 1a, 1b, 2a and 2b in this chapter). The main advantage of an unsupervised clustering method such as Ward's is that the number of clusters is not predefined. This allows any number of clusters to be identified based on the parameters entered. Ward's method has been used in other studies attempting similar clustering of electrophysiological data (Romanò et al., 2013; Cauli et al., 2000). Despite being unsupervised, two largely different cell types were identified that each displayed similarities to excitatory pyramidal neurons and inhibitory interneurons that may be found in the forebrain (Cauli et al., 2000; Lee et al., 2010; Chen et al., 1996). The main disadvantage of a clustering method such as this is that it weighs each parameter equally when calculating the hierarchy. This does not reflect reality, where some factors (such as fAHP and firing frequency) are more indicative of neuronal identity than others (such as sEPSCs or AP threshold). However, assigning weights to a clustering algorithm in itself presents further issues, such as properly defining appropriate relative weights for each parameter, and furthermore raises the question of whether the intrinsic properties important for identifying forebrain neurons are the same for PAG neurons. Due to these issues, and to maintain an unbiased approach to clustering, Ward's was deemed the most appropriate method for clustering this dataset.

Cytoarchitectural studies from the 1980s and 1990s (Mantyh, 1982; Beitz and Shepard, 1985; Meller and Dennis, 1990; Liu and Hamilton, 1980; Gioia et al., 1985; Chieng and Christie, 1994) sought to characterise the morphology of cell types in the PAG.

Each of these studies identifies a different number of cell morphologies, however pyramidal/triangular, fusiform/bipolar and multipolar/stellate are consistently reported by all. I successfully identified these three morphology types in biocytin-filled neurons from whole-cell patch clamp recordings, and found that type 1 cells were predominantly pyramidal, and type 2 cells were fusiform or multipolar. Although not infallible, this clustering and correlation provides a method of identifying PAG cell types where genetic identification methods are unavailable.

Previous studies have characterised specific neuronal subtypes in the PAG; for example, vGluT2$^+$ neurons (Evans et al., 2018), or opioid-sensitive neurons (Heinisch et al., 2011). Several similarities can be drawn between the properties of neurons described in these studies and the electrophysiologically-defined clusters identified in this chapter. The vGluT2$^+$ neurons described by Evans et al. (2018) have similar passive properties to the type 1 (closest to type 1b) neurons defined in this chapter, suggesting type 1 neurons may indeed be excitatory in nature. Heinisch et al. (2011) describes the effects of PAG neurons that were sensitive to μ-opioid receptor agonists CXCL12 and CX3CL1, and report responding PAG neurons to have a depolarised RMPs (-45 to -55 mV) and low input resistances ($>$ 300 MΩ). Within the clusters defined in this chapter, type 2a neurons have the most depolarised RMP, however these neurons displayed a much higher average input resistance (Table 3.1). A subset of type 1 neurons displayed depolarised RMPs and $>$ 300 MΩ input resistance, so it is possible that opioid-sensitive neurons represent a small proportion of neurons that fall within the type 1 category described in this chapter.

The PAG is over 2 mm in length in adult rats (Paxinos and Watson, 2007), and there are known functional differences in the anterior and posterior subdivisions of the dorsal PAG (Keay and Bandler, 2004). Despite this, I found that almost all parameters measured were not correlated with the position of the cell in the A-P axis of the PAG, with the exception of sEPSC frequency. sEPSC frequency was highly correlated with A-P axis position, with more posterior cells displaying lower sEPSC frequencies. This suggests that posterior PAG cells receive fewer excitatory inputs than anterior PAG cells, however as AP firing rate was not altered along this axis, posterior cells may also receive more inhibitory input. To further investigate this phenotype, mEPSC and mIPSC recordings could be carried out along the A-P axis of the PAG.

3.3.2 Hyperexcitability of dPAG neurons in *Nlgn3$^{-/y}$* rats

Nlgn3$^{-/y}$ rats display increased flight behaviour in response to fearful stimuli. The execution of flight-freeze responses involves distinct subregions of the PAG; dPAG stimulation results in flight responses (Bandler and Depaulis, 1988; Bandler and Carrive, 1988; Tomaz et al., 1988; Fanselow, 1991; Fanselow et al., 1995), whereas stimulation of the vPAG elicits freezing (Zhang et al., 1990; Fanselow, 1991; Fanselow et al., 1995). The results in this chapter provide evidence that neurons in the dPAG, but not vPAG, of *Nlgn3$^{-/y}$* rats are intrinsically hyperexcitable. This may affect the excitation/ inhibition balance within the PAG, leading to a disruption of flight-freeze response circuitry. A region-specific hyperexcitability of dPAG neurons in *Nlgn3$^{-/y}$* is likely to bring the resting state of the dPAG closer to the "threshold" of eliciting an escape response (Evans et al., 2018) and promote output to downstream areas controlling escape behaviour. Clustering analysis shown in Appendix B.1 suggested this phenotype is driven by increased intrinsic excitability of type 2 rather than type 1 neurons, however the clustering may be confounded by the effect of neuroligin-3 loss on intrinsic cell properties. Further investigation of the nature of the neurons contributing to this phenotype is therefore required.

Interestingly, I found no overall change in input resistance or AP threshold to explain the hyperexcitability of dPAG neurons in *Nlgn3$^{-/y}$* rats. However, I found that fAHP amplitude was significant decreased in dPAG neurons of *Nlgn3$^{-/y}$* rats. fAHP is a K^+ current that lasts 2-5 ms following an AP repolarisation (Storm, 1989). fAHP has been shown to be mediated by BK channels (large-conductance K^+ channel) (Poolos and Johnston, 1999) which are activated by Ca^{2+} influx and contribute towards repolarisation of APs. Antagonism of BK channels decreases fAHP and increases neuronal firing frequency (Springer et al., 2015). Reduced BK currents could therefore underlie the change in excitability of dPAG neurons in *Nlgn3$^{-/y}$* rats. It is also possible the stress levels of the animal before culling differentially affected intrinsic excitability (Varela et al., 2012; Matovic et al., 2019; Urban and Valentino, 2017). It is important to note that the change in firing frequency is not due to sampling different populations of neurons in each genotype. There is a great diversity of neurons in the PAG, as discussed in section 3.3.1, however post-hoc clustering analysis revealed that equal proportions of type 1 and type 2 neurons were sampled from WT and *Nlgn3$^{-/y}$* rats (see Appendix B.1, Fig. S4).

Neuroligin-3 is a postsynaptic cell adhesion molecule, and therefore it is unlikely to directly affect intrinsic excitability. However, the intrinsic excitability of neurons could be affected indirectly by neuroligin-3 deficiency. Both neuroligin-3 and BK channels have been shown to associate with PSD-95 (Irie et al., 1997; Sailer et al., 2006), so the loss of neuroligin-3 may have knock-on effects on BK channel binding to PSD-95 or recruitment to the postsynaptic membrane. Investigation of BK channel expression and binding to PSD-95 (using Western blotting and co-immunoprecipitation) would provide further insight into the effect of neuroligin-3 loss in PAG neurons.

3.3.3 Normal excitability of vPAG neurons in *Nlgn3*$^{-/y}$ rats

Additional to increased flight behaviour (Figs. 1.7, 1.8), *Nlgn3*$^{-/y}$ rats display reduced freezing behaviour during auditory fear conditioning and recall (Fig. 1.5). However, no corresponding change to the cellular excitability of vPAG neurons was observed in *Nlgn3*$^{-/y}$ rats. This indicates that PAG circuitry responsible for executing freezing behaviour may be intact in *Nlgn3*$^{-/y}$ rats but is superseded by hyperexcitability of flight-promoting dPAG neurons.

To test this hypothesis, a further behavioural experiment was carried out by V. Kapgal to create a scenario in which *Nlgn3*$^{-/y}$ rats may display typical freezing behaviour. This experiment revealed when both tone and context information are presented during the recall phase of fear conditioning, *Nlgn3*$^{-/y}$ rats display normal freezing behaviour, despite not freezing to the tone or context individually (Fig. 3.19). This agrees with electrophysiological data suggesting that circuits contributing to freezing behaviour are intact. Escape behaviours are exhibited by WT rats in situations where escape is possible (for example see Calvo et al. (2019)), and rarely in contexts such as this where no escape route exists. Failure to identify an escape route usually results in freezing behaviour, as is robustly observed in WT rats during fear conditioning (Figs. 1.5, 3.19). *Nlgn3*$^{-/y}$ rats exhibit flight behaviours in fearful situations much more readily than WT rats (Figs. 1.7, 1.8), not even exhibiting completely passive responses in the enclosed chambers used for fear conditioning and recall (Fig. 1.5D), so therefore may view almost all fearful situations as escapable. Perhaps the presentation of both tone and context is enough information for the situation to be viewed as inescapable, and therefore freezing responses are exhibited.

The addition of context presentation during cued fear recall involves the ventral

hippocampus, which was not previously required for cue-only fear recall (Hobin et al., 2006; Phillips and LeDoux, 1992). This may have affected fear response output, as projections from the hippocampus to the BA and mPFC (Ishikawa and Nakamura, 2006; Herry et al., 2008) are thought to encode sensory and contextual information that provoke appropriate fear response behaviour. As both the mPFC and BA project to the PAG in turn (for the BA, these projections are indirect through the CeM) (Tovote et al., 2016; Rozeske et al., 2018), the activation of circuits responding to both cued and contextual fear condition may result in increased inhibition of the dPAG or increased activation of the vPAG, leading to the freezing behaviour observed in *Nlgn3*$^{-/y}$ rats during this part of the paradigm. Investigation of coherence between these brain regions *in vivo* is an interesting future experiment to further explore this phenotype.

In combination with the finding that vPAG neurons display normal intrinsic excitability in *Nlgn3*$^{-/y}$ rats, this suggests that there are no major deficits in freezing circuitry, and it is the hyper-function of the dPAG that is overriding normal freezing-provoking circuits and causing the preference of flight responses to fear.

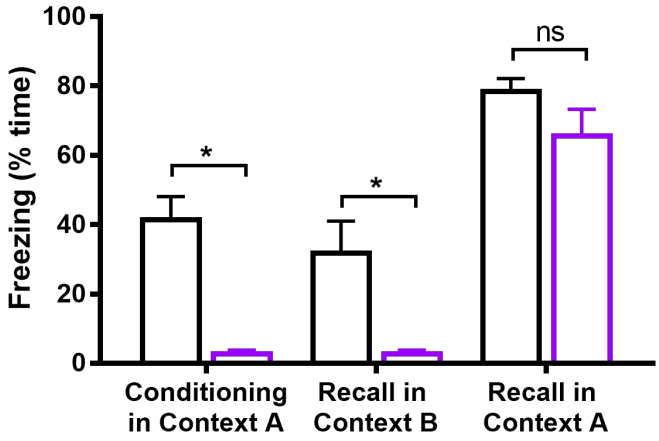

Figure 3.19: Presentation of both cue and context restores freezing behaviour in *Nlgn3*$^{-/y}$ rats. Experiment carried out by V. Kapgal, CBDR. (A) *Nlgn3*$^{-/y}$ rats show significantly less classic freezing behaviour during conditioning and recall of context, however freezing behaviour is restored to WT levels when the animals are presented with both tone and context (WT n = 8, KO n = 8, conditioning: $p < 0.0001$, context recall: $p = 0.0033$, both recall: $p = 0.33$, $F = 31.83$, repeated measures two-way ANOVA).

Despite there being no gross alterations in intrinsic excitability of vPAG cells in *Nlgn3*$^{-/y}$ rats, they are not entirely unaffected by the mutation. There is a significant decrease in membrane time constant and increase in AP height and half-height duration

in vPAG neurons of *Nlgn3*$^{-/y}$ rats, however, there is no significant change in input resistance of these cells, implying number of active channels is equivalent between genotypes but ion channel conductance may be altered in *Nlgn3*$^{-/y}$ vPAG neurons. Further investigation of the biophysical mechanisms that could account for these changes, and the functional implications of this, are needed.

3.3.4 Synaptic function of PAG neurons of *Nlgn3*$^{-/y}$ rats

In addition to intrinsic excitability, the excitability of a neuron depends on the synaptic input it receives. As *Nlgn3*$^{-/y}$ is a synaptic protein known to be involved in the development and maintenance of synapses (reviewed in Lisé and El-Husseini (2006)), it is surprising that mEPSCs are unaffected in *Nlgn3*$^{-/y}$ dPAG and vPAG cells. A possible explanation for this result is that is the role of neuroligin-3 in synapse development and function is being compensated for by an increase in expression of neuroligins 1 and 2, which localise to excitatory and inhibitory synapses, respectively (Futai et al., 2013; Gibson et al., 2009; Levinsoni et al., 2005; Chubykin et al., 2007). Indeed, preliminary RNA sequencing data from our lab shows that *Nlgn1* and *Nlgn2* are upregulated in *Nlgn3*$^{-/y}$ rats (*Nlgn1* p = 0.047, *Nlgn2* p = 0.00017), however further evidence is required to confirm this finding. A previous study reported neuroligin-1 loss leads to upregulation of neuroligin-2 by 30 %, suggesting these proteins can homeostatically regulate to maintain normal function (Blundell et al., 2010). Chanda et al. (2017) reported the complete deletion of any of the neuroligins results in no or little change in synapse number, but had a large effect on synaptic maintenance. However, I found that neuroligin-3 loss in rats does not affect mEPSC frequency or amplitude in PAG neurons, suggesting excitatory synaptic formation and maintenance are unaffected. Yet, given the low number of animals recorded from for this dataset (dPAG: WT n = 6, KO n = 6, vPAG: WT n = 5, KO n = 6), and that the distinct cell populations identified in the first half of this chapter were not analysed separately here, it is possible this dataset is underpowered and unable to detect small changes in mEPSC amplitudes or frequencies. Additional animals would need to be recorded from to increase the confidence with which we can accept the null hypothesis of this experiment.

Several studies have investigated the effect of *Nlgn3* mutations on mEPSCs/IPSCs in mice. Etherton et al. (2011) reported decreased mEPSC frequencies in hippocampal pyramidal cells of *Nlgn3*$^{-/y}$ mice, and Baudouin et al. (2012) reported the same pheno-

type in cerebellar purkinje neurons, yet this does not appear to be the case in the Calyx of Held, striatal medium spiny neurons, or somatosensory cortex pyramidal neurons in which *Nlgn3*$^{-/y}$ mice have normal mEPSC amplitudes and frequencies (Zhang et al., 2017; Rothwell et al., 2014; Tabuchi et al., 2007). Interestingly, there are considerably more reports of altered mEPSCs/IPSCs in mice with the *R451C* mutation (Zhang et al., 2017; Rothwell et al., 2014; Tabuchi et al., 2007), or *R704C* mutation (Etherton et al., 2011; Zhang et al., 2017; Chanda et al., 2013) (NB. Chanda et al. (2013) shows this effect not in mice, but in human induced-neuronal cells containing this mutation), than in mice with full *Nlgn3* deletions. Given this, it is likely that the complete loss of the neuroligin-3 protein, rather than the gain-of-function mutations *R451C* and *R704C*, may be what is required in order for other proteins to compensate.

Additionally, the mEPSC frequency of PAG neurons reported in the literature is lower than that observed here (Ho et al., 2018). The most parsimonious explanation for this difference is flow rate of ACSF (3-4 ml/min in Ho et al. (2018), 5-7 ml/min here), which markedly affects mEPSC frequency in slice. Alternatively, differences in the sampled population of cells could account for this. Nonetheless, these results provide evidence that the excitatory synaptic input on to PAG neurons is equivalent in *Nlgn3*$^{-/y}$ and WT rats. I did not record mIPSCs in these neurons, which would have provided additional information about the excitation:inhibition balance received by PAG neurons.

I hypothesised that increased excitability of dPAG neurons in *Nlgn3*$^{-/y}$ rats would not only promote flight behaviour via dPAG efferents to downstream pre-motor areas, but also increase local inhibition of the vPAG in order to suppress freezing behaviour (Tovote et al., 2016). Tovote et al. (2016) provided evidence that (in mice) glutamatergic dPAG neurons synapsing onto GABAergic vPAG neurons suppress freezing behaviour by inhibition of freeze-promoting glutamatergic vPAG neurons. The majority of these connections were ipsilateral, with a mean of 7 glutamatergic dPAG synapses per GABAergic vPAG cell. I investigated these synapses in *Nlgn3*$^{-/y}$ rats firstly by examining activity-dependent synaptic transmission for both AMPA and GABA receptors. I found that excitatory and inhibitory transmission at dPAG-vPAG synapses were relatively equal, and on average there was no change in the $GABA_AR$/ AMPAR ratios of *Nlgn3*$^{-/y}$ rats. The loss of neuroligin-3 therefore does not appear to affect overall excitatory/ inhibitory

drive at dPAG-vPAG synapses. Interestingly, Chanda et al. (2013) also reported no change in $GABA_AR$/ AMPAR ratios in *NLGN3 R704C*-mutated induced neurons.

Examination of putative single synapses by minimal stimulation provides further information about the strength of connections. Minimally stimulated EPSCs are known to be highly variable (for example see Allen and Stevens (1994); Dobrunz and Stevens (1997)) and depend on both the size and the replenishment rate of the readily-releasable pool (RRP). Overall, failure rate and response size of minimally-stimulated EPSCs were not different between WT and *Nlgn3*$^{-/y}$ rats. However, confirmation of these cells' morphology revealed a significant increase in release probability in vPAG fusiform cells alone in *Nlgn3*$^{-/y}$ rats. The immmunoreactivity of these fusiform neurons is not known; immunocytochemical staining for GAD65/67 or GABA (see Methods section 2.5) was applied to provide a marker for GABAergic neurons, however this was unsuccessful due to the fixation process for these slices. Determining the nature of the fusiform neurons that contribute towards this phenotype is crucial for a clearer understanding of this intra-PAG circuit. In the forebrain, fusiform cells have been characterised as GABAergic (Cauli et al., 2000, 1997; Benson et al., 1994; Esclapez et al., 1987). Additional characterisation of these neurons and this pathway in *Nlgn3*$^{-/y}$ rats is an interesting future experiment. For example, using optogenetic stimulation of opsin-expressing glutamatergic neurons in the dPAG and recording visually identifiable (eg. via GFP) vPAG GABAergic neurons. A rat line that co-expresses a yellow fluorescent protein (Venus) with vesicular GABA transporter (VGAT) has already been created (Uematsu et al., 2008), and would be a useful tool for further investigation of this finding. Nonetheless, the 'catch-all' approach I have used allows for several interesting conclusions and questions to be drawn:

1. **vPAG-projecting dPAG neurons preferentially target fusiform neurons.** Identification of vPAG cells that responded to dPAG stimulation revealed vastly different proportions of neuronal morphologies to those identified in WT rats in section 3.2.1. Pseudo-random sampling of vPAG neurons in WT rats revealed fusiform neurons account for 18.5 % of the total cell population (Fig. 3.9A, and also Gioia et al. (1985), 14 %; Meller and Dennis (1990), 30 %), however they represented 53 % and 56 % (in WT and *Nlgn3*$^{-/y}$) of the neurons that responded to dPAG stimulation.

2. **Existence of other dPAG-vPAG synapses besides glutamatergic - GABAergic.** Minimally-stimulated EPSCs were evoked in cells of all identified cell types, including pyramidal cells. This suggests that, although the specific function and immunoreactivity of each cell morphology has not been confirmed for the PAG, vPAG-projecting dPAG neurons do not only target a single cell type. This highlights the need for further investigation, and confirmation of the nature of these cells types and connections, which has not yet been explored in PAG literature.

3. **Increased release probability of dPAG synapses to vPAG fusiform neurons.** From the results presented here, it is likely that these cells represent those in the pathway identified by Tovote et al. (2016). Release probability of dPAG neurons projecting to vPAG fusiform neurons is increased in *Nlgn3*$^{-/y}$ rats (shown as a decrease in failure rate). These results suggest that the behavioural manifestation of dPAG neuron hyperexcitability may be exacerbated by increased suppression of freezing-promoting vPAG neurons.

4. **Short-term plasticity of dPAG-vPAG synapses may be reduced.** Fusiform cells, which show a highly significant decrease in failure rate in *Nlgn3*$^{-/y}$ rats, do not show an accompanying change in PPF. PPF and failure rate have been shown to be inversely proportional to each other (Dobrunz and Stevens, 1997; Huang and Stevens, 1997), yet there is also evidence to suggest they are directly proportional (Chen et al., 1996). The percentage of PPF is thought to reflect residual Ca^{2+} in the axon terminal (Zucker, 1989). The lack of PPF change in these neurons may indicate a loss of presynaptic plasticity in *Nlgn3*$^{-/y}$ rats. Further investigation of this is required.

It is important to note that the vPAG cells reported in this chapter displaying evoked EPSCs to minimal or non-minimal dPAG stimulation do not represent the response of all cells in the vPAG. Approximately half of all vPAG cells recorded showed no response to dPAG stimulation, and therefore are not included in this analysis. To further understand the intra-PAG circuitry in *Nlgn3*$^{-/y}$ rats, the use of optogenetics may provide more insight (see Chapter 6 for further details), however these data suggest release probability of a subpopulation of dPAG-vPAG synapses is increased in *Nlgn3*$^{-/y}$ rats.

3.4 Summary

In summary, the results in this chapter demonstrate that PAG neurons can be subdivided into electrophysiologically distinct groups that are reflective of neuronal morphology. Within these groups of neurons, I find that there is increased cellular excitability within the dPAG of *Nlgn3*$^{-/y}$ rats, driven by decreased fAHP amplitude, which could lead to the behavioural manifestation of increased flight behaviours. This may be exacerbated by increased released probability of dPAG-vPAG synapses. Furthermore, I provide the first evidence of PAG dysfunction in a model of ASD/ID. Despite fear behaviour being well characterised in many models of ASD/ID, the physiology of the PAG has never been considered as a contributing factor. Further study of the involvement of the PAG in autism may provide additional insight into the mechanisms behind anxiety disorders and abnormal emotional responses seen in people with ASD/ID.

The findings of this chapter led to the hypothesis that the PAG may be functionally altered in *Nlgn3*$^{-/y}$ rats *in vivo* during the presentation of fearful stimuli. Hyperexcitability of the dorsal, but not ventral PAG shown through slice electrophysiology recordings suggests the activity of the dPAG may be overriding that of the vPAG. Thus, the following chapter aims to investigate the physiology of the dPAG *in vivo*.

Chapter 4

Fear response behaviour and *in vivo* physiology of the periaqueductal grey

4.1 Introduction

In vivo electrophysiology has the advantage of being able to perform recordings during a behavioural task, or alternatively can be used to evoke a specific behaviour. Additionally, long-range connectivity which is lost in acute brain slices, is intact during this method of recording. In order to gain more information about the (dys)function of the PAG in *Nlgn3*$^{-/y}$ rats, and begin to develop an understanding of intact networks in this model, a combination of *ex vivo* and *in vivo* methods have been utilised in this thesis. Following the identification of fear-response behaviour abnormalities in *Nlgn3*$^{-/y}$ rats outlined in section 1.7, and the hyperexcitability of the dPAG described in Chapter 3, I investigated the physiology of the PAG in *Nlgn3*$^{-/y}$ rats *in vivo*.

For many years the PAG has been considered as a final common path for the execution of fear responses. Descending projections from the central amygdala, hypothalamus, mPFC, and superior colliculus convey threat level and contextual information about the fearful stimuli which are relayed to the PAG in order to evoke the appropriate defensive response: fight, flight or freeze (Tovote et al., 2016; Wang et al., 2015; Rozeske et al., 2018; Evans et al., 2018). Fight-flight-freeze reactions can be induced directly by electrical or chemical stimulation of the dorsal/ventral regions of the PAG (see section 3.1 for details), as well as by presentation of fearful stimuli.

4.1.1 The PAG in fear conditioning

The majority of studies investigating fear conditioning in rodents focus on freezing behaviour as the primary output of fear, as this appears to be the default response for rodents during this task. Reduction of freezing behaviour in models of ASD/ID (notably in the *Nlgn3*$^{-/y}$ rat (Hamilton et al., 2014), and mouse (Radyushkin et al., 2009)) is therefore normally interpreted as a deficit in **fear learning**, however the data presented in the introduction of this thesis demonstrates that changes in **fear response** behaviour may also account for decreases in freezing behaviour during fear recall.

During fear conditioning, lesioning of the dPAG has been shown to abolish the activity burst occurring during foot-shock, whereas vPAG lesions reduce the conditioned freezing response during recall (Fanselow, 1991). Additionally, PAG neurons are activated in response to CS presentation following fear conditioning (Tovote et al., 2016; Watson et al., 2016; Halladay and Blair, 2015). It seems, however, that whilst defensive reactions mediated by the dPAG are context independent (i.e will occur during both innate and learned fear (Kim et al., 2013; DeOca et al., 1998), vPAG-mediated freezing is suspected to be only involved in conditioned fear (Vianna et al., 2001). Supporting this, Watson et al. (2016) found more robust responses of dPAG, rather than vPAG, neurons during innate fear, however both dPAG and vPAG neurons were active during learned fear. This suggests different roles for the dorsal and ventral subdivisions of the PAG in the processing of fear, as well as the execution of responses. Furthermore, Watson et al. (2016) reported a correlation between local field potential (LFP) amplitude in the PAG and percentage of time the rat spends freezing during fear recall. Given this reported correlation, and the significantly reduced freezing behaviour observed in *Nlgn3*$^{-/y}$ rats (Fig. 1.5), it is possible that the amplitude of LFPs are atypical in *Nlgn3*$^{-/y}$ rats during this fear recall.

Stimulation of the dPAG acts as an unconditioned stimulus in itself, and results in fear conditioning (Di Scala et al., 1987; Kim et al., 2013), whereas the same is not true for the vPAG (Kim et al., 2013). Additionally, reciprocal projections between the the PAG and amygdala (Nicholson et al., 2017) provides further evidence for a role of the PAG more complex than simply an exit pathway for fear response implementation. PAG inactivation has been shown to reduce US-evoked responses in amygdala neurons (Johansen et al., 2010), and Kim et al. (2013) demonstrated that electrical priming (at 1 mA) of dPAG neurons resulted in long term depression of BLA-ventral subiculum

synapses. In summary, the PAG appears to be involved in both the execution of fear responses and encoding of fear memories.

4.1.2 Hypotheses and aims

Abnormal flight-freeze behaviour (see section 1.7) and increased intrinsic excitability of dPAG neurons (Fig. 3.13) indicates dysfunction of the PAG may be responsible for the altered fear expression in *Nlgn3*$^{-/y}$ rats. I hypothesised firstly that activity in the dPAG would be altered in *Nlgn3*$^{-/y}$ rats during recall of learned fear, and secondly that *Nlgn3*$^{-/y}$ rats would require lower dPAG stimulation to evoke escape responses. In this chapter, I use a combination of behavioural testing paired with local field potential recordings, and *in vivo* electrical dPAG stimulation to investigate these hypotheses.

4.2 Results

4.2.1 dPAG local field potentials in *Nlgn3*$^{-/y}$ rats

During recall of CS-US association in fear conditioning, *Nlgn3*$^{-/y}$ rats display significantly reduced freezing behaviour (Fig. 1.5C). However, these rats do not appear to have a major fear learning deficit, as they are responding to the CS-onset with another behaviour (Fig. 1.5D). Instead of freezing, *Nlgn3*$^{-/y}$ rats display cessation of exploratory behaviours, immobility of paws and body, followed by head movements from side-to-side. This unusual behaviour has been described previously in rats confronted with a snake (Uribe-Mario et al., 2012; Calvo et al., 2019), and described as "threat assessment" or "defensive attention". Furthermore, active place avoidance testing provided additional evidence of intact associative fear learning in *Nlgn3*$^{-/y}$ rats (Fig. 1.9). I hypothesised that this behaviour is due to a hyperfunction of escape-response circuitry, as opposed to a hypofunction of freezing-response circuitry, as *Nlgn3*$^{-/y}$ rats do display freezing behaviour equivalent to WT levels when presented with additional contextual information (Fig. 3.19), suggesting that circuitry mediating freezing behaviour is intact, but overridden. This is supported by evidence from acute slice recordings displayed in the previous chapter showing that dPAG neurons are hyperexcitable in *Nlgn3*$^{-/y}$ rats, but vPAG neurons remain unchanged (Fig. 3.13).

This chapter aims to further investigate if the phenotype seen during fear conditioning in *Nlgn3*$^{-/y}$ rats is mediated by PAG dysfunction. Following work carried out by my

colleague (see Watson et al. (2016)) examining the activity of the PAG in fear recall, I investigated LFPs in the dPAG of *Nlgn3*$^{-/y}$ rats during auditory fear conditioning.

No change in dPAG LFP amplitude of *Nlgn3*$^{-/y}$ rats during fear recall

To further investigate if the phenotype seen during fear conditioning in *Nlgn3*$^{-/y}$ rats is mediated by PAG dysfunction, and investigate if the previously identified correlation between freezing behaviour and PAG LFP amplitude (Watson et al., 2016) holds true for *Nlgn3*$^{-/y}$ rats, WT and *Nlgn3*$^{-/y}$ rats were implanted unilaterally with electrodes in the dPAG. Rats were allowed to recover for a minimum of one week before undergoing fear conditioning (Fig. 4.1A). CS (tone)-evoked LFPs were recorded from the dPAG during fear recall. Unlike the original fear conditioning paradigm shown in the introduction of this thesis (Fig. 1.5A), the paradigm shown here included a tone habituation phase immediately prior to the conditioning. In a subset of the animals (WT n = 5, KO n = 6), tone-evoked LFPs were recorded to the unconditioned tones presented during tone habituation, however no significant LFPs were observed (Fig. 4.1E), and additionally no freezing behaviour was seen in either WT or *Nlgn3*$^{-/y}$ rats (Fig. 4.1B).

During conditioning, where three CS-US pairings were given, there was no difference in time spent freezing between WT and *Nlgn3*$^{-/y}$ rats, both of which exhibited freezing that increased up to around 25 % (Fig. 4.1C). However, during the recall phase, freezing behaviour of WT rats was approximately 75 % during CS presentations, whereas *Nlgn3*$^{-/y}$ rats displayed significantly lower freezing levels (defined as no movement except for respiration) of around 25 % (Fig. 4.1D). Tone-evoked LFPs were observed in the dPAG of both WT and *Nlgn3*$^{-/y}$ rats with z-scored amplitudes that remained relatively consistent throughout fear recall (Fig. 4.1F-I). Z-scored amplitude of these tone-evoked LFPs (or event-related potentials (ERPs)), was not different between WT and *Nlgn3*$^{-/y}$ rats (Fig. 4.1J). These results show that, despite significant changes to fear response behaviour in *Nlgn3*$^{-/y}$ rats, LFPs evoked in the dPAG by CS presentation are robust.

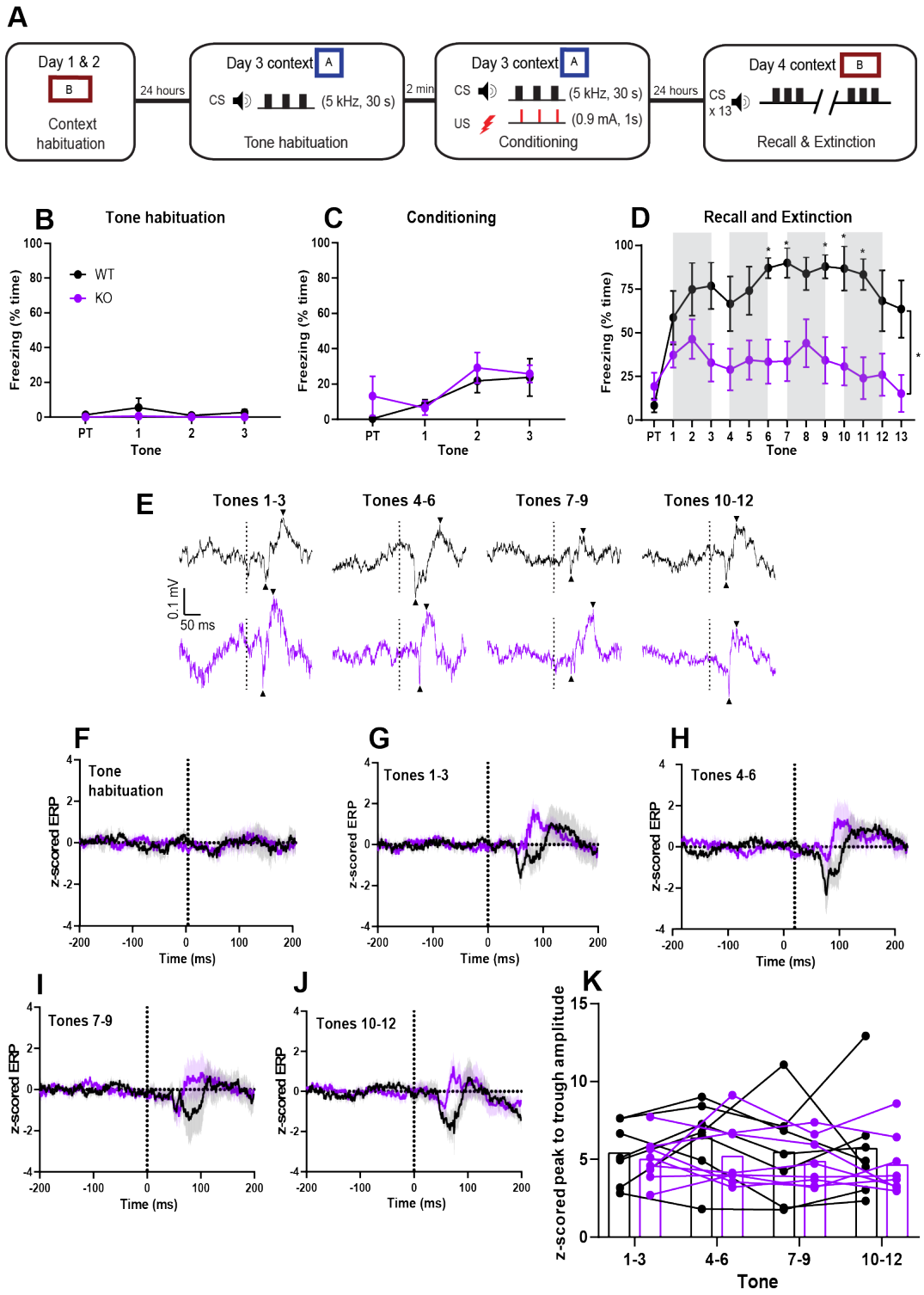

Figure 4.1: Tone-evoked LFP amplitude is unchanged in *Nlgn3*$^{-/y}$ rats during fear recall

Figure 4.1 ***(previous page)*****: Tone-evoked LFP amplitude is unchanged in *Nlgn3*$^{-/y}$ rats during fear recall.** (A) Protocol diagram for auditory fear conditioning paradigm. (B) Both WT and *Nlgn3*$^{-/y}$ rats display very little freezing behaviour during tone habituation (WT n = 7, KO n = 8, p = 0.082, F = 3.78, repeated measures two way ANOVA). (C) Comparable % time freezing in WT and *Nlgn3*$^{-/y}$ rats during conditioning (WT n = 7, KO n = 8, p = 0.41, F = 0.74, repeated measures two way ANOVA). (D) Reduced time spent freezing in *Nlgn3*$^{-/y}$ rats in comparison to WT throughout fear recall (WT n = 7, KO n = 8, p = 0.0061, F = 12.45, repeated measures two way ANOVA). (E) Representative ERP traces taken from tones 1-3, 4-6, 7-9, and 10-12 for WT (black) and *Nlgn3*$^{-/y}$ (purple) rats. Black arrows denote peak and trough, dotted line represents tone onset. (F) No significant ERPs during tone habituation for WT (n = 5, p = 0.25, paired t-test) or *Nlgn3*$^{-/y}$ (n = 6, p = 0.093, paired t-test) rats. (G) Significant ERPs were observed in average LFP waveforms after CS onset for tones 1-3 for both WT (n = 7, p = 0.0032, paired t-test) and *Nlgn3*$^{-/y}$ (n = 8, p = 0.0099, paired t-test) rats. (H) Significant ERPs were seen in average LFP waveforms after CS onset for tones 4-6 for both WT (n = 7, p = 0.0030, paired t-test) and *Nlgn3*$^{-/y}$ (n = 8, p = 0.0084, paired t-test) rats. (I) Significant ERPs were observed in average LFP waveforms after CS onset for tones 7-9 for both WT (n = 7, p = 0.029, paired t-test) and *Nlgn3*$^{-/y}$ (n = 8, p = 0.0040, paired t-test) rats. (J) Significant ERPs were seen in average LFP waveforms after CS onset for tones 10-12 for both WT (n = 7, p = 0.0158, paired t-test) and *Nlgn3*$^{-/y}$ (n = 8, p = 0.0046, paired t-test) rats. (K) No significant difference in tone-evoked LFP amplitude during fear recall in WT and *Nlgn3*$^{-/y}$ rats (WT n = 7, KO n = 8, p = 0.42, F = 0.73, repeated measures two-way ANOVA).

Decreased dPAG LFP duration in *Nlgn3*$^{-/y}$ rats during fear recall

The main factor contributing to amplitude of LFPs is thought to be synaptic input. In addition to this, voltage gated ion channels (Reimann et al., 2013) as well as sub-threshold conductances such as I_h (Ness et al., 2016) contribute to LFP waveform. The tone-evoked LFPs recorded during fear recall were similar in amplitude for WT and *Nlgn3*$^{-/y}$ rats, however the duration of these LFPs was significantly decreased throughout recall and extinction in *Nlgn3*$^{-/y}$ rats (Fig. 4.2). This demonstrates that although amplitude is not changed, the tone-evoked LFPs seen in the dPAG of *Nlgn3*$^{-/y}$ rats are not comparable to those of WT rats.

Histology

Following auditory fear conditioning and recording of LFPs, the electrode placement was confirmed via lesioning. All animals included in the analyses above had electrode sites confirmed within the boundaries of the dPAG (Fig. 4.3).

4.2.2 *In vivo* dPAG stimulation in *Nlgn3*$^{-/y}$ rats

Behavioural testing of *Nlgn3*$^{-/y}$ rats showed that, when given repeated foot-shocks of increasing intensities, shock threshold required to elicit first response was not different

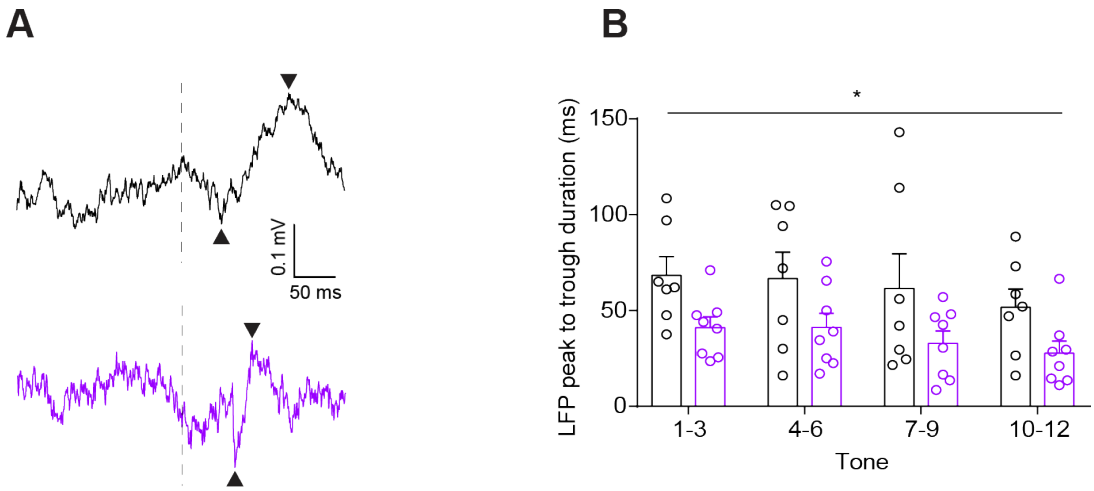

Figure 4.2: Shorter duration ERPs in dPAG of *Nlgn3*$^{-/y}$ rats during fear recall. (A) Representative raw ERP traces for WT (black) and *Nlgn3*$^{-/y}$ (purple) rats. Black arrows indicate trough and peak of ERP. (B) *Nlgn3*$^{-/y}$ rats show significantly faster LFPs evoked by tone onset during fear recall (WT n = 7, KO n = 8, p = 0.042, F = 5.09, two-way ANOVA).

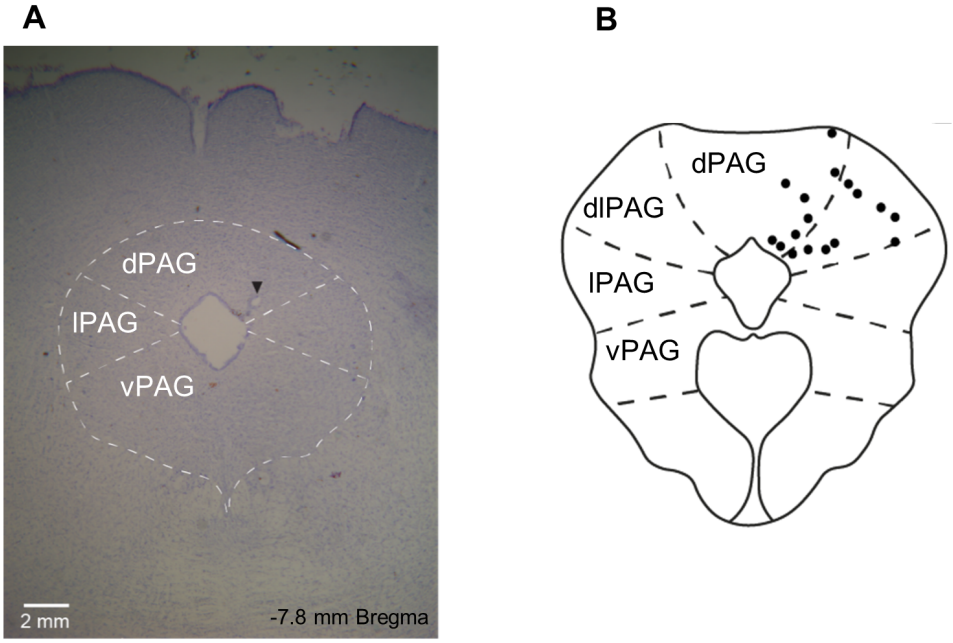

Figure 4.3: Confirmation of LFP electrode sites (A) Example of a nissl stained section showing electrode site in dorsal PAG. Black arrow denotes lesion site. (B) Electrode sites from all animals included in analysis projected onto a schematic of the PAG. Black dots represent individual animals.

between *Nlgn3*$^{-/y}$ and WT rats (Fig. 1.8B-C), however, they do display significantly more jumps in response to the foot-shocks (Fig. 1.8D). If the foot-shocks in Figure 1.8 are preferentially activating the dPAG in *Nlgn3*$^{-/y}$ rats, we would expect that increasing intensities of direct dPAG stimulation would cause similar jumping behaviour at a lower threshold in *Nlgn3*$^{-/y}$ rats in comparison to WTs. Accordingly, I examined behavioural responses of WT and *Nlgn3*$^{-/y}$ rats to *in vivo* electrical stimulation of the dPAG.

Increased jumping behaviour in *Nlgn3*$^{-/y}$ rats in response to dPAG stimulation

Incremental stimulation of the dPAG has been shown to elicit jumping responses (Kim et al., 2013; Vianna and Brandão, 2003; Bittencourt et al., 2004; Schenberg et al., 1990; Fanselow et al., 1995). Furthermore, *Nlgn3*$^{-/y}$ rats have been shown to display increased jumping behaviour (Fig. 1.8). In order to assess fear responses elicited by dPAG stimulation, rats were bilaterally implanted with stimulating electrodes, and following 1 week recovery, habituated to a context for 2 days. The next day, these rats were reintroduced to the context and given increasing dPAG stimulations from 30-75 μA in 5 μA steps (Fig. 4.4A). Behavioural response to each stimulation was observed. As seen in paradigms utilising foot-shocks (Figs. 1.5, 3.19), throughout the entire protocol classic freezing behaviour was significantly lower in *Nlgn3*$^{-/y}$ rats in comparison to WT (Fig. 4.4C). Freezing increased with dPAG stimulation up to a maximum of ∼60 % in WT rats, and only ∼35 % in *Nlgn3*$^{-/y}$ rats. It is important to note that freezing behaviour was rarely seen as an initial response to dPAG stimulation, and instead occurred for a prolonged period following the initial reaction (also described in Brandão and Lovick (2019)).

Immediately following stimulation of the dPAG, an initial reaction could be observed in the period of approximately 1-5 seconds following the stimulation. Analysis of this period revealed that a significantly higher percentage of *Nlgn3*$^{-/y}$ rats exhibited jumping behaviour in response to dPAG stimulations in comparison to WT rats (Fig. 4.4E). This was particularly the case at higher dPAG stimulations of 60 μA (20 % WT, 77.8 % KO), 65 μA (20 % WT, 66.7 % KO) and 70 μA (20 % WT, 77.8 % KO). Furthermore, over the course of the stimulations, this jumping behaviour resulted in escape out of the arena in 56 % (5/9) of *Nlgn3*$^{-/y}$ rats; significantly more than the 20 % (1/5) WT that also successfully escaped. Running behaviour was also significantly increased in

Nlgn3$^{-/y}$ rats (Fig. 4.4F). Running behaviour was seen more in *Nlgn3*$^{-/y}$ rats at medium stimulation intensities of 50 μA (20 % WT, 55.56 % KO) and 55 μA (0 % WT, 66.67 % KO). There were no differences between genotypes in the occurrence of startle or attention responses (Fig. 4.4G-H). For details on behavioural response classification see Methods section 2.6.5.

These results show that *in vivo* dPAG stimulation results in more active fear responses and less passive responses in *Nlgn3*$^{-/y}$ rats in comparison to WT rats. This provides further support of the hypothesis that *Nlgn3*$^{-/y}$ rats display a circuit bias towards flight, rather than freeze, behaviours in response to fearful stimuli.

No difference in jumping of *Nlgn3*$^{-/y}$ rats in response to single dPAG stimulation

Stimulation of the dPAG is known to act as a US and cause fear conditioning (Di Scala et al., 1987; Kim et al., 2013), and therefore animals undergoing the protocol depicted in Figure 4.4A were likely forming an association between their context and the US (dPAG stimulation). The relatively high levels of freezing shown even 3-6 minutes following 75 μA stimulation in both WT and *Nlgn3*$^{-/y}$ rats (Fig. 4.4B) suggests evidence of fear conditioning during this paradigm.

In order to assess the effect of escape-provoking dPAG stimulation in *Nlgn3*$^{-/y}$ rats without the cumulative effect of repeated stimulations, the same animals were given a single 60 μA dPAG stimulation approximately 1 week later (Fig. 4.5A). Both WT and *Nlgn3*$^{-/y}$ rats did not respond with freezing behaviour on re-entry into the arena (Fig. 4.5B), suggesting any contextual fear conditioning undergone had been extinguished or forgotten. Following a single 60 μA stimulation to dPAG, similar percentages of WT and *Nlgn3*$^{-/y}$ rats displayed jumping (40 % WT, 44.44 % KO), startle (0 % WT, 11.11 % KO), and attention (20 % WT, 33.33 % KO) responses (Fig. 4.5C). Significantly fewer *Nlgn3*$^{-/y}$ rats responded with running behaviour (60 % WT, 33.33 % KO, Fig. 4.5C). Additionally, WT rats exhibited post-response freezing for an average of 41.49 % of the following 3 minutes, and *Nlgn3*$^{-/y}$ rats also displayed similar freezing levels; an average of 52.69 % of 3 minutes (Fig. 4.5B).

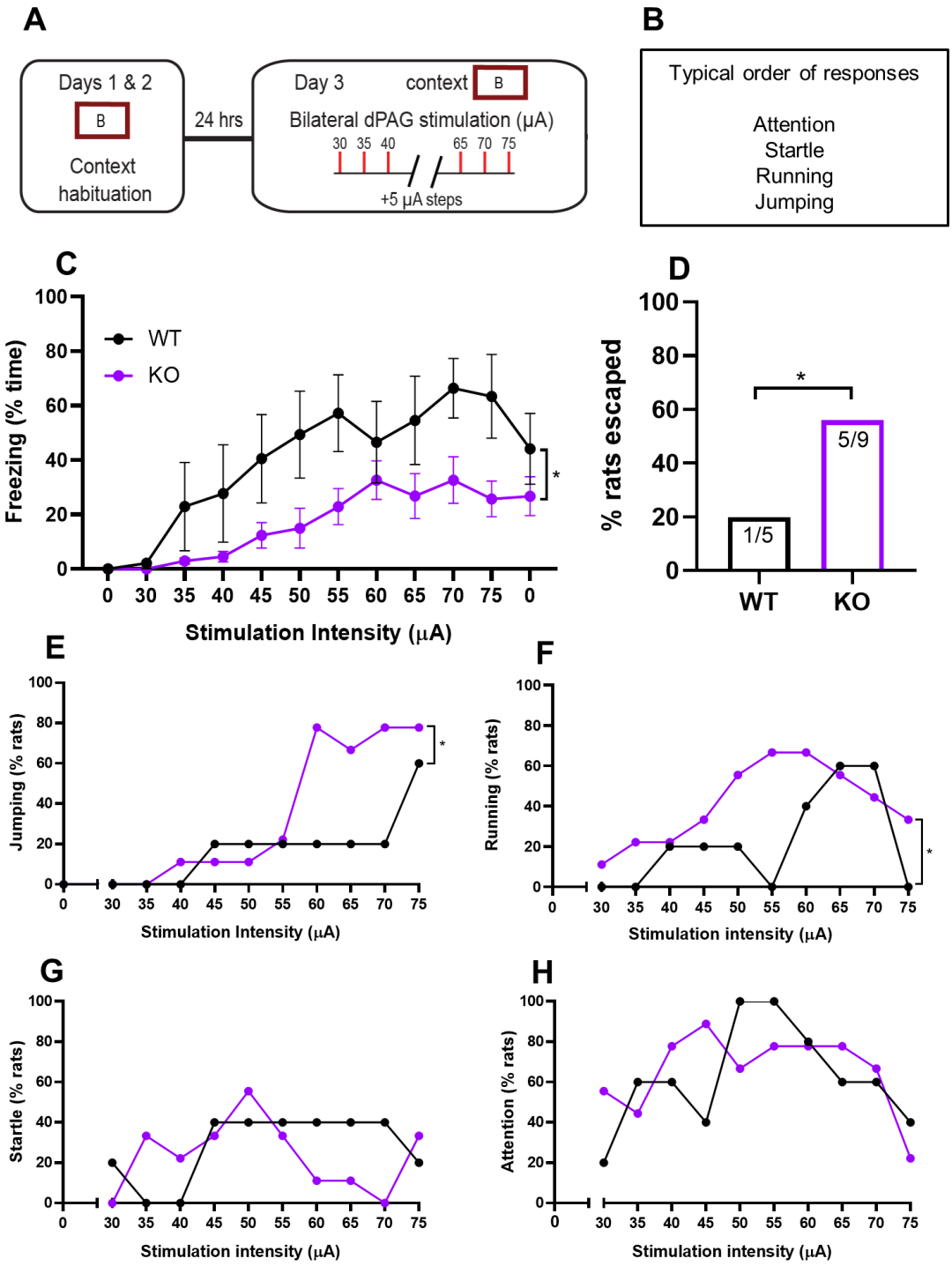

Figure 4.4: Decreased freezing and increased jumping in *Nlgn3*$^{-/y}$ rats in response to increasing dPAG stimulations.

Figure 4.4 ***(previous page)*****: Decreased freezing and increased jumping in** ***Nlgn3*** $^{-/y}$ **rats in response to increasing dPAG stimulations.** (A) Protocol diagram depicting dPAG stimulation paradigm. (B) Typical order of responses seen in rats receiving repeated dPAG stimulations in incremental steps. (C) Percentage time freezing is significantly lower for WT in comparison to *Nlgn3*$^{-/y}$ rats (WT n = 5, KO, n = 9, p = 0.025, F = 6.58, repeated measures two-way ANOVA). Each data point is average % time freezing over the entire 3 minute interval following stimulation. (D) Significantly more *Nlgn3*$^{-/y}$ rats successfully escaped the arena following dPAG stimulation in comparison to WT rats (WT n = 5, KO n = 9, p < 0.0001, Fisher's exact test). (E) Significantly higher proportion of *Nlgn3*$^{-/y}$ rats display jumping behaviour in comparison to WT (WT n = 5, KO n = 9, p = 0.0065, Fisher's exact test). (F) Increased percentage of *Nlgn3*$^{-/y}$ rats display running behaviour in comparison to WT (WT n = 5, KO n = 9, p = 0.0059, Fisher's exact test). (G) No difference in percentage of rats displaying startle responses between WT and *Nlgn3*$^{-/y}$ rats (WT n = 5, KO n = 9, p = 0.52, Fisher's exact test). (H) No difference between WT and *Nlgn3*$^{-/y}$ rats in occurrence of attention response (WT n = 5, KO n = 9, p = 0.66, Fisher's exact test).

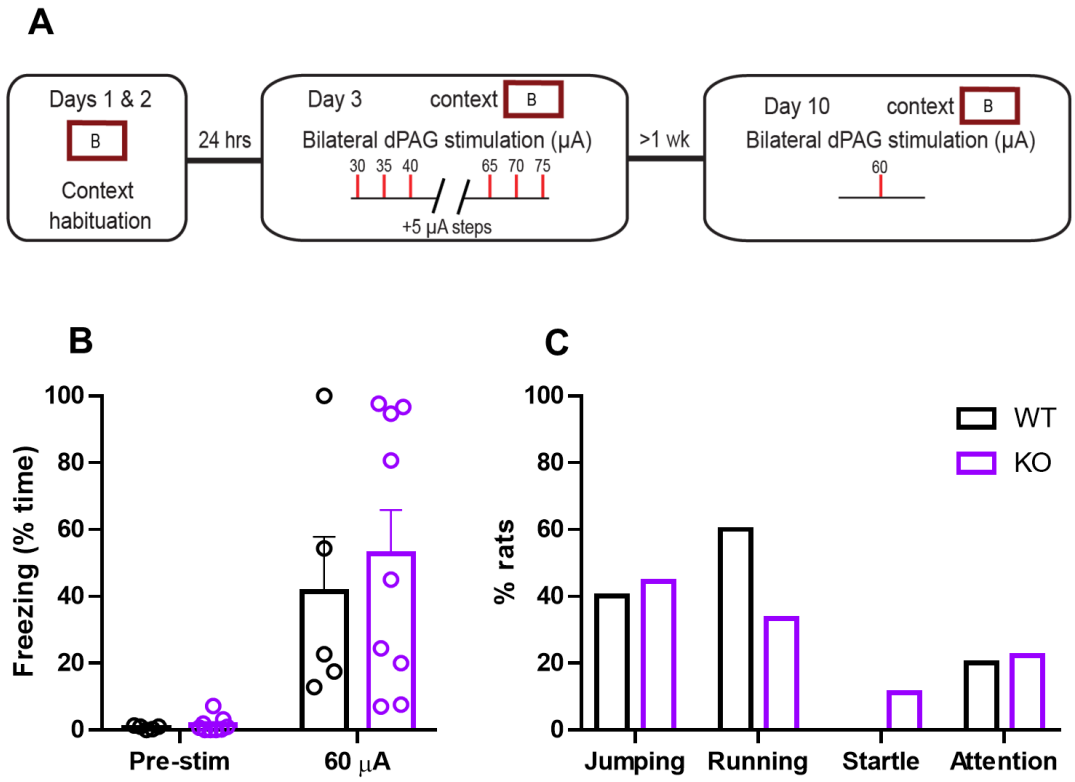

Figure 4.5: No difference in response behaviour of ***Nlgn3*** $^{-/y}$ **rats following single dPAG stimulation.** (A) Protocol diagram depicting dPAG single stimulation paradigm. (B) Percentage time freezing is comparable between WT and *Nlgn3*$^{-/y}$ rats both before dPAG stimulation and after (WT n = 5, KO n = 9, p = 0.59, F = 0.31, repeated measures two-way ANOVA). (C) Similar percentages of rats exhibited jumping (p = 0.67) and attention (p = 0.86) responses, and significantly fewer *Nlgn3*$^{-/y}$ rats exhibited running responses (p = 0.0002) immediately following dPAG stimulation (n = 5 WT, n = 9 KO, Fisher's exact tests). Statistical testing was not performed on startle responses as 0 WT and 1 *Nlgn3*$^{-/y}$ rat exhibited this response.

Therefore although dPAG stimulation caused increased active fear responses when repeated stimulations were given, the fear response of *Nlgn3*$^{-/y}$ rats is comparable to WTs when given a single stimulation following potential priming a week prior. This suggests that the effect seen in Figure 4.4 may be in part a consequence of the fear conditioning properties of dPAG stimulation (Di Scala et al., 1987; Kim et al., 2013), rather than dPAG stimulation alone.

No defensive responses evoked by somatosensory cortex stimulation in WT or *Nlgn3*$^{-/y}$ rats

To confirm that defensive reactions evoked by increasing stimulations of the dPAG were due to activation of the PAG and not a direct reaction of electrical stimulation itself, a subset of WT and *Nlgn3*$^{-/y}$ rats (WT n = 2, KO n = 2) were implanted with stimulating electrodes in primary somatosensory cortex. Repeated increasing stimulations from 30-75 μA to S1 resulted in none of the previously seen (Fig. 4.4) fear responses at any stimulation intensity. Freezing behaviour was also scored throughout this protocol, and although some immobility indistinguishable from true fearful freezing was observed (Fig. 4.6), the same profile of post-stimulation activity burst followed by freezing behaviour (Fig. 4.4C) was not seen. This result suggests that dPAG stimulation elicits defensive reactions that are due to activation of dPAG neurons as opposed to by the stimulation itself.

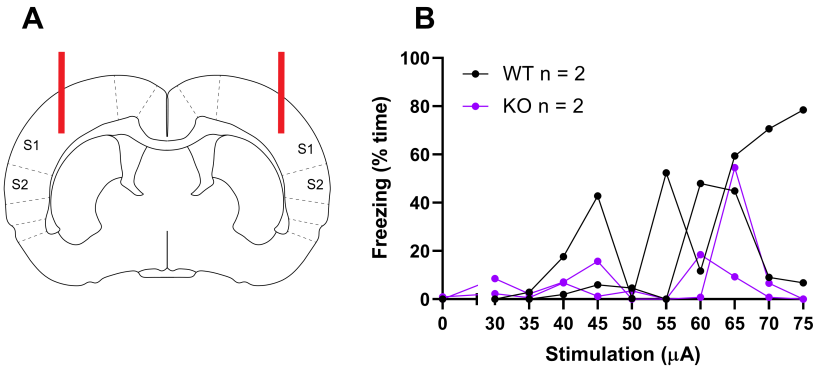

Figure 4.6: No defensive reactions elicited by S1 barrel cortex stimulation. (A) Schematic depicting electrode implant site. Red lines denote stimulating electrodes. (B) Freezing behaviour, defined as no movement except for respiration, in 2 WT and 2 *Nlgn3*$^{-/y}$ rats throughout repeated increasing intensities of S1 stimulation. Connected lines represent an individual animal, points represent average freezing time for 3 minutes post-stimulation.

Histology

After dPAG stimulation experiments, the electrode placements were confirmed through lesioning. All animals included in the analysis above had electrode sites confirmed within the boundaries of the dPAG/lPAG (Fig. 4.7).

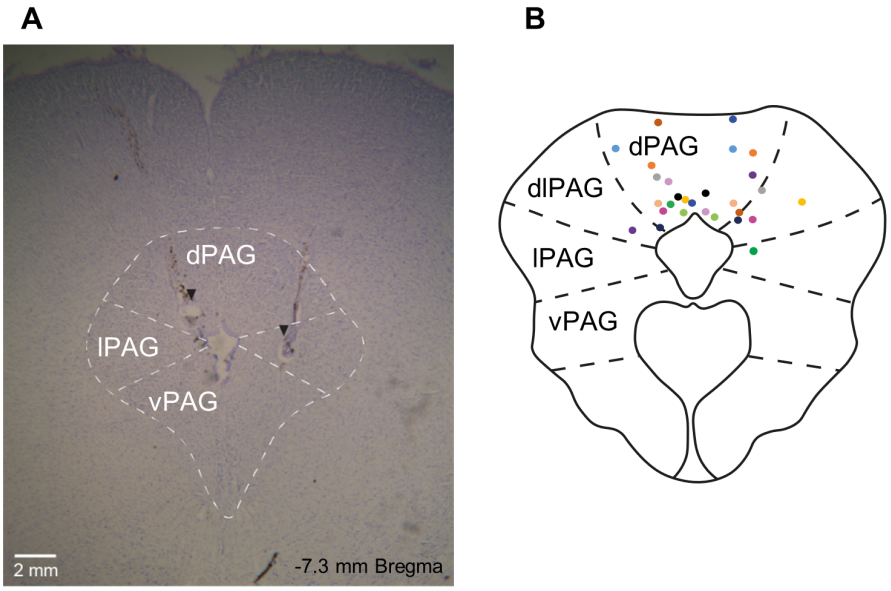

Figure 4.7: Confirmation of stimulation electrode sites (A) Example of a nissl stained section showing electrode site in dorsal PAG. Black arrow denotes lesion site. (B) Electrode sites from all animals included in analysis projected onto a schematic of the PAG. Pairs of coloured dots represent electrodes in each dPAG hemisphere of an individual animal.

4.3 Discussion

The results presented in this chapter build both on the behavioural data shown in introductory Figures 1.5, 1.7, 1.9 and 1.8, and on the *ex vivo* electrophysiology data shown in the previous chapter of this thesis (Figs. 3.13, 3.16, 3.18). The data presented here provide evidence that *Nlgn3*$^{-/y}$ rats display tone-evoked LFPs in the dPAG during fear recall that are of a similar amplitude, but shorter duration, than those of WT rats. Furthermore, this chapter describes the effect of repeated *in vivo* dPAG stimulation in WT and *Nlgn3*$^{-/y}$ rats, showing increased incidence of active fear responses and decreased incidence of passive fear responses in *Nlgn3*$^{-/y}$ rats. This effect however, was not observed when WT and *Nlgn3*$^{-/y}$ rats were given only a single dPAG stimulation.

4.3.1 Reduced freezing behaviour in *Nlgn3*$^{-/y}$ rats during fear recall

The auditory fear conditioning paradigm shown in Figure 4.1 was carried out as similarly as possible to that shown in Figure 1.5. In both cohorts of animals, *Nlgn3*$^{-/y}$ rats display significantly less classic freezing behaviour than their respective WT controls. However, it is important to note that the freezing profiles differ between the two experiments for both WT and *Nlgn3*$^{-/y}$ rats. Firstly, in Figure 4.1C, during the conditioning phase, the genotype effect observed in 1.5B is not seen. This is not due to a relative increase in freezing of *Nlgn3*$^{-/y}$ rats, but the overall amount of freezing behaviour exhibited by WTs is lower in comparison to Figure 1.5B. Secondly, the extinction profile of reduced freezing over time seen in Figure 1.5C cannot be seen to the same extent in Figure 4.1D. Lastly, overall freezing behaviour exhibited by *Nlgn3*$^{-/y}$ rats during fear recall is, although significantly lower than WT controls, slightly higher than was seen in Figure 1.5C. These differences in the fear conditioning and extinction profiles may be due to several unavoidable differences between the experimental procedures, as discussed below.

First, animals contributing to the data presented in this chapter had undergone surgery one week prior to auditory fear conditioning. Although care was taken to ensure full recovery of the animals, and all animals were handled for three days prior to the start of the experiment, this undoubtedly stressful procedure may have had consequences on the prior 'fear state' of rats before fear conditioning had even begun. Furthermore, post-operative cognitive dysfunction is a phenomenon known to occur particularly in

elderly humans (reviewed in Kotekar et al. (2018)), however literature investigating the causes of this in rodents often find contradicting results (An et al., 2013; Wan et al., 2007; Wuri et al., 2011; Netto et al., 2018). Nonetheless, it is possible that surgery influences both the stress level and learning abilities of rats.

Second, as animals used for the experiments in this chapter had undergone surgery, they were also single-housed following the procedure to allow full recovery of the wound under the Home Office guidelines. Animals used for behavioural experiments shown in Figure 1.5 were housed in groups of 4. Social isolation of adult for 3-4 weeks has been shown to impair fear extinction (Pibiri et al., 2008), and longer term (12 week) isolation in adult rats results in more risk-taking behaviours and increased spontaneous exploration (Thorsell et al., 2006). Although social isolation was only for one week here, some effects on fear conditioning encoding and exploratory behaviour could be present.

Third, in order to record LFPs evoked by the CS-onset, a tone habituation phase also needed to be included in the protocol used for Figure 4.1 in order to confirm the unconditioned tone does not cause significant LFPs in the dPAG. The introduction of this tone habituation phase immediately prior to conditioning could have interfered with the encoding of the CS-US association, and resulted in an effect more similar to a trace conditioning paradigm, which is known to cause generalised freezing behaviour, rather than classical CS-US associative pairing (Curzon et al., 2014).

Fourth, in the fear conditioning experiment presented in this chapter, animals were handled for three days prior to habituation. Contrastingly, animals contributing to the data shown in Figure 1.5 had undergone two other behavioural tasks on the weeks prior to these experiments; marble burying and object recognition. These behavioural tasks were not expected to interfere with auditory fear conditioning, however the differences in the amount of handling may have affected the fear extinction profiles. Campeau et al. (1991) showed increases in c-fos expression in the amygdala caused by handling alone, however this effect was eliminated by repeated handling for ten days. Furthermore, Cho et al. (2017) provided evidence that four days of handling did not attenuate handling-induced c-fos expression in the amygdala. This could therefore have resulted in differences in the fear expression profiles observed between the two experiments.

Overall, despite the preservation of the phenotype in *Nlgn3*$^{-/y}$ rats during fear recall, the differences between these two protocols introduced several important considerations that may have affected rat behaviour. Although this does not affect the conclusions

that can be drawn from this data, it highlights the complexity of controlling all the variables for a behavioural paradigm, and provides further evidence that factors such as social isolation and handling do affect the fear state of an animal.

4.3.2 Tone-evoked LFPs in the dPAG during fear recall

Recall of a fear memory following fear conditioning is known to evoke activity in PAG neurons (Watson et al., 2016). Additionally, Watson et al. (2016) showed that tone-evoked LFPs in the PAG reduce in amplitude during CS-US extinction, correlating with reduction in freezing behaviour. However, despite significant decreases in classic freezing behaviour observed in *Nlgn3*$^{-/y}$ rats (Fig. 4.1D) no changes in LFP amplitude were observed (Fig. 4.1J). Interestingly, duration of the LFPs were significantly decreased throughout fear recall in *Nlgn3*$^{-/y}$ rats in comparison to WTs (Fig. 4.2).

The amplitude of LFPs are thought to predominantly reflect the synaptic input received by a population of neurons. Combined intracellular and LFP recordings have demonstrated a close relationship between LFP activity and synaptic potentials (Haider et al., 2016), and in addition, active conductances are thought to affect LFP waveform (Ness et al., 2016, 2018; Reimann et al., 2013). Conversely, action potentials themselves are thought to contribute very little to the size of an LFP (Herreras, 2016). In Chapter 3, I provide evidence that there is no change in excitatory synaptic input onto dPAG neurons. If synaptic input is the predominant factor contributing to LFP size, these data agree with the results in this chapter showing that tone-evoked LFPs in the dPAG during fear recall are comparable in amplitude to WT.

Furthermore, the results presented in section 4.2.1 demonstrate that LFPs recorded from the dPAG during fear recall are not reflective of fear response behaviour. Watson et al. (2016) reported attenuation of tone-evoked LFP size in the PAG during fear extinction, corresponding with a reduction in freezing behaviour exhibited by the mice. However, despite significantly decreased freezing behaviour seen in *Nlgn3*$^{-/y}$ rats (Fig. 4.1D), LFPs observed in the dPAG were largely normal. This suggests that the reduction LFP amplitude reported by Watson et al. (2016) may reflect the extinction of fear, rather than the change in freezing behaviour. This distinction is interesting, as it suggests that LFPs recorded from the PAG may indicate activities of neurons involved in encoding fear, rather than the physical responses of flight or freeze. Furthermore, if this is the case, then the presence of normal amplitude LFPs in the dPAG of *Nlgn3*$^{-/y}$

rats provides further evidence of CS-US association in this model, again suggesting that the reduced freezing is a change in fear response behaviour rather than a fear learning deficit.

Observed LFPs were not, however, completely analogous between WT and *Nlgn3*$^{-/y}$ rats. Figure 4.2 shows a decrease in LFP duration in *Nlgn3*$^{-/y}$ rats in comparison to WTs. The duration of an LFP may be, in part, affected by the presence of active conductances. Studies modelling LFPs have demonstrated the presence of active conductances in the neuronal membrane result in decreased LFP duration (Ness et al., 2016; Reimann et al., 2013). The changes in fAHP reported in Chapter 3 (Fig. 3.14) indicates altered active currents, perhaps involving BK channels (Poolos and Johnston, 1999), in *Nlgn3*$^{-/y}$ dPAG neurons and which may contribute towards changes in LFP width observed here. Interestingly, Kurt et al. (2008) reported increased tone-evoked LFP width (recorded from auditory cortex in gerbils) with application of bicuculline, a potent antagonist of $GABA_A$ receptors. Therefore, another possible explanation for decreased LFP duration in *Nlgn3*$^{-/y}$ rats is increased $GABA_A$-mediated inhibitory synaptic drive to dPAG neurons, which may have led to homeostatic increases in intrinsic excitability (Turrigiano and Nelson, 2004) and thus increased flight behaviour. Further investigation is needed to interrogate this.

Direct comparisons between arbitrary measurements such as LFP size/shape and biologically relevant conclusions must be drawn with care, as many factors can contribute to the size and shape of LFPs, most notably the geometry of the brain area recorded (Herreras, 2016). Furthermore, the spatial resolution of LFPs is a point of debate within the field. There is evidence to show LFPs have a spatial resolution of <1 mm (for example see Destexhe et al. (1999); Katzner et al. (2009); Xing et al. (2009)), however several studies also show volume conductance within some brain regions allows the recording of LFPs originating many millimetres from the electrode site (Herreras, 2016; Kajikawa and Schroeder, 2011).

Accordingly, to further investigate the activity of the dPAG during fear recall of *Nlgn3*$^{-/y}$ rats, single-unit recordings may provide an interesting source of information. As dPAG neurons *ex vivo* displayed increased firing frequencies both at resting membrane potential (Fig. 3.12) and in response to depolarising current injections (Fig. 3.13), recording single-unit spiking *in vivo* would allow investigation of the hypothesis that hyperexcitability of this brain area underpins the increased flight behaviours observed

in *Nlgn3*$^{-/y}$ rats.

4.3.3 Behavioural responses to dPAG stimulation

The second part of this chapter describes the behavioural responses caused by dPAG stimulation in WT and *Nlgn3*$^{-/y}$ rats. There have been many studies demonstrating that dPAG stimulation results in active fear responses such as jumping and running (Kim et al., 2013; Vianna and Brandão, 2003; Bittencourt et al., 2004; Schenberg et al., 1990; Fanselow et al., 1995). Additionally, following this initial burst of activity, dPAG stimulation is known to induce freezing behaviour (Carvalho et al., 2015; Brandão and Lovick, 2019; Kim et al., 2013). Both initial active responses and post-stimulation freezing were observed in WT and *Nlgn3*$^{-/y}$ rats following dPAG stimulation. Similar dPAG stimulation amplitudes were used to evoke flight responses in the experiments contributing to this chapter as in Kim et al. (2013), however *Nlgn3*$^{-/y}$ rats displayed a tendancy to exhibit flight responses at lower dPAG stimulation intensities (Fig. 4.4).

It is possible that, rather than an increase in active fear responses, the results presented in this chapter and the introduction of this thesis could be interpreted as motor hyperfunction causing jumping behaviour. However, as both running and jumping responses were increased in dPAG-stimulated *Nlgn3*$^{-/y}$ rats, this provides evidence that it is not a single motor activity that is increased in these rats but rather the elicitation of escape-like behaviours. Furthermore, the data presented in Figures 4.4D and 1.7 shows *Nlgn3*$^{-/y}$ rats demonstrating goal-directed escape out of the arena, as opposed to indiscriminate jumping. Additionally, in an open field task *Nlgn3*$^{-/y}$ rats did not show changes in distance travelled or velocity (Fig. 1.6), suggesting basal activity levels in neutral (non-fearful) contexts are not increased in *Nlgn3*$^{-/y}$ rats. Overall, these data suggest that active defensive responses involving the dPAG are increased in *Nlgn3*$^{-/y}$ rats.

When considering increased dPAG-induced flight behaviours in *Nlgn3*$^{-/y}$ rats, two main points of consideration must be highlighted: first, that repeated dPAG stimulations are themselves likely to have an additive effect on behaviour, and second, that the implementation of repeated dPAG stimulations are likely to have long lasting effects on future behavioural testing.

With regard the first point, fear conditioning that can be caused by dPAG stimulation (Di Scala et al., 1987; Kim et al., 2013) may have been causing further fear

responses in these rats in addition to the post-stimulation freezing behaviour (Fig. 4.4C) (Carvalho et al., 2015; Brandão and Lovick, 2019; Kim et al., 2013). Johansen et al. (2010) demonstrated that the conditioning effect of dPAG stimulation was eliminated by lesioning of the basolateral amygdala. As the results presented in this chapter show an increase in active fear response behaviours in *Nlgn3*$^{-/y}$ rats given repeated dPAG stimulations, but not in *Nlgn3*$^{-/y}$ rats given a single dPAG stimulation, this phenotype may therefore be due to increased strength of dPAG-BLA connectivity activated during fear conditioning, and not hyperexcitability of the dPAG alone. Supporting this, data from whole-cell patch-clamp recordings of the lateral amygdala revealed neurons in this area are hyperexcitable in *Nlgn3*$^{-/y}$ rats (Dr Anna Toft, University of Edinburgh, PhD thesis, 2019).

With regard to second point, studies carried out by de Almeida et al. (2006) and Carvalho et al. (2018) investigated the effects of dPAG stimulation on 'long-term' behaviour. In these studies, rats were given repeated incremental dPAG stimulations until an active fear response such as running or jumping was observed. Following this, an increase in generalised anxiety-like behaviours were seen in these rats for up to 7 days post-stimulation. Therefore, even though rats contributing to the results in this chapter did not display context-dependent freezing behaviour when they were reintroduced to the arena (Fig. 4.5B), their behavioural responses may still have been influenced by previous stimulations the week prior.

Interestingly, both of these studies (de Almeida et al., 2006; Carvalho et al., 2018) reported large inter-animal variability in the stimulation required to evoke defensive behaviours. This may be due to differences between the animals themselves, or due to specific electrode placement or impedance. It therefore may have been more pertinent for the single-stimulation experiment to give each animal the appropriate stimulation that elicited defensive reactions in that particular rat, rather than using 60 μA for all animals. This may have resulted in less inter-animal variability in the behaviours seen in response to a single dPAG stimulation.

Overall, *in vivo* stimulation of the dPAG in WT and *Nlgn3*$^{-/y}$ rats provided further evidence of reduced threshold in the dPAG for elicitation of active fear responses in *Nlgn3*$^{-/y}$ rats. The contradictory phenotype observed during single, rather than repeated, dPAG stimulation has implications for the involvement of other brain areas in the wider fear circuitry in this phenotype; particularly the involvement of dPAG-BLA connectivity.

The effect of a single 60 μA stimulation without the potentially priming effects of previous repeated stimulations is still to be determined, but would provide further information regarding this phenotype.

4.3.4 Conclusions on PAG dysfunction in the *Nlgn3*$^{-/y}$ rat model

The results presented in this chapter, in combination with Chapter 3, leads to several interesting potential conclusions that can be drawn using data that are a combination of *ex vivo* and *in vivo* experimental approaches. In Chapter 3, I provide evidence that dPAG, but not vPAG, neurons are hyperexcitable and display increased release probability in *Nlgn3*$^{-/y}$ rats. The nature of neurons contributing to this hyperexcitability is not known, however clustering analysis suggests they may be GABAergic. In this chapter, I find that *Nlgn3*$^{-/y}$ rats display shorter duration, but normal amplitude, LFPs during fear recall, and reduced threshold of dPAG-evoked escape behaviours. Together, these data suggest that the increased excitability of neurons in the dPAG of *Nlgn3*$^{-/y}$ rats may lead to reduced "synaptic threshold" (Evans et al., 2018), meaning less input from sensory and limbic brain regions might be required in order for an active fear response to be elicited by the dPAG. Understanding the true nature of the dPAG neurons that are contributing to this hyperexcitability in *Nlgn3*$^{-/y}$ rats is of great importance, as it will affect conclusions regarding how circuitry is affected in this model of ASD. Furthermore, the increased release probability in a subpopulation of dPAG-vPAG synapses in *Nlgn3*$^{-/y}$ rats agrees with data from Tovote et al. (2016). It suggests that the increased flight behaviour of *Nlgn3*$^{-/y}$ rats shown in this chapter is not simply a consequence of increased dPAG activity, but also of increased dPAG-induced suppression of the freeze-promoting vPAG.

In addition, the decreased freezing behaviour during fear recall was not associated with decreased tone-evoked LFP amplitude in the PAG of *Nlgn3*$^{-/y}$ rats; a correlation that was previously identified by Watson et al. (2016). This implies tone-evoked PAG LFP amplitudes during fear recall are reflective of fear, as oppose to fear response behaviour. Nonetheless, the data shown in this chapter demonstrates that the LFPs recorded in the dPAG of *Nlgn3*$^{-/y}$ rats during fear recall were of shorter duration than those of WT rats. The biological relevance of this finding is still unclear, however one explanation is provided by the increased fAHP amplitude identified in *ex vivo* whole-cell patch clamp recordings in chapter 3. As voltage-gated ion channels have been suggested

to affect LFP waveform (Reimann et al., 2013; Ness et al., 2016, 2018), the altered BK channel conductance implicated by the reduced fAHP observed in dPAG neurons may be contributing towards this phenotype.

Overall, the data presented in Chapters 3 and 4 of this thesis suggests that alterations in the properties of dPAG neurons in *Nlgn3*$^{-/y}$ rats leads to atypical fear response behaviours exhibited in these rats.

4.4 Summary

In summary, the results presented in this chapter provide further evidence that *Nlgn3*$^{-/y}$ rats display decreased freezing and increased flight responses. Additionally, these results suggest that the threshold of dPAG activation required to elicit flight responses is reduced in *Nlgn3*$^{-/y}$ rats, however synaptic input to this brain area is unchanged. This exposes several interesting potential avenues of further research examining the circuit dysfunction leading to this phenotype, which may provide important information regarding the pathophysiologies leading to anxiety and panic disorders in ASD/ID.

Chapter 5

Physiology of the hippocampus and prefrontal cortex

5.1 Introduction

The hippocampus (HC) and medial-prefrontal cortex (mPFC) are key parts of the fear circuit (Apps and Strata, 2015; Tovote et al., 2015), crucial for fear learning, recall, and extinction (see section 1.6). In light of the fear-related behavioural phenotypes seen in the *Nlgn3*$^{-/y}$ rat (see section 1.7), further investigation of other brain areas involved in fear learning was required to gain a broader picture of what could be underlying these behaviours. Besides altered flight-freeze responses, *Nlgn3*$^{-/y}$ rats display prolonged avoidance of the previous shock zone during the probe trial of the APA task, in contrast to WTs which learn the zone is now safe (Fig. 1.9H-L). This lack of 're-learning' indicates *Nlgn3*$^{-/y}$ rats may have cognitive inflexibility in this task. Cognitive flexibility is the ability to switch between tasks and learn new rules, and is dependent on plasticity of the mPFC (Torres-García et al., 2017; Bravo-Rivera et al., 2014; Diehl et al., 2018). However, *Nlgn3*$^{-/y}$ rats display enhanced initial learning of the shock zone location in the APA task, suggesting that associative and spatial learning abilities are intact (Figs. 1.9B-G). This chapter therefore firstly aims to investigate cellular correlates of these behaviours by examining the physiology of the HC and mPFC in *Nlgn3*$^{-/y}$ rats.

In addition to this, the work presented in this chapter addresses another question: do genetically diverse models of ASD/ID display common cellular and circuit pathophysiologies? Several previous studies, along with considerable work from our lab (Krumm et al., 2014; Pinto et al., 2014; Barnes et al., 2015; Baudouin et al., 2012) has suggested that there is convergence of cellular and molecular phenotypes between

genetically distinct models of ASD/ID. The prospect of such a diverse spectrum of disorders having converging pathophysiologies is highly attractive, as this suggests that common treatment strategies may be possible.

One potential convergent phenotype between genetically distinct models of ASD/ID that has been highlighted in previous research is dysregulation of protein homeostasis. Increased protein synthesis has been reported in models of Fragile-X syndrome (Osterweil et al., 2010; Barnes et al., 2015; Auerbach et al., 2011), MRD5 (Barnes et al., 2015) and *Eif4ebp*-deletion (Gkogkas et al., 2013). Furthermore, decreased protein synthesis has been reported in a model of Tuberous Sclerosis (Auerbach et al., 2011), and increased protein degradation has been shown to be present in a model of Angelman syndrome (hui Jiang et al., 1998). Changes in protein synthesis are likely to affect synaptic plasticity; and correspondingly abnormal mGluR-dependent LTD has been shown to be a convergent property between many models of ASD/ID, including Fragile-X syndrome (Huber et al., 2002; Barnes et al., 2015; Auerbach et al., 2011), MRD5 (Barnes et al., 2015), *Nlgn3*-deletion (Baudouin et al., 2012), Angelman syndrome (hui Jiang et al., 1998), and Cowden syndrome (Butler et al., 2005). Impaired LTP has also been demonstrated in several models (reviewed in Louros and Osterweil (2016)). Together, these findings suggest convergence at a molecular and synaptic level may exist between genetically distinct forms of ASD/ID. However, convergence or divergence of cellular excitability has not yet been reported. The work presented in this chapter aims to expand on this research by investigating synaptic plasticity and transmission, in addition to cellular intrinsic properties, of the *Nlgn3*$^{-/y}$ and *Nrxn1*$^{+/-}$ rat models of ASD. Due to the similar roles of adhesion molecules that neurexin-1 and neuroligin-3 fulfil at pre- and postsynaptic membranes, depletion of these proteins may result in converging effects on synaptic function and cellular excitability.

5.1.1 *Nrxn1*$^{+/-}$ and ASD/ID

Neurexins (gene: *NRXN*) are brain-specific presynaptic cell-adhesion proteins discovered through study of α-latrotoxin; the toxin from black widow spider venom (Ushkaryov et al., 1992), and are the binding partners of neuroligins. Neurexins are encoded for by three genes; *NRXN1*, *NRXN2*, and *NRXN3*, which are controlled by three promoters (Ullrich et al., 1995; Rowen et al., 2002; Sterky et al., 2017; Yan et al., 2015):

- **α-neurexin.** The α-neurexin promoter is upstream of exon 1 and yields a longer

protein with 6 LNS (laminin/neurexin/sex hormone binding globulin) domains. There are 5 alternative splice sites within α-neurexin.

- **β-neurexin.** The β-neurexin promoter is within the intron downstream of exon 17, and yields a shorter protein with just one LNS domain. There are 2 alternative splice sites within β-neurexin.

- **γ-neurexin.** The γ-neurexin promoter was relatively recently identified and is largely uncharacterised. γ-neurexins lack all extracellular domains (Sterky et al., 2017; Yan et al., 2015).

The combination of several genes, promoters, and extensive alternative splicing, generates thousands of neurexin isoforms, which are thought to encode synapse specificity (Ullrich et al., 1995). Neurexins localise to both excitatory and inhibitory neurons, however each neurexin sub-type (1α, 2α 3α, 1β, 2β, 3β, 1γ, 2γ, 3γ) is differentially distributed in the brain (Ullrich et al., 1995). Similarly to neuroligins, neurexins alone can elicit both excitatory and inhibitory postsynaptic formations in dendrites (Graf et al., 2004; Nam and Chen, 2005), and triple KO mutations of all three α-neurexins (leaving β-neurexins intact) are perinatally lethal (Missler et al., 2003). The extracellular domains of α-neurexins are vital for correct functioning of presynaptic Ca^{2+} channels, including Ca^{2+}-triggered synaptic vesicle release (Missler et al., 2003; Zhang, 2005).

Neurexins (notably neurexin-1α) are known to be involved in the control of synaptic plasticity (Li et al., 2015; Choi et al., 2011; Larkin et al., 2015; Anderson et al., 2015), synaptic transmission (Zhang, 2005; Etherton et al., 2009; Anderson et al., 2015; Missler et al., 2003), and behaviours relating to cognitive function (Dachtler et al., 2015; Anderson et al., 2015; Esclassan et al., 2015). Furthermore, mutations in the *NRXN* genes have been repeatedly found in individuals with ASD and ID. The first evidence for *NRXN1* mutations being involved in the manifestation of ASD was by Friedman et al. (2006), who noted a heterozygous *de novo* CNV in the neurexin-1α promoter in a child with ASD, borderline ID, and ADHD, as well as some vertebral and facial abnormalities. Since this 2006 study, there has been numerous reports of *NRXN1* mutations in patients with neurodevelopmental disorders, including ASD, ID, and schizophrenia (Szatmari et al., 2007; Bucan et al., 2009; Ching et al., 2010; Dabell et al., 2013; Gauthier et al., 2011; Glessner et al., 2009; Kim et al., 2008; Yan et al., 2008; Morrow et al., 2008; Duong et al., 2012; Shah et al., 2010; Pinto et al., 2010;

Harrison et al., 2011; Liu et al., 2012a; Schaaf et al., 2012; Prasad et al., 2012; Girirajan et al., 2013; De Rubeis et al., 2014; O'Roak et al., 2014; Lowther et al., 2017; Wang et al., 2016; Stessman et al., 2017; Onay et al., 2016; Woodbury-Smith et al., 2017; Leblond et al., 2019; Wiśniowiecka-Kowalnik et al., 2010).

The vast majority of individuals presenting with *NRXN1*-associated neurodevelopmental disorders have heterozygote mutations; although biallelic *NRXN1* mutations have also been reported (Castronovo et al., 2019). The *Nrxn1*$^{+/-}$ rat model used in our lab has a heterozygous mutation upstream of exon 1, and therefore disrupts the α-neurexin promoter. It is unknown if the downstream β-neurexin translation is also affected.

5.1.2 Hippocampal and prefrontal cortex dysfunction in ASD/ID

Behavioural data shown in section 1.7 demonstrates that *Nlgn3*$^{-/y}$ rats show decreased freezing during fear recall, however further analysis suggested that this may not be a deficit in fear learning, but a change in fear response behaviour (Fig. 1.5). This hypothesis is supported by the results presented in Chapters 3 and 4, which indicate a circuit bias towards the execution of flight over freeze responses. Furthermore, *Nlgn3*$^{-/y}$ rats display intact spatial learning during the active place avoidance task (Fig. 1.9). The extinction of fear memories and the spatial associative learning in the active place avoidance task are dependent on hippocampal function (Kim et al., 1993; Tang et al., 2003; Cimadevilla et al., 2000).

Additionally, *Nlgn3*$^{-/y}$ rats show decreased entries into the previous shock zone during the probe trial of the active place avoidance task, suggesting that these rats may have impairments in brain areas involved in cognitive flexibility, such as the mPFC (Torres-García et al., 2017; Bravo-Rivera et al., 2014; Diehl et al., 2018). Moreover, the mPFC sends direct connections to the dPAG, which are thought to relay contextual information regarding the fearful stimuli which is important for eliciting appropriate defensive responses (Rozeske et al., 2018; Corcoran and Quirk, 2007; Courtin et al., 2014).

Behavioural testing of the *Nrxn1*$^{+/-}$ rat model revealed that they display a small but significant increase in freezing behaviour during fear recall (Fig. 5.1), which may be reflective of increased basal anxiety or reduced ability to extinguish fear memories. As both the HC and mPFC are required for the acquisition, recall, and extinction of fear

memories, these results suggests there may also be impairments in these brain regions in the *Nrxn1*$^{+/-}$ rat. For these reasons, this chapter examines hippocampal and mPFC physiology in the *Nlgn3*$^{-/y}$ and *Nrxn1*$^{+/-}$ rat models of ASD/ID.

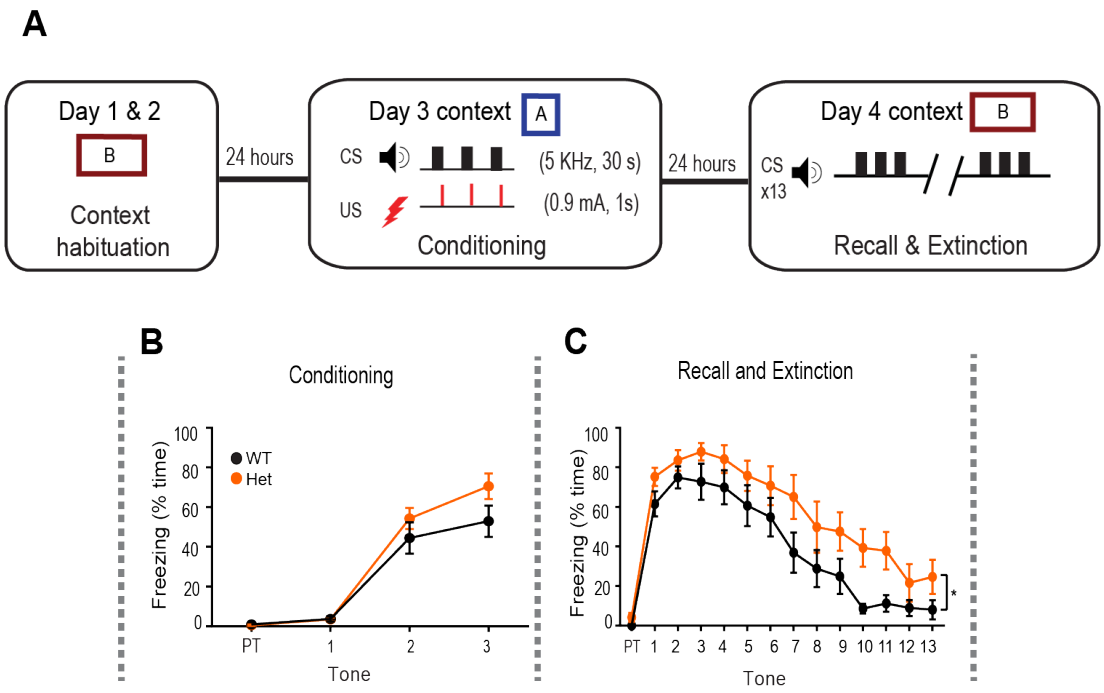

Figure 5.1: *Nrxn1*$^{+/-}$ rats display increased freezing during auditory fear recall. (A) Schematic of auditory fear conditioning paradigm. (B) WT and *Nrxn1*$^{+/-}$ rats display similar freezing levels during auditory fear conditioning (WT n = 12, Het n = 12, p = 0.14, F = 2.36, repeated measures two-way ANOVA). (C) *Nrxn1*$^{+/-}$ rats freeze for significantly more time during fear recall (WT n = 12, Het n = 12, p = 0.038, F = 4.9, repeated measures two-way ANOVA).

5.1.3 Hypothesis and Aims

Neurexin-1 and neuroligin-3 are binding partners required for the maintenance of synapses (Varoqueaux et al., 2006; Missler et al., 2003). Loss of these proteins may lead to impairments in synaptic function, reflected by changes in synaptic plasticity and transmission. Altered synaptic function can also lead to changes in intrinsic excitability (Turrigiano and Nelson, 2004), so neuronal intrinsic properties were also assessed in *Nlgn3*$^{-/y}$ and *Nrxn1*$^{+/-}$ rats. I hypothesised that *Nlgn3*$^{-/y}$ and *Nrxn1*$^{+/-}$ rats would display converging cellular and circuit-level pathophysiologies due to their similar roles at the synapse.

Furthermore, the behavioural studies described in the introduction of this thesis indicate that *Nlgn3*$^{-/y}$ rats have normal associative learning, however they may display cognitive inflexibility (see section 1.7, Fig. 1.9). Given the role of the HC and mPFC in

these executive functions, this chapter addresses the hypotheses that synaptic plasticity in these two brain regions are unaffected and reduced in *Nlgn3*$^{-/y}$ rats, respectively. Moreover, changes in the fear extinction behaviour seen in Figure 5.1 also indicate possible impairments in HC and mPFC plasticity in the *Nrxn1*$^{+/-}$ rat.

I use a combination of extracellular field recordings and whole-cell patch-clamp electrophysiology to assess synaptic plasticity, synaptic function, and neuronal excitability to address these questions.

5.2 Results

5.2.1 Hippocampal plasticity in *Nlgn3*$^{-/y}$ and *Nrxn1*$^{+/-}$ rats

Extracellular field recordings were made from the *stratum radiatum* of pyramidal cells in CA1 of the hippocampus. Electrical stimulation of the Schaffer collateral (SC) pathway reliably results in a fEPSP with a pre-synaptic volley followed by a smooth rising phase, peak, and decay phase which can contain a population-spike. For all analyses performed, the slope of the rising phase was used for quantification as opposed to the peak amplitude. This is because the slope linearly correlates with synaptic conductance, whereas the measurement of peak amplitude may be contaminated by the presence of population-spikes (Johnston and Wu, 1994).

As neuroligin-3 and neurexin-1 are synaptic proteins, full or partial loss may result in reduced synaptic plasticity. To investigate changes in synaptic plasticity in the hippocampus, I applied chemical or electrical stimulation to hippocampal slices from WT, *Nrxn1*$^{+/-}$ and *Nlgn3*$^{-/y}$ rats in which fEPSPs were being recorded.

LTP and LTD can be induced reliably in Schaffer collateral synapses

There are many protocols, both chemical and electrical, for inducing plasticity in CA3-CA1 synapses described in the literature. In this chapter, I utilised a high-frequency stimulation (HFS) protocol of 2 x 100 Hz to produce LTP, a low-frequency stimulation (LFS) protocol of 900 x 1 Hz to induce LTD, and application of S-DHPG (50 μM, 5 minutes) to induce mGluR-dependent LTD. I demonstrated that, following acquisition of a stable baseline, tetanic stimulation of 2 x 100 Hz reliably induced LTP in acute hippocampal slices from p25-35 rats (Fig. 5.2A-B). This form of LTP was NMDAR-dependent (Komiyama et al., 2002) (Fig. 5.2A-B). Secondly, I established

that LFS of 900 pulses at 1 Hz resulted in LTD, which was also NMDAR-dependent (Mulkey and Malenka, 1992) (Fig. 5.2C-D). Lastly, I confirmed that application of S-DHPG resulted in an NMDAR-independent form of LTD in these slices (Oliet et al., 1997) (Fig. 5.2E-F).

NMDAR-dependent LTP is reduced in both *Nlgn3*$^{-/y}$ and *Nrxn1*$^{+/-}$ rats

Nlgn3 R415C mice have previously been shown to have increased hippocampal LTP, whereas *Nlgn3*$^{-/y}$ mice display comparable LTP to WT mice (Etherton et al., 2011). However, Anderson et al. (2015) demonstrated reduced LTP in hippocampal subiculum neurons in *Nrxn1β*$^{-/-}$ mice. Thus, I investigated whether LTP was altered in our *Nrxn1*$^{+/-}$ and *Nlgn3*$^{-/y}$ rat models, using the stimulation protocol outlined above. I found that following HFS, both *Nlgn3*$^{-/y}$ and *Nrxn1*$^{+/-}$ rats displayed LTP (*Nlgn3*$^{-/y}$ 10.6% ± 5.53%; *Nrxn1*$^{+/-}$ 11.74% ± 4.56%) that was significantly reduced in comparison to WT controls (Fig. 5.3, *Nlgn3*$^{+/y}$ 42.7% ± 8.96%; *Nrxn1*$^{+/+}$ 35.52% ± 5.64%). This suggests that both models of ASD/ID show some converging phenotypes in the hippocampus which may be due to NMDAR dysfunction.

Reduced NMDAR-dependent LTD in hippocampal slices from *Nlgn3*$^{-/y}$ but not *Nrxn1*$^{+/-}$ rats

As NMDAR-dependent LTP was affected in both of these rat models of ASD/ID, further investigations of NMDAR-dependent plasticity were deemed necessary. I carried out LFS to induce LTD in slices from *Nrxn1*$^{+/-}$ and *Nlgn3*$^{-/y}$ rats; a protocol that is NMDAR-dependent (Dudek and Bear, 1992) (Fig. 5.2). I found that LTD magnitude (as a percentage of baseline) was significantly reduced in *Nlgn3*$^{-/y}$ rats (11.20 ± 2.87 %) in comparison to WT controls (21.65 ± 2.87 %, Fig. 5.4). However, *Nrxn1*$^{+/-}$ showed an average of 12.90 ± 3.50 % LTD, which was comparable to that found in WT controls (15.36 ± 6.07 %, Fig. 5.4). These data suggest that even though both *Nlgn3*$^{-/y}$ and *Nrxn1*$^{+/-}$ showed a converging phenotype of reduced LTP, NMDAR-dependent plasticity is affected only in *Nlgn3*$^{-/y}$ rats.

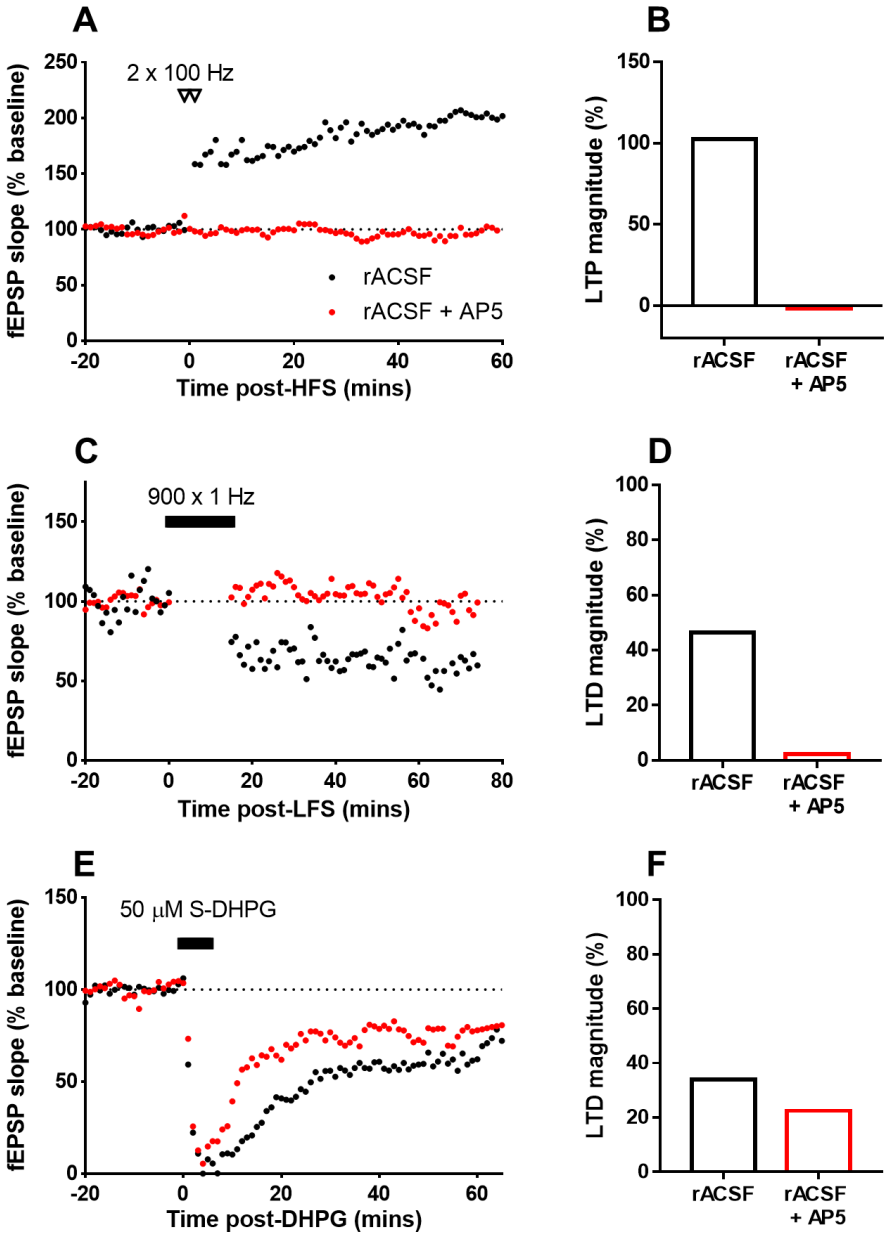

Figure 5.2: Induction of LTP and LTD in CA3-CA1 synapses.

Figure 5.2 ***(previous page)*****: Induction of LTP and LTD in CA3-CA1 synapses.** (A) fEPSP recording from hippocampal SCs of a WT rat showing induction of LTP following HFS. This LTP is abolished when AP5 (50 μM) was present in rACSF throughout recording (n = 1 slice/ 1 rat). (B) Summary of LTP magnitude, calculated as average fEPSP slope 50-60 minutes following induction divided by average baseline fEPSP slope (n = 1 slice/ 1 rat). (C) fEPSP recording from hippocampal SCs of a WT rat showing induction of LTD following LFS. This LTD is suppressed when AP5 (50 μM) was present in rACSF throughout recording (n = 1 slice/ 1 rat). (D) Summary of LTD magnitude, calculated as average fEPSP slope 65-75 minutes following beginning of induction protocol divided by average baseline fEPSP slope (n = 1 slice/ 1 rat). (E) fEPSP recording from hippocampal SCs of a WT rat showing induction of LTD following application of 50 μM S-DHPG for 5 minutes. This LTD is unaffected by the presence of AP5 (50 μM) in rACSF throughout recording (n = 1 slice/ 1 rat). (F) Summary of LTP magnitude, calculated as average fEPSP slope 55-65 minutes following start of S-DHPG application divided by average baseline fEPSP slope (n = 1 slice/ 1 rat).

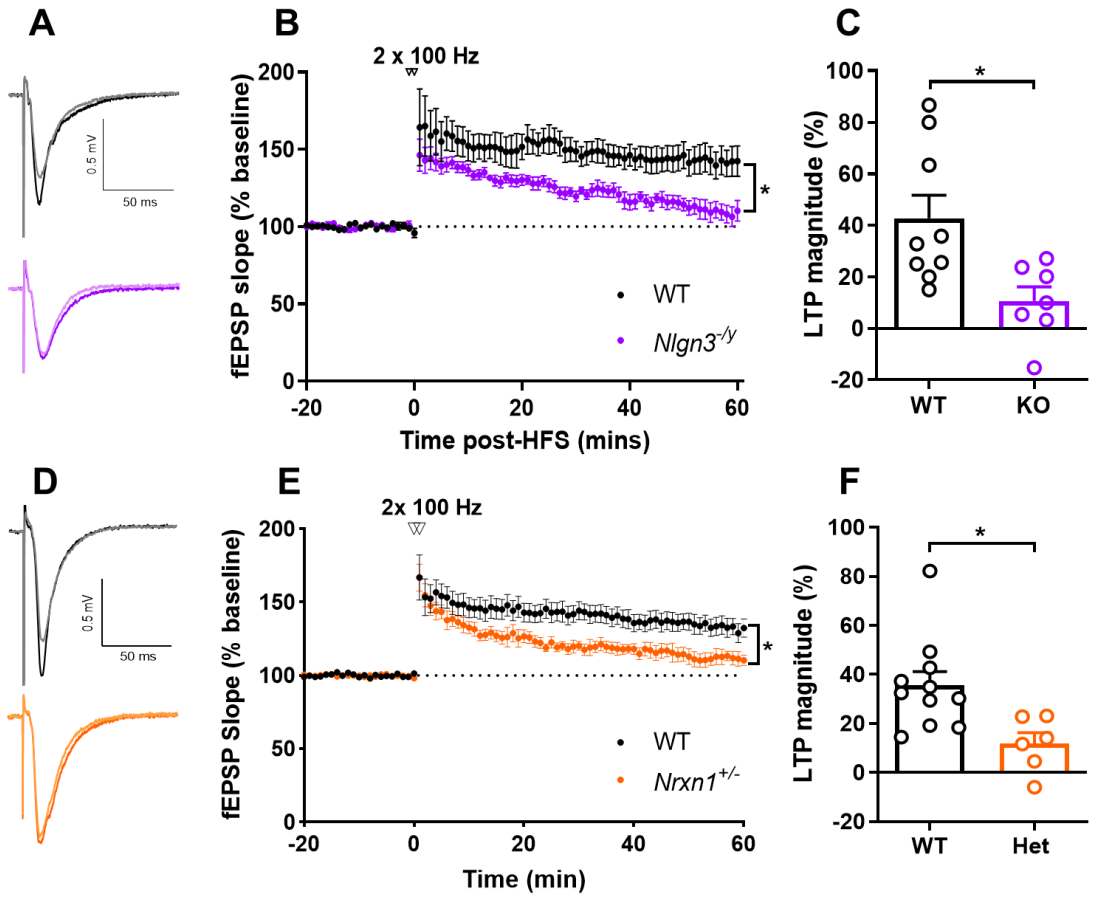

Figure 5.3: Reduced hippocampal LTP in both *Nlgn3*$^{-/y}$ and *Nrxn1*$^{+/-}$ rats. (A) Representative traces of WT (black) and *Nlgn3*$^{-/y}$ (purple) recordings. Baseline shown as grey/pink lines. (B). Time-course of LTP recordings. *Nlgn3*$^{-/y}$ rats show significantly reduced LTP following 2 x 1 second trains of 100 Hz stimulation (WT n = 9, KO n = 7, p = 0.015, F = 7.65, two-way ANOVA). (C) % LTP, defined as EPSP magnitude 50-60 minutes post- high frequency stimulation (HFS) normalised to baseline, is significantly lower in *Nlgn3*$^{-/y}$ rats compared to WT (WT n = 9, KO n = 7, p = 0.0133, unpaired t-test). (D) Representative traces of WT (black) and *Nrxn1*$^{+/-}$(orange) recordings. Baseline shown as grey/light orange lines. (E) Timecourse of LTP recordings. *Nrxn1*$^{+/-}$ rats show reduced LTP following 2 x 1 second trains of 100 Hz stimulation (WT n = 11, Het n = 6, p = 0.047, F = 4.68 two-way ANOVA). (F) % LTP, defined as EPSP magnitude 50-60 minutes post- high frequency stimulation (HFS) normalised to baseline, is significantly lower in *Nrxn1*$^{+/-}$ rats compared to WT (WT n = 11, Het n = 6, p = 0.0128, unpaired t-test).

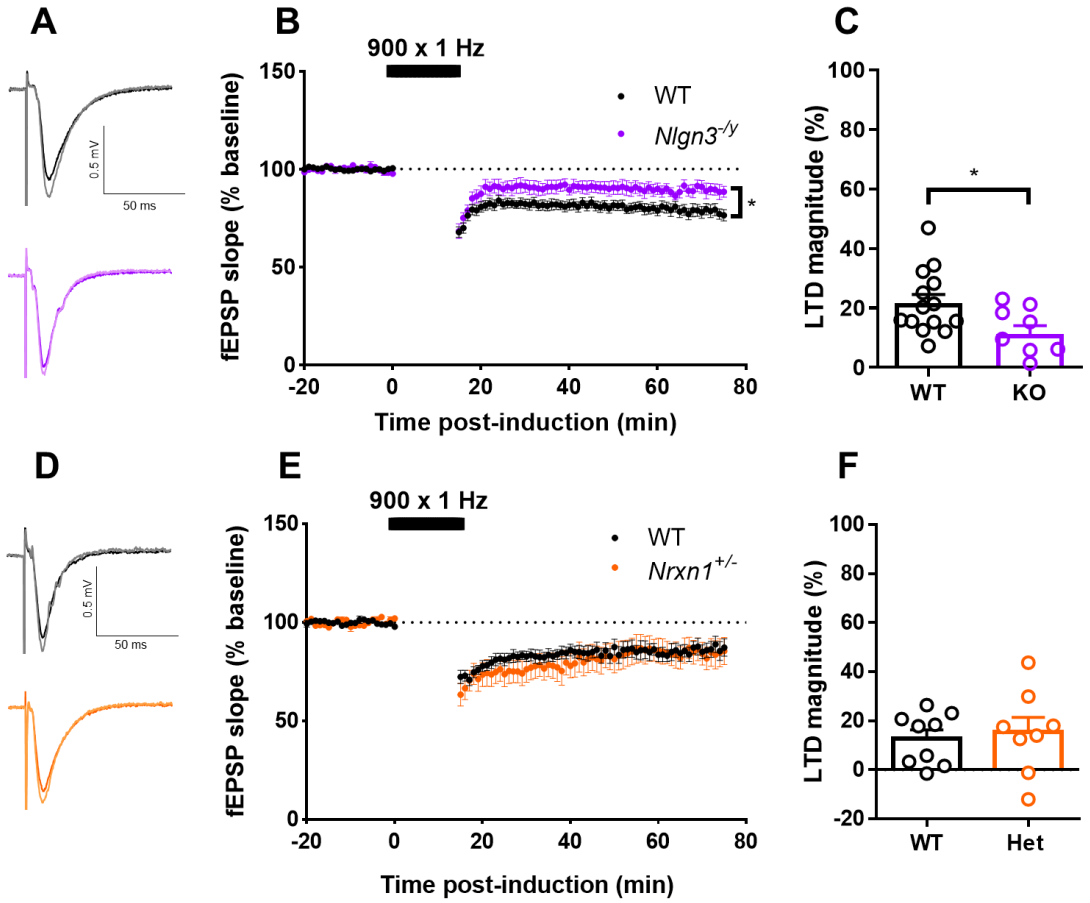

Figure 5.4: Reduced hippocampal NMDAR-dependent LTD in *Nlgn3*$^{-/y}$ but not *Nrxn1*$^{+/-}$ rats. (A) Representative traces of WT (black) and *Nlgn3*$^{-/y}$ (purple) recordings. Baseline shown as grey/pink lines. (B). Time-course of LTP recordings. *Nlgn3*$^{-/y}$ rats show significantly reduced LTD following 15 minutes of 1 Hz stimulation (WT n = 14, KO n = 9, p = 0.030, F = 5.43, two-way ANOVA). (C) % LTD, defined as EPSP magnitude 65-75 minutes following the beginning of LFS normalised to baseline, is significantly lower in *Nlgn3*$^{-/y}$ rats compared to WT (WT n = 14, KO n = 9, p = 0.023, unpaired t-test). (D) Representative traces of WT (black) and *Nrxn1*$^{+/-}$(orange) recordings. Baseline shown as grey/light orange lines. (E) Timecourse of LTP recordings. *Nrxn1*$^{+/-}$ rats show comparable levels of LTD to WT controls (WT n = 8, Het n = 8, p = 0.63, F = 0.25, two-way ANOVA). (F) % LTD, defined as EPSP magnitude 65-75 minutes following the beginning of LFS normalised to baseline, is significantly lower in *Nrxn1*$^{+/-}$ rats compared to WT (WT n = 8, Het n = 8, p = 0.72, unpaired t-test).

mGluR-dependent LTD is unaffected in both *Nlgn3$^{-/y}$* and *Nrxn1$^{+/-}$* rats

mGluR-dependent LTD has been well studied in the context of ASD/ID following the description of the mGluR theory of Fragile-X syndrome (Bear et al., 2004). Our lab and others have shown that hippocampal DHPG-induced mGluR-LTD is enhanced in *Fmr1$^{-/y}$* mice (Nosyreva and Huber, 2006; Huber et al., 2002; Barnes et al., 2015) and rats (Asiminas et al., 2019; Till et al., 2015). Barnes et al. (2015) described convergence of this phenotype between *Syngap$^{+/-}$* and *Fmr1$^{-/y}$* mice. In addition, Baudouin et al. (2012) found that mGluR-dependent LTD was occluded in *Nlgn3$^{-/y}$* mice in cerebellar slices; whereas exaggerated mGluR-dependent LTD has been reported in cerebellar purkinje neurons lacking *Fmr1* (Koekkoek et al., 2005). Not surprisingly, altered synaptic plasticity in response to deletion of *Nlgn3* appears to be brain-region specific, as no such changes are seen in striatum (Rothwell et al., 2014).

To date, no studies have investigated mGluR-dependent LTD in the hippocampus in *Nlgn3$^{-/y}$* or *Nrxn1$^{+/-}$* rat models. Therefore, I investigated the effect of DHPG-application to hippocampal slices in an identical manner as shown in Till et al. (2015). Interestingly, I found that both *Nlgn3$^{-/y}$* and *Nrxn1$^{+/-}$* rats show analogous LTD magnitudes 1 hour after brief S-DHPG application (Fig. 5.5, *Nlgn3$^{+/y}$* 55.40 ± 6.86 %, *Nlgn3$^{-/y}$* 55.21 ± 2.87 %; *Nrxn1$^{+/+}$* 43.94 ± 5.76 %, *Nrxn1$^{+/-}$* 43.38 ± 4.83 %). This provides evidence that neurexin-1 and neuroligin-3 are not involved this form of in mGluR-dependent LTD in rat hippocampus. These results also imply that, although abnormal mGluR-dependent LTD is a conserved phenotype between *Nlgn3$^{-/y}$* and *Fmr1$^{-/y}$* mice in cerebellar parallel fibre synapses (Baudouin et al., 2012; Koekkoek et al., 2005), it is not conserved between *Nlgn3$^{-/y}$* and *Fmr1$^{-/y}$* rats in the hippocampus.

To further confirm this finding, and to investigate whether potential changes to mGluR-dependent LTD were dosage-dependent in *Nlgn3$^{-/y}$* rats, additional experiments testing different concentrations of S-DHPG were carried out on *Nlgn3$^{-/y}$* rats and their corresponding WT littermates. It is possible that the magnitude of LTD was saturated using 50 μM S-DHPG; occluding potential phenotypes. The concentration of DHPG to elicit mGluR-dependent LTD varies between published work, so 25 μM and 100 μM were therefore used in addition to the 50 μM shown in Figure 5.5. This confirmed that concentration of S-DHPG proportionally affects the amount of LTD elicited in SC synapses; 30.34 ± 4.96 % in WT and 23.96 ± 3.46 % in *Nlgn3$^{-/y}$* using 25 μM S-DHPG (Fig. 5.6A-C), 55.40 ± 6.86 %, in WT and 55.21 ± 2.87 % in *Nlgn3$^{-/y}$* using 50 μM

S-DHPG (Fig. 5.5A-C), and 64.03 ± 7.6 % in WT and 53.00 ± 12.46 % in *Nlgn3*$^{-/y}$ using 100 μM S-DHPG (Fig. 5.6). The magnitude of LTD was not different between WT and in *Nlgn3*$^{-/y}$ rats at any DHPG concentration, providing further evidence that mGluR-dependent LTD is unaffected by the loss of neuroligin-3 in rat hippocampal slices.

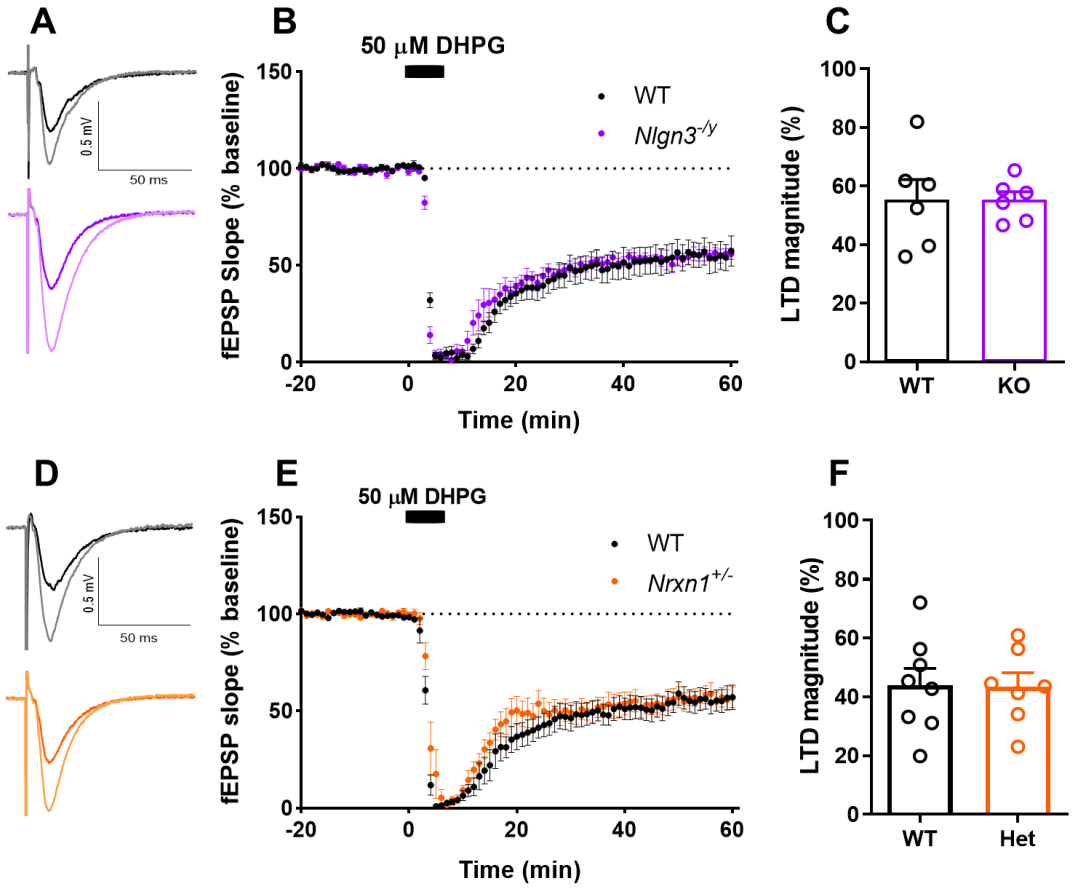

Figure 5.5: Hippocampal mGluR-dependent LTD is unaffected in *Nlgn3*$^{-/y}$ and *Nrxn1*$^{+/-}$ rats. (A) Representative traces of WT (black) and *Nlgn3*$^{-/y}$ (purple) recordings. Baseline shown as grey/pink lines. (B) Time-course of LTD recordings in *Nlgn3*$^{-/y}$ and WT rats showing comparable LTD following S-DHPG application for 5 minutes (WT n = 6, KO n = 6, p = 0.75, F = 1.01, two-way ANOVA). (C) % LTD, defined as EPSP magnitude 55-65 minutes following initial S-DHPG application normalised to baseline, is similar in *Nlgn3*$^{-/y}$ rats compared to WT (WT n = 6, KO n = 6, p = 0.98, unpaired t-test). (D) Representative traces of WT (black) and *Nrxn1*$^{+/-}$(orange) recordings. Baseline shown as grey/light orange lines. (E) Timecourse of LTD recordings showing similar LTD following S-DHPG application in *Nrxn1*$^{+/-}$ rats to WT controls (WT n = 8, Het n = 7, p = 0.45, F = 0.60, two-way ANOVA). (F) % LTD, defined as EPSP magnitude 65-75 minutes following the beginning of LFS normalised to baseline, is significantly lower in *Nrxn1*$^{+/-}$ rats compared to WT (WT n = 7, Het n = 6, p = 0.94, unpaired t-test).

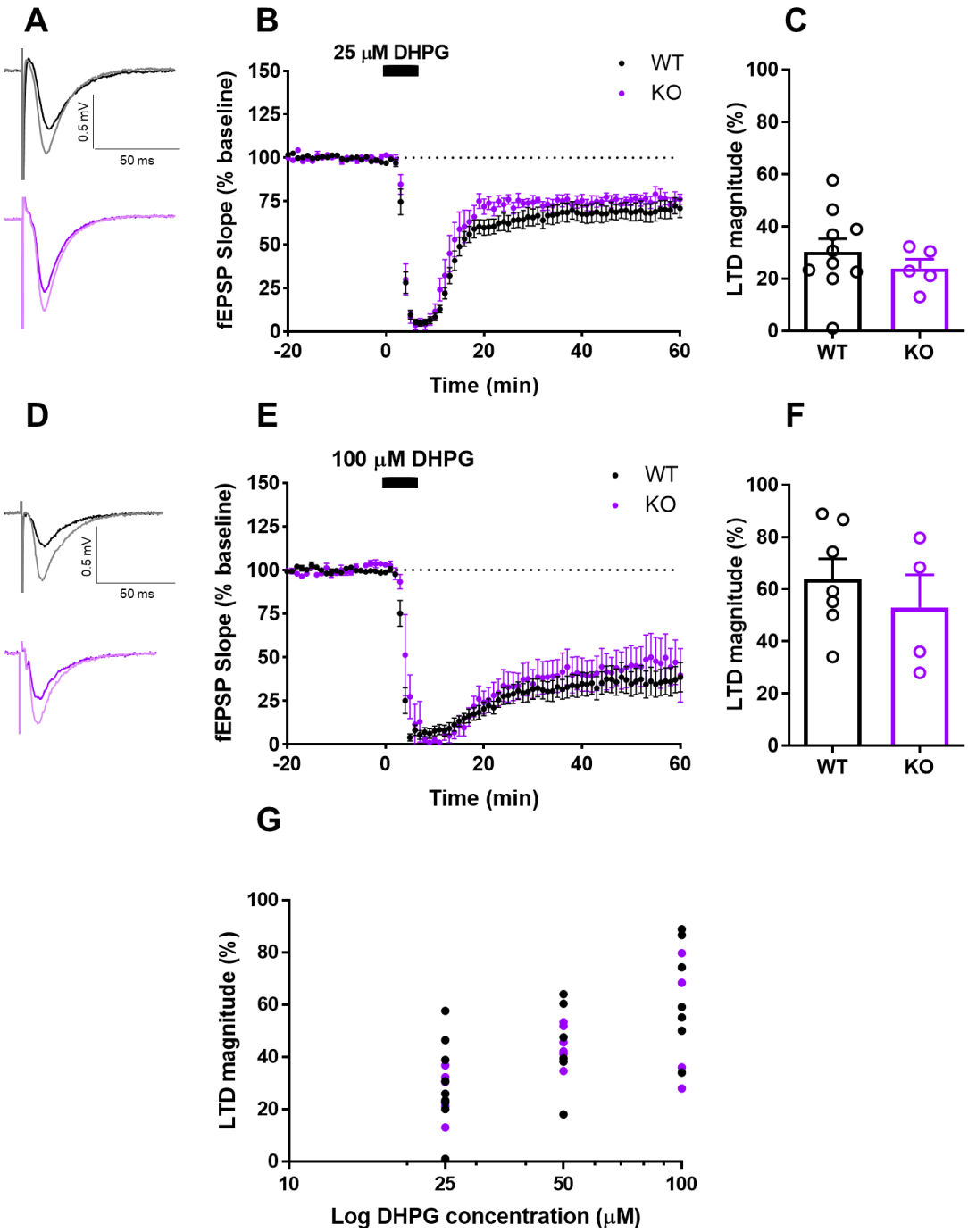

Figure 5.6: Different DHPG concentrations do not affect mGluR-dependent LTD in *Nlgn3*$^{-/y}$ rats. (A, D) Representative traces of WT (black) and *Nlgn3*$^{-/y}$ (purple) recordings. Baseline shown as grey/pink lines. (B) Time-course of LTD recordings in *Nlgn3*$^{-/y}$ and WT rats showing comparable LTD following 25 μM S-DHPG application for 5 minutes (WT n = 10, KO n = 5, p = 0.25, F = 1.39, two-way ANOVA). (C) % LTD, defined as EPSP magnitude 55-65 minutes following 25 μM S-DHPG application normalised to baseline, is similar in *Nlgn3*$^{-/y}$ rats compared to WT (WT n = 10, KO n = 5, p = 0.41, unpaired t-test). (E) Time-course of LTD recordings in *Nlgn3*$^{-/y}$ and WT rats showing comparable LTD following 100 μM S-DHPG application for 5 minutes (WT n = 7, KO n = 4, p = 0.47, F = 0.56, two-way ANOVA). (F) % LTD, defined as EPSP magnitude 55-65 minutes following 100 μM S-DHPG application normalised to baseline, is similar in *Nlgn3*$^{-/y}$ rats compared to WT (WT n = 7, KO n = 4, p = 0.44, unpaired t-test). (G) % LTD plotted against log S-DHPG concentration.

5.2.2 Intrinsic properties *Nlgn3*$^{-/y}$ and *Nrxn1*$^{+/-}$ CA1 neurons

Changes in the effectiveness of neural circuits are correlated not only with changes in synaptic strength, but also with changes in intrinsic excitability (Xu et al., 2005; Fan et al., 2005; Brager and Johnston, 2007). As intrinsic excitability was increased in the dPAG (Fig. 3.13), it may be the case that loss of neuroligin-3 also affects cell intrinsic properties in the hippocampus. Furthermore, previous work from our lab has provided evidence that intrinsic properties in the BLA of *Nlgn3*$^{-/y}$ rats are differentially affected throughout development (Toft, 2019), therefore I assessed cell properties at an additional earlier age point; p13-15 as well as p25-35. I examined the intrinsic properties of CA1 pyramidal cells (PCs) in *Nrxn1*$^{+/-}$ and *Nlgn3*$^{-/y}$ rats using whole-cell patch clamp recording.

Passive membrane properties are altered in *Nrxn1*$^{+/-}$ but not *Nlgn3*$^{-/y}$ CA1 PCs

Passive membrane properties of CA1 PCs examined were resting membrane potential (RMP), input resistance, membrane time constant (τ), capacitance, and sag potential (voltage change initiated by the hyperpolarisation-activated currents, I_h). I found no changes between WT and *Nlgn3*$^{-/y}$ rats in passive membrane properties of CA1 PCs at p13-15 or p25-35 (Table 5.1, Fig. 5.7A-E). However, at p13-15, hyperpolarisation-activated sag potential was increased in *Nrxn1*$^{+/-}$ CA1 PCs in comparison to WT (Table 5.2, Fig. 5.7J). Furthermore, at p25-35, cell capacitance was increased in *Nrxn1*$^{+/-}$ CA1 PCs (Table 5.2, Fig. 5.7I), driven by a small downward trend in input resistance (Table 5.2, Fig. 5.7G). Power analyses revealed that a further 52 and 45 cells per group (for WT and Het, respectively) would be required to achieve significance given the level of variability in this dataset. Overall, these data suggest that passive membrane properties of CA1 PCs are affected by neurexin-1, but not neuroligin-3, depletion.

Active properties are altered in *Nrxn1*$^{+/-}$ but not *Nlgn3*$^{-/y}$ CA1 PCs

The intrinsic excitability of cells was assessed in whole-cell patch clamp by applying incremental depolarising current injections. I found no changes to intrinsic excitability in CA1 PCs at p13-15 or p25-35 in *Nlgn3*$^{-/y}$ rats (Fig. 5.8A-D). In agreement with this, rheobase current and action potential (AP) threshold were unchanged in *Nlgn3*$^{-/y}$ CA1 PCs in comparison to WT at both time points (Table 5.1, Fig. 5.8E, F). Conversely,

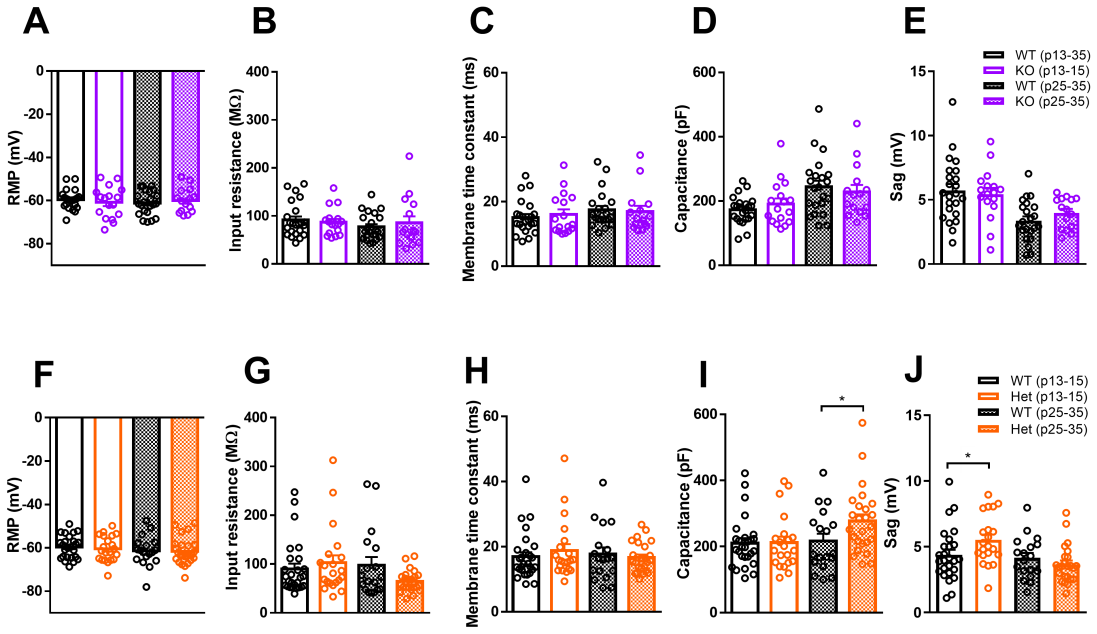

Figure 5.7: Altered CA1 pyramidal cell passive membrane properties in *Nrxn1*$^{+/-}$ (orange) but not *Nlgn3*$^{-/y}$ (purple) rats. (A, F) There is no difference in RMP in CA1 PCs of *Nlgn3*$^{-/y}$ or *Nrxn1*$^{+/-}$ in comparison to WT rats at either p13-15 (*Nlgn3*$^{+/y}$ 23 cells/ 8 rats, *Nlgn3*$^{-/y}$ 18 cells/ 6 rats; *Nrxn1*$^{+/+}$ 26 cells/ 10 rats, *Nrxn1*$^{+/-}$ 20 cells/ 9 rats) or p25-35 (*Nlgn3*$^{+/y}$ 21 cells/ 8 rats, *Nlgn3*$^{-/y}$ 17 cells/ 6 rats; *Nrxn1*$^{+/+}$ 15 cells/ 6 rats, *Nrxn1*$^{+/-}$ 24 cells/ 8 rats). (B, G) There is no difference in the input resistance of *Nlgn3*$^{-/y}$ or *Nrxn1*$^{+/-}$ CA1 PCs in response to a -10pA current step in comparison to WT rats at either p13-15 (*Nlgn3*$^{+/y}$ 23 cells/ 8 rats, *Nlgn3*$^{-/y}$ 18 cells/ 6 rats; *Nrxn1*$^{+/+}$ 26 cells/ 10 rats, *Nrxn1*$^{+/-}$ 20 cells/ 9 rats) or p25-35 (*Nlgn3*$^{+/y}$ 21 cells/ 8 rats, *Nlgn3*$^{-/y}$ 17 cells/ 6 rats; *Nrxn1*$^{+/+}$ 15 cells/ 6 rats, *Nrxn1*$^{+/-}$ 24 cells/ 8 rats). (C, H) There is no difference in membrane time constant (τ) in *Nlgn3*$^{-/y}$ or *Nrxn1*$^{+/-}$ CA1 PCs in comparison to WT PCs at either p13-15 (*Nlgn3*$^{+/y}$ 23 cells/ 8 rats, *Nlgn3*$^{-/y}$ 18 cells/ 6 rats; *Nrxn1*$^{+/+}$ 26 cells/ 10 rats, *Nrxn1*$^{+/-}$ 20 cells/ 9 rats) or p25-35 (*Nlgn3*$^{+/y}$ 21 cells/ 8 rats, *Nlgn3*$^{-/y}$ 17 cells/ 6 rats; *Nrxn1*$^{+/+}$ 15 cells/ 6 rats, *Nrxn1*$^{+/-}$ 24 cells/ 8 rats). (D, I) Cell capacitance of CA1 PCs is unchanged in *Nlgn3*$^{-/y}$ and *Nrxn1*$^{+/-}$ rats at p13-15 (*Nlgn3*$^{+/y}$ 23 cells/ 8 rats, *Nlgn3*$^{-/y}$ 18 cells/ 6 rats; *Nrxn1*$^{+/+}$ 26 cells/ 10 rats, *Nrxn1*$^{+/-}$ 20 cells/ 9 rats), but is increased in *Nrxn1*$^{+/-}$ rats at p25-35 (*Nrxn1*$^{+/+}$ 15 cells/ 6 rats, *Nrxn1*$^{+/-}$ 24 cells/ 8 rats). Cell capacitance is unaltered in *Nlgn3*$^{-/y}$ rats at p25-35 (*Nlgn3*$^{+/y}$ 21 cells/ 8 rats, *Nlgn3*$^{-/y}$ 17 cells/ 6 rats). (E, J) 'Sag' is increased in *Nrxn1*$^{+/-}$ rats at p13-15 (*Nrxn1*$^{+/+}$ 26 cells/ 10 rats, *Nrxn1*$^{+/-}$ 20 cells/ 9 rats), but not in *Nlgn3*$^{-/y}$ rats (*Nlgn3*$^{+/y}$ 23 cells/ 8 rats, *Nlgn3*$^{-/y}$). At p25-25, sag potential is unchanged in both models (*Nlgn3*$^{+/y}$ 21 cells/ 8 rats, *Nlgn3*$^{-/y}$ 17 cells/ 6 rats; *Nrxn1*$^{+/+}$ 15 cells/ 6 rats, *Nrxn1*$^{+/-}$ 24 cells/ 8 rats).
Dots represent cells, GLMM results shown in Tables 5.1 and 5.2.

I found that although intrinsic excitability and rheobase current were not altered in p13-15 CA1 PCs of *Nrxn1*$^{+/-}$ rats (Table 5.2, Fig. 5.8G, H, K), AP threshold was significantly reduced in p13-15 *Nrxn1*$^{+/-}$ CA1 PCs.

Cell capacitance was increased in *Nrxn1*$^{+/-}$ CA1 PCs at p25-35 (Fig. 5.7I), therefore a change in intrinsic excitability of these neurons would be expected. Accordingly, I found that *Nrxn1*$^{+/-}$ CA1 PCs displayed decreased firing frequencies in response to incremental current injections (Fig. 5.8I, J) at p25-35. Although no changes in rheobase or AP threshold were observed at p25-35 in *Nrxn1*$^{+/-}$ CA1 PCs, rheobase current displayed a trending increase (Table 5.2, Fig. 5.8K, L). Power analysis of p25-35 rheobase current dataset revealed that an additional 20 and 13 cells would be required for WT and Het groups, respectively, to show significance with 80 % power.

The waveform and kinetics of the first rheobase AP were also analysed to glean information regarding AP propagation. Parameters measured were AP peak height, AP duration (measured at half AP height), depolarisation speed, and repolarisation speed. In *Nlgn3*$^{-/y}$ rats, no changes to the first AP waveform or kinetics in CA1 PCs were observed at p13-15 or p25-35 (Table 5.1, Fig. 5.9A-D). However, in *Nrxn1*$^{+/-}$ rats, the peak height of the rheobase AP of CA1 PCs was significantly decreased in comparison to WT at p13-15 (Table 5.2, Fig. 5.9E). Furthermore, at p25-35, both depolarisation speed and repolarisation speed were decreased in *Nrxn1*$^{+/-}$ CA1 PCs in comparison to WT (Table 5.2, Fig. 5.8G, H). These results suggest again that neurexin haploinsufficiency affects the intrinsic properties of CA1 PCs, whilst loss of neuroligin-3 does not.

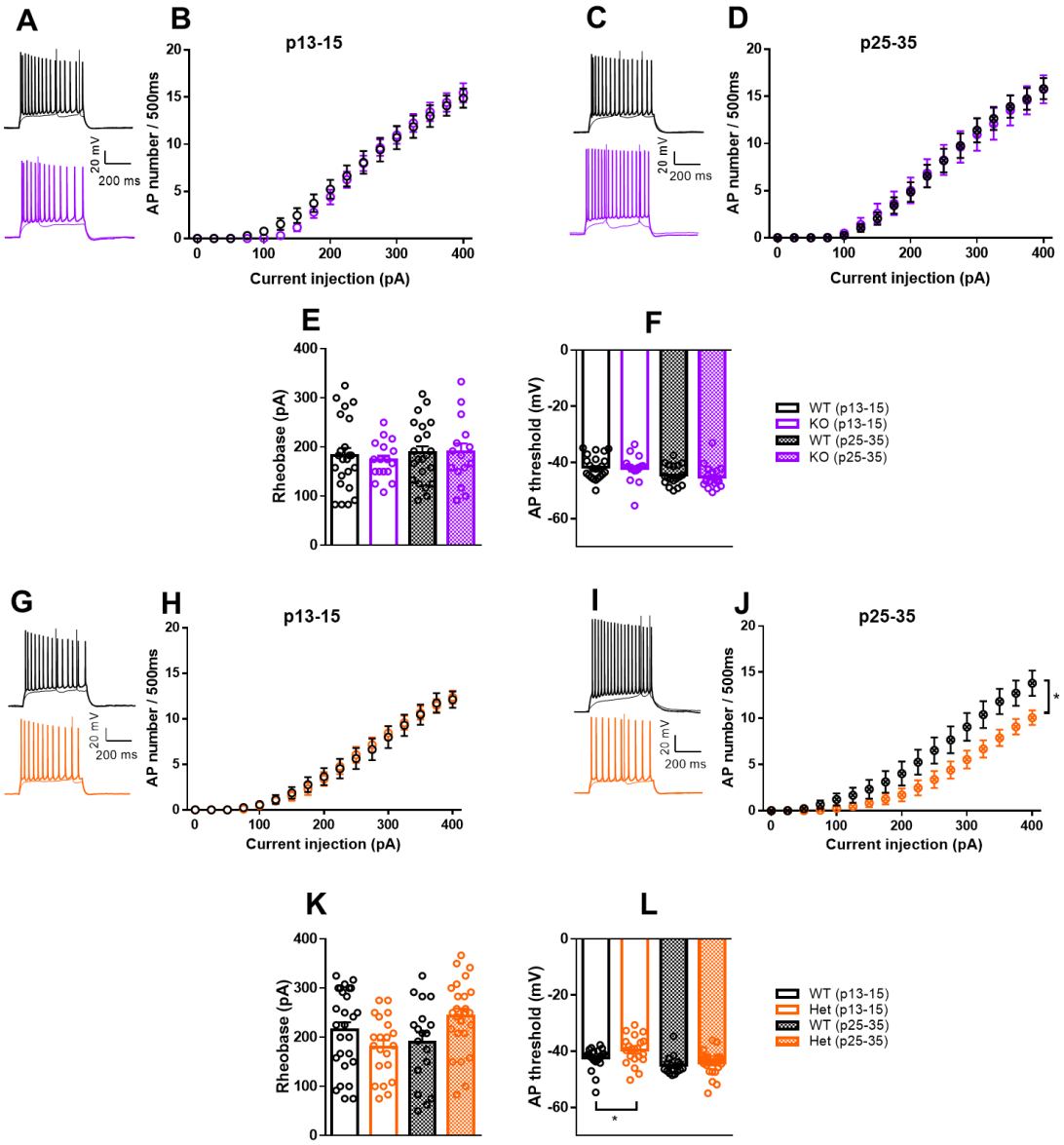

Figure 5.8: Hypoexcitability of *Nrxn1*$^{+/-}$ but not *Nlgn3*$^{-/y}$ CA1 pyramidal cells.

Figure 5.8 ***(previous page)*****: Hypoexcitability of *Nrxn1*$^{+/-}$ (orange) but not *Nlgn3*$^{-/y}$ (purple) CA1 pyramidal cells.** (A) Representative traces of WT (black) and *Nlgn3*$^{-/y}$ (purple) CA1 PCs from p13-15 rats firing in response to rheobase and +400 pA current steps. (B) No difference in the input-frequency curve of p13-15 *Nlgn3*$^{-/y}$ CA1 PCs in comparison to WT controls (*Nlgn3*$^{+/y}$ 23 cells/ 8 rats, *Nlgn3*$^{-/y}$ 18 cells/ 6 rats, p = 0.83, F = 0.047, two-way ANOVA). (C) Representative traces of WT (black) and *Nlgn3*$^{-/y}$ (purple) CA1 PCs from p25-35 rats firing in response to rheobase and +400 pA current steps. (D) No difference in the input-frequency curve of p25-35 *Nlgn3*$^{-/y}$ CA1 PCs in comparison to WT controls (*Nlgn3*$^{+/y}$ 21 cells/ 8 rats, *Nlgn3*$^{-/y}$ 17 cells/ 6 rats, p = 0.99, F = 0.0001 two-way ANOVA). (E) No change in rheobase current in *Nlgn3*$^{+/y}$ p13-15 (*Nlgn3*$^{+/y}$ 23 cells/ 8 rats, *Nlgn3*$^{-/y}$ 18 cells/ 6 rats) or p25-35 (*Nlgn3*$^{+/y}$ 21 cells/ 8 rats, *Nlgn3*$^{-/y}$ 17 cells/ 6 rats) CA1 PCs. (F) No difference in AP threshold in *Nlgn3*$^{+/y}$ p13-15 (*Nlgn3*$^{+/y}$ 23 cells/ 8 rats, *Nlgn3*$^{-/y}$ 18 cells/ 6 rats) or p25-35 (*Nlgn3*$^{+/y}$ 21 cells/ 8 rats, *Nlgn3*$^{-/y}$ 17 cells/ 6 rats) CA1 PCs. (G) Representative traces of WT (black) and *Nrxn1*$^{+/-}$ (orange) CA1 PCs from p13-15 rats firing in response to rheobase and +400 pA current steps. (H) No difference in the input-frequency curve of p13-15 *Nrxn1*$^{+/-}$ CA1 PCs in comparison to WT controls (*Nrxn1*$^{+/+}$ 26 cells/ 10 rats, *Nrxn1*$^{+/-}$ 20 cells/ 9 rats, p = 0.37, F = 0.0018, two-way ANOVA). (I) Representative traces of WT (black) and *Nrxn1*$^{+/-}$ (orange) CA1 PCs from p25-35 rats firing in response to rheobase and +400 pA current steps. (J) Rightward shift in the input-frequency curve of p25-35 *Nrxn1*$^{+/-}$ CA1 PCs in comparison to WT controls (*Nrxn1*$^{+/+}$ 15 cells/ 6 rats, *Nrxn1*$^{+/-}$ 24 cells/ 8 rats, p = 0.041, F = 4.46, two-way ANOVA). (K) Rheobase current is unchanged in *Nrxn1*$^{+/-}$ CA1 PCs at both p13-15 (*Nrxn1*$^{+/+}$ 26 cells/ 10 rats, *Nrxn1*$^{+/-}$ 20 cells/ 9 rats) and p25-25 (*Nrxn1*$^{+/+}$ 15 cells/ 6 rats, *Nrxn1*$^{+/-}$ 24 cells/ 8 rats). (L) AP threshold was decreased in *Nrxn1*$^{+/-}$ CA1 PCs at p13-15 (*Nrxn1*$^{+/+}$ 26 cells/ 10 rats, *Nrxn1*$^{+/-}$ 20 cells/ 9 rats) but not p25-25 (*Nrxn1*$^{+/+}$ 15 cells/ 6 rats, *Nrxn1*$^{+/-}$ 24 cells/ 8 rats).
Dots represent cells, GLMM results shown in Tables 5.1 and 5.2.

Post-AP currents are affected in *Nrxn1*$^{+/-}$ but not *Nlgn3*$^{-/y}$ CA1 PCs

Next, currents activated following AP repolarisation were examined in *Nrxn1*$^{+/-}$ and *Nlgn3*$^{-/y}$ CA1 PCs at p13-15 and p25-35. These were after-depolarisation potential (ADP, measured as the peak depolarisation following an AP), and medium after-hyperpolarisation potential (mAHP, measured as the peak hyperpolarisation following a train of 5 APs at 20, 40, 60, 80 or 100 Hz). I found that mAHP was increased in p25-35 *Nrxn1*$^{+/-}$ CA1 PCs (Fig. 5.10F), however was unchanged in p13-15 *Nrxn1*$^{+/-}$ CA1 PCs (Fig. 5.10E) in comparison to WT. mAHP was also unaffected in *Nlgn3*$^{-/y}$ rat CA1 PCs at both p13-15 and p25-35 (Fig. 5.10B, C). Furthermore, ADP was unchanged in both models at p13-15 and p25-35 (Tables 5.1, 5.2, Fig. 5.10A, D). These results suggest that changes in post-AP currents may contribute to the hypoexcitability phenotype observed in *Nrxn1*$^{+/-}$ rat CA1 PCs at p25-35.

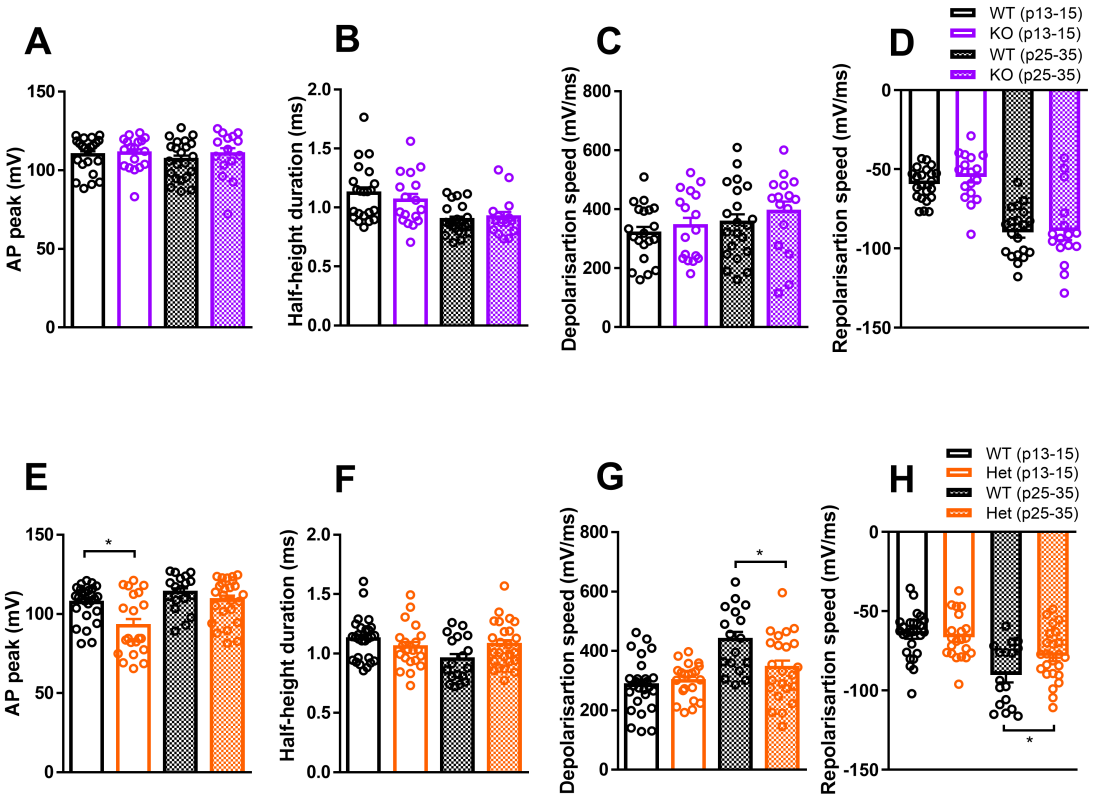

Figure 5.9: Altered AP waveform and kinetics in *Nrxn1*$^{+/-}$ (orange) but not *Nlgn3*$^{-/y}$ (purple) CA1 pyramidal cells. (A, E) Rheobase AP peak height is reduced in *Nrxn1*$^{+/-}$ but not *Nlgn3*$^{-/y}$ at p13-15 (*Nlgn3*$^{+/y}$ 23 cells/ 8 rats, *Nlgn3*$^{-/y}$ 18 cells/ 6 rats; *Nrxn1*$^{+/+}$ 26 cells/ 10 rats, *Nrxn1*$^{+/-}$ 20 cells/ 9 rats). No change in AP peak in either model at p25-35 (*Nlgn3*$^{+/y}$ 21 cells/ 8 rats, *Nlgn3*$^{-/y}$ 17 cells/ 6 rats; *Nrxn1*$^{+/+}$ 15 cells/ 6 rats, *Nrxn1*$^{+/-}$ 24 cells/ 8 rats). (B, F) No difference in half-height duration of rheobase AP in either *Nlgn3*$^{-/y}$ or *Nrxn1*$^{+/-}$ CA1 PCs at p13-15 (*Nlgn3*$^{+/y}$ 23 cells/ 8 rats, *Nlgn3*$^{-/y}$ 18 cells/ 6 rats; *Nrxn1*$^{+/+}$ 26 cells/ 10 rats, *Nrxn1*$^{+/-}$ 20 cells/ 9 rats) or p25-35 (*Nlgn3*$^{+/y}$ 21 cells/ 8 rats, *Nlgn3*$^{-/y}$ 17 cells/ 6 rats; *Nrxn1*$^{+/+}$ 15 cells/ 6 rats, *Nrxn1*$^{+/-}$ 24 cells/ 8 rats). (C, G) AP depolarisation speed was decreased in *Nrxn1*$^{+/-}$ but not *Nlgn3*$^{-/y}$ CA1 PCs at p25-35 (*Nlgn3*$^{+/y}$ 23 cells/ 8 rats, *Nlgn3*$^{-/y}$ 18 cells/ 6 rats; *Nrxn1*$^{+/+}$ 26 cells/ 10 rats, *Nrxn1*$^{+/-}$ 20 cells/ 9 rats). No change in either model at p13-15 (*Nlgn3*$^{+/y}$ 21 cells/ 8 rats, *Nlgn3*$^{-/y}$ 17 cells/ 6 rats; *Nrxn1*$^{+/+}$ 15 cells/ 6 rats, *Nrxn1*$^{+/-}$ 24 cells/ 8 rats). (D, H) AP repolarisation speed was decreased in *Nrxn1*$^{+/-}$ but not *Nlgn3*$^{-/y}$ CA1 PCs at p25-35 (*Nlgn3*$^{+/y}$ 23 cells/ 8 rats, *Nlgn3*$^{-/y}$ 18 cells/ 6 rats; *Nrxn1*$^{+/+}$ 26 cells/ 10 rats, *Nrxn1*$^{+/-}$ 20 cells/ 9 rats). No change in either model at p13-15 (*Nlgn3*$^{+/y}$ 21 cells/ 8 rats, *Nlgn3*$^{-/y}$ 17 cells/ 6 rats; *Nrxn1*$^{+/+}$ 15 cells/ 6 rats, *Nrxn1*$^{+/-}$ 24 cells/ 8 rats).
Dots represent cells, GLMM results shown in Tables 5.1 and 5.2.

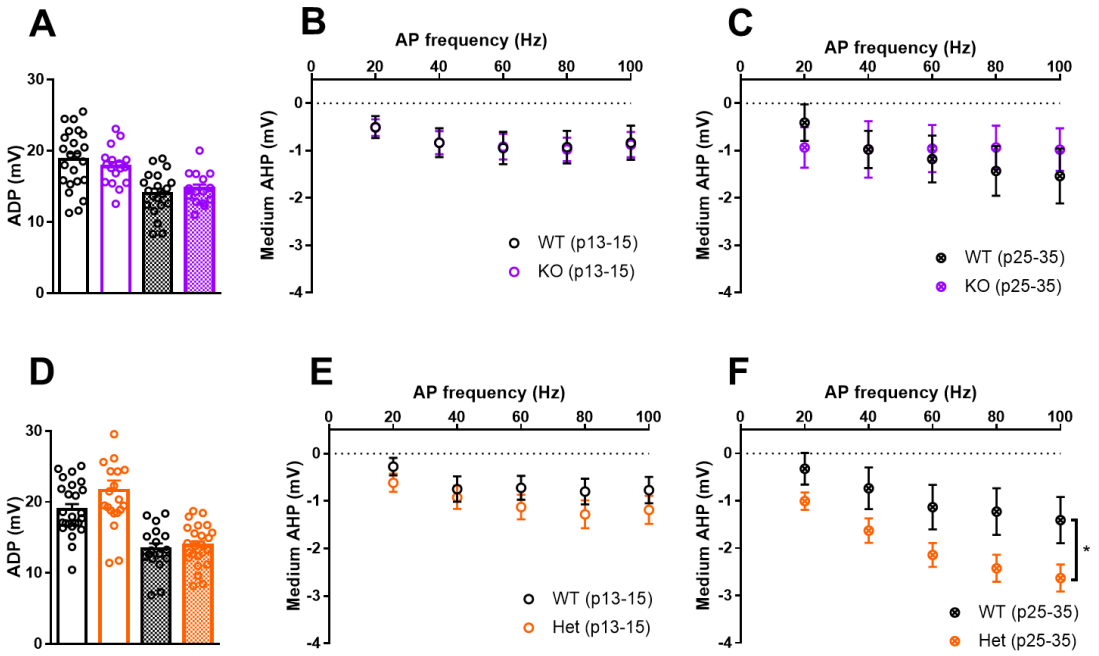

Figure 5.10: Increased medium after-hyperpolarisation potential in *Nrxn1*$^{+/-}$ (orange) but not *Nlgn3*$^{-/y}$ (purple) CA1 pyramidal cells (A, D) No change in after-depolarisation potential amplitude in *Nlgn3*$^{-/y}$ or *Nrxn1*$^{+/-}$ CA1 PCs at either p13-15 (*Nlgn3*$^{+/y}$ 23 cells/ 8 rats, *Nlgn3*$^{-/y}$ 18 cells/ 6 rats; *Nrxn1*$^{+/+}$ 26 cells/ 10 rats, *Nrxn1*$^{+/-}$ 20 cells/ 9 rats) or p25-35 (*Nlgn3*$^{+/y}$ 21 cells/ 8 rats, *Nlgn3*$^{-/y}$ 17 cells/ 6 rats; *Nrxn1*$^{+/+}$ 15 cells/ 6 rats, *Nrxn1*$^{+/-}$ 24 cells/ 8 rats). Dots represent cells, GLMM results shown in Tables 5.1 and 5.2. (B) No change in medium AHP amplitude in p13-15 *Nlgn3*$^{-/y}$ CA1 PCs in comparison to WT (*Nlgn3*$^{+/y}$ 20 cells/ 8 rats, *Nlgn3*$^{-/y}$ 15 cells/ 6 rats, p = 0.97, F = 0.0012, two-way ANOVA). (C) No difference in medium AHP amplitude in p25-35 *Nlgn3*$^{-/y}$ CA1 PCs in comparison to WT (*Nlgn3*$^{+/y}$ 11 cells/ 6 rats, *Nlgn3*$^{-/y}$ 4 cells/ 3 rats, p = 0.50, F = 0.025, two-way ANOVA). (E) Medium AHP amplitude is unaltered in *Nrxn1*$^{+/-}$ p13-15 CA1 PCs in comparison to WT (*Nrxn1*$^{+/+}$ 21 cells/ 10 rats, *Nrxn1*$^{+/-}$ 9 cells/ 6 rats, p = 0.23, F = 1.13, two-way ANOVA). (F) Medium AHP amplitude is increased in *Nrxn1*$^{+/-}$ p25-35 CA1 PCs compared to WT (*Nrxn1*$^{+/+}$ 14 cells/ 6 rats, *Nrxn1*$^{+/-}$ 18 cells/ 7 rats, p = 0.043, F = 4.46, two-way ANOVA).

Table 5.1: GLMM for CA1 PC intrinsic properties in WT and *Nlgn3*$^{-/y}$ rats.

	WT	***Nlgn3*$^{-/y}$**	**p-value**
RMP			
p13-15:	-59.65 ± 0.92 mV	-60.81 ± 1.75 mV	p = 0.49
p25-35:	-61.14 ± 1.18 mV	-60.02 ± 1.46 mV	p = 0.83
Input resistance			
p13-15:	97.79 ± 16.58 MΩ	64.60 ± 4.231 MΩ	p = 0.38
p25-35:	77.04 ± 5.96 MΩ	85.77 ± 13.50 MΩ	p = 0.87
Membrane time constant			
p13-15:	15.07 ± 1.09 ms	16.09 ms ± 1.53 ms	p = 0.20
p25-35:	17.46 ± 1.19 ms	17.00 ms ± 1.73 ms	p = 0.40
Capacitance			
p13-15:	172.9 ± 9.012 pF	175.5 ± 19.08 pF	p = 0.51
p25-35:	244.6 ± 18.88 pF	228.9 ± 21.53 pF	p = 0.49
Sag			
p13-15:	5.72 ± 0.50 mV	5.45 ± 0.47 mV	p = 0.35
p25-35:	3.37 ± 0.34 mV	3.98 ± 0.31 mV	p = 0.19
Rheobase			
p13-15:	183.0 ± 15.32 pA	173.0 ± 9.36 pA	p = 0.77
p25-35:	188.3 ± 13.30 pA	189.4 ± 17.70 pA	p = 0.66
AP threshold			
p13-15:	-41.66 ± 0.86 mV	-42.04 ± 1.14 mV	p = 0.70
p25-35:	-44.55 ± 0.86 mV	-45.14 ± 1.03 mV	p = 0.55
AP height			
p13-15:	105.9 ± 4.41 mV	111.5 ± 2.54 mV	p = 0.22
p25-35:	106.7 ± 2.61 mV	110.3 ± 3.80 mV	p = 0.57
AP width			
p13-15:	1.12 ± 0.050 ms	1.061 ± 0.054 ms	p = 0.70
p25-35:	0.90 ± 0.027 ms	0.92 ± 0.044 ms	p = 0.31
AP depolarisation speed			
p13-15:	318.9 ± 21.53 mV/ms	343.5 ± 27.72 mV/ms	p = 0.27
p25-35:	355.4 ± 27.49 mV/ms	393.2 ± 33.51 mV/ms	p = 0.96
AP repolarisation speed			
p13-15:	-59.49 ± 2.22 mV/ms	-54.79 ± 3.48 mV/ms	p = 0.53
p25-35:	-89.93 ± 3.31 mV/ms	-88.94 ± 5.83 mV/ms	p = 0.39
ADP			
p13-15:	18.77 ± 0.87 mV/ms	17.79 ± 0.65 mV/ms	p = 0.40
p25-35:	14.00 ± 0.68 mV/ms	14.68 ± 0.60 mV/ms	p = 0.48

Table 5.2: GLMM for CA1 PC intrinsic properties in WT and *Nrxn1*$^{+/-}$ rats.

	WT	***Nrxn1*$^{+/-}$**	**p-value**
RMP			
p13-15:	-59.66 ± 0.98 mV	-60.62 ± 1.90 mV	p = 0.68
p25-35:	-61.41 ± 1.62 mV	-61.69 ± 1.22 mV	p = 0.98
Input resistance			
p13-15:	90.31 ± 10.50 MΩ	74.22 ± 9.484 MΩ	p = 0.49
p25-35:	97.79 ± 16.58 MΩ	64.60 ± 4.23 MΩ	p = 0.057
Membrane time constant			
p13-15:	16.91 ± 3.52 ms	17.81 ms ± 2.03	p = 0.41
p25-35:	17.75 ± 1.99 ms	16.67 ms ± 0.90	p = 0.55
Capacitance			
p13-15:	210.3 ± 14.87 pF	250.8 ± 25.16 pF	p = 0.95
p25-35:	216.9 ± 21.73 pF	277.5 ± 19.98 pF	p = 0.048
Sag			
p13-15:	4.38 ± 0.39 mV	4.32 ± 0.45 mV	p = 0.045
p25-35:	4.15 ± 0.37 mV	3.67 ± 0.29 mV	p = 0.30
Rheobase			
p13-15:	214.8 ± 15.77 pA	217.6 ± 16.10 pA	p = 0.11
p25-35:	190.3 ± 19.60 pA	243.7 ± 14.77 pA	p = 0.065
AP threshold			
p13-15:	-42.50 ± 0.67 mV	-40.91 ± 1.40 mV	p = 0.02
p25-35:	-45.01 ± 0.75 mV	-44.22 ± 0.84 mV	p = 0.77
AP height			
p13-15:	107.2 ± 2.15 mV	112.6 ± 2.37 mV	p = 0.0002
p25-35:	113.5 ± 2.71 mV	108.8 ± 2.71 mV	p = 0.34
AP width			
p13-15:	1.12 ± 0.035 ms	1.012 ± 0.030 ms	p = 0.27
p25-35:	0.95 ± 0.044 ms	1.074 ± 0.038 ms	p = 0.07
AP depolarisation speed			
p13-15:	285.0 ± 17.68 mV/ms	299.7 ± 13.07 mV/ms	p = 0.67
p25-35:	438.0 ± 26.33 mV/ms	344.3 ± 23.28 mV/ms	p = 0.0079
AP repolarisation speed			
p13-15:	-64.77 ± 2.73 mV/ms	-66.38 ± 3.11 mV/ms	p = 0.83
p25-35:	-90.19 ± 4.73 mV/ms	-78.19 ± 3.34 mV/ms	p = 0.04
ADP			
p13-15:	18.99 ± 0.74 mV/ms	21.62 ± 1.42 mV/ms	p = 0.09
p25-35:	13.42 ± 0.78 mV/ms	13.89 ± 0.60 mV/ms	p = 0.63

5.2.3 Synaptic properties of *Nlgn3$^{-/y}$* and *Nrxn1$^{+/-}$* CA1 neurons

Miniature excitatory post-synaptic potentials (mEPSCs) and miniature inhibitory post-synaptic potentials (mIPSCs) were recorded in whole-cell configuration of patch-clamp in the presence of tetrodotoxin (TTX) to block action potential formation. The frequency and amplitude of mEPSCs/mIPSCs reflect the number of synaptic vesicles fusing the presynaptic membrane, and the postsynaptic response to these vesicles. *Nlgn3$^{-/y}$* and *Nrxn1$^{+/-}$* are known to be involved in the correct functioning of synapses (see section 1.3.1). Therefore, I hypothesised that full or partial loss of neurexin-1 or neuroligin-3 would result in decreased mEPSC/mIPSC amplitude and/or frequency.

mEPSCs are affected in *Nlgn3$^{-/y}$* but not *Nrxn1$^{+/-}$* CA1 PCs

Changes in synaptic transmission have been reported in both *Nlgn3$^{-/y}$* and *Nrxn1$^{-/-}$* mouse models (Baudouin et al., 2012; Etherton et al., 2009), and *Nrxn1$^{+/-}$* human induced neurons (Pak et al., 2015). Identical conditions are particularly crucial for comparisons of mEPSCs/mIPSCs as they are highly sensitive to changes in temperature and ACSF flow rate. I recorded mEPSCs in the presence of both TTX and picrotoxin (PTX) in CA1 PCs from *Nlgn3$^{-/y}$* and *Nrxn1$^{+/-}$* rats, along with appropriate WT controls. I found that mEPSC amplitude was increased in *Nlgn3$^{-/y}$* rat CA1 PCs (Table 5.3, Fig. 5.11B), but not *Nrxn1$^{+/-}$* CA1 PCs (Table 5.3, Fig. 5.11E). Neither model displayed changes in mEPSC frequency in comparison to WT rats (Table 5.3, Fig. 5.11C, F). These results imply that excitatory synaptic input to CA1 PCs in *Nlgn3$^{-/y}$* is increased, but synapse number is unchanged.

mIPSCs are unaffected in both *Nlgn3$^{-/y}$* and *Nrxn1$^{+/-}$* CA1 PCs

Neuroligin-3 and neurexin-1 are present at both excitatory and inhibitory synapses (Budreck and Scheiffele, 2007; Missler et al., 2003). Etherton et al. (2009) reported reduced mEPSCs in *Nrxn1$^{-/-}$* mice, however no change in mIPSCs was observed. Accordingly, I also examined mIPSCs in these models, in the presence of both TTX and cyanquixaline (CNQX). I found no differences in mIPSC amplitude or frequency in either *Nlgn3$^{-/y}$* or *Nrxn1$^{+/-}$* CA1 PCs (Table, 5.3, Fig. 5.12). This provides evidence that there are no changes in inhibitory synaptic input to CA1 PCs in *Nlgn3$^{-/y}$* and *Nrxn1$^{+/-}$* rat models.

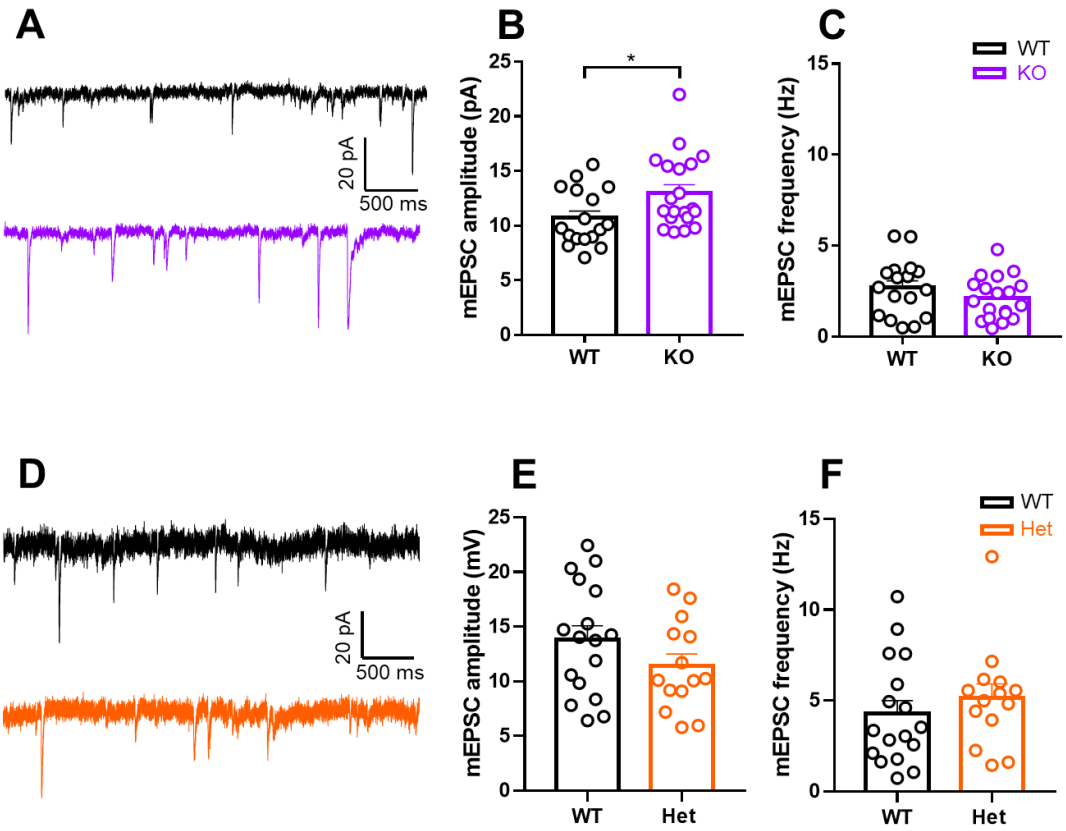

Figure 5.11: mEPSCs are unaffected in *Nlgn3*$^{-/y}$ and *Nrxn1*$^{+/-}$ CA1 pyramidal cells. (A) Representative traces of mEPSCs recorded from WT (black) and *Nlgn3*$^{-/y}$ (purple) rats. (B) Increased mEPSC amplitude in *Nlgn3*$^{-/y}$ CA1 PCs in comparison to WT (WT n = 17 cells/ 6 rats, KO n = 20 cells/ 8 rats). (C) mEPSC frequencies are not different between WT and *Nlgn3*$^{-/y}$ CA1 PCs (WT n = 17 cells/ 6 rats, KO n = 20 cells/ 8 rats). (D) Representative traces of mEPSCs recorded from WT (black) and *Nrxn1*$^{+/-}$ (orange) rats. (E) No change in mEPSC amplitude between WT and *Nrxn1*$^{+/-}$ CA1 PCs (WT n = 17 cells/ 7 rats, Het n = 14 cells/ 5 rats). (F) mEPSC frequencies are unchanged in *Nrxn1*$^{+/-}$ in comparison to WT CA1 PCs (WT n = 17 cells/ 7 rats, Het n = 14 cells/ 5 rats). Dots represent cells, GLMM results shown in Table 5.3.

Table 5.3: GLMM for hippocampus mEPSCs/IPSCs in WT, *Nlgn3*$^{-/y}$ and *Nrxn1*$^{+/-}$ rats.

	WT	***Nlgn3*$^{-/y}$**	**p-value**
mEPSC amplitude (pA)	10.72 ± 0.63	13.02 ± 0.74	0.036
mEPSC frequency (Hz)	2.70 ± 0.38	2.11 ± 0.27	0.20
mIPSC amplitude (pA)	26.15 ± 2.85	25.58 ± 1.94	0.87
mIPSC frequency (Hz)	5.74 ± 0.53	6.74 ± 0.62	0.28
	WT	***Nrxn1*$^{+/-}$**	**p-value**
mEPSC amplitude (pA)	13.84 ± 1.25	11.42 ± 1.10	0.35
mEPSC frequency (Hz)	4.30 ± 0.71	5.17 ± 0.75	0.52
mIPSC amplitude (pA)	30.90 ± 2.82	28.94 ± 3.71	0.87
mIPSC frequency (Hz)	8.70 ± 0.50	8.10 ± 0.45	0.65

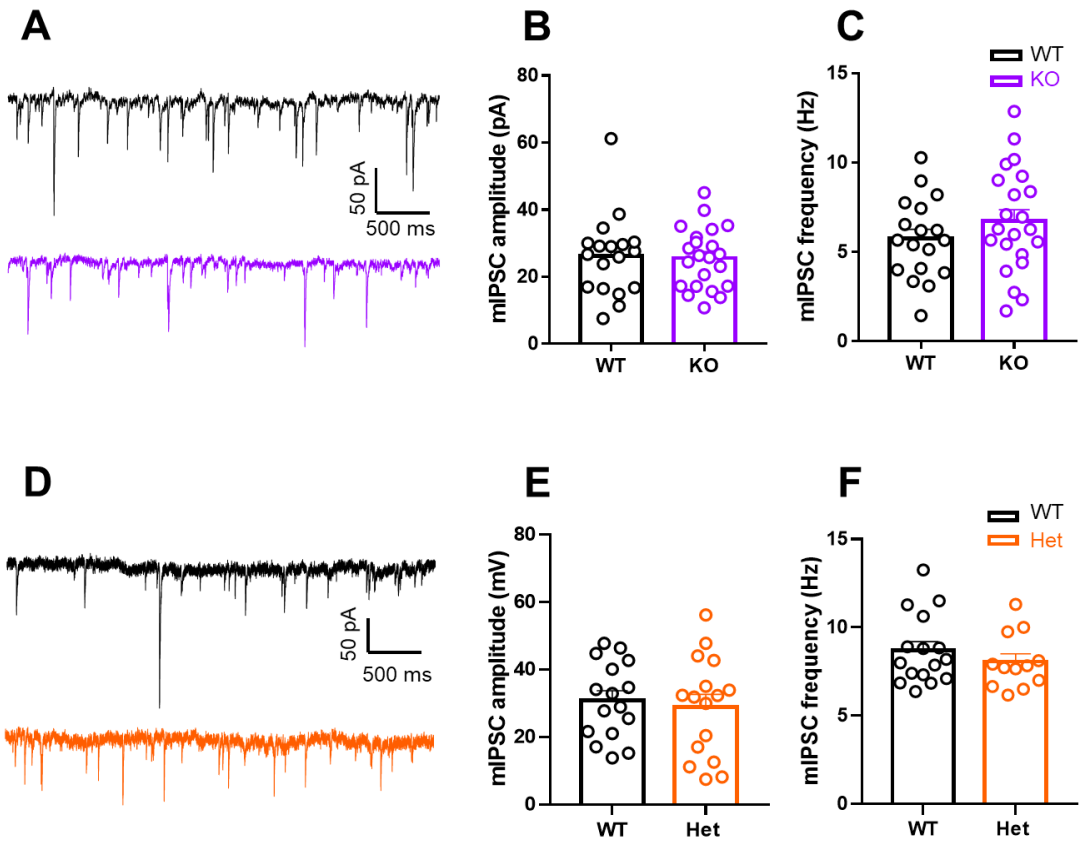

Figure 5.12: mIPSCs are unaffected in *Nlgn3*$^{-/y}$ and *Nrxn1*$^{+/-}$ CA1 pyramidal cells. (A) Representative traces of mIPSCs recorded from WT (black) and *Nlgn3*$^{-/y}$ (purple) rats. (B) No change in mIPSC amplitude between WT and *Nlgn3*$^{-/y}$ CA1 PCs (WT n = 18 cells/ 6 rats, KO n = 22 cells/ 8 rats). (C) mIPSC frequencies are not different between WT and *Nlgn3*$^{-/y}$ CA1 PCs (WT n = 18 cells/ 6 rats, KO n = 22 cells/ 8 rats). (D) Representative traces of mIPSCs recorded from WT (black) and *Nrxn1*$^{+/-}$ (orange) rats. (E) No change in mIPSC amplitude between WT and *Nrxn1*$^{+/-}$ CA1 PCs (WT n = 16 cells/ 7 rats, Het n = 16 cells/ 5 rats). (F) mIPSC frequencies are unchanged in *Nrxn1*$^{+/-}$ in comparison to WT CA1 PCs (WT n = 16 cells/ 7 rats, Het n = 16 cells/ 5 rats).
Dots represent cells, GLMM results shown in Table 5.3.

5.2.4 mPFC plasticity in *Nlgn3$^{-/y}$* and *Nrxn1$^{+/-}$* rats

Extracellular field recordings were made from layer 2/3 (L2/3) to layer 5 (L5) synapses in the prelimbic (PL) mPFC. Electrical stimulation of these synapses results in an fEPSP that has been shown to undergo plasticity (Huang et al., 2004; Asiminas et al., 2019; Kang et al., 2018; Kolomiets et al., 2009; Matsuda et al., 2006). Reduced plasticity of these synapses has been demonstrated in several other models of ASD/ID, including the *Fmr1$^{-/y}$* rat (Asiminas et al., 2019) and *Syngap$^{+/-}$* rat (A. Jackson, unpublished). The PL mPFC has many excitatory long range connections, notably to the PAG (Floyd et al., 2000; An et al., 2006; Beitz, 1982) and basolateral amygdala (McDonald et al., 1996), both of which are intrinsically hyperexcitable in *Nlgn3$^{-/y}$* rats (Fig. 3.13; Toft (2019)). Additionally, the active place avoidance task revealed that *Nlgn3$^{-/y}$* rats display prolonged avoidance of the shock zone that could be interpreted as cognitive inflexibility, which is an mPFC dependent process (reviewed in Park and Moghaddam (2017)). Cognitive flexibility has also been shown to be reduced in *Nlgn3$^{-/y}$* mice (Norris et al., 2019). Finally, as I observed reduced LTP in both *Nlgn3$^{-/y}$* and *Nrxn1$^{+/-}$* rats in hippocampal SC synapses, I hypothesised that neuroligin-3 or neurexin-1 deficiency would also result in LTP deficits in the PL mPFC.

LTP can be induced in L2/3-L5 synapses in the mPFC

There are fewer studies describing plasticity of L2/3-L5 synapses in the mPFC than CA3-CA1 synapses in the hippocampus, however the protocol defined by Huang et al. (2004) has been utilised by our lab (Asiminas et al., 2019) to successfully assess mPFC plasticity. This protocol consists of 5 x 300 Hz stimulation, and produces LTP in these synapses that is blocked by the presence of AP5 (Fig. 5.13).

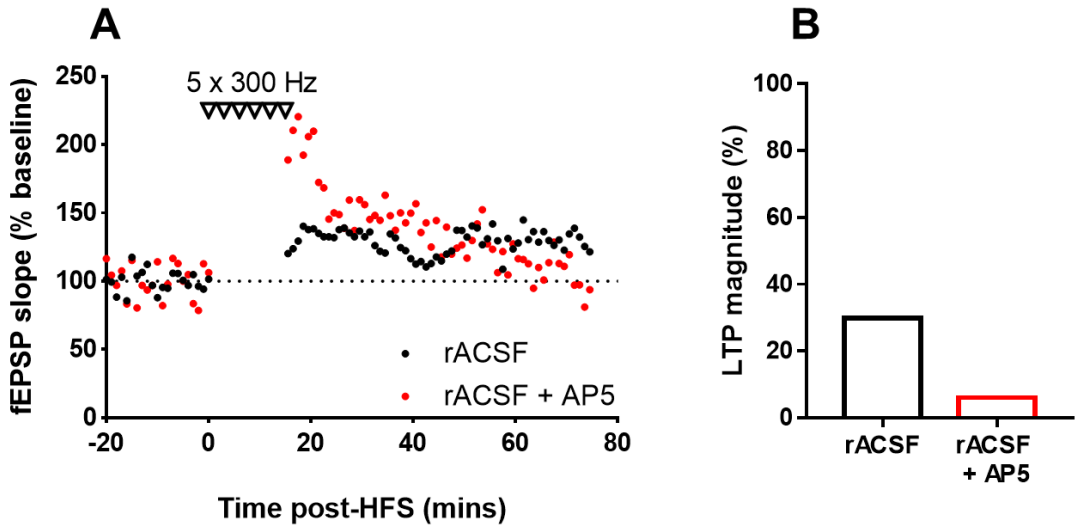

Figure 5.13: Induction of LTP at L2/3-L5 synapses in prelimbic mPFC. (A) fEPSP recordings from mPFC slices from a WT rat showing induction of LTP following 5 x 300 Hz stimulation. This LTP is reduced when AP5 (50 μM) is present in rACSF (n = 1 slice/ 1 rat). (B) Summary of LTP magnitude, calculated as average fEPSP slope 65-75 minutes following beginning of LTP induction (n = 1 slice/ 1 rat).

LTP is intact in both *Nrxn1*$^{+/-}$ and *Nlgn3*$^{-/y}$ L2/3-L5 mPFC synapses

To investigate if synaptic plasticity is impaired in the mPFC in addition to the hippocampus in *Nrxn1*$^{+/-}$ and *Nlgn3*$^{-/y}$ rats, I stimulated PL mPFC L2/3-L5 synapses in slices from both *Nrxn1*$^{+/-}$ and *Nlgn3*$^{-/y}$ rats and WT controls. I found that following HFS, slices from both *Nrxn1*$^{+/-}$ and *Nlgn3*$^{-/y}$ rats showed LTP that was comparable to that of WTs (Fig. 5.14; *Nlgn3*$^{+/y}$ 18.30 ± 4.99 %, *Nlgn3*$^{-/y}$ 13.57 ± 3.49 %; *Nrxn1*$^{+/+}$ 20.25 ± 4.67 %, *Nrxn1*$^{+/-}$ 19.97 ± 7.35 %). This suggests that the reduced plasticity seen in hippocampal slices from both these models is a brain area specific phenotype, and not conserved in the mPFC.

5.2.5 Intrinsic properties of *Nlgn3*$^{-/y}$ and *Nrxn1*$^{+/-}$ mPFC neurons

In order to compare cellular function not only across models, but also across brain regions, I examined the intrinsic properties of layer 5 PCs in the prelimbic (PL) mPFC. Layer 5 is the main output region of the PL mPFC, projecting to both the BLA and PAG (Senn et al., 2014; Rozeske et al., 2018). Again, I assessed these cell properties at two age points, p13-15 and p25-35, and all experiments were conducted identically to as described for hippocampal CA1 recordings.

Passive membrane properties are affected in *Nrxn1*$^{+/-}$ but not *Nlgn3*$^{-/y}$ layer 5 mPFC PCs

Passive membrane properties recorded from *Nlgn3*$^{-/y}$ and *Nrxn1*$^{+/-}$ layer 5 PL mPFC PCs were RMP, input resistance, membrane time constant (τ), capacitance, and sag. I found that input resistance was significantly increased, and capacitance significantly decreased, in layer 5 mPFC PCs recorded from p13-15 but not p25-35 *Nrxn1*$^{+/-}$ rats (Table 5.5, Fig. 5.15G, I). However, no difference in any passive membrane properties were observed in cells from *Nlgn3*$^{-/y}$ rats, at either age point (Table 5.4, Fig. 5.15A-E). These results suggest that, unlike the HC, in layer 5 mPFC neurons, depletion of neurexin-1 causes changes to cell size earlier in development. However, this phenotype is recovered by the time rats reach juvenile adult stage.

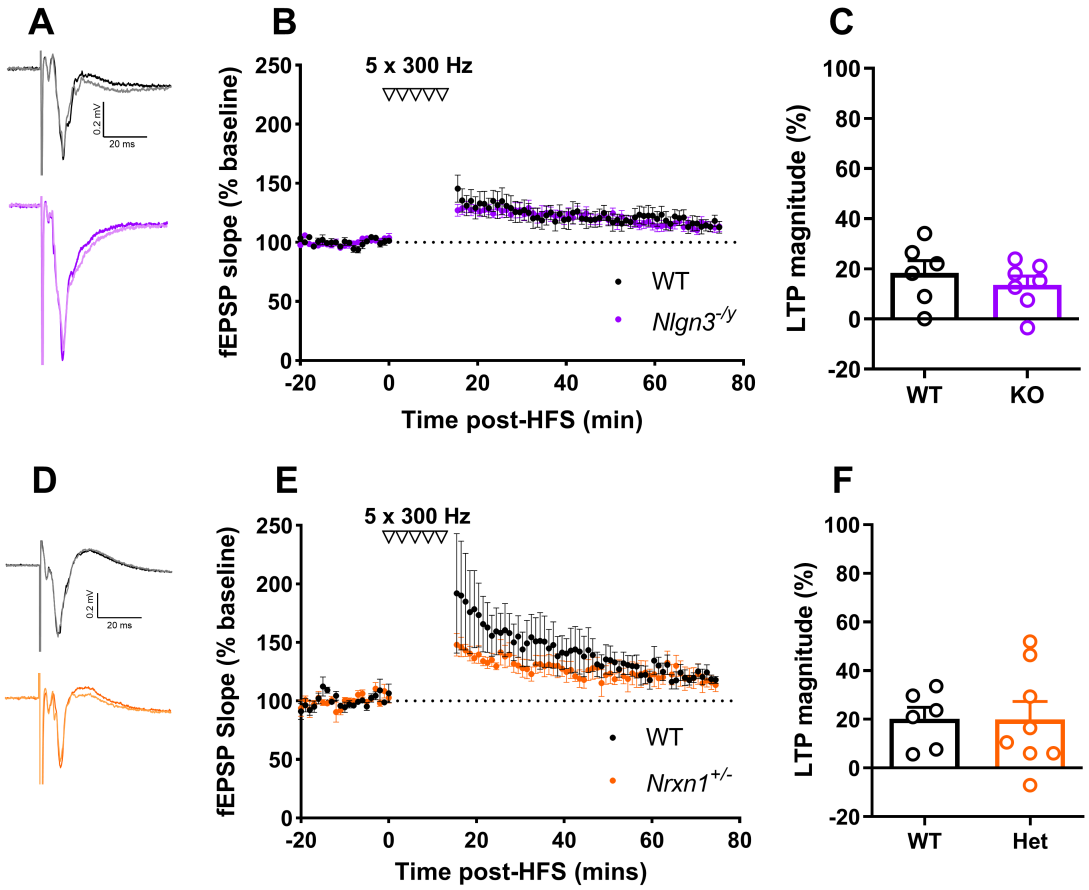

Figure 5.14: No difference in LTP of L2/3-L5 mPFC synapses in either *Nlgn3*$^{-/y}$ or *Nrxn1*$^{+/-}$ rats. (A) Representative traces of WT (black) and *Nlgn3*$^{-/y}$ (purple) recordings. Baseline shown as grey/pink lines. (B) Timecourse of LTP recordings. *Nlgn3*$^{-/y}$ rats show comparable LTP following 5 trains of 300 Hz stimulation (WT n = 6, KO n = 7, p = 0.78, F = 0.072, two-way ANOVA). (C) % LTP, defined as EPSP magnitude 65-75 minutes after start of LTP induction, normalised to baseline, is unaffected in *Nlgn3*$^{-/y}$ rats compared to WT (WT n = 6, KO n = 7, p = 0.44, unpaired t-test). (D) Representative traces of WT (black) and *Nrxn1*$^{+/-}$ (orange) recordings. Baseline shown as grey/light orange lines. (E) Timecourse of LTP recordings. *Nrxn1*$^{+/-}$ rats show comparable LTP following 5 trains of 300 Hz stimulation (WT n = 6, KO n = 8, p = 0.31, F = 1.11, two-way ANOVA). (F) % LTP, defined as EPSP magnitude 65-75 minutes after start of LTP induction, normalised to baseline, is unaffected in *Nrxn1*$^{+/-}$ rats compared to WT (WT n = 6, KO n = 8, p = 0.97, unpaired t-test).

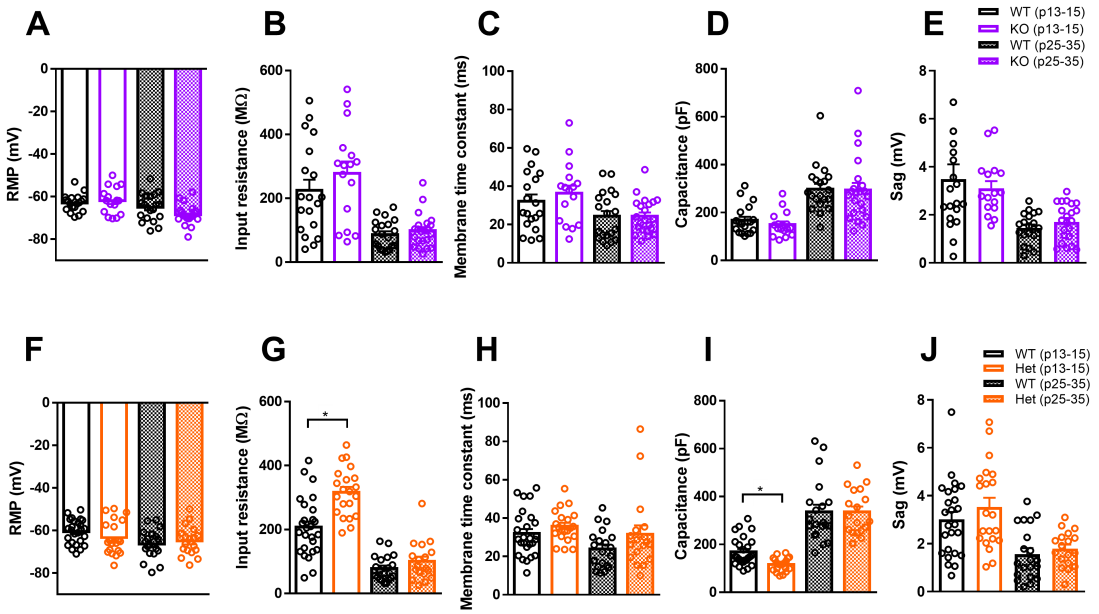

Figure 5.15: Altered mPFC pyramidal cell passive membrane properties in *Nrxn1*$^{+/-}$ (orange) but not *Nlgn3*$^{-/y}$ (purple) rats. (A, F) There is no difference in RMP in layer 5 mPFC PCs of *Nlgn3*$^{-/y}$ or *Nrxn1*$^{+/-}$ in comparison to WT rats at either p13-15 (*Nlgn3*$^{+/y}$ 19 cells/ 8 rats, *Nlgn3*$^{-/y}$ 16 cells/ 7 rats; *Nrxn1*$^{+/+}$ 26 cells/ 10 rats, *Nrxn1*$^{+/-}$ 21 cells/ 9 rats) or p25-35 (*Nlgn3*$^{+/y}$ 20 cells/ 8 rats, *Nlgn3*$^{-/y}$ 22 cells/ 8 rats; *Nrxn1*$^{+/+}$ 20 cells/ 6 rats, *Nrxn1*$^{+/-}$ 18 cells/ 7 rats). (B, G) Input resistance in response to a -10pA current step is significantly increased in layer 5 mPFC neurons of p13-15 *Nrxn1*$^{+/-}$ (*Nrxn1*$^{+/+}$ 26 cells/ 10 rats, *Nrxn1*$^{+/-}$ 21 cells/ 9 rats) but not in *Nlgn3*$^{-/y}$ rats (*Nlgn3*$^{+/y}$ 19 cells/ 8 rats, *Nlgn3*$^{-/y}$ 16 cells/ 7 rats). Input resistance at p25-35 was comparable to WT in both models (*Nlgn3*$^{+/y}$ 20 cells/ 8 rats, *Nlgn3*$^{-/y}$ 22 cells/ 8 rats; *Nrxn1*$^{+/+}$ 20 cells/ 6 rats, *Nrxn1*$^{+/-}$ 18 cells/ 7 rats). (C, H) There is no difference in membrane time constant (τ) in *Nlgn3*$^{-/y}$ or *Nrxn1*$^{+/-}$ mPFC PCs in comparison to WT at either p13-15 (*Nlgn3*$^{+/y}$ 19 cells/ 8 rats, *Nlgn3*$^{-/y}$ 16 cells/ 7 rats; *Nrxn1*$^{+/+}$ 26 cells/ 10 rats, *Nrxn1*$^{+/-}$ 21 cells/ 9 rats) or p25-35 (*Nlgn3*$^{+/y}$ 20 cells/ 8 rats, *Nlgn3*$^{-/y}$ 22 cells/ 8 rats; *Nrxn1*$^{+/+}$ 20 cells/ 6 rats, *Nrxn1*$^{+/-}$ 18 cells/ 7 rats). (D, I) Cell capacitance of mPFC PCs is reduced in *Nrxn1*$^{+/-}$ rats at p13-15 (*Nrxn1*$^{+/+}$ 26 cells/ 10 rats, *Nrxn1*$^{+/-}$ 21 cells/ 9 rats), but unchanged in *Nlgn3*$^{-/y}$ rats in comparison to WT (*Nlgn3*$^{+/y}$ 19 cells/ 8 rats, *Nlgn3*$^{-/y}$ 16 cells/ 7 rats). No difference in cell capacitance in either model at p25-35 (*Nlgn3*$^{+/y}$ 20 cells/ 8 rats, *Nlgn3*$^{-/y}$ 22 cells/ 8 rats; *Nrxn1*$^{+/+}$ 20 cells/ 6 rats, *Nrxn1*$^{+/-}$ 18 cells/ 7 rats). (E, J) 'Sag' was unchanged in both *Nlgn3*$^{-/y}$ and *Nrxn1*$^{+/-}$ rats at p13-15 (*Nlgn3*$^{+/y}$ 19 cells/ 8 rats, *Nlgn3*$^{-/y}$ 16 cells/ 7 rats; *Nrxn1*$^{+/+}$ 26 cells/ 10 rats, *Nrxn1*$^{+/-}$ 21 cells/ 9 rats) or p25-35 (*Nlgn3*$^{+/y}$ 20 cells/ 8 rats, *Nlgn3*$^{-/y}$ 22 cells/ 8 rats; *Nrxn1*$^{+/+}$ 20 cells/ 6 rats, *Nrxn1*$^{+/-}$ 18 cells/ 7 rats).
Dots represent cells, GLMM results shown in Tables 5.4 and 5.5

Active membrane properties are affected in both *Nlgn3$^{-/y}$* and *Nrxn1$^{+/-}$* layer 5 mPFC PCs

Cao et al. (2018) reported normal intrinsic excitability of mPFC PCs in *Nlgn3 R451C* mice. To determine if this is the case in *Nlgn3$^{-/y}$* rats, the intrinsic excitability of layer 5 mPFC PCs was assessed using a series of depolarising current injections. Despite a change in input resistance and capacitance of p13-15 layer 5 mPFC *Nrxn1$^{+/-}$* PCs, I found no corresponding change in intrinsic cell excitability in *Nrxn1$^{+/-}$* PCs (Fig. 5.16G, H). Furthermore, I found no change in the excitability of p25-35 *Nrxn1$^{+/-}$* mPFC PCs (Fig. 5.16I, J), or in *Nlgn3$^{-/y}$* mPFC PCs at either time point (Fig. 5.16A-D). However, there was a significant decrease in rheobase current in p13-15 *Nrxn1$^{+/-}$* neurons (Table 5.5, Fig. 5.17K). Conversely, no changes in rheobase was observed at p25-35 in *Nrxn1$^{+/-}$* PCs (Table 5.5, Fig. 5.17K), or in *Nlgn3$^{-/y}$* mPFC PCs at either age point (Table 5.4, Fig. 5.17E). AP threshold was unaltered in both models at both time points (Tables 5.4 and 5.5, Fig. 5.17F, L).

The change in rheobase of p13-15 *Nrxn1$^{+/-}$* mPFC PCs was not accompanied by any changes in AP waveform or kinetics (Table 5.5, Fig. 5.17E-H). Additionally, no change in AP waveform/kinetics were observed at p25-35 in *Nrxn1$^{+/-}$* mPFC PCs. However, p25-35, but not p13-15, layer 5 mPFC cells from *Nlgn3$^{-/y}$* rats showed a decrease in AP duration and an increase in repolarisation speed (Table 5.4, Fig. 5.17B, D). Together, these results suggest that active intrinsic properties of layer 5 mPFC PCs are differentially affected by *Nrxn1* and *Nlgn3* mutations.

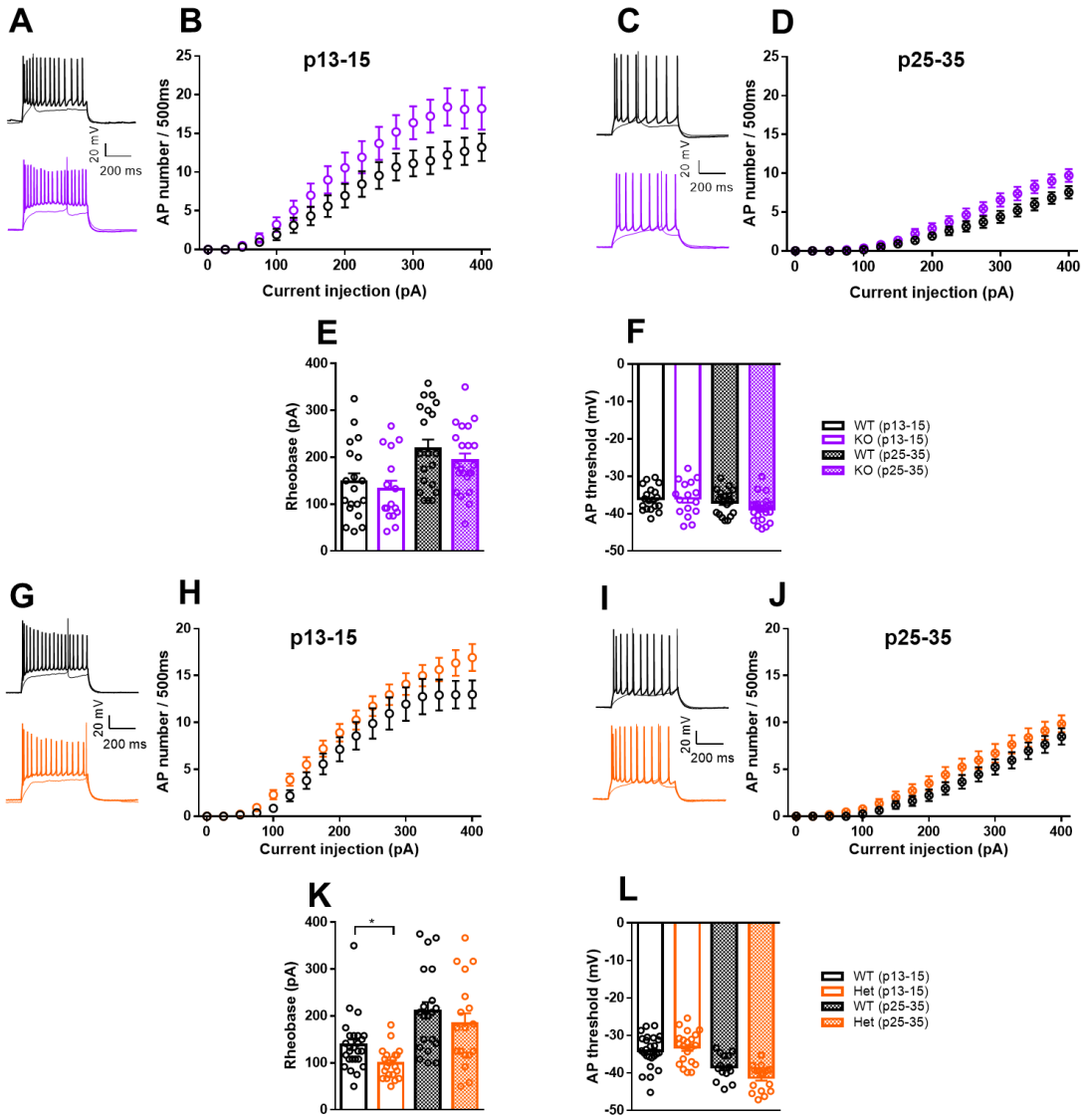

Figure 5.16: Altered active properties of *Nrxn1*$^{+/-}$ but not *Nlgn3*$^{-/y}$ mPFC pyramidal cells.

Figure 5.16 ***(previous page)*****: Altered active properties of *Nrxn1*$^{+/-}$ (orange) but not *Nlgn3*$^{-/y}$ (purple) mPFC pyramidal cells.** (A) Representative traces of WT (black) and *Nlgn3*$^{-/y}$ (purple) mPFC PCs from p13-15 rats firing in response to rheobase and +400 pA current steps. (B) No difference in the input-frequency curve of p13-15 *Nlgn3*$^{-/y}$ mPFC PCs in comparison to WT controls (*Nlgn3*$^{+/y}$ 19 cells/ 8 rats, *Nlgn3*$^{-/y}$ 16 cells/ 7 rats, p = 0.072, F = 3.44, two-way ANOVA). (C) Representative traces of WT (black) and *Nlgn3*$^{-/y}$ (purple) mPFC PCs from p25-35 rats firing in response to rheobase and +400 pA current steps. (D) No difference in the input-frequency curve of p25-35 *Nlgn3*$^{-/y}$ mPFC PCs in comparison to WT controls (*Nlgn3*$^{+/y}$ 20 cells/ 8 rats, *Nlgn3*$^{-/y}$ 22 cells/ 8 rats, p = 0.12, F = 2.52, two-way ANOVA). (E) No change in rheobase current in *Nlgn3*$^{+/y}$ p13-15 (*Nlgn3*$^{+/y}$ 19 cells/ 8 rats, *Nlgn3*$^{-/y}$ 16 cells/ 7 rats) or p25-35 (*Nlgn3*$^{+/y}$ 20 cells/ 8 rats, *Nlgn3*$^{-/y}$ 22 cells/ 8 rats) mPFC PCs. (F) AP threshold is unchanged in *Nlgn3*$^{+/y}$ p13-15 (*Nlgn3*$^{+/y}$ 19 cells/ 8 rats, *Nlgn3*$^{-/y}$ 16 cells/ 7 rats) or p25-35 (*Nlgn3*$^{+/y}$ 20 cells/ 8 rats, *Nlgn3*$^{-/y}$ 22 cells/ 8 rats) mPFC PCs. (G) Representative traces of WT (black) and *Nrxn1*$^{+/-}$ (orange) mPFC PCs from p13-15 rats firing in response to rheobase and +400 pA current steps. (H) No difference in the input-frequency curve of p13-15 *Nrxn1*$^{+/-}$ mPFC PCs in comparison to WT controls (*Nrxn1*$^{+/+}$ 26 cells/ 10 rats, *Nrxn1*$^{+/-}$ 21 cells/ 9 rats, p = 0.19, F = 1.78, two-way ANOVA). (I) Representative traces of WT (black) and *Nrxn1*$^{+/-}$ (orange) mPFC PCs from p25-35 rats firing in response to rheobase and +400 pA current steps. (J) No difference in the input-frequency curve of p25-35 *Nrxn1*$^{+/-}$ mPFC PCs in comparison to WT controls (*Nrxn1*$^{+/+}$ 20 cells/ 6 rats, *Nrxn1*$^{+/-}$ 18 cells/ 7 rats, p = 0.19, F = 1.75 two-way ANOVA). (K) Rheobase current is reduced in *Nrxn1*$^{+/-}$ mPFC PCs at p13-15 (*Nrxn1*$^{+/+}$ 26 cells/ 10 rats, *Nrxn1*$^{+/-}$ 21 cells/ 9 rats) but not p25-25 (*Nrxn1*$^{+/+}$ 20 cells/ 6 rats, *Nrxn1*$^{+/-}$ 18 cells/ 7 rats). (L) AP threshold was decreased in *Nrxn1*$^{+/-}$ mPFC PCs at p13-15 (*Nrxn1*$^{+/+}$ 26 cells/ 10 rats, *Nrxn1*$^{+/-}$ 21 cells/ 9 rats) but not p25-25 (*Nrxn1*$^{+/+}$ 20 cells/ 6 rats, *Nrxn1*$^{+/-}$ 18 cells/ 7 rats).
Dots represent cells, GLMM results shown in Tables 5.4 and 5.5.

Post-AP currents are affected in *Nrxn1*$^{+/-}$ but not *Nlgn3*$^{-/y}$ mPFC PCs

Following examination of active and passive intrinsic properties, post-AP currents were examined in *Nrxn1*$^{+/-}$ and *Nlgn3*$^{-/y}$ mPFC PCs at p13-15 and p25-35. I found no changes in ADP or mAHP in *Nlgn3*$^{-/y}$ mPFC PCs at either age point (Table 5.4, Fig. 5.18A-C). However, ADP in mPFC PCs from *Nrxn1*$^{+/-}$ p13-15, but not p25-35, rats was increased in comparison to WT rats (Table 5.5, Fig. 5.18D). mAHP amplitude was unchanged in *Nrxn1*$^{+/-}$ layer 5 mPFC PCs at both time points (Table 5.5, Fig. 5.18E, F).

These results suggest that, whilst neuroligin-3 loss has minimal effects on cell intrinsic properites in both the hippocampus and mPFC, heterozygote mutations in *Nrxn1* cause altered intrinsic properties of neurons that are distinct between brain regions and points throughout development.

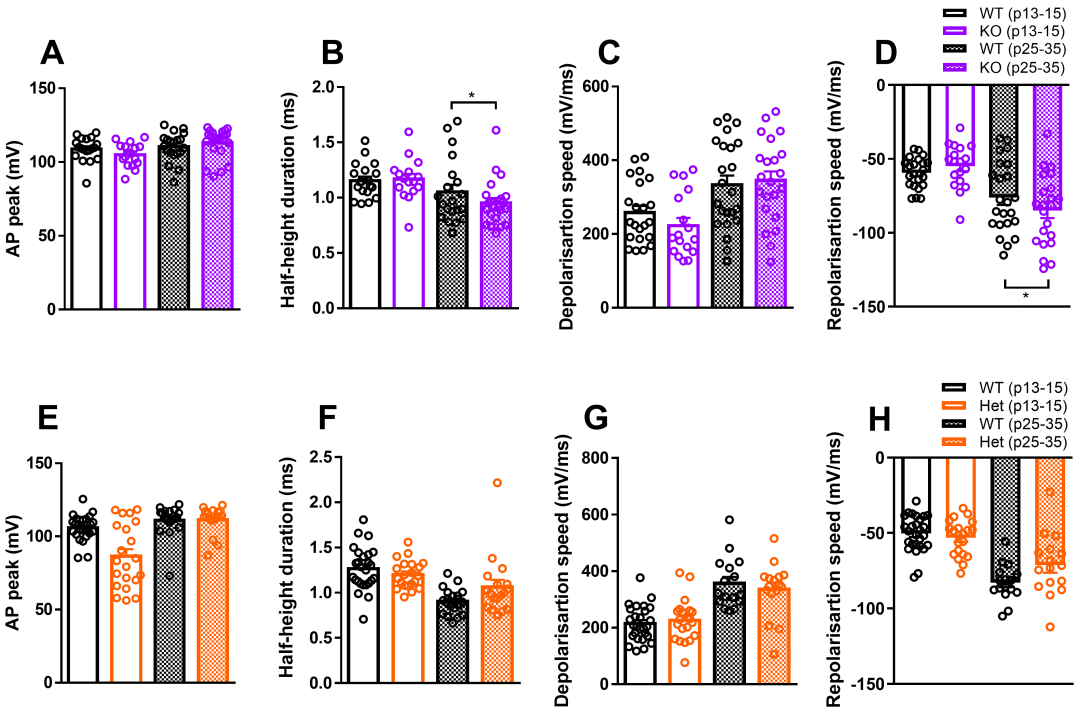

Figure 5.17: Altered AP waveform and kinetics in *Nlgn3*$^{-/y}$ (purple) but not *Nrxn1*$^{+/-}$ (orange) mPFC pyramidal cells. (A, E) Rheobase AP peak height is unchanged in both *Nrxn1*$^{+/-}$ and *Nlgn3*$^{-/y}$ at p13-15 (*Nlgn3*$^{+/y}$ 19 cells/ 8 rats, *Nlgn3*$^{-/y}$ 16 cells/ 7 rats; *Nrxn1*$^{+/+}$ 26 cells/ 10 rats, *Nrxn1*$^{+/-}$ 21 cells/ 9 rats) and p25-35 (*Nlgn3*$^{+/y}$ 20 cells/ 8 rats, *Nlgn3*$^{-/y}$ 22 cells/ 8 rats; *Nrxn1*$^{+/+}$ 20 cells/ 6 rats, *Nrxn1*$^{+/-}$ 18 cells/ 7 rats). (B, F) Half-height duration of rheobase AP was decreased in p25-35 layer 5 mPFC neurons in *Nlgn3*$^{-/y}$ (*Nlgn3*$^{+/y}$ 20 cells/ 8 rats, *Nlgn3*$^{-/y}$ 22 cells/ 8 rats) but not *Nrxn1*$^{+/-}$ rats (*Nrxn1*$^{+/+}$ 20 cells/ 6 rats, *Nrxn1*$^{+/-}$ 18 cells/ 7 rats) in comparison to WT. (C, G) Depolarisation speed of rheobase AP was unaffected in both *Nlgn3*$^{-/y}$ and *Nrxn1*$^{+/-}$ layer 5 mPFC PCs at p13-15 (*Nlgn3*$^{+/y}$ 19 cells/ 8 rats, *Nlgn3*$^{-/y}$ 16 cells/ 7 rats; *Nrxn1*$^{+/+}$ 26 cells/ 10 rats, *Nrxn1*$^{+/-}$ 21 cells/ 9 rats) or p25-35 (*Nlgn3*$^{+/y}$ 20 cells/ 8 rats, *Nlgn3*$^{-/y}$ 22 cells/ 8 rats; *Nrxn1*$^{+/+}$ 20 cells/ 6 rats, *Nrxn1*$^{+/-}$ 18 cells/ 7 rats). (D, H) AP repolarisation speed was increased in in p25-35 layer 5 mPFC neurons in *Nlgn3*$^{-/y}$ (*Nlgn3*$^{+/y}$ 20 cells/ 8 rats, *Nlgn3*$^{-/y}$ 22 cells/ 8 rats) but not *Nrxn1*$^{+/-}$ rats (*Nrxn1*$^{+/+}$ 20 cells/ 6 rats, *Nrxn1*$^{+/-}$ 18 cells/ 7 rats) in comparison to WT.
Dots represent cells, GLMM results shown in Tables 5.4 and 5.5.

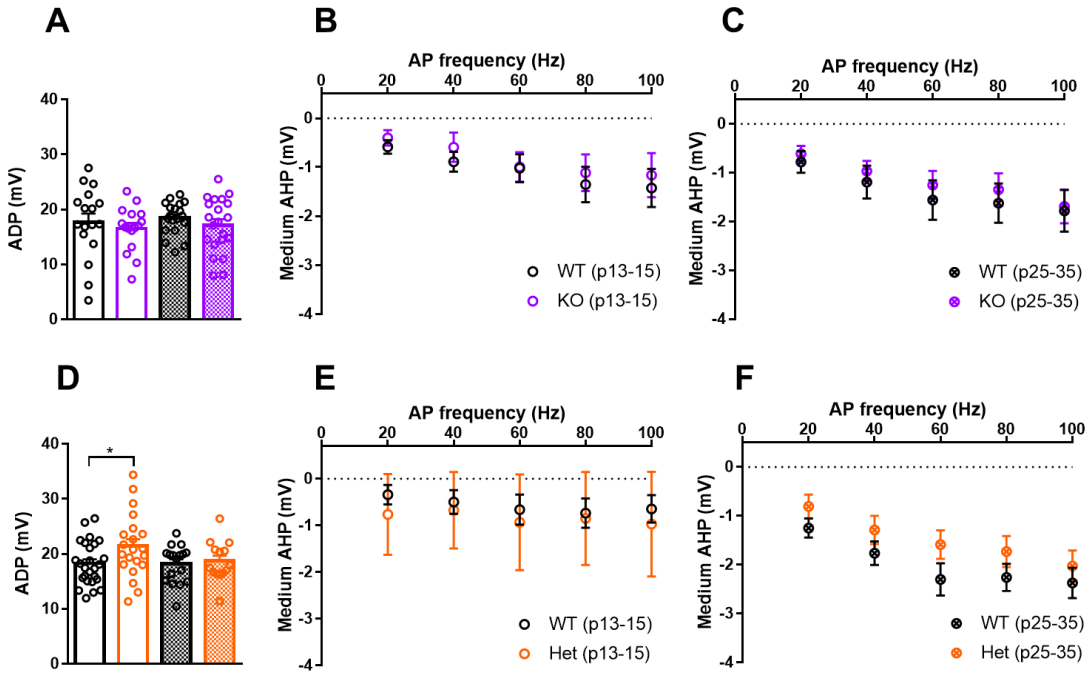

Figure 5.18: After-depolarisation potential is unaffected in *Nrxn1*$^{+/-}$ (orange) but not *Nlgn3*$^{-/y}$ (purple) mPFC pyramidal cells. (A, D) After-depolarisation potential amplitude is increased in *Nrxn1*$^{+/-}$ (*Nrxn1*$^{+/+}$ 26 cells/ 10 rats, *Nrxn1*$^{+/-}$ 21 cells/ 9 rats) but not*Nlgn3*$^{-/y}$ (*Nlgn3*$^{+/y}$ 19 cells/ 8 rats, *Nlgn3*$^{-/y}$ 16 cells/ 7 rats) mPFC PCs at p13-15. No change in after-depolarisation in either model at p25-35 (*Nlgn3*$^{+/y}$ 20 cells/ 8 rats, *Nlgn3*$^{-/y}$ 22 cells/ 8 rats; *Nrxn1*$^{+/+}$ 20 cells/ 6 rats, *Nrxn1*$^{+/-}$ 18 cells/ 7 rats). Dots represent cells, GLMM results shown in Tables 5.4 and 5.5. (B) No change in medium AHP amplitude in p13-15 *Nlgn3*$^{-/y}$ layer 5 mPFC PCs in comparison to WT (*Nlgn3*$^{+/y}$ 12 cells/ 8 rats, *Nlgn3*$^{+/y}$ 13 cells/ 7 rats p = 0.63, F = 0.24, two-way ANOVA). (C) No difference in medium AHP amplitude in p25-35 *Nlgn3*$^{-/y}$ layer 5 mPFC PCs in comparison to WT (*Nlgn3*$^{+/y}$ 16 cells/ 8 rats, *Nlgn3*$^{+/y}$ 17 cells/ 8 rats p = 0.62, F = 0.24, two-way ANOVA). (E) Medium AHP amplitude is unaltered in *Nrxn1*$^{+/-}$ p13-15 layer 5 mPFC PCs in comparison to WT ((*Nrxn1*$^{+/+}$, *Nrxn1*$^{+/-}$ 20 cells/ 9 rats, p = 0.40, F = 0.73, two-way ANOVA). (F) Medium AHP amplitude is unchanged in *Nrxn1*$^{+/-}$ p25-35 layer 5 mPFC PCs compared to WT (*Nrxn1*$^{+/+}$ 15 cells/ 8 rats, *Nrxn1*$^{+/-}$ 15 cells/ 7 rats, p = 0.2, F = 1.72, two-way ANOVA).

Table 5.4: GLMM for mPFC PC intrinsic properties in WT and *Nlgn3*$^{-/y}$ rats.

	WT	***Nlgn3*$^{-/y}$**	**p-value**
RMP			
p13-15:	-63.00 ± 0.93 mV	-61.92 ± 1.58 mV	p = 0.88
p25-35:	-65.07 ± 1.41 mV	-68.50 ± 0.96 mV	p = 0.15
Input resistance			
p13-15:	225.4 ± 32.98 MΩ	277.8 ± 37.35 MΩ	p = 0.27
p25-35:	86.36 ± 10.14 MΩ	98.56 ± 11.17 MΩ	p = 0.41
Membrane time constant			
p13-15:	32.17 ± 3.52 ms	36.30 ms ± 4.02 ms	p = 0.45
p25-35:	24.28 ± 2.76 ms	24.38 ms ± 1.95 ms	p = 0.89
Capacitance			
p13-15:	168.4 ± 13.81 pF	149.7 ± 13.05 pF	p = 0.28
p25-35:	297.9 ± 21.70 pF	294.4 ± 29.45 pF	p = 0.27
Sag			
p13-15:	3.49 ± 0.61 mV	3.11 ± 0.29 mV	p = 0.86
p25-35:	1.46 ± 0.14 mV	1.71 ± 0.16 mV	p = 0.79
Rheobase			
p13-15:	147.4 ± 18.49 pA	132.0 ± 1.16 pA	p = 0.55
p25-35:	218.3 ± 19.65 pA	193.2 ± 14.87 pA	p = 0.53
AP threshold			
p13-15:	-35.95 ± 0.73 mV	-35.88 ± 0.29 mV	p = 0.61
p25-35:	-36.93 ± 0.73 mV	-38.74 ± 0.70 mV	p = 0.34
AP height			
p13-15:	108.8 ± 1.83 mV	104.9 ± 2.04 mV	p = 0.11
p25-35:	110.4 ± 2.17 mV	113.0 ± 2.19 mV	p = 0.30
AP width			
p13-15:	1.16 ± 0.036 ms	1.17 ± 0.047 ms	p = 0.29
p25-35:	1.05 ± 0.065 ms	0.95 ± 0.045 ms	p = 0.018
AP depolarisation speed			
p13-15:	258.4 ± 17.64 mV/ms	222.9 ± 20.94 mV/ms	p = 0.38
p25-35:	333.8 ± 25.04 mV/ms	345.5 ± 24.09 mV/ms	p = 0.67
AP repolarisation speed			
p13-15:	-59.49 ± 22.22 mV/ms	-54.79 ± 3.48 mV/ms	p = 0.046
p25-35:	-76.16 ± 5.01 mV/ms	-84.88 ± 5.17 mV/ms	p = 0.98
ADP			
p13-15:	17.68 ± 1.58 mV/ms	16.51 ± 1.03 mV/ms	p = 0.54
p25-35:	18.45 ± 0.68 mV/ms	17.13 ± 1.08 mV/ms	p = 0.32

Table 5.5: GLMM for mPFC PC intrinsic properties in WT and *Nrxn1*$^{+/-}$ rats.

	WT	***Nrxn1*$^{+/-}$**	**p-value**
RMP			
p13-15:	-60.58 ± 1.13 mV	-62.76 ± 3.13 mV	p = 0.11
p25-35:	-66.37 ± 1.49 mV	-64.90 ± 1.62 mV	p = 0.51
Input resistance			
p13-15:	207.4 ± 17.96 MΩ	304.0 ± 30.48 MΩ	p = 0.00031
p25-35:	78.39 ± 8.813 MΩ	100.6 ± 14.51 MΩ	p = 0.34
Membrane time constant			
p13-15:	31.95 ± 2.32 ms	37.31 ms ± 2.12	p = 0.34
p25-35:	23.96 ± 2.24 ms	31.63 ms ± 4.56	p = 0.19
Capacitance			
p13-15:	169.2 ± 11.67 pF	127.5 ± 6.897 pF	p = 0.00016
p25-35:	336.4 ± 29.08 pF	335.7 ± 22.36 pF	p = 0.78
Sag			
p13-15:	3.014 ± 0.31 mV	2.94 ± 0.52 mV	p = 0.84
p25-35:	1.57 ± 0.24 mV	1.79 ± 0.17 mV	p = 0.69
Rheobase			
p13-15:	138.5 ± 11.29 pA	100.9 ± 9.47 pA	p = 0.011
p25-35:	209.7 ± 19.89 pA	183.8 ± 22.06 pA	p = 0.61
AP threshold			
p13-15:	-34.12 ± 0.85 mV	-31.53 ± 1.56 mV	p = 0.57
p25-35:	-38.37 ± 0.93 mV	-41.21 ± 0.79 mV	p = 0.10
AP height			
p13-15:	106.0 ± 1.71 mV	108.7 ± 3.30 mV	p = 0.96
p25-35:	111.1 ± 2.30 mV	111.5 ± 2.16 mV	p = 0.21
AP width			
p13-15:	1.27 ± 0.047 ms	1.21 ± 0.068 ms	p = 0.12
p25-35:	0.91 ± 0.031 ms	1.063 ± 0.078 ms	p = 0.071
AP depolarisation speed			
p13-15:	214.9 ± 11.84 mV/ms	226.5 ± 16.25 mV/ms	p = 0.49
p25-35:	357.4 ± 22.49 mV/ms	336.2 ± 24.2 mV/ms	p = 0.52
AP repolarisation speed			
p13-15:	-50.37 ± 2.31 mV/ms	-53.2 ± 2.58 mV/ms	p = 0.42
p25-35:	-82.91 ± 3.01 mV/ms	-71.29 ± 5.09 mV/ms	p = 0.057
ADP			
p13-15:	18.21 ± 0.77 mV	21.43 ± 1.26 mV	p = 0.03
p25-35:	18.18 ± 0.83 mV	18.71 ± 0.97 mV	p = 0.67

5.2.6 Synaptic properties of *Nlgn3$^{-/y}$* and *Nrxn1$^{+/-}$* mPFC neurons

Synaptic transmission of CA1 PCs was significantly altered in *Nlgn3$^{-/y}$*, however no differences were observed in *Nrxn1$^{+/-}$* CA1 PCs. Nonetheless, the data shown so far in this chapter provides evidence that several phenotypes are brain-region specific. I therefore hypothesised that mutations in *Nlgn3* or *Nrxn1* would lead to altered mEPSC/mIPSCs in layer 5 mPFC neurons.

No change in mEPSCs in mPFC PCs of *Nlgn3$^{-/y}$* or *Nrxn1$^{+/-}$* rats

In order to assess basal excitatory synaptic transmission in layer 5 mPFC neurons in *Nlgn3$^{-/y}$* and *Nrxn1$^{+/-}$* rats, I examined mEPSCs in the presence of TTX and PTX from acute mPFC slices. I found no changes in mEPSC amplitude or frequency in either model compared to WT (Table 5.6, Fig. 5.19). This suggests that excitatory synaptic input to layer 5 PCs in the mPFC is unchanged in both *Nlgn3$^{-/y}$* and *Nrxn1$^{+/-}$* rats.

No change in mIPSCs in mPFC PCs of *Nlgn3$^{-/y}$* or *Nrxn1$^{+/-}$* rats

To determine if there were changes in inhibitory synapses onto layer 5 mPFC PCs, I examined mIPSCs in the presence of TTX and CNQX. I found no differences in mIPSC amplitude or frequency in either rat model (Table 5.6, Fig. 5.20). These results suggest that inhibitory input to layer 5 PCs is unaffected in the mPFC of *Nlgn3$^{-/y}$* and *Nrxn1$^{+/-}$* rats in comparison to WT.

Table 5.6: GLMM for mPFC PC mEPSCs/mIPSCs in WT, *Nlgn3$^{-/y}$* and *Nrxn1$^{+/-}$* rats.

	WT	***Nlgn3$^{-/y}$***	**p-value**
mEPSC amplitude (pA)	9.80 ± 0.37	10.52 ± 0.62	0.36
mEPSC frequency (Hz)	4.93 ± 0.87	3.92 ± 0.39	0.5
mIPSC amplitude (pA)	29.92 ± 3.45	28.43 ± 2.71	0.87
mIPSC frequency (Hz)	5.65 ± 0.66	5.40 ± 0.56	0.93
	WT	***Nrxn1$^{+/-}$***	**p-value**
mEPSC amplitude (pA)	12.42 ± 1.29	12.81 ± 1.65	0.93
mEPSC frequency (Hz)	9.27 ± 1.04	7.67 ± 0.84	0.31
mIPSC amplitude (pA)	26.73 ± 1.93	34.47 ± 6.10	0.32
mIPSC frequency (Hz)	6.49 ± 0.52	9.19 ± 1.38	0.085

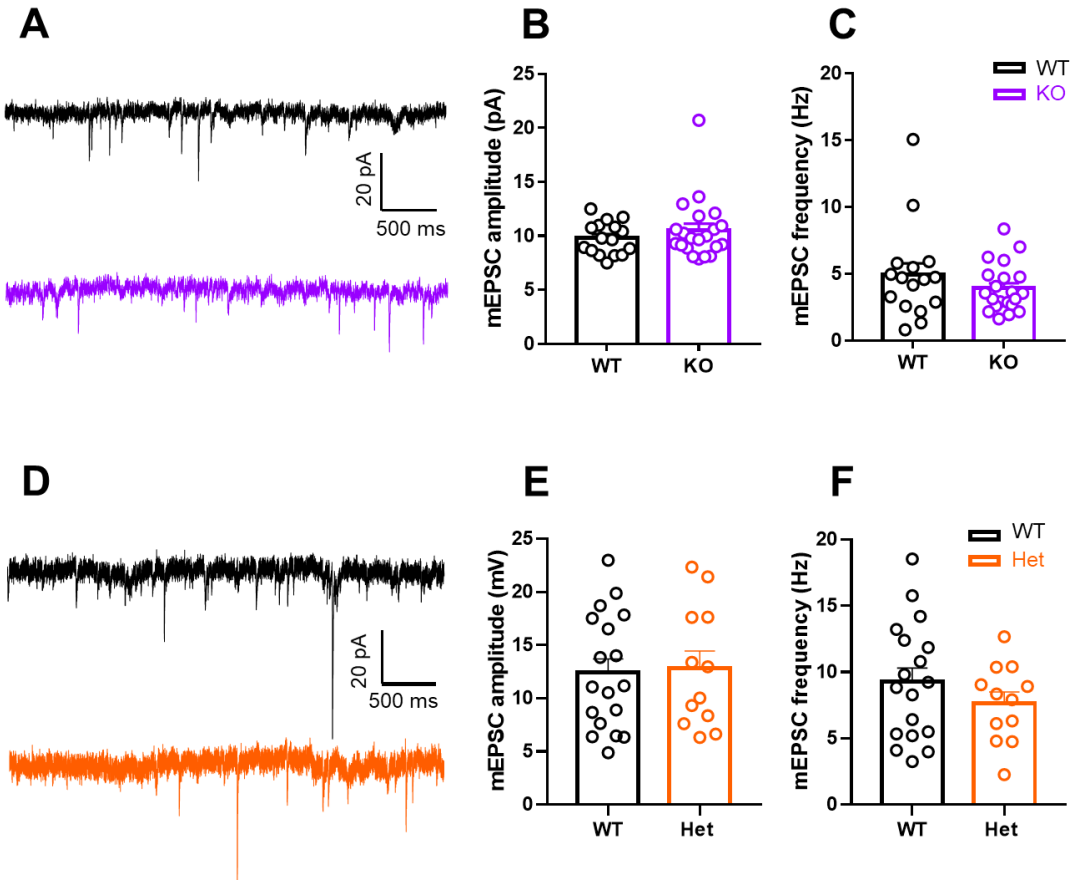

Figure 5.19: mEPSCs are unaffected in *Nlgn3*$^{-/y}$ and *Nrxn1*$^{+/-}$ mPFC PCs. (A) Representative traces of mEPSCs recorded from WT (black) and *Nlgn3*$^{-/y}$ (purple) rats. (B) No change in mEPSC amplitude between WT and *Nlgn3*$^{-/y}$ mPFC PCs (WT n = 16 cells/ 6 rats, KO n = 21 cells/ 8 rats). (C) mEPSC frequencies are not different between WT and *Nlgn3*$^{-/y}$ mPFC PCs (WT n = 16 cells/ 6 rats, KO n = 21 cells/ 8 rats). (D) Representative traces of mEPSCs recorded from WT (black) and *Nrxn1*$^{+/-}$ (orange) rats. (E) No change in mEPSC amplitude between WT and *Nrxn1*$^{+/-}$ mPFC PCs (WT n = 18 cells/ 7 rats, Het n = 12 cells/ 5 rats). (F) mEPSC frequencies are unchanged in *Nrxn1*$^{+/-}$ in comparison to WT mPFC PCs (WT n = 18 cells/ 7 rats, Het n = 12 cells/ 5 rats).
Dots represent cells, GLMM results shown in Table 5.6.

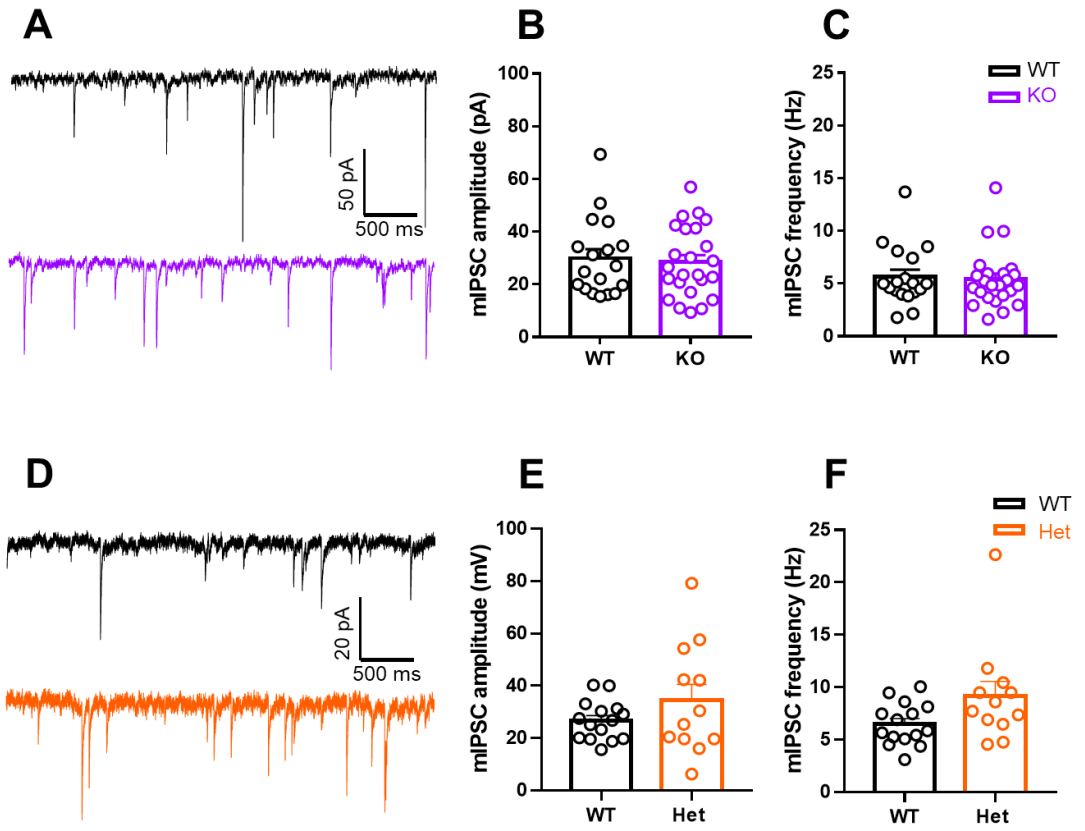

Figure 5.20: mIPSCs are unaffected in *Nlgn3*$^{-/y}$ and *Nrxn1*$^{+/-}$ mPFC PCs. (A) Representative traces of mIPSCs recorded from WT (black) and *Nlgn3*$^{-/y}$ (purple) rats. (B) No change in mIPSC amplitude between WT and *Nlgn3*$^{-/y}$ mPFC PCs (WT n = 18 cells/ 6 rats, KO n = 24 cells/ 8 rats). (C) mIPSC frequencies are not different between WT and *Nlgn3*$^{-/y}$ mPFC PCs (WT n = 18 cells/ 6 rats, KO n = 24 cells/ 8 rats). (D) Representative traces of mIPSCs recorded from WT (black) and *Nrxn1*$^{+/-}$ (orange) rats. (E) No change in mIPSC amplitude between WT and *Nrxn1*$^{+/-}$ mPFC PCs (WT n = 15 cells/ 7 rats, Het n = 12 cells/ 5 rats). (F) mIPSC frequencies are unchanged in *Nrxn1*$^{+/-}$ in comparison to WT mPFC PCs (WT n = 15 cells/ 7 rats, Het n = 12 cells/ 5 rats).
Dots represent cells, GLMM results shown in Table 5.6.

5.3 Discussion

The results presented in this chapter sought to examine synaptic plasticity, synaptic transmission, and neuronal excitability in the HC and mPFC of *Nlgn3*$^{-/y}$ and *Nrxn1*$^{+/-}$ rats in comparison to WT. I find that overall, the electrophysiology of neurons in these brain regions are different to WT controls in both models, which may provide cellular correlates for identified behavioural phenotypes implicating HC and mPFC dysfunction (Figs. 1.9, 5.1). Interestingly, I find that synaptic plasticity is reduced in both *Nlgn3*$^{-/y}$ and *Nrxn1*$^{+/-}$ rats at hippocampal SC synapses. In *Nlgn3*$^{-/y}$ rats, this impaired plasticity may be due to altered glutamatergic transmission, as mEPSC amplitudes are increased in these neurons. In *Nrxn1*$^{+/-}$ rats, however, show no changes in mEPSCs/mIPSCs, but instead display increased mAHP that could explain the reduced LTP observed in the HC. Furthermore, increased mAHP also results in hypoexcitability of CA1 PCs in *Nrxn1*$^{+/-}$ rats. However, these altered intrinsic properties were not consistent over different developmental stages.

In contrast to the HC, synaptic plasticity, synaptic transmission, and PC intrinsic properties were largely normal in the prelimbic mPFC of *Nlgn3*$^{-/y}$ and *Nrxn1*$^{+/-}$ rats. Some changes to the intrinsic properties were observed in layer 5 mPFC PCs in both models, however these effects were again age-dependent and different between *Nlgn3*$^{-/y}$ and *Nrxn1*$^{+/-}$ rats.

These results suggest that both *Nlgn3*$^{-/y}$ and *Nrxn1*$^{+/-}$ rats display significant alterations in cellular physiology, more so in the HC than in the mPFC. *Nlgn3*$^{-/y}$ and *Nrxn1*$^{+/-}$ rats display convergence of synaptic pathophysiologies in the case of LTP at CA3-CA1 synapses, however further investigations into cellular and synaptic mechanisms suggests distinct mechanisms underpin this phenotype in each model. Together, these data suggest that both convergence and divergence of pathophysiologies exist in the *Nlgn3*$^{-/y}$ and *Nrxn1*$^{+/-}$ rat models of ASD and ID.

5.3.1 Altered synaptic plasticity in *Nlgn3*$^{-/y}$ and *Nrxn1*$^{+/-}$ rats

Changes in hippocampal and mPFC plasticity has been shown to be correlated with reduced learning and memory in models of ASD/ID (Till et al., 2015; Asiminas et al., 2019). Behaviour experiments investigating fear learning and responses presented in the introduction of this thesis implicated that *Nlgn3*$^{-/y}$ rats have intact associative learning.

In addition to this, Etherton et al. (2011) demonstrated that full deletions of *Nlgn3* in mice have minimal effects on synaptic plasticity in the hippocampus, despite the crucial role neuroligin-3 plays in synapse development and maintenance (Scheiffele et al., 2000; Varoqueaux et al., 2006; Chih et al., 2005).

For these reasons, I hypothesised that hippocampal plasticity would be unaffected in *Nlgn3*$^{-/y}$ rats. However, I found they have reduced plasticity at hippocampal SC synapses. Specifically, forms of plasticity that are dependent on NMDAR function were affected in the hippocampus of *Nlgn3*$^{-/y}$ rats, whilst mGluR-dependent LTD was intact. Neuroligin-3 is known to associate with NMDARs through interactions with PSD-95 (Kim and Sheng, 2004; Walkup et al., 2016; Irie et al., 1997), therefore the loss of neuroligin-3 may cause decreased localisation of NMDARs to the postsynapse. This hypothesis is not supported by previous research in *Nlgn3*$^{-/y}$ mice which found no change in AMPAR/ NMDAR ratios in the hippocampus, however this study also reported no change in LTP at CA3-CA1 syanpses (Etherton et al., 2011). Even though phenotypes between *Nlgn3*$^{-/y}$ mice and rats are not conserved, further investigation of mechanisms behind the reduced NMDAR-dependent plasticity in the *Nlgn3*$^{-/y}$ rat is required. Recording AMPAR/ NMDAR ratios in hippocampal PCs would allow investigation of NMDAR currents which may be contributing to this reduced NMDAR-dependent plasticity phenotype.

High frequency stimulation of L2/3-L5 synapses in the prelimbic mPFC is also NMDAR-dependent (Fig. 5.13) but is unaffected in *Nlgn3*$^{-/y}$ rats. Brain region specific phenotypes of *Nlgn3* mutations have also been described by previous studies on mouse models (Etherton et al., 2011) despite relatively consistent expression of *Nlgn3* throughout the brain (Varoqueaux et al., 2006; Uhlén et al., 2015; Uchigashima et al., 2020). This could be due to compensation for the functional loss of neuroligin-3 by the other neuroligins, or employment of NMDAR-independent mechanisms to elicit LTP following high frequency stimulation in the mPFC. LTP recordings performed in mPFC slices from *Nlgn3*$^{-/y}$ rats in the presence of the NMDAR-antagonist AP5 would test the latter theory. Furthermore, this method of LTP induction in the mPFC is limited by the amount of LTP possible to achieve in these synapses using 5 x 300 Hz induction protocol. In slices from WT rats, average LTP magnitude 50-60 minutes following induction is only an 18 % fEPSP increase in comparison to baseline. Conversely, average LTP elicited in WT hippocampal slices was 43 %. When considering small magnitude

effects it is difficult to observe decreases in the amount potentiation without a large n and low variability (an increase in LTP, on the other hand, would be easier to detect using this protocol). More animals may therefore be required to determine if there is a decrease in mPFC LTP using this protocol. Alternatively, a theta-burst paradigm (such as utilised in Kerkhofs et al. (2018)) could be used, as this provides firstly a larger magnitude of LTP and secondly is more physiologically relevant than HFS induction.

Nonetheless, if cellular correlates of cognitive flexibility are intact in *Nlgn3*$^{-/y}$ rats, another interpretation of the behavioural data shown in Figure 1.9 is that *Nlgn3*$^{-/y}$ rats display increased avoidance of the shock zone to such an extent that they never re-enter the shock zone and therefore are never able to go through reversal learning. This interpretation would be in line with the conclusions drawn from Chapters 3 and 4, implying that *Nlgn3*$^{-/y}$ rats have a circuit bias promoting escape behaviour. Further behavioural testing of cognitive flexibility that do not include fearful stimuli would give a better understanding of this phenotype.

The results presented in this chapter suggest that cellular correlates of memory are reduced in *Nlgn3*$^{-/y}$ rats, whereas cellular correlates of cognitive flexibility are unaffected. It is important to note that the recordings performed in this chapter were carried out on slices taken from p25-35 rats, whereas behavioural experiments were on p60-70 animals. This difference in ages may explain the disparity between the expected and observed outcomes of these experiments. Supporting this, preliminary evidence from our lab suggests that hippocampal LTP in slices from p60 rats is unaffected in *Nlgn3*$^{-/y}$ rats (Teresa Spanò, unpublished). This suggests that hippocampal synaptic plasticity in *Nlgn3*$^{-/y}$ rats is impaired earlier in development, and then is restored by adulthood. Moreover, amygdalar LTP, shown to be required for the acquisition of fear memories (Rogan et al., 1997; Quirk et al., 1995) is reduced in p25-35 *Nlgn3*$^{-/y}$ rats (Toft, 2019). Together, these results suggest that associative fear learning, and cellular correlates of this, may be impaired in juvenile *Nlgn3*$^{-/y}$ rats but is recovered in adult rats. Conditional deletion of *Nlgn3* in adult rats would allow dissection of which phenotypes are the direct cause of neuroligin-3 loss at the synapse, and which are a consequence of abnormal synapse and circuit development.

Furthermore, I found that hippocampal slices from *Nlgn3*$^{-/y}$ rats do not display altered mGluR-dependent LTD. Hamilton et al. (2014) suggested that on a behavioural level, *Fmr1*$^{-/y}$ and *Nlgn3*$^{-/y}$ rats display converging phenotypes, and Baudouin et al.

(2012) provided evidence of shared synaptic pathophysiologies between *Fmr1*$^{-/y}$ and *Nlgn3*$^{-/y}$ mice. However, I provide evidence that the exaggerated mGluR-dependent LTD reported in *Fmr1*$^{-/y}$ rats (Till et al., 2015) is not present in *Nlgn3*$^{-/y}$ rats. This suggests that, although behavioural phenotypes may be similar between these two models of ASD/ID, cellular and synaptic pathophysiologies are divergent. FMRP, the protein encoded by *Fmr1*, is a translational repressor required to suppress proteins required for mGluR-dependent LTD (Bear et al., 2004). As neuroligin-3 is a synaptic adhesion molecule, and not directly involved in protein translation, convergence of synaptic properties between *Nlgn3*$^{-/y}$ and *Fmr1*$^{-/y}$ rats may not be expected. This was also the case for *Nrxn1*$^{+/-}$ rats, in which mGluR-dependent LTD was also unaffected in hippocampal slices. Nonetheless, the converging phenotype of abnormal mGluR-dependent LTD between *Fmr1*$^{-/y}$ and *Nlgn3*$^{-/y}$ mice in cerebellar slices reported by Baudouin et al. (2012) and Koekkoek et al. (2005) warrants further investigation of mGluR-dependent LTD in the cerebellum of *Nlgn3*$^{-/y}$ rats.

Unlike *Nlgn3*$^{-/y}$ and *Fmr1*$^{-/y}$ rats, behavioural experiments revealed diverging phenotypes between *Nlgn3*$^{-/y}$ and *Nrxn1*$^{+/-}$ rats (Figs. 1.5, 5.1). Both models, however, displayed some common synaptic plasticity impairments; the reduced hippocampal LTP observed in *Nlgn3*$^{-/y}$ rats was also present in *Nrxn1*$^{+/-}$ rats. This indicates that convergence of pathophysiologies between genetically distinct models of autism can occur at different levels. It is possible that therapeutic intervention at a biological level where convergence is present may also result in rescue of behavioural phenotypes despite their diverging nature between models. However, it is not known if this LTP impairment prevails into adulthood in *Nrxn1*$^{+/-}$ rats, so age-matching physiology and behavioural experiments would provide information on whether this is a developmentally transient phenotype. *Nrxn1*$^{+/-}$ rats did not, however, show the same decrease in NMDAR-dependent LTD as was observed in *Nlgn3*$^{-/y}$ hippocampal slices. Unlike neuroligin-3, the presynaptically localised neurexin-1 is not directly involved in the recruitment of NMDARs, which may explain why this form of LTD is unaffected in this model. It is possible that distinct mechanisms lead to reduced hippocampal LTP in *Nlgn3*$^{-/y}$ and *Nrxn1*$^{+/-}$ rats. The NR2A and NR2B subunits of NMDARs are thought to have differential roles in LTP and LTD; the NR2B subunit is required for CaMKII binding and therefore LTP induction (Barria and Malinow, 2005), however is not required for LTD (Morishita et al., 2007). In addition, the NR2A subunit is required for NMDAR-

dependent LTD but not LTP (Morishita et al., 2007; Massey et al., 2004). Differences in these subunits would account for the distinct effects of *Nlgn3* and *Nrxn1* mutations on LTP and LTD, if *Nrxn1*$^{+/-}$ rats have altered NR2B but not NR2A subunits. This hypothesis could be tested using Western blotting for the individual NMDAR subunits.

Alternatively, as neurexin and neuroligin localise to the pre- and postsynapse, respectively, it is possible that the reduced LTP results from a presynaptic effect in one model, and a postsynaptic effect in the other. One way of investigating whether the basis of LTP is pre- or postsynaptic is using coefficient of variation (CV^2) analysis. This was performed on LTP recording data from *Nlgn3*$^{-/y}$ and *Nrxn1*$^{+/-}$ (see Appendix B.1, Fig. S6), and revealed both pre- and postsynaptic interpretations of recordings from *Nlgn3*$^{-/y}$ and *Nrxn1*$^{+/-}$ LTP recordings, however the low magnitudes of LTP caused by the mutations made these data difficult to interpret. Further investigation of pre- and postsynaptic LTP mechanisms in *Nlgn3*$^{-/y}$ and *Nrxn1*$^{+/-}$ is required.

Although potentially arising from distinct mechanisms in *Nlgn3*$^{-/y}$ and *Nrxn1*$^{+/-}$ rats, the results shown in this chapter demonstrate convergence of reduced hippocampal LTP between these two models of ASD/ID. Impaired LTP has been reported in models many other models of ASD/ID in addition to *Nlgn3*$^{-/y}$ and *Nrxn1*$^{+/-}$ rats described here, including Fragile-X syndrome, Neurofibromatosis, MRD5, Cowden syndrome, Tuberous Sclerosis, and Angelman syndrome (Louros and Osterweil, 2016), which suggests synaptic plasticity may be a relevant therapeutic target. Further investigation of drugs that ameliorate plasticity deficits, such as modulators of cAMP and cGMP signalling pathways (recently shown to rescue LTP deficits in models of Alzheimer's disease (Prieto et al., 2017)), may provide significant insight into potential treatments for ASD/ID.

In summary, the changes in synaptic plasticity presented in this chapter are:

1. Species specific: *Nlgn3*$^{-/y}$ mice did not show reduced hippocampal LTP (Etherton et al., 2011), but it is observed here in *Nlgn3*$^{-/y}$ rats, despite the similar ages of rats in these two experiments (p28-40 in Etherton et al. (2011), p25-35 here).

2. Model specific: Reduced NMDAR-dependent LTD is not conserved between *Nlgn3*$^{-/y}$ and *Nrxn1*$^{+/-}$ rats.

3. Brain region specific: LTP impairments were observed in the hippocampus but not in the mPFC in both *Nlgn3*$^{-/y}$ and *Nrxn1*$^{+/-}$ rats.

4. Age specific (preliminary): Preliminary data (Teresa Spanò, unpublished) suggests

that the reduced hippocampal LTP present in p25-35 rats is intact in p60-70 rats.

5.3.2 Increased mEPSC amplitudes in *Nlgn3$^{-/y}$* CA1 neurons

Changes in subthreshold synaptic activity may explain the observed plasticity deficits in *Nlgn3$^{-/y}$* and *Nrxn1$^{+/-}$* rats. I found no changes in the mEPSCs/mIPSCs of *Nrxn1$^{+/-}$* rats in either CA1 or layer 5 mPFC PCs (Figs. 5.11, 5.12, 5.19, 5.20) however CA1 PCs of *Nlgn3$^{-/y}$* rats displayed increased mEPSC amplitudes (Fig. 5.11). As with the reduced LTP observed in this model, this mEPSC change was specific to the hippocampus and not observed in layer 5 mPFC neurons (Fig. 5.19), or indeed in PAG neurons of *Nlgn3$^{-/y}$* rats (Fig. 3.15). This increase in mEPSC amplitude of CA1 PCs is in contrast to previously reported data from *Nlgn3$^{-/y}$* mice, which showed a decrease in mEPSC amplitude in cerebellar slices (Baudouin et al., 2012), and hippocampal slices which showed a decrease in mEPSC frequency with no change in amplitude (Etherton et al., 2011).

Whilst changes in mEPSCs/mIPSC frequency (unchanged in both models and both brain regions) indicate altered synaptic inputs or release probability, changes in mEPSCs/mIPSC amplitude may reflect an increase in synaptic efficacy. As mEPSCs are recorded at -70 mV, the current contributing to them is AMPAR-mediated, suggesting AMPAR-mediated currents are increased in *Nlgn3$^{-/y}$* rats. One explanation for the impaired NMDAR-dependent plasticity in *Nlgn3$^{-/y}$* rats is reduced NMDAR recruitment to synapses due to the loss of neuroligin-3, which may have knock-on effects on AMPAR recruitment. There is evidence to suggest that NMDAR signalling restricts AMPAR recruitment in developing synapses in the cortex, and loss of the NMDAR NR1 subunit leads to increased AMPAR-mediated currents (Ultanir et al., 2007). If this is the case in *Nlgn3$^{-/y}$* rats, chronic inactivation of NMDARs should have no further effect on AMPAR currents in the hippocampus. Investigation of AMPAR/ NMDAR ratios in *Nlgn3$^{-/y}$* CA1 PCs would also provide further information regarding this hypothesis.

Additionally, it is important to highlight the lack of changes to mEPSCs and mIPSCs recorded from *Nrxn1$^{+/-}$* rats. Neurexins have been shown to be crucial for Ca^{2+}-triggered synaptic vesicle release (Missler et al., 2003; Zhang, 2005), yet I observe no change in synaptic transmission either the amplitude or frequency of miniature events in *Nrxn1$^{+/-}$* rats in either the HC or mPFC. Pak et al. (2015) reported heterozygous *Nrxn1* mutations introduced into human induced neurons result in significant reduction

in mEPSC frequency; a phenotype also observed in the hippocampus of *Nrxn1α*$^{-/-}$ mice (Etherton et al., 2009). Whether heterozygous mutation of *Nrxn1* in mice has the same effect is not known. Interestingly, Avazzadeh et al. (2019) reported the opposite effect in patient-derived *Nrxn1α*$^{+/-}$ neurons; an increase in Ca^{2+} transients was observed. One explanation for the different findings in these models of *Nrxn*-associated ASD is the distinct functions of α and β-neurexins. α-neurexins are required for synaptic transmission (Missler et al., 2003), whereas β-neurexins are required for binding to neuroligins (Boucard et al., 2005). The heterozygous mutations introduced into the human neurons described in Pak et al. (2015) caused loss of both α and β-neurexin, and Avazzadeh et al. (2019) demonstrated that their patient derived *Nrxn1α*$^{+/-}$ neurons displayed an 262 % increase in *NRXN1β* that may be compensating for the depletion of *NRXN1α*, suggesting that the phenotypes found by Pak et al. (2015) were due to loss of compensation by *NRXN1β*. It is not known whether *Nrxn1β* is also affected in the rat model utilised in this thesis, however these studies demonstrate the ability for different neurexin isoforms to take on a compensatory role which may explain why no change to synaptic transmission was observed in *Nrxn1*$^{+/-}$ rats.

5.3.3 Minor changes to cell intrinsic properties in *Nlgn3*$^{-/y}$ rats

Evidence of altered intrinsic excitability of neurons in *Nlgn3*$^{-/y}$ rats has been demonstrated in the dPAG (Fig. 3.13) and in the lateral amygdala (Toft, 2019). Furthermore, Modi et al. (2019) reported increased intrinsic excitability cells recorded from CA2 in *Nlgn3*$^{-/y}$ mice. However, I provide evidence that loss of neuroligin-3 largely does not disrupt the intrinsic properties of neurons in CA1, at either p13-15 or p25-35. Furthermore, the intrinsic properties of layer 5 mPFC neurons are also unaffected in *Nlgn3*$^{-/y}$ rats at p13-15. However, minimal changes to AP duration and ADP were observed in *Nlgn3*$^{-/y}$ mPFC PCs at p25-35, suggesting there may be some disruption of K^+ channel function (Kang et al., 2000) in these neurons. These results highlight the differential effects of neuroligin-3 loss in distinct brain regions. Normal intrinsic excitability in naïve *Nlgn3*$^{-/y}$ rats therefore suggests that the output of hippocampal and mPFC regions to the BLA and PAG is likely to be unaffected. However, as was noted for the extracellular field recordings, the intrinsic excitability of these neurons was assessed at an earlier time point to the behaviour, making it difficult to draw direct conclusions between physiological and behavioural phenotypes.

Changes in intrinsic excitability of PCs in CA1 and mPFC have been reported after fear conditioning (McKay et al., 2009; Santini et al., 2008). The intrinsic excitability of CA1 or mPFC neurons has not been assessed in *Nlgn3*$^{-/y}$ rats following fear conditioning, and it is possible that experience-dependent plasticity of intrinsic excitability in PCs may be impaired, even if basal excitability is normal.

5.3.4 Hypoexcitability of CA1 pyramidal cells in *Nrxn1*$^{+/-}$ rats

Neurexin-1 is a presynaptic cell adhesion protein and, for this reason, direct effects in intrinsic excitability would be unlikely. However, changes in intrinsic excitability could occur via indirect means. Synaptic transmission, measured via the recording of mEPSCs/mIPSCs, was unaffected in *Nrxn1*$^{+/-}$ HC, however altered synaptic transmission at an earlier age (not investigated here) may have led to long lasting alterations in intrinsic excitability (Turrigiano and Nelson, 2004). Furthermore, synaptic plasticity was impaired in *Nrxn1*$^{+/-}$ HC which may lead to homeostatic changes in intrinsic excitability.

There is evidence to suggest that intrinsic neuronal excitability (and mAHP) may affect recruitment of neurons into memory engrams (Saar et al., 1998). Investigation of cell properties revealed that in slices taken from p25-35 *Nrxn1*$^{+/-}$ rats, CA1 PCs are intrinsically hypoexcitable and have increased mAHP, which may caused decreased recruitment of hippocampal neurons to during fear conditioning or extinction. Moreover, this hypoexcitability was accompanied by an increase in capacitance and a decrease in both depolarisation and repolarisation speeds. Increased cell capacitance suggests an increase in cell size, and therefore more current required to elicit AP firing. Decreased depolarisation and repolarisation speeds suggest that Na^+ and K^+ channels are affected by the *Nrxn1* mutation, slowing AP propagation and resulting in fewer APs fired in response to depolarising current injections. K^+ currents are also implicated in the increased mAHP observed in *Nrxn1*$^{+/-}$ CA1 PCs. mAHP is dependent on the activation of several channels, including M-channels (Gu et al., 2005; Storm, 1989; Tzingounis et al., 2010), Na^+/K^+-ATPase (Gulledge et al., 2013), and HCN channels (I_h) (Oswald et al., 2009). Given that sag, a measure of I_h, is unaffected in p25-35 *Nrxn1*$^{+/-}$ CA1 PCs, it is unlikely that altered I_h is contributing to the increased mAHP of these neurons. However, increased M-channels would explain an increase in mAHP and hypoexcitability.

M-channels are voltage-gated non-inactivating potassium channels comprising of subunits of Kv7 channels: Kv7.2, Kv7.3 and Kv7.5 (Wang et al., 1998; Selyanko et al., 1999; Lerche et al., 2000; Shah et al., 2002). They activate at subthreshold potentials in neurons, allowing slow (tens of milliseconds) efflux of K^+. They do not contribute to the initial repolarisation phase of an AP, but instead act to suppress repetitive firing given sustained depolarisation (Brown and Passmore, 2009). For this reason, while altered M-current could contribute to alterations in capacitance, mAHP, and hypoexcitability, it is unlikely to explain the change in AP waveform observed in *Nrxn1*$^{+/-}$ CA1 PCs.

Mutations in M-channels have also been implicated in ID and epilepsy (Borgatti et al., 2004; Biervert et al., 1998). In addition to their contributions to neuronal excitability (Peters et al., 2005) and mAHP (Gu et al., 2005; Storm, 1989; Tzingounis et al., 2010), inhibition of Kv7 channels has been shown to enhance LTP through NMDAR-dependent mechanisms (Petrovic et al., 2012). Given the reduction of LTP in *Nrxn1*$^{+/-}$ hippocampus, in addition to hypoexcitability and increased mAHP of CA1 PCs, there may be overexpression of M-channels in CA1 of *Nrxn1*$^{+/-}$ rats. Although neurexin-1 does not directly interact with K^+ channels, partial loss of this protein may have knock-on effects on neuroligin and PSD-95, which could affect the recruitment of ion channels to the postsynapse. However, M-channels have also been shown to affect ADP (Yue, 2004), RMP, and release probability (Huang and Trussell, 2011), and no changes in these parameters were observed in *Nrxn1*$^{+/-}$ PCs. Nonetheless, examination of the effects of M-channel inactivation in *Nrxn1*$^{+/-}$ rats would be an interesting future experiment.

Altered intrinsic excitability and mAHP may affect neuronal recruitment to memory engrams (Saar et al., 1998). Moreover, AHP and neuronal excitability in CA1 PCs have been shown to increase following fear conditioning (McKay et al., 2009) (although this study uses contextual and trace fear conditioning paradigms, not cued). In combination with the reduced LTP also identified in *Nrxn1*$^{+/-}$ hippocampus, these results suggest that *Nrxn1*$^{+/-}$ rats may have reduced learning abilities that contribute towards the increased freezing behaviour and reduced extinction following fear conditioning (Fig. 5.1).

5.3.5 Age-dependent cell intrinsic property changes in *Nrxn1*$^{+/-}$ rats

Hypoexcitability of CA1 pyramidal cells in *Nrxn1*$^{+/-}$ rats was only observed in slices from p25-35 rats. When slices taken from rats at an earlier time point (p13-15) were examined, no changes in cellular excitability were detected. However, a small but significant increase in sag was observed in p13-15 *Nrxn1*$^{+/-}$ CA1 PCs, along with a decrease in AP threshold and AP height (Figs. 5.7, 5.8, 5.9). Changes to AP threshold and height implicate a dysfunction of Na^+ channels; AP threshold has been shown to be logarithmically correlated with Na^+ channel density (Platkiewicz and Brette, 2010), so reductions may indicate a decrease in Na^+ channels in p13-15 *Nrxn1*$^{+/-}$ CA1 PCs. AP threshold is also affected by A-type K^+ channels, however these also influence AP width and RMP (Carrasquillo et al., 2012) which were not altered in *Nrxn1*$^{+/-}$ CA1 PCs, suggesting dysfunction of A-type K^+ channels is not responsible for the change in AP threshold observed.

Furthermore, increased sag indicates increased I_h; mediated by HCN channels. HCN channels are activated in response to hyperpolarising membrane voltages, and conduct both Na^+ and K^+. Interestingly, deletion of HCN1 in mice has been reported to cause impaired rotarod performance (Nolan et al., 2003; Lewis et al., 2011), and *Nrxn1*$^{+/-}$ rats perform better than WT on the rotarod (V. Kapgal, S. Tiwari; unpublished). However, rotarod experiments on *Nrxn1*$^{+/-}$ rats were carried out at 2-3 months of age, and changes to sag, threshold and AP peak height were only altered in p13-15 rats. It is therefore possible that these early alterations in neuronal intrinsic properties lead to developmental changes that contribute to altered circuitry in *Nrxn1*$^{+/-}$ rats.

These age-dependent pathophysiologies observed in *Nrxn1*$^{+/-}$ rats highlights the importance of investigating more than one developmental time point when studying models of neurodevelopmental disorders, as many of these phenotypes may not be the direct result of neurexin-1 loss at the synapse, but rather an effect of compensatory changes such as altered synaptic transmission earlier in development (not investigated in this thesis). To examine potential compensatory effects, rats with conditional *Nrxn1* mutations could be utilised. Conditional mutations allow spatial and temporal manipulation of protein expression, therefore permitting investigation of whether neurexin-1 haploinsufficiency results in the same changes to neuronal intrinsic properties when the mutation is introduced later in development.

In cells recorded from layer 5 mPFC, age-dependent phenotypes were also observed.

Whilst the intrinsic properties of p25-35 *Nrxn1*$^{+/-}$ layer 5 mPFC PCs were unaffected, p13-15 *Nrxn1*$^{+/-}$ neurons displayed increased input resistance (leading to decreased capacitance) and decreased rheobase in this brain region (Figs. 5.15, 5.16). This was accompanied by a trend towards hyperexcitability, which was not statistically significant. The contrast of this phenotype in comparison to the hypoexcitability observed in *Nrxn1*$^{+/-}$ CA1 PCs again highlights that ASD/ID-associated mutations can cause phenotypes that are not only age specific but also brain region specific.

5.3.6 Convergence and divergence of pathophysiologies in *Nlgn3*$^{-/y}$ and *Nrxn1*$^{+/-}$ rats

Convergence of molecular and cellular pathophysiologies between genetically distinct models of ASD/ID would firstly help explain how the genetic heterogeneity of mutations resulting in autism and ID in humans can result in the presentation of similar behavioural traits. Secondly, identifying common phenotypes between models of ASD/ID may allow the identification of therapeutics interventions that are relevant and ameliorative for a large proportion of individuals with ASD. Several studies have identified phenotypic convergence between genetically distinct models of ASD/ID (Krumm et al., 2014; Pinto et al., 2014; Barnes et al., 2015; Baudouin et al., 2012). As neurexin-1 and neuroligin-3 have similar roles as synaptic cell adhesion proteins, in addition to being binding partners, I hypothesised *Nlgn3*$^{-/y}$ and *Nrxn1*$^{+/-}$ rat models would show converging cellular and synaptic pathophysiologies. The data presented in this chapter provides evidence that partially supports this hypothesis; I find that both *Nlgn3*$^{-/y}$ and *Nrxn1*$^{+/-}$ rats display impaired hippocampal LTP. However, this converging phenotype appears to manifest as a result of diverging mechanisms in the two models. In *Nlgn3*$^{-/y}$ rats, I hypothesise that reduced hippocampal LTP is a consequence of impaired NMDAR function (see section 5.3.2), whereas in *Nrxn1*$^{+/-}$ rats altered M-current may underpin the change in synaptic plasticity (see section 5.3.4). Impaired LTP has been reported many other rodent models of ASD/ID (Louros and Osterweil, 2016; Chung et al., 2012), highlighting the potential importance of impaired synaptic plasticity in contributing to the expression of ASD/ID-related behaviours. This idea is not novel (for example, Barnes et al. (2015)), but the results presented in this chapter provide additional evidence that supports impaired LTP as a converging phenotype across genetically distinct models of ASD/ID. Together, the results presented in this chapter, in addition to previous

research, suggest that synaptic plasticity may be a relevant therapeutic target. However, as this phenotype is likely the result of differing molecular impairments within each model, finding drug treatments may prove difficult. As the data in this chapter has demonstrated, these phenotypes may be both age and brain region specific; reduced LTP was not observed in the mPFC in *Nlgn3*$^{-/y}$ or *Nrxn1*$^{+/-}$ rats, and may not be impaired in older *Nlgn3*$^{-/y}$ rats (Teresa Spanò, unpublished). Thus, there is a need to identify drugs that target the affected biological level and brain region, in addition to determining the most appropriate treatment age. Nonetheless, these data suggest that alterations in synaptic plasticity may be a common core pathophysiology underlying ASD/ID. Furthermore, convergence at a molecular level is not investigated in this thesis, and could still be possible between *Nlgn3*$^{-/y}$ and *Nrxn1*$^{+/-}$ rats (discussed further in Chapter 6).

5.4 Summary

Overall, the results presented in this chapter suggest that physiology of hippocampus and mPFC neurons in *Nlgn3*$^{-/y}$ and *Nrxn1*$^{+/-}$ rats are affected in terms of their synaptic plasticity, intrinsic properties, and synaptic properties. The results of these experiments are summarised in Table 5.7. These differences may lead to impaired fear learning or extinction. *Nlgn3*$^{-/y}$ and *Nrxn1*$^{+/-}$ rats display both converging and diverging cellular and synaptic physiologies; notably impaired hippocampal LTP was observed in both models. In *Nlgn3*$^{-/y}$ rats the reduced LTP is likely caused by a decrease in NMDAR function, and in *Nrxn1*$^{+/-}$ rats the decreased LTP may be a result of increased M-channel function. Further experiments are needed to confirm this. In addition, identified phenotypes in *Nlgn3*$^{-/y}$ and *Nrxn1*$^{+/-}$ rats changed over development, highlighting the importance of studying physiology across developmental trajectories in models of neurodevelopmental disorders. This chapter provides additional evidence (Louros and Osterweil, 2016; Chung et al., 2012) that impaired synaptic plasticity may be a core phenotype leading to the manifestation of ASD and ID.

Table 5.7: Summary table of HC and mPFC physiology in *Nlgn3*$^{-/y}$ and *Nrxn1*$^{+/-}$ rats.

	Hippocampus				mPFC			
	***Nlgn3*$^{-/y}$**		***Nrxn1*$^{+/-}$**		***Nlgn3*$^{-/y}$**		***Nrxn1*$^{+/-}$**	
	p13-15	p25-35	p13-15	p25-35	p13-15	p25-35	p13-15	p25-35
LTP		↓		↓		–		–
NMDAR-dependent LTD		↓		–				
mGluR-dependent LTD		–		–				
RMP	–	–	–	–	–	–	–	–
Input resistance	–	–	–	–	–	–	↑	–
Membrane time constant	–	–	–	–	–	–	–	–
Capacitance	–	–	–	↑	–	–	↓	–
Sag	–	–	↑	–	–	–	–	–
Intrinsic excitability	–	–	–	↓	–	–	–	–
Rheobase	–	–	–	–	–	–	↓	–
Threshold	–	–	↓	–	–	–	–	–
AP peak	–	–	↓	–	–	–	–	–
AP width	–	–	–	–	–	↓	–	–
Depolarisation speed	–	–	–	↓	–	–	–	–
Repolarisation speed	–	–	–	↓	–	↑	–	–
After-depolarisation potential	–	–	–	–	–	↑	–	–
Medium after-hyperpolarisation potential	–	–	–	↑	–	–	–	–
mEPSC amplitude		↑		–		–		–
mEPSC frequency		–		–		–		–
mIPSC amplitude		–		–		–		–
mIPSC frequency		–		–		–		–

Chapter 6

Concluding remarks

6.1 Concluding remarks

This thesis aimed to address a number of hypotheses relating to how the physiology of brain regions involved in fear learning and expression may be disrupted in rat models of ASD/ID. Behavioural studies carried out on *Nlgn3*$^{-/y}$ and *Nrxn1*$^{+/-}$ rats were used as a platform for identifying potentially affected brain regions. The work presented does not provide a comprehensive investigation of all brain areas involved in fear, however it does highlight several novel research avenues that provide potential mechanistic explanations of the high occurance of anxiety disorders and altered emotional responses in individuals with ASD/ID.

6.1.1 Different behaviour, different physiology

Previous work investigating the behaviour of *Nlgn3*$^{-/y}$ and *Nrxn1*$^{+/-}$ mice has identified converging behavioural deficits between these models of ASD/ID. For example, both *Nlgn3*$^{-/y}$ and *Nrxn1*$^{+/-}$ mice show impairments in social behaviour and hyperactivity (Dachtler et al., 2015; Radyushkin et al., 2009). However, we find that *Nlgn3*$^{-/y}$ and *Nrxn1*$^{+/-}$ rats display differing behavioural responses in fearful situations (Figs. 1.5, 5.1). These behaviours are underpinned by distinct physiological deficits in these two models of ASD/ID.

The results presented in Chapter 3 demonstrate a great diversity of neurons in the PAG and, within these classes, increased cellular excitability and altered release probability in the PAG of *Nlgn3*$^{-/y}$ rats. These findings provide a cellular correlate for the manifestation of increased flight behaviours in *Nlgn3*$^{-/y}$ rats. Chapter 4 provides

evidence that the PAG of *Nlgn3*$^{-/y}$ rats has a decreased threshold for eliciting flight responses *in vivo*, however further experimentation is still required to determine the specific neurons and circuits responsible for the bias towards flight responses in *Nlgn3*$^{-/y}$ rat behaviour.

I also hypothesised that cellular correlates of fear learning would be unimpaired in *Nlgn3*$^{-/y}$ rats, however experimental evidence in Chapter 5 suggests the contrary; hippocampal LTP was reduced. Further investigation of learning and memory is therefore required in *Nlgn3*$^{-/y}$ rats. *Nrxn1*$^{+/-}$ rats also displayed impaired hippocampal LTP, in addition to altered neuronal excitability in the hippocampus. These physiological changes may underpin the small but significant change in fear extinction observed in *Nrxn1*$^{+/-}$ rats. Further investigation is needed to confirm this, as discussed in section 6.2.

The majority of the work presented in this thesis utilises *ex vivo* electrophysiology to investigate cellular and synaptic properties of neurons involved in fear learning and expression. *Ex vivo* recordings are extremely useful for providing a wealth of information regarding the effects of a genetic mutation on channels, synapses, local circuits, and individual neuronal function. However, conclusions drawn between these recordings and behavioural phenotypes must be done so with caution. Utilising a combination of *in vivo* and *ex vivo* techniques allows a clearer link to be drawn between physiology and behaviour. The research presented in this thesis encourages further *in vivo* experimentation to understand the potential circuit dysfunctions implicated in these models of ASD/ID.

6.1.2 The PAG and autism

The results displayed in Chapters 3 and 4 demonstrate the first implication of PAG dysfunction in a model of autism. Despite many studies describing models of ASD/ID display reduced freezing behaviour during fear conditioning and recall, changes in the expression of fear responses have been overlooked as an explanation for this. The altered fear response behaviour observed in *Nlgn3*$^{-/y}$ rats highlights the importance of careful investigation of behavioural data. In studies that report decreases in a certain behaviour (eg. freezing), the question of what alternative behaviour is being expressed is often neglected. For example, Radyushkin et al. (2009) reported reduced freezing of *Nlgn3*$^{-/y}$ mice during cued and contextual fear conditioning, yet conclude these mice likely have

no learning deficits due to their successful performance in the Morris water maze task. These conclusions are similar to those we have made regarding the behaviour of the *Nlgn3*$^{-/y}$ rat, and it would be of great interest to know if *Nlgn3*$^{-/y}$ mice also display increased flight behaviour. In this way, deeper examination of rodent behaviour may lead to alternative explanations for the data. The evidence that *Nlgn3*$^{-/y}$ rats adopt a different strategy for responding to fearful stimuli led to investigation of the PAG in this thesis, which presents an interesting new research avenue for understanding fear and anxiety in ASD.

To date, the research presented in this thesis shows the first phenotypic link between PAG dysfunction and ASD/ID in a model of these disorders, despite anxiety and altered emotional responses being a key feature of ASD. The investigation of fear learning and responses in the *Nlgn3*$^{-/y}$ rat in this thesis highlights the importance of in-depth behavioural phenotyping. Previous research into children with ASD has suggested that fight-flight-freeze responses are easier to trigger in these individuals in comparison to typically developing children (Panju et al., 2015), and it is possible that this aspect of the disorder is underpinned by physiological changes in the PAG. Abnormal sensory integration that has been identified in many models of ASD has been thought to affect fear response behaviour (reviewed in Robertson and Baron-Cohen (2017)), however it is possible that changes brain areas such as the PAG which directly control appropriate fear responses are also responsible.

Investigating PAG dysfunction in the context of ASD has several key advantages: firstly the structure and function of the PAG is highly conserved across species (see section 3.1), and secondly it is important in the control of several ASD-related behaviours. This includes the execution of appropriate responses to fearful stimuli which are explored here, but also analgesia, sleep, and communication (reviewed in Benarroch (2012)). Decreased PAG activity has been reported in fMRI studies of individuals with ASD (Schneider et al., 2013; Fan et al., 2014), suggesting that changes in this brain region may be translated into humans with the disorder. Further investigation of the role of the PAG in contributing to the pathophysiology of ASD would be an interesting future research avenue, and may allow a better understanding of the underlying physiological mechanisms that result in abnormal emotional reactions in individuals with ASD.

6.1.3 Compensation

Considering the importance of neuroligin-3 and neurexin-1 in the maintenance of synaptic efficacy (Nam and Chen, 2005; Missler et al., 2003; Varoqueaux et al., 2006), very minor effects on synaptic transmission were observed in *Nlgn3*$^{-/y}$ and *Nrxn1*$^{+/-}$ rats. Altered synaptic transmission has been reported in mouse models of *Nlgn3* and *Nrxn1*-associated ASD/ID (Etherton et al., 2011; Zhang et al., 2017; Rothwell et al., 2014; Tabuchi et al., 2007; Chanda et al., 2013; Pak et al., 2015; Etherton et al., 2009; Baudouin et al., 2012), however from the literature it is clear that full deletions of *Nlgn3* in mice are less detrimental to physiology than the *R451C* point mutations. The reason for this is likely to be homeostatic compensation by neuroligins 1 and 2, or for the case of *Nrxn1*$^{+/-}$ rats by neurexins 2 and 3 (or by β-neurexins if these are unaffected (Avazzadeh et al., 2019)). Research carried out by Jiang et al. (2017) provides evidence that neuroligin-1 is able to compensate for neuroligin-3 loss, but not vice versa. Conditional ablation of neuroligins 1 and 3 in mice suggested that the function of neuroligin-3 was almost redundant in the presence of neuroligin 1, however double KO neurons lacking both neuroligins 1 and 3 displayed disruption of excitatory synaptic transmission that was further increased in comparison to loss of neuroligin-1 alone (Chanda et al., 2017). This provides additional evidence of the ability of neuroligin-1 to compensate for neuroligin-3 loss. In addition, preliminary RNA sequencing data from our lab shows that *Nlgn1* and *Nlgn2* are upregulated in *Nlgn3*$^{-/y}$ rats (*Nlgn1* $p = 0.047$, *Nlgn2* $p = 0.00017$).

Upgregulation of the other neuroligins may cause additional effects on fear learning and response behaviour. Fear learning has been shown to cause endogenous upregulation of both neuroligins 1 and 2 through BDNF activity in the mPFC, and the increase of these proteins is required for fear memory formation and appropriate extinction (Ye et al., 2017). Therefore the knock-on effects of *Nlgn3* mutations on *Nlgn1* and *Nlgn2* may also be detrimental.

Neuroligin-3 and neurexin-1 are expressed throughout development (Scheiffele et al., 2000; Song et al., 1999; Varoqueaux et al., 2006; Harkin et al., 2017; Górecki et al., 1999). It is possible that some pathophysiologies observed in *Nlgn3*$^{-/y}$ and *Nrxn1*$^{+/-}$ rats are a result of abnormal synaptic and circuit development following the loss of these proteins in critical periods, rather than their direct physical absence at the synapse during the time of physiological measurement. Baudouin et al. (2012) reported the

rescue of some phenotypes in the *Nlgn3*$^{-/y}$ mouse following the reintroduction of *Nlgn3* into Purkinje cells of p30 mice. Discerning between phenotypes caused by abnormal development and those caused by continued loss of a protein (such as those described in the *Mecp2* mouse (Guy et al., 2007)) allows better understanding of protein function and cellular pathophysiologies in models of neurodevelopmental disorders.

6.1.4 Convergence or divergence?

In Chapter 5, I assess cellular and synaptic physiology in an identical manner in two brain regions in *Nlgn3*$^{-/y}$ and *Nrxn1*$^{+/-}$ rats, and find very few common phenotypes between these models. There are several potential conclusions that can be drawn from these results. One conclusion is that the lack of converging physiological phenotypes may reflect that different pathways are affected in *Nlgn3*$^{-/y}$ and *Nrxn1*$^{+/-}$ rats, and therefore it is unlikely a common treatment could be found for the disorders associated with these mutations. Alternatively, these genetic mutations could provoke completely different compensatory mechanisms that result may in these distinct phenotypes. In this case, it is still possible these mutations result in convergent core pathophysiologies. It is also important to consider the level at which there could be convergence between these models. Although we can conclude that *Nlgn3*$^{-/y}$ and *Nrxn1*$^{+/-}$ rats display largely diverging phenotypes at a cellular physiology and behavioural level, it is not known if there is convergence at a molecular or biochemical level between these models.

One form of convergence at the molecular level that has been repeatedly implicated in several genetically distinct models of ASD/ID is dysregulation of mGluR signalling. Following the 'mGluR' theory of Fragile-X syndrome (Bear et al., 2004), which proposes loss of FMRP leads to an increase in mGluR-regulated protein synthesis (Osterweil et al., 2010; Barnes et al., 2015; Auerbach et al., 2011), increased protein synthesis has been reported in *SynGAP*-haploinsufficiency (Barnes et al., 2015) and *Eif4ebp*-deletion (Gkogkas et al., 2013), and mGluR expression has been shown to be increased in *Nlgn3*$^{-/y}$ mice (Baudouin et al., 2012). I demonstrate that mGluR-dependent LTD is unaffected in *Nlgn3*$^{-/y}$ and *Nrxn1*$^{+/-}$ rats, however whether protein synthesis or mGluR expression is affected in these models is not known. Compensatory mechanisms that take place at each level of the biological hierarchy (molecular, cellular, circuit, behavioural) may result in distinct phenotypes observed at these higher levels. This may therefore be what is leading to the observed divergence between these models of ASD/ID, as oppose

to a true divergence at the level of biochemistry.

6.1.5 Translation between species

Multiple pre-clinical models of a disorder allows the comparison of core cellular pathophysiologies and behavioural phenotypes across species. The investigation of the *Nlgn3*$^{-/y}$ and *Nrxn1*$^{+/-}$ rat models has provided significant insight into the roles of neuroligin-3 and neurexin-1 at the mammalian synapse that is not necessarily limited to mice. Till et al. (2015) provided evidence of cross-species conservation of cellular pathophysiologies but not behavioural impairments in *Fmr1*$^{-/y}$ mice and rats, however the opposite may be true for *Nlgn3*$^{-/y}$ mice; I find divergence of phenotypes at a cellular level, yet behavioural deficits appear to be conserved in *Nlgn3*$^{-/y}$ rats to those previously reported in mice.

Nlgn3$^{-/y}$ rats display impaired hippocampal LTP, whilst LTP of *Nlgn3*$^{-/y}$ mice appears unaffected (Etherton et al., 2011). Furthermore, I report no change in mGluR-dependent LTD of *Nlgn3*$^{-/y}$ rats, whilst mGluR-dependent LTD was reported to be decreased in *Nlgn3*$^{-/y}$ mice (Baudouin et al., 2012) (although note these recordings were from cerebellar slices). The amplitude of mEPSCs was found to be increased in hippocampal PCs of *Nlgn3*$^{-/y}$ rats, whereas Etherton et al. (2011) found decreased frequencies and normal amplitudes of mEPSCs in *Nlgn3*$^{-/y}$ mice. However, in agreement with Tabuchi et al. (2007), I also find no change in inhibitory synaptic transmission in the hippocampus of *Nlgn3*$^{-/y}$ rats.

The ecological niche of rats in the wild is different to that of mice. Despite this, freezing behaviour during cued fear recall is reduced in both *Nlgn3*$^{-/y}$ mice (Radyushkin et al., 2009) and *Nlgn3*$^{-/y}$ rats (Figs. 1.5, 4.1). Cognitive flexibility, which may be affected in *Nlgn3*$^{-/y}$ rats, was also reported to be impaired in *Nlgn3*$^{-/y}$ mice (Norris et al., 2019). In addition to this, increased rotarod performance has been identified as a consequence of *Nlgn3* loss in both species (Rothwell et al., 2014) (V. Kapgal, S. Tiwari, unpublished). On the other hand, hyperactivity in an open field arena does not appear to be conserved between *Nlgn3*$^{-/y}$ mice and rats (Radyushkin et al., 2009) (Fig. 1.6). Radyushkin et al. (2009) did not investigate whether the reduced freezing behaviour of *Nlgn3*$^{-/y}$ mice was a result of altered fear expression, however Hosie et al. (2018) reported increased jumping behaviour in *Nlgn3 R451C* mice, suggesting that increased flight responses may also be conserved between *Nlgn3*$^{-/y}$ mice and rats.

Cross-species validation of phenotypes strengthens the relevance of genetic models of ASD to the human disorder. The work presented in this thesis implicates the existence of both translated and species-specific physiological and behavioural impairments in *Nlgn3*$^{-/y}$ and *Nrxn1*$^{+/-}$ mice and rats, highlighting the importance of utilising more than one animal model of a disorder to draw conclusions regarding potential deficits and mechanistic explanations. Together, the use of rat and mouse models of a disorder may provide new insight into the identification of pathophysiogies and potential treatment options for neurological disorders.

6.2 Future Directions

6.2.1 The physiology of fear learning in *Nlgn3*$^{-/y}$ and *Nrxn1*$^{+/-}$ rats

Reduced freezing behaviour during fear recall initially suggested that fear learning behaviour may be impaired in *Nlgn3*$^{-/y}$ rats, however the combination of altered fear response behaviour and normal associative learning during the active place avoidance task provide evidence that this is not the case. I hypothesised that hippocampal plasticity, a cellular correlate of learning and memory (Bliss and Collingridge, 1993), would be unaffected in *Nlgn3*$^{-/y}$ rats, however I found that it was impaired. Preliminary evidence from a co-worker implied that this plasticity impairment was limited to juvenile (p25-35) rats, and was not the case in p60-70 rats age matched with behavioural experiments (Teresa Spanò, unpublished). Further confirmation of this is required. Moreover, amygdalar LTP is a well characterised cellular correlate of fear learning (Li et al., 2013) that has not been investigated in this thesis. LTP of the thalamic inputs to the LA has been shown to be impaired in juvenile *Nlgn3*$^{-/y}$ rats (Toft, 2019), and it would therefore be interesting to know if this phenotype perseveres into adulthood. In addition to this, investigation of fear learning behaviour in juvenile *Nlgn3*$^{-/y}$ rats is an interesting further research avenue.

Lastly, these results provoke questions as to whether learning in *Nlgn3*$^{-/y}$ rats is impaired in the absence of fearful stimuli. Behavioural readouts of learning abilities during fear conditioning and active place avoidance (i.e. freezing, successful avoidance) tasks were occluded by the abnormal fear expression in *Nlgn3*$^{-/y}$ rats, so behavioural testing of hippocampal-dependent memory during non-fearful contexts may provide further information regarding potential learning impairments.

In contrast to *Nlgn3*$^{-/y}$ rats, *Nrxn1*$^{+/-}$ rats display a small but significant increase in freezing behaviour during fear extinction. This increase in freezing behaviour may be indicative of an impairment in fear extinction-related physiology. Supporting this, hippocampal LTP was impaired in *Nrxn1*$^{+/-}$ rats. It would therefore also be interesting to examine *Nrxn1*$^{+/-}$ rats in a non-fearful hippocampal-dependent learning task, such as the 'object-place-context' task (Langston and Wood, 2010).

There are several other brain regions implicated in fear extinction that may be disrupted in *Nrxn1*$^{+/-}$ rats but are not investigated in this thesis. Synaptic plasticity of inputs to the LA is required for successful fear extinction (Sotres-Bayon et al., 2007; Herry et al., 2006), and the infralimbic (IL) mPFC has also been implicated in extinction learning (Milad and Quirk, 2002; Laurent and Westbrook, 2009). Investigation of these regions may provide further insight into the physiological underpinnings of this behavioural phenotype in *Nrxn1*$^{+/-}$ rats.

6.2.2 The physiology of fear response behaviour in *Nlgn3*$^{-/y}$ rats

Behavioural studies of *Nlgn3*$^{-/y}$ rats demonstrated that they display an imbalance of flight-freeze responses heavily biased towards flight. This thesis provides evidence that this is underpinned by hyperexcitability of neurons in the dPAG and reduced threshold of dPAG-induced flight behaviours.

What are the neurons responsible for the manifestation of this behaviour?

I provide evidence that neurons in the dPAG of *Nlgn3*$^{-/y}$ rats display an overall increase in cellular excitability, however I did not fully identify the type of neuron that contributes towards this phenotype. Based on the characterisation of WT neurons in section 3.2.1, I used clustering analysis to determine this population-level hyperexcitability in *Nlgn3*$^{-/y}$ rats was driven by an increase in cellular excitability of type 2 neurons. To further investigate this, utilisation of GM rats expressing fluorescent reporter proteins in specific neuronal populations crossed with the *Nlgn3*$^{-/y}$ rat line (eg. Venus-VGAT, Uematsu et al. (2008)), would allow visualisation of excitatory or inhibitory neurons in the PAG, and therefore more targeted *ex vivo* electrophysiological recordings. This would provide additional information regarding changes in neuronal excitability and local circuitry in the PAG of *Nlgn3*$^{-/y}$ rats, by allowing further investigation of the nature of neuronal subtypes contributing to the hyperexcitability and increased released

probability phenotypes. Similarly, the results presented in Chapter 4 demonstrate reduced threshold of flight behaviours during increasing dPAG stimulation in *Nlgn3*$^{-/y}$ rats. Optogenetically or chemogenetically stimulating only excitatory or only inhibitory neurons of the PAG both *ex vivo* and *in vivo* would allow further dissection of cellular pathophysiologies.

Additionally, recording single-units in the PAG *in vivo* during the expression of flight behaviours may highlight differentially active neurons in WT and *Nlgn3*$^{-/y}$ rats. I provide evidence that LFP recordings in the PAG are largely normal in *Nlgn3*$^{-/y}$ rats during fear recall, however the firing of single units may still differ between genotypes.

What are the circuits involved in this behavioural imbalance?

Increased cellular excitability may be a result of homeostatic plasticity in response to altered connectivity. There are several possible circuit dysfunctions that may contribute towards abnormal fear response behaviour in *Nlgn3*$^{-/y}$ rats that I hope to investigate in the continuation of this project:

1. **CeA to vPAG** Tovote et al. (2016) identified disinhibitory projections from the CeA to vPAG, activation of which resulted in freezing behaviour. Given the reduced freezing behaviour observed in *Nlgn3*$^{-/y}$ rats, this pathway may be disrupted. However, this thesis provides behavioural and physiological evidence that both freezing and cellular correlates of this behaviour are intact in *Nlgn3*$^{-/y}$ rats, only overridden by a bias towards escape responses.

2. **mPFC to vPAG** Rozeske et al. (2018) described projections from the mPFC pyramidal cells to the vPAG, and activation of these neurons resulted in decreased freezing behaviour. This study provided evidence that the decreased freezing was not a result of increased avoidance or escape behaviours. Thus, although decreased freezing was observed during fear recall in *Nlgn3*$^{-/y}$ rats, it is unlikely that impairments in this pathway results in the increased flight behaviours. This is further supported by the absence of changes to intrinsic and synaptic properties of mPFC pyramidal cells in *Nlgn3*$^{-/y}$ rats.

3. **Hypothalamus to dPAG** (Wang et al., 2015) described projections from the ventromedial hypothalamus (VMH) to dPAG. These projections are thought to be inhibitory in nature, as activation resulted in freezing behaviour. Disruption

of this projection in *Nlgn3*$^{-/y}$ rats may result in decreased suppression of flight-promoting neurons in the dPAG, and increased output of flight responses.

4. **Superior colliculus to dPAG** Evans et al. (2018) described excitatory connections between the superior colliculus (SC) and dPAG that are required for the expression of flight responses. Sustained activation of the SC causes potentiation of SC-dPAG synapses, which overcomes a 'threshold' in dPAG neurons to elicit flight responses. If these connections are more numerous, or have increased synaptic efficacy at a basal level in *Nlgn3*$^{-/y}$ rats, this may account for the increased flight responses observed.

Further investigation of these connections, in particular VMH-dPAG and SC-dPAG pathways, may provide additional information regarding circuit dysfunction in *Nlgn3*$^{-/y}$ rats. Optogenetic or chemogenetic modulation of these pathways *in vivo* may lead to distinct behavioural manifestations in WT and *Nlgn3*$^{-/y}$ rats.

6.3 Summary

This thesis provides evidence that fear responses behaviours are atypical in a model of ASD/ID, and these changes in fear responses could potentially account for previously reported "fear learning deficits". Furthermore, I identify dysfunction of the PAG as a likely mechanism underlying this behavioural change; highlighting the potential relevance of this brain region to ASD pathophysiologies. Finally, I describe both converging and diverging phenotypes between two genetically distinct models of ASD/ID. This suggests that despite the genetic heterogeneity of these disorders there may be common core pathophysiologies which can be targeted to develop treatments that are effective for many individuals.

In conclusion, my findings encourage further experiments, with the particular focus on understanding the role of the PAG in models of ASD/ID. Investigating the physiological correlates of fear is important for understanding the pathophysiology of anxiety disorders and altered emotional responses in individuals with ASD and ID, and will hopefully lead to the identification of novel pharmacological targets and treatment options for these disorders.

Appendix A

A.1 Behaviour Paradigms

All rats were handled for a minimum of 3 consecutive days prior to any behavioural testing.

A.1.1 Auditory fear conditioning

Auditory fear conditioning was performed as described in Methods section 2.6.3, however no tone habituation phase was carried out, and rats were not tethered to electrophysiology recording equipment during the experiment.

A.1.2 Active place avoidance

Habituation: day 1 Rats were habituated to a rotating arena with a grid floor (as described in Lesburguères et al. (2016)), except a transparent lid was added in (Fig. 1.9) to prevent the animals from escaping the arena. Large brightly coloured cues were hung around the room external to the arena. Each rat was placed in one quadrant (counterbalanced between animals and genotypes) of the arena and behaviour was recorded for 10 minutes. Rats were then returned to their home cage, which was stored inside a dark cupboard, for a minimum of 10 minutes before being placed again inside the arena for a second habituation session. Each rat was then returned to their home cage.

Training: days 2 &3 One quandrant of the arena floor grid was electrified with an 0.2 mA, 500 ms shock. The position of the shock-zone was counterbalanced between animals and genotypes. Each rat was placed into the arena facing the outer wall in one of the adjacent quadrants to the shock-zone, and behaviour was recorded for 10 minutes

as the rats learned the location of the shock-zone. Movement of rats was scored live using open-source software Carousel Maze Manager (Bahník, 2014). Rats were then returned to their home cage, which was stored inside a dark cupboard, for 10 minutes. Rats were reintroduced to the arena for another 10 minutes and then returned to their home cage for 10 minutes. This was repeated until each rat had completed 8 10-minute training sessions. After all training sessions were complete rats were returned to their home cages.

Probe trial: day 4 The shock zone was removed from the arena. Each rat was placed into the arena facing the outer wall in one of the adjacent quadrants to the previous shock-zone, and behaviour was recorded for 10 minutes as the rats learned the shock-zone was no longer dangerous. Movement of rats was scored live using Carousel Maze Manager. After all training sessions were complete rats were returned to their home cages.

Behavioural analysis Carousel Maze Manager was used for all data parameters in this task.

A.1.3 Shock-ramp test

Rats were placed within context A from the fear conditioning task (Fig. 1.5). Each rat was placed in the centre of the arena, and given 2.5 minutes to explore their environment. Rats were then presented with 3 scrambled foot shocks for 1 second per shock, with 1.5 minutes between each shock (Fig. 1.8A). This was repeated with the foot shock intensity increased (0.06, 0.1, 0.2, 0.3, 0.5, 0.7, 1.0 mA).

Appendix B

B.1 Additional electrophysiology analysis

B.1.1 Access resistance measurements

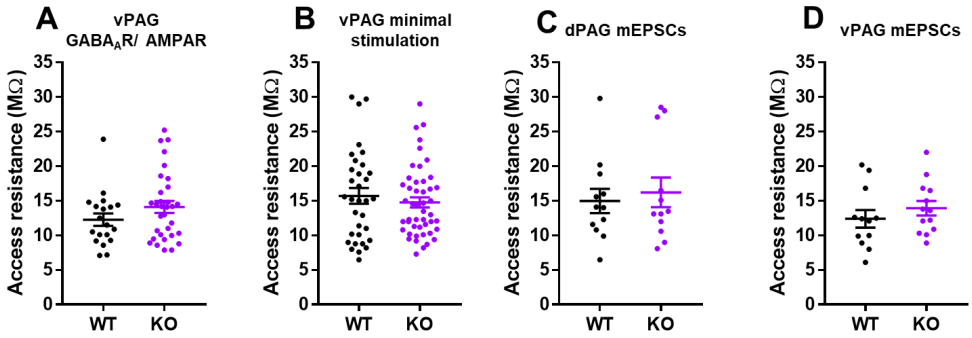

Figure S1: Access resistance of recordings in Chapter 3. (A) Access resistances of $GABA_AR$/ AMPAR ratio recordings from WT and *Nlgn3*$^{-/y}$ vPAG neurons are not different between genotypes (WT n = 19 cells, KO n = 32 cells, p = 0.17, unpaired t-test). (B) Minimal stimulation recordings from WT and *Nlgn3*$^{-/y}$ rats do not differ in access resistance (WT n = 33, KO n = 47, p = 0.48, unpaired t-test). (C) Overall access resistance is not different between WT and *Nlgn3*$^{-/y}$ rats for mEPSC recordings from dPAG neurons (WT n = 12, KO n = 12, p = 0.66, unpaired t-test). (D) No change in average access resistance of mEPSC recordings from vPAG neurons between WT and *Nlgn3*$^{-/y}$ rats (WT n = 12, KO n = 13, p = 0.37, unpaired t-test).

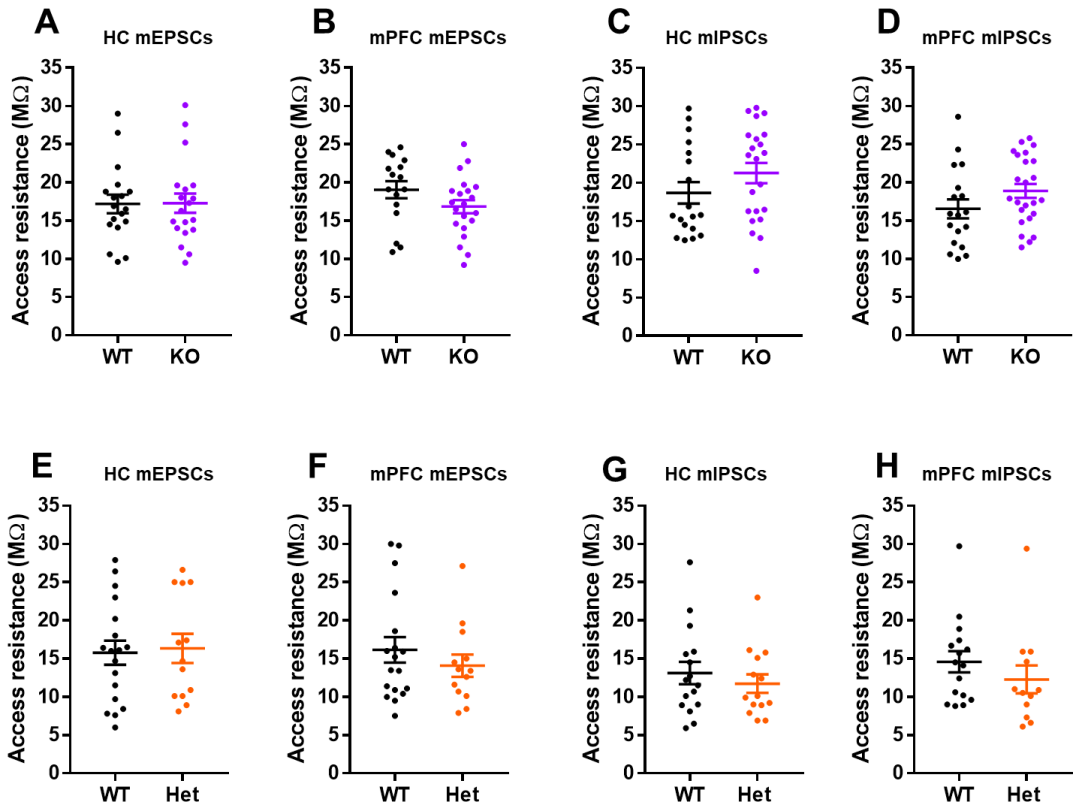

Figure S2: Access resistance of recordings in Chapter 5. (A) Access resistance of mEPSC recordings from WT and *Nlgn3*$^{-/y}$ HC neurons was not different between groups (WT n = 18, KO n = 19, p = 0.96, unpaired t-test). (B) No change in access resistance of mPFC neuron mEPSC recordings between WT and *Nlgn3*$^{-/y}$ rats (WT n = 16, KO n = 21, p = 0.13, unpaired t-test). (C) Access resistance of mIPSC recordings from WT and *Nlgn3*$^{-/y}$ HC neurons did not differ between genotypes (WT n = 18, KO n = 22, p = 0.19, unpaired t-test). (D) Access resistance was not different between WT and *Nlgn3*$^{-/y}$ mPFC neuron mIPSC recordings (WT n = 18, KO n = 24, p = 0.13, unpaired t-test). (E) Access resistance of mEPSC recordings from WT and *Nrxn1*$^{+/-}$ HC neurons was not different between groups (WT n = 18, Het n = 13, p = 0.82, unpaired t-test). (F) No change in access resistance of mPFC neuron mEPSC recordings between WT and *Nrxn1*$^{+/-}$ rats (WT n = 18, Het n = 13, p = 0.38, unpaired t-test). (G) Access resistance of mIPSC recordings from WT and *Nrxn1*$^{+/-}$ HC neurons did not differ between genotypes (WT n = 16, Het n = 14, p = 0.47, unpaired t-test). (H) Access resistance was not different between WT and *Nrxn1*$^{+/-}$ mPFC neuron mIPSC recordings (WT n = 16, Het n = 12, p = 0.32, unpaired t-test).

B.1.2 PAG neuron intrinsic properties and A-P axis position

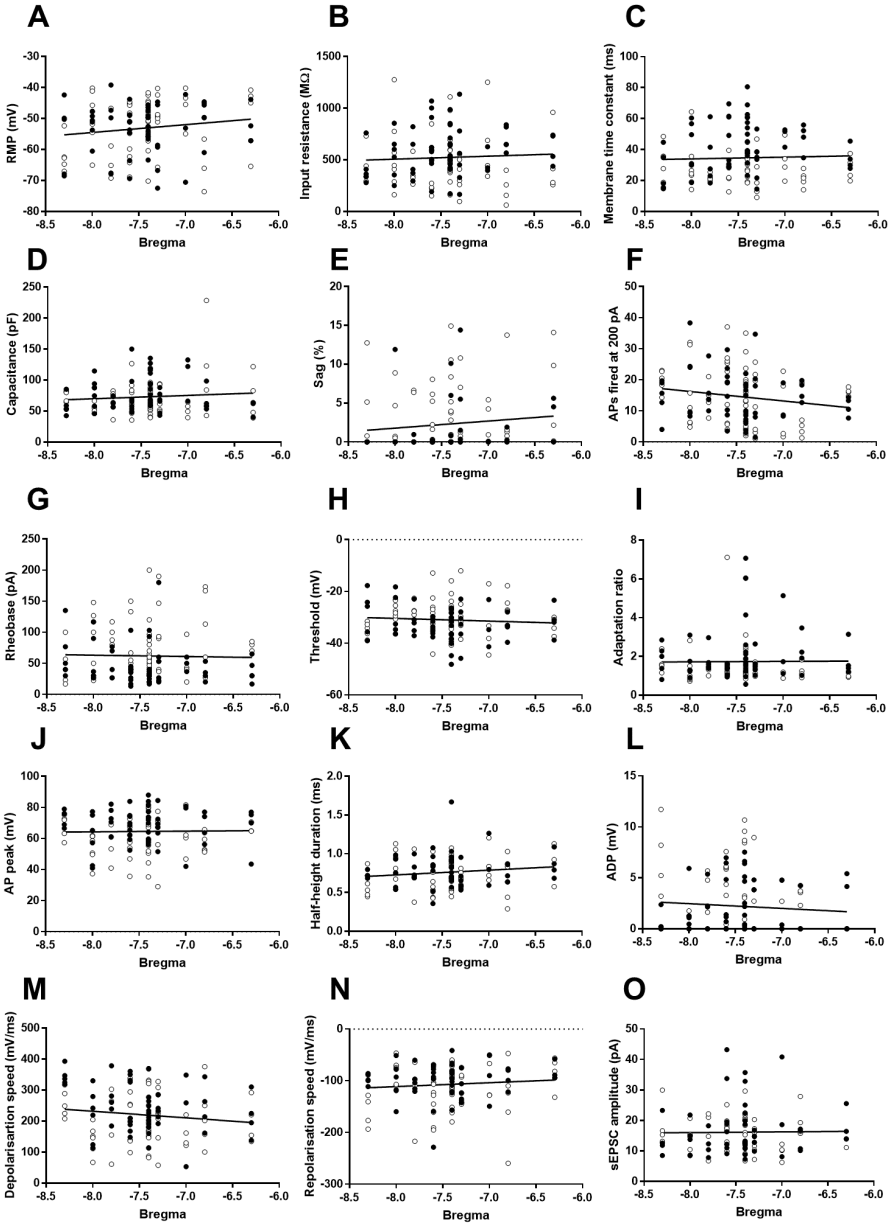

Anterior-posterior axis variation of WT PAG neuron properties

Figure S3 ***(previous page)*****: Anterior-posterior axis variation of PAG neuron properties** (A) No correlation between A-P axis position and RMP ($p = 0.12$, $R^2 = 0.021$, Pearson's R correlation). (B) A-P axis position and input resistance were not correlated ($p = 0.53$, $R^2 = 0.0033$, Pearson's R correlation). (C) A-P axis position and membrane time constant did not show significant correlation($p = 0.67$, $R^2 = 0.0015$, Pearson's R correlation). (D) No correlation between A-P axis position and capacitance ($p = 0.31$, $R^2 = 0.0087$, Pearson's R correlation). (E) No correlation was observed between A-P axis position and sag ($p = 0.21$, $R^2 = 0.014$, Pearson's R correlation). (F) A-P axis position and number of APs fired at 200 pA current injection were not significantly correlated ($p = 0.055$, $R^2 = 0.031$, Pearson's R correlation). (G) No correlation between A-P axis position and rheobase ($p = 0.79$, $R^2 = 0.00061$, Pearson's R correlation). (H) A-P axis position and threshold were not correlated ($p = 0.42$, $R^2 = 0.006$, Pearson's R correlation). (I) No significant correlation between A-P axis position and adaptation ratio ($p = 0.93$, $R^2 = <0.0001$, Pearson's R correlation). (J) A-P axis position and AP peak showed no correlation ($p = 0.85$, $R^2 = 0.00031$, Pearson's R correlation). (K) No correlation between A-P axis position and AP width ($p = 0.12$, $R^2 = 0.021$, Pearson's R correlation). (L) A-P axis position and ADP were not correlated ($p = 0.39$, $R^2 = 0.006$, Pearson's R correlation). (M) A-P axis position and AP depolarisation speed did not show significant correlation ($p = 0.32$, $R^2 = 0.009$, Pearson's R correlation). (N) No correlation between A-P axis position and AP repolarisation speed ($p = 0.22$, $R^2 = 0.014$, Pearson's R correlation). (O) A-P axis position and sEPSC amplitude were not correlated($p = 0.87$, $R^2 = 0.00025$, Pearson's R correlation).
Clear symbols represent cells in dPAG, filled symbols represent cells in vPAG.

B.1.3 Ward's clustering analysis of WT and *Nlgn3*$^{-/y}$ PAG neurons

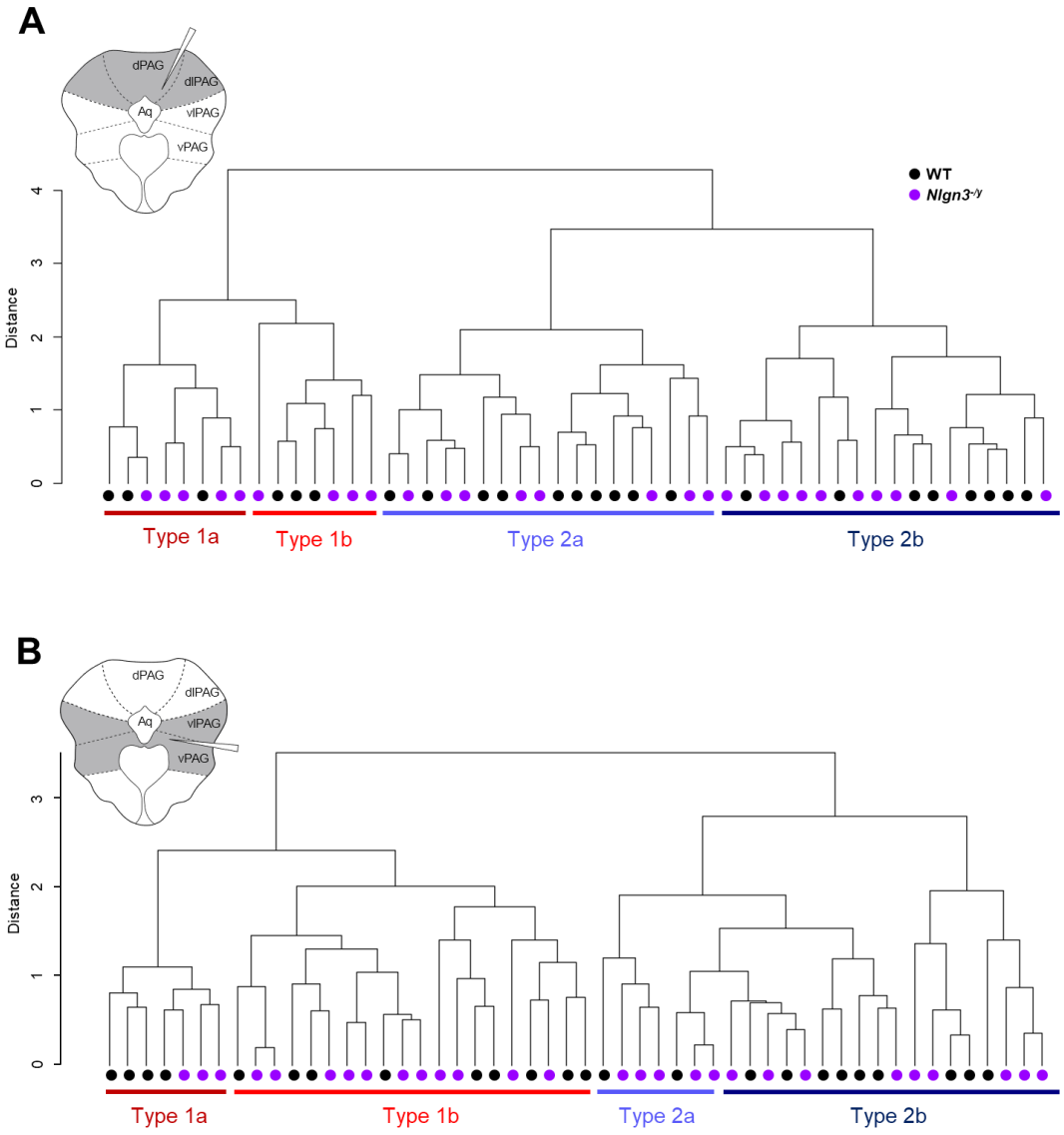

Figure S4: Ward's method clustering of WT and *Nlgn3*$^{-/y}$ PAG neurons (A) Dendrogram of dPAG neurons. (B) Dendrogram of vPAG neurons.

Table B.1: Means of dPAG neuron intrinsic properties for type 1 and type 2 neurons for WT and *Nlgn3*$^{-/y}$ rats. Mean values ± SEM for each intrinsic property recorded and used for cluster analysis.

	Type 1		**Type 2**		**Type 1**		**Type 2**	
	WT		**KO**		**WT**		**KO**	
	Average	± SEM	Average	± SEM	Average	± SEM	Average	± SEM
RMP (mV)	-57.13	2.92	-59.89	3.04	-50.92	1.66	-48.77	1.77
Input resistance (MΩ)	345.06	46.53	427.61	60.16	597.19	41.22	724.28	53.66
Membrane time constant (ms)	32.54	4.5	31.98	3.59	44.32	3.34	45.92	3.31
Capacitance (pF)	104.03	18.34	89.08	6.94	77.45	6.08	64.64	2.73
APs at 100 pA	2.13	0.52	3.28	1.12	7.2	1.25	12.43	1.87
APs at 200 pA	12.15	2.16	10.04	2.19	20.77	2.12	20.29	2.72
Rheobase (pA)	85.14	5.03	74.26	9.84	59.17	5.89	33.13	3.78
Threshold (mV)	-34.78	1.66	-33.3	2.12	-31.7	1.11	-32.33	1.12
Adaptation ratio	1.94	0.79	1.30	0.27	1.20	0.10	1.49	0.22
AP height (mV)	38.01	2.36	30.78	10.48	39.14	1.54	42.76	1.58
AP width (ms)	0.70	0.06	0.75	0.08	0.9	0.03	1.02	0.05
Depolarisation (mV/ms)	103.06	6.33	105.1	12.74	84.02	4.81	86.91	7.03
Repolarisation (mV/ms)	-74.87	3.42	-74.16	7.7	-62.39	3.81	-59.53	4.29

Table B.2: Means of vPAG neuron intrinsic properties for type 1 and type 2 neurons for WT and *Nlgn3*$^{-/y}$ rats. Mean values ± SEM for each intrinsic property recorded and used for cluster analysis.

	Type 1		**Type 2**		**Type 1**		**Type 2**	
	WT		**KO**		**WT**		**KO**	
	Average	± SEM	Average	± SEM	Average	± SEM	Average	± SEM
RMP (mV)	-49.58	1.88	-50.14	2.26	-58.06	2.1	-55.11	2.84
Input resistance (MΩ)	808.56	59.54	821.85	69.64	583.7	58.15	508.63	44.65
Membrane time constant (ms)	57.57	4.06	50.34	5.09	54.49	7.67	39.65	2.49
Capacitance (pF)	73.97	5.74	61.74	3.58	96.56	10.78	83.51	5.8
APs at 100 pA	44.08	2.68	49.43	2.16	44.84	2.75	49.24	2.15
APs at 200 pA	9.46	1.18	9.38	1.88	7.13	0.68	6.15	1.2
Rheobase (pA)	12.95	2.26	8.83	2.53	18.08	1.89	14.6	1.98
Threshold (mV)	-31.37	1.27	-33.54	1.3	-35.3	1.01	-34.08	1.27
Adaptation ratio	1.81	0.24	2.92	0.94	2.64	1.07	2.13	0.21
AP height (mV)	33.14	3.51	33.1	3.75	41.44	4.95	52.98	8.46
AP width (ms)	1.06	0.05	1.31	0.09	0.83	0.04	0.9	0.05
Depolarisation (mV/ms)	89.92	6.95	87.13	7.00	111.71	8.93	113.78	5.55
Repolarisation (mV/ms)	-52.64	2.8	-50.01	2.38	-70.99	5.12	-71.07	3.44

B.1.4 Minimally stimulated responses of pyramidal and multipolar WT and *Nlgn3*$^{-/y}$ PAG neurons

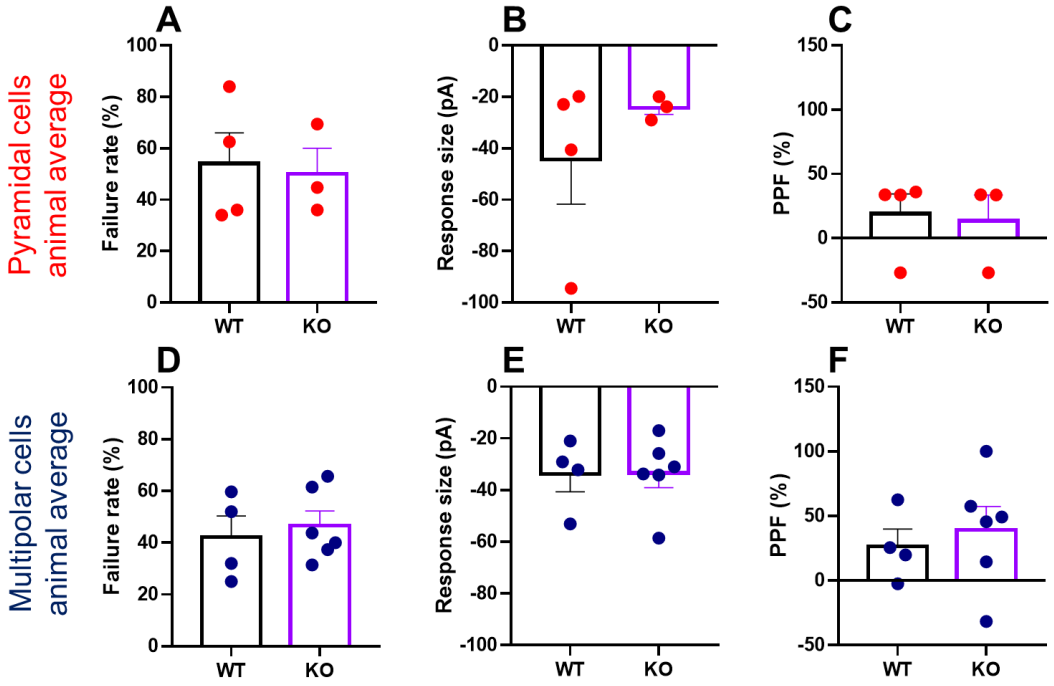

Figure S5: No change in minimaly stimulated responses of pyramidal and multipolar neurons in *Nlgn3*$^{-/y}$ rats. (A) Animal average of pyramidal cell failure rate is unchanged in *Nlgn3*$^{-/y}$ rats compared to WT (WT 6 cells/ 4 rats, KO 5 cells/ 3 rats, p = 0.81, unpaired t-test). (B) Animal average of WT and *Nlgn3*$^{-/y}$ EPSC size when only considering pyramidal cells is comparable (WT 6 cells/ 4 rats, KO 5 cells/ 3 rats, p = 0.37, unpaired t-test). (C) Animal average of WT and *Nlgn3*$^{-/y}$ pyramidal cell % PPF are not significantly differentt (WT 6 cells/ 4 rats, KO 5 cells/ 3 rats, p = 0.83, unpaired t-test). (D) Animal average of multipolar cell failure rate is unchanged in *Nlgn3*$^{-/y}$ rats compared to WT (WT 8 cells/ 4 rats, KO 13 cells/ 6 rats, p = 0.65, unpaired t-test). (E) Animal average of WT and *Nlgn3*$^{-/y}$ failure rate when only considering multipolar cells is unchanged in *Nlgn3*$^{-/y}$ compared to WT rats (WT 8 cells/ 4 rats, KO 13 cells/ 6 rats, p = 0.96, unpaired t-test). (F) Animal average of WT and *Nlgn3*$^{-/y}$ failure rate is unchanged for multipolar cells (WT 8 cells/ 4 rats, KO 13 cells/ 6 rats, p = 0.62, unpaired t-test).

B.1.5 CV^2 analysis

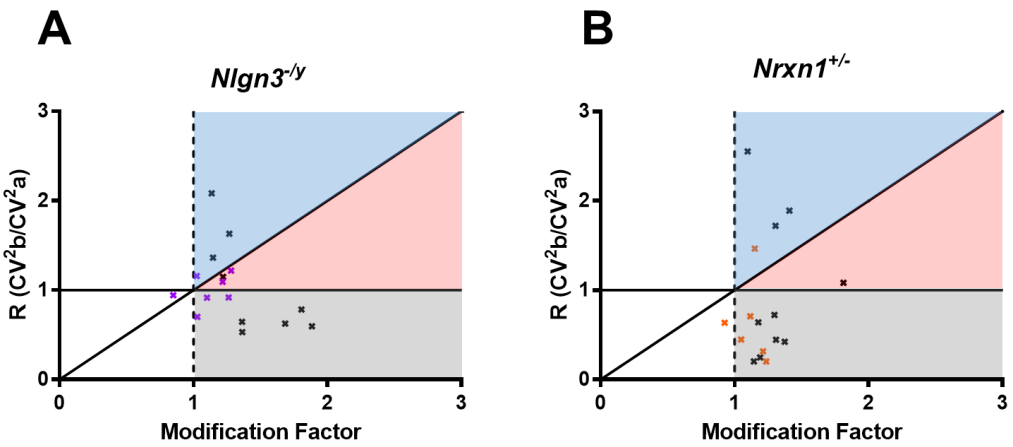

Figure S6: CV^2 analysis of *Nlgn3*$^{-/y}$ and *Nrxn*$^{+/-}$ LTP recordings. (A) CV^2 analysis of *Nlgn3*$^{-/y}$ LTP recordings. (B) CV^2 analysis of *Nrxn*$^{+/-}$ LTP recordings.
Data points located on or below the horizontal line (grey region) signify a postsynaptic interpretation, above the diagonal line (blue region) signifies a presynaptic interpretation, and in between (red region) signifies both (Faber and Korn, 1991).

Chapter 7

Bibliography

Bibliography

Allen C, Stevens CF (1994) An evaluation of causes for unreliability of synaptic transmission. *Proceedings of the National Academy of Sciences of the United States of America* 91:10380–10383.

Amano T, Unal CT, Paré D (2010) Synaptic correlates of fear extinction in the amygdala. *Nature Neuroscience* 13:489–494.

An LN, Yue Y, Guo WZ, Miao YL, Mi WD, Zhang H, Lei ZL, Han SJ, Dong L (2013) Surgical trauma induces iron accumulation and oxidative stress in a rodent model of postoperative cognitive dysfunction. *Biological Trace Element Research* 151:277–283.

An X, Bandler R, Ongur D, Price JL (2006) Prefrontal Cortical Projections to Longitudinal Columns in the Midbrain Periaqueductal Gray in Macaque Monkeys. *Journal of Comparative Neurology* 479:455–479.

Anderson GR, Aoto J, Tabuchi K, Földy C, Covy J, Yee AX, Wu D, Lee SJ, Chen L, Malenka RC, Südhof TC (2015) β-Neurexins Control Neural Circuits by Regulating Synaptic Endocannabinoid Signaling. *Cell* 162:593–606.

Andrásfalvy BK, Magee JC (2004) Changes in AMPA receptor currents following LTP induction on rat CA1 pyramidal neurones. *Journal of Physiology* 559:543–554.

Anwyl R (1999) Metabotropic glutamate receptors: Electrophysiological properties and role in plasticity. *Brain Research Reviews* 29:83–120.

Apps R, Strata P (2015) Neuronal circuits for fear and anxiety-the missing link. *Nature Reviews Neuroscience* 16:642–643.

Araya R, Vogels TP, Yuste R (2014) Activity-dependent dendritic spine neck changes are correlated with synaptic strength. *Proceedings of the National Academy of Sciences of the United States of America* 111.

Asiminas A, Jackson AD, Louros SR, Till SM, Spano T, Dando O, Bear MF, Chattarji S, Hardingham GE, Osterweil EK, Wyllie DJ, Wood ER, Kind PC (2019) Sustained correction of associative learning deficits after brief, early treatment in a rat model of Fragile X Syndrome. *Science Translational Medicine* 11:1–11.

Assareh N, Bagley EE, Carrive P, McNally GP (2017) Brief optogenetic inhibition of rat lateral or ventrolateral periaqueductal gray augments the acquisition of pavlovian fear conditioning. *Behavioral Neuroscience* 131:454–459.

Auerbach BD, Osterweil EK, Bear MF (2011) Mutations causing syndromic autism define an axis of synaptic pathophysiology. *Nature* 480:63–68.

Avazzadeh S, McDonagh K, Reilly J, Wang Y, Boomkamp SD, McInerney V, Krawczyk J, Fitzgerald J, Feerick N, O'Sullivan M, Jalali A, Forman EB, Lynch SA, Ennis S, Cosemans N, Peeters H, Dockery P, O'Brien T, Quinlan LR, Gallagher L, Shen S (2019) Increased Ca2+ signaling in NRXN1α +/- neurons derived from ASD induced pluripotent stem cells. *Molecular Autism* 10:1–16.

Avdjieva-Tzavella DM, Todorov TP, Todorova AP, Kirov AV, Hadjidekova SP, Rukova BB, Litvinenko IO, Hristova-Naydenova DN, Tincheva RS, Toncheva DI (2012) Analysis of the genes encoding neuroligins NLGN3 and NLGN4 in Bulgarian patients with autism. *Genetic Counseling* 23:505–511.

Bahník Š (2014) Carousel maze manager. Version 0.4.0 [Software].

Bailey A, Le Couteur A, Gottesman I, Bolton P, Simonoff E, Yuzda E, Rutter M (1995) Autism as a strongly genetic disorder: Evidence from a british twin study. *The Science of Mental Health: Volume 2: Autism* pp. 91–105.

Bandler R, Carrive P (1988) Integrated defence reaction elicited by excitatory amino acid microinjection in the midbrain periaqueductal grey region of the unrestrained cat. *Brain Research* 439:95–106.

Bandler R, Depaulis A (1988) Elicitation of intraspecific defence reactions in the rat from midbrain periaqueductal grey by microinjection of kainic acid, without neurotoxic effects. *Neuroscience Letters* 88:291–296.

Bandler R, Depaulis A, Vergnes M (1985) Indentification of midbrain neurones mediating defensive behaviour in the rat by microinjections of excitatory amino acids. *Behavioural Brain Research* 15:107–119.

Barnes SA, Wijetunge LS, Jackson AD, Katsanevaki D, Osterweil EK, Komiyama NH, Grant SGN, Bear MF, Nagerl UV, Kind PC, Wyllie DJA (2015) Convergence of Hippocampal Pathophysiology in Syngap+/- and Fmr1-/y Mice. *Journal of Neuroscience* 35:15073–15081.

Barria A, Malinow R (2005) NMDA receptor subunit composition controls synaptic plasticity by regulating binding to CaMKII. *Neuron* 48:289–301.

Bashir ZI, Jane DE, Sunter DC, Watkins JC, Collingridge GL (1993a) Metabotropic glutamate receptors contribute to the induction of long-term depression in the CA1 region of the hippocampus. *European journal of pharmacology* 239:265–6.

Bashir ZI, Bortolotto ZA, Davies CH, Berretta N, Irving AJ, Seal AJ, Henley JM, Jane DE, Watkins JC, Collingridge GL (1993b) Induction of LTP in the hippocampus needs synaptic activation of glutamate metabotropic receptors. *Nature* 363:347–350.

Baudouin S, Gaudias J, Gerharz S, Hatstatt L, Zhou K, Punnakkal P, Tanaka K, Spooren W, Hen R, Zeeuw C, Kaspar V, Scheiffele P (2012) Shared Synaptic Pathophysiology in Syndromic and Nonsyndromic Rodent Models of Autism. *Science* 338:1–6.

Bauer EP, Schafe GE, LeDoux JE (2002) NMDA Receptors and L-Type Voltage-Gated Calcium Channels Contribute to Long-Term Potentiation and Different Components of Fear Memory Formation in the Lateral Amygdala. *Journal of Neuroscience* 22:5239–5249.

Bear MF, Huber KM, Warren ST (2004) The mGluR theory of fragile X mental retardation.

Behbehani MM (1995) Functional characteristics of the midbrain periaqueductal gray. *Progress in Neurobiology* 46:575–605.

Beitz AJ (1982) The organisation of afferent projections to the midbrain periaqueductal gray of the rat. *Neuroscience* 7:133–159.

Beitz AJ, Shepard RD (1985) The midbrain periaqueductal gray in the rat. II. A Golgi analysis. *Journal of Comparative Neurology* 237:460–475.

Bellini S (2004) Social Skill Deficits and Anxiety in High-Functioning Adolescents With Autism Spectrum Disorders. *Focus on Autism and Other Developmental Disabilities* .

Bellini S (2006) The Development of Social Anxiety in Adolescents With Autism Spectrum Disorders. *Focus on Autism and Other Developmental Disabilities* 21:138–145.

Belova MA, Paton JJ, Morrison SE, Salzman CD (2007) Expectation Modulates Neural Responses to Pleasant and Aversive Stimuli in Primate Amygdala. *Neuron* 55:970–984.

Benarroch EE (2012) Periaqueductal gray: An interface for behavioral control. *Neurology* 78:210–270.

Benson DL, Watkins FH, Steward O, Banker G (1994) Characterization of GABAergic neurons in hippocampal cell cultures. *Journal of Neurocytology* 23:279–295.

Besag FM (2018) Epilepsy in patients with autism: Links, risks and treatment challenges. *Neuropsychiatric Disease and Treatment* 14:1–10.

Biederer T, Südhof TC (2000) Mints as adaptors. Direct binding to neurexins and recruitment of Munc18. *Journal of Biological Chemistry* 275:39803–39806.

Biervert C, Schroeder BC, Kubisch C, Berkovic SF, Propping P, Jentsch TJ, Steinlein OK (1998) A potassium channel mutation in neonatal human epilepsy. *Science* 279:403–406.

Bittencourt AS, Carobrez AP, Zamprogno LP, Tufik S, Schenberg LC (2004) Organization of single components of defensive behaviors within distinct columns of periaqueductal gray matter of the rat: Role of N-methyl-D-aspartic acid glutamate receptors. *Neuroscience* 125:71–89.

Blasi F, Bacchelli E, Pesaresi G, Carone S, Bailey AJ, Maestrini E (2006) Absence of coding mutations in the X-linked genes neuroligin 3 and neuroligin 4 in individuals with autism from the IMGSAC collection. *American Journal of Medical Genetics - Neuropsychiatric Genetics* 141 B:220–221.

Bliss TV, Gardner-Medwin aR (1973) Long-lasting potentiation of synaptic transmission in the dentate area of the unanaestetized rabbit following stimulation of the perforant path. *The Journal of physiology* 232:357–374.

Bliss TVP, Lømo T (1973) Long-lasting potentiation of synaptic transmission in the dentate area of the anaesthetized rabbit following stimulation of the perforant path. *The Journal of Physiology* 232:331–356.

Bliss T, Collingridge G (1993) A synaptic model of memory: LTP in the hippocampus. *Nature* 361:31–39.

Blundell J, Blaiss CA, Etherton MR, Espinosa F, Tabuchi K, Walz C, Bolliger MF, Südhof TC, Powell CM (2010) Neuroligin-1 deletion results in impaired spatial memory and increased repetitive behavior. *Journal of Neuroscience* 30:2115–2129.

Bolliger MF, Pei J, Maxeiner S, Boucard AA, Grishin NV, Südhof TC (2008) Unusually rapid evolution of Neuroligin-4 in mice. *Proceedings of the National Academy of Sciences of the United States of America* 105:6421–6426.

Booker SA, Vida I (2018) Morphological diversity and connectivity of hippocampal interneurons. *Cell and Tissue Research* 373:619–641.

Borgatti R, Zucca C, Cavallini A, Ferrario M, Panzeri C, Castaldo P, Soldovieri MV, Baschirotto C, Bresolin N, Bernardina BD, Taglialatela M, Bassi MT (2004) A novel mutation in KCNQ2-associated with BFNC, drug resistant epilepsy, and mental retardation. *Neurology* 63:57–65.

Boucard AA, Chubykin AA, Comoletti D, Taylor P, Südhof TC (2005) A splice code for trans-synaptic cell adhesion mediated by binding of neuroligin 1 to α- and β-neurexins. *Neuron* 48:229–236.

Brager DH, Johnston D (2007) Plasticity of Intrinsic Excitability during Long-Term Depression Is Mediated through mGluR-Dependent Changes in Ih in Hippocampal CA1 Pyramidal Neurons. *Journal of Neuroscience* 27:13926–13937.

Brandão ML, Lovick TA (2019) Role of the dorsal periaqueductal gray in posttraumatic stress disorder: mediation by dopamine and neurokinin. *Translational Psychiatry* 9.

Bravo-Rivera C, Roman-Ortiz C, Brignoni-Perez E, Sotres-Bayon F, Quirk GJ (2014) Neural structures mediating expression and extinction of platform-mediated avoidance. *Journal of Neuroscience* 34:9736–9742.

Bravo-Rivera C, Roman-Ortiz C, Montesinos-Cartagena M, Quirk GJ (2015) Persistent active avoidance correlates with activity in prelimbic cortex and ventral striatum. *Frontiers in Behavioral Neuroscience* 9:1–8.

Brown DA, Passmore GM (2009) Neural KCNQ (Kv7) channels. *British Journal of Pharmacology* 156:1185–1195.

Bucan M, Abrahams BS, Wang K, Glessner JT, Herman EI, Sonnenblick LI, Alvarez Retuerto AI, Imielinski M, Hadley D, Bradfield JP, Kim C, Gidaya NB, Lindquist I, Hutman T, Sigman M, Kustanovich V, Lajonchere CM, Singleton A, Kim J, Wassink TH, McMahon WM, Owley T, Sweeney JA, Coon H, Nurnberger JI, Li M, Cantor RM, Minshew NJ, Sutcliffe JS, Cook EH, Dawson G, Buxbaum JD, Grant SF, Schellenberg GD, Geschwind DH, Hakonarson H (2009) Genome-wide analyses of exonic copy number variants in a family-based study point to novel autism susceptibility genes. *PLoS Genetics* 5.

Budreck EC, Kwon OB, Jung JH, Baudouin S, Thommen A, Kim HS, Fukazawa Y, Harada H, Tabuchi K, Shigemoto R, Scheiffele P, Kim JH (2013) Neuroligin-1 controls synaptic abundance of NMDA-type glutamate receptors through extracellular coupling. *Proceedings of the National Academy of Sciences of the United States of America* 110:725–730.

Budreck EC, Scheiffele P (2007) Neuroligin-3 is a neuronal adhesion protein at GABAergic and glutamatergic synapses. *European Journal of Neuroscience* 26:1738–1748.

Burrows EL, Laskaris L, Koyama L, Churilov L, Bornstein JC, Hill-Yardin EL, Hannan AJ (2015) A neuroligin-3 mutation implicated in autism causes abnormal aggression and increases repetitive behavior in mice. *Molecular Autism* 6.

Butler MG, Dazouki MJ, Zhou XP, Talebizadeh Z, Brown M, Takahashi TN, Miles JH, Wang CH, Stratton R, Pilarski R, Eng C (2005) Subset of individuals with autism spectrum disorders and extreme macrocephaly associated with germline PTEN tumour suppressor gene mutations. *Journal of Medical Genetics* 42:318–321.

Calvo F, Lobão-soares B, Freitas RLD, Paschoalin-maurin T, Anjos-garcia T, Medeiros P, Almeida J, Lovick TA, Coimbra NC (2019) The endogenous opioid system modulates defensive behavior evoked by Crotalus durissus terrificus : Panicolytic-like effect of intracollicular non-selective opioid receptors blockade. *Psychopharmacology* 33:51–61.

Campeau S, Hayward MD, Hope BT, Rosen JB, Nestler EJ, Davis M (1991) Induction of the c-fos proto-oncogene in rat amygdala during unconditioned and conditioned fear. *Brain Research* 565:349–352.

Canteras NS (2002) The medial hypothalamic defensive system : Hodological organization and functional implications. *Pharmacology, Biochemistry and Behavior* 71:481–491.

Cao W, Lin S, qiang Xia Q, lan Du Y, Yang Q, ying Zhang M, qing Lu Y, Xu J, min Duan S, Xia J, Feng G, Xu J, hong Luo J (2018) Gamma Oscillation Dysfunction in mPFC Leads to Social Deficits in Neuroligin 3 R451C Knockin Mice. *Neuron* 97:1253–1260.e7.

Carrasquillo Y, Burkhalter A, Nerbonne JM (2012) A-type K+ channels encoded by Kv4.2, Kv4.3 and Kv1.4 differentially regulate intrinsic excitability of cortical pyramidal neurons. *Journal of Physiology* 590:3877–3890.

Carrive P, Bandler R, Dampney RA (1988) Anatomical evidence that hypertension associated with the defence reaction in the cat is mediated by a direct projection from a restricted portion of the midbrain periaqueductal grey to the subretrofacial nucleus of the medulla. *Brain Research* .

Carrive P (1993) The periaqueductal gray and defensive behavior: Functional representation and neuronal organization. *Behavioural Brain Research* 58:27–47.

Carrive P, Bandler R (1991) Viscerotopic organization of neurons subserving hypotensive reactions within the midbrain periaqueductal grey: a correlative functional and anatomical study. *Brain Research* 541:206–215.

Carroll RC, Beattie EC, Xia H, Lüscher C, Altschuler Y, Nicoll RA, Malenka RC, Von Zastrow M (1999a) Dynamin-dependent endocytosis of ionotropic glutamate receptors. *Proceedings of the National Academy of Sciences of the United States of America* 96:14112–14117.

Carroll RC, Lissin DV, Von Zastrow M, Nicoll RA, Malenka RC (1999b) Rapid redistribution of glutamate receptors contributes to long-term depression in hippocampal cultures. *Nature Neuroscience* 2:454–460.

Carvalho MC, Santos JM, Brandão ML (2015) Dorsal periaqueductal gray post-stimulation freezing is counteracted by neurokinin-1 receptor antagonism in the central nucleus of the amygdala in rats. *Neurobiology of Learning and Memory* 121:52–58.

Carvalho MC, Veloni AC, Genaro K, Brandão ML (2018) Behavioral sensitization induced by dorsal periaqueductal gray electrical stimulation is counteracted by NK1 receptor antagonism in the ventral hippocampus and central nucleus of the amygdala. *Neurobiology of Learning and Memory* 148:60–68.

Castronovo P, Baccarin M, Ricciardello A, Picinelli C, Tomaiuolo P, Cucinotta F, Frittoli M, Lintas C, Sacco R, Persico AM (2019) Phenotypic spectrum of NRXN1 mono- and bi-allelic deficiency: A systematic review. *Clinical Genetics* 484:125–137.

Cauli B, Audinat E, Lambolez B, Angulo MC, Ropert N, Tsuzuki K, Hestrin S, Rossier J (1997) Molecular and physiological diversity of cortical nonpyramidal cells. *Journal of Neuroscience* 17:3894–3906.

Cauli B, Porter JT, Tsuzuki K, Lambolez B, Rossier J, Quenet B, Audinat E (2000) Classification of fusiform neocortical interneurons based on unsupervised clustering. *Proceedings of the National Academy of Sciences of the United States of America* 97:6144–6149.

Chadman KK, Gong S, Scattoni ML, Boltuck SE, Gandhy U, Heintz N, Crawley JN (2008) Minimal Aberrant Behavioral Phenotypes of Neuroligin-3 R451C Knockin Mice. *Autism* 1:147–158.

Chanda S, Aoto J, Lee SJ, Wernig M, Südhof TC (2016) Pathogenic mechanism of an autism-associated neuroligin mutation involves altered AMPA-receptor trafficking. *Molecular Psychiatry* 21:169–177.

Chanda S, Hale WD, Zhang B, Wernig M, Südhof TC (2017) Unique versus Redundant Functions of Neuroligin Genes in Shaping Excitatory and Inhibitory Synapse Properties. *The Journal of Neuroscience* 37:6816–6836.

Chanda S, Marro S, Wernig M, Südhof TC (2013) Neurons generated by direct conversion of fibroblasts reproduce synaptic phenotype caused by autism-associated neuroligin-3 mutation. *Proceedings of the National Academy of Sciences of the United States of America* 110:16622–16627.

Chen W, Zhang JJ, Hu GY, Wu CP (1996) Electrophysiological and morphological properties of pyramidal and nonpyramidal neurons in the cat motor cortex in vitro. *Neuroscience* 73:39–55.

Chen Y, Chad JE, Wheal HV (1996) Synaptic release rather than failure in the conditioning pulse results in paired-pulse facilitation during minimal synaptic stimulation in the rat hippocampal CA1 neurones. *Neuroscience Letters* 218:204–208.

Chieng B, Christie MJ (1994) Hyperpolarization by opioids acting on μ receptors of a subpopulation of rat periaqueductal gray neurones in vitro. *British Journal of Pharmacology* 113:121–128.

Chih B, Afridi SK, Clark L, Scheiffele P (2004) Disorder-associated mutations lead to functional inactivation of neuroligins. *Human Molecular Genetics* 13:1471–1477.

Chih B, Engelman H, Scheiffele P (2005) Control of excitatory and inhibitory synapse formation by neuroligins. *Science* 307:1324–1328.

Chih B, Gollan L, Scheiffele P (2006) Alternative Splicing Controls Selective Trans-Synaptic Interactions of the Neuroligin-Neurexin Complex. *Neuron* 51:171–178.

Ching MSL, Shen Y, Tan WH, Jeste SS, Morrow EM, Chen X, Mukaddes NM, Yoo SY, Hanson E, Hundley R, Austin C, Becker RE, Berry GT, Driscoll K, Engle EC, Friedman S, Gusella JF, Hisama FM, Irons MB, Lafiosca T, LeClair E, Miller DT, Neessen M, Picker JD, Rappaport L, Rooney CM, Sarco DP, Stoler JM, Walsh CA, Wolff RR, Zhang T, Nasir RH, Wu BL (2010) Deletions of NRXN1 (neurexin-1) predispose to a wide spectrum of developmental disorders. *American Journal of Medical Genetics, Part B: Neuropsychiatric Genetics* 153:937–947.

Chiou Lc, Fan SH, Guerrini R, Calo G (2002) [Nphe1]N/OFQ-(1-13)-NH2 is a competitive and selective antagonist at nociceptin/orphanin FQ receptors mediating K+ channel activation in rat periaqueductal gray slices. *Neuropharmacology* 42:246–252.

Cho JH, Rendall SD, Gray JM (2017) Brain-wide maps of Fos expression during fear learning and recall. *Learning and Memory* 24:169–181.

Choi YB, Li HL, Kassabov SR, Jin I, Puthanveettil SV, Karl KA, Lu Y, Kim JH, Bailey CH, Kandel ER (2011) Neurexin-Neuroligin Transsynaptic Interaction Mediates Learning-Related Synaptic Remodeling and Long-Term Facilitation in Aplysia. *Neuron* 70:468–481.

Chubykin AA, Atasoy D, Etherton MR, Brose N, Kavalali ET, Gibson JR, Südhof TC (2007) Activity-Dependent Validation of Excitatory versus Inhibitory Synapses by Neuroligin-1 versus Neuroligin-2. *Neuron* 54:919–931.

Chung L, Bey AL, Jiang YH (2012) Synaptic plasticity in mouse models of autism spectrum disorders. *Korean Journal of Physiology and Pharmacology* 16:369–378.

Cimadevilla JM, Fenton AA, Bures J (2000) Functional inactivation of dorsal hippocampus impairs active place avoidance in rats. *Neuroscience Letters* 285:53–56.

Ciocchi S, Herry C, Grenier F, Wolff SB, Letzkus JJ, Vlachos I, Ehrlich I, Sprengel R, Deisseroth K, Stadler MB, Müller C, Lüthi A (2010) Encoding of conditioned fear in central amygdala inhibitory circuits. *Nature* 468:277–282.

Clements JD, Bekkers JM (1997) Detection of spontaneous synaptic events with an optimally scaled template. *Biophysical Journal* 73:220–229.

Coan EJ, Saywood W, Collingridge GL (1987) MK-801 blocks NMDA receptor-mediated synaptic transmission and long term potentiation in rat hippocampal slices. *Neuroscience Letters* 80:111–114.

Coimbra NC, Calvo F, Almada RC, Freitas RL, Paschoalin-Maurin T, dos Anjos-Garcia T, Elias-Filho DH, Ubiali WA, Lobão-Soares B, Tracey I (2017) Opioid neurotransmission modulates defensive behavior and fear-induced antinociception in dangerous environments. *Neuroscience* 354:178–195.

Colacicco G, Welzl H, Lipp HP, Würbel H (2002) Attentional set-shifting in mice: Modification of a rat paradigm, and evidence for strain-dependent variation. *Behavioural Brain Research* 132:95–102.

Collingridge GL, Kehl SJ, McLennan H (1983) Excitatory amino acids in synaptic transmission in the Schaffer collateral-commissural pathway of the rat hippocampus. *The Journal of Physiology* 334:33–46.

Comoletti D, De Jaco A, Jennings LL, Flynn RE, Gaietta G, Tsigelny I, Ellisman MH, Taylor P (2004) The Arg451Cys-neuroligin-3 mutation associated with autism reveals a defect in protein processing. *The Journal of neuroscience : the official journal of the Society for Neuroscience* 24:4889–93.

Comoletti D, Flynn RE, Boucard AA, Demeler B, Schirf V, Shi J, Jennings LL, Newlin HR, Südhof TC, Taylor P (2006) Gene selection, alternative splicing, and post-translational processing regulate neuroligin selectivity for β-neurexins. *Biochemistry* 45:12816–12827.

Constals A, Penn AC, Compans B, Toulmé E, Phillipat A, Marais S, Retailleau N, Hafner AS, Coussen F, Hosy E, Choquet D (2015) Glutamate-Induced AMPA Receptor Desensitization Increases Their Mobility and Modulates Short-Term Plasticity through Unbinding from Stargazin. *Neuron* 85:787–803.

Corcoran KA, Quirk GJ (2007) Activity in prelimbic cortex is necessary for the expression of learned, but not innate, fears. *Journal of Neuroscience* 27:840–844.

Courtin J, Bienvenu TC, Einarsson EÖ, Herry C (2013) Medial prefrontal cortex neuronal circuits in fear behavior. *Neuroscience* 240:219–242.

Courtin J, Chaudun F, Rozeske RR, Karalis N, Gonzalez-Campo C, Wurtz H, Abdi A, Baufreton J, Bienvenu TC, Herry C (2014) Prefrontal parvalbumin interneurons shape neuronal activity to drive fear expression. *Nature* 505:92–96.

Cracco JB, Serrano P, Moskowitz SI, Bergold PJ, Sacktor TC (2005) Protein synthesis-dependent LTP in isolated dendrites of CA1 pyramidal cells. *Hippocampus* 15:551–556.

Craig AM, Kang Y (2007) Neurexin-neuroligin signaling in synapse development. *Current Opinion in Neurobiology* 17:43–52.

Curzon P, Nr R, Ke B (2014) Chapter 2 - Cued and Contextual Fear Conditioning for Rodents In *Methods of Behavior Analysis in Neuroscience*, pp. 1–11. Taylor & Francis Group, LLC.

Dabell MP, Rosenfeld JA, Bader P, Escobar LF, El-Khechen D, Vallee SE, Dinulos MBP, Curry C, Fisher J, Tervo R, Hannibal MC, Siefkas K, Wyatt PR, Hughes L, Smith R, Ellingwood S, Lacassie Y, Stroud T, Farrell SA, Sanchez-Lara PA, Randolph LM, Niyazov D, Stevens CA, Schoonveld C, Skidmore D, Mackay S, Miles JH, Moodley M, Huillet A, Neill NJ, Ellison JW, Ballif BC, Shaffer LG (2013) Investigation of NRXN1 deletions: Clinical and molecular characterization. *American Journal of Medical Genetics, Part A* 161:717–731.

Dachtler J, Ivorra JL, Rowland TE, Lever C, John Rodgers R, Clapcote SJ (2015) Heterozygous deletion of α-neurexin I or α-neurexin II results in behaviors relevant to autism and schizophrenia. *Behavioral Neuroscience* 129:765–776.

Dalzell L, Connor S, Penner M, Saari MJ, Leboutillier JC, Weeks AC (2011) Fear conditioning is associated with synaptogenesis in the lateral amygdala. *Synapse* 65:513–519.

Davis E, Ollendick T (2014) Chapter 10- Fear: Autism Spectrum Disorder and/or Specific Phobia In *The Handbook of Autism and Anxiety*, pp. 137–152. Springer US.

Davis TE, Hess JA, Moree BN, Fodstad JC, Dempsey T, Jenkins WS, Matson JL (2011) Anxiety symptoms across the lifespan in people diagnosed with Autistic Disorder. *Research in Autism Spectrum Disorders* 5:112–118.

de Almeida LP, Ramos PL, Pandossio JE, Landeira-Fernandez J, Zangrossi H, Nogueira RL (2006) Prior electrical stimulation of dorsal periaqueductal grey matter or deep layers of the superior colliculus sensitizes rats to anxiety-like behaviors in the elevated T-maze test. *Behavioural Brain Research* 170:175–181.

de Git KC, van Tuijl DC, Luijendijk MC, Wolterink-Donselaar IG, Ghanem A, Conzelmann KK, Adan RA (2018) Anatomical projections of the dorsomedial hypothalamus to the periaqueductal grey and their role in thermoregulation: a cautionary note. *Physiological Reports* 6:1–16.

De Jaco A, Lin MZ, Dubi N, Comoletti D, Miller MT, Camp S, Ellisman M, Butko MT, Tsien RY, Taylor P (2010) Neuroligin trafficking deficiencies arising from mutations in the α/β-hydrolase fold protein family. *Journal of Biological Chemistry* 285:28674–28682.

De Rubeis S, He X, Goldberg AP, Poultney CS, Samocha K, Cicek AE, Kou Y, Liu L, Fromer M, Walker S, Singh T, Klei L, Kosmicki J, Fu SC, Aleksic B, Biscaldi M, Bolton PF, Brownfeld JM, Cai J, Campbell NG, Carracedo A, Chahrour MH, Chiocchetti AG, Coon H, Crawford EL, Crooks L, Curran SR, Dawson G, Duketis E, Fernandez BA, Gallagher L, Geller E, Guter SJ, Hill RS, Ionita-Laza I, Gonzalez PJ, Kilpinen H, Klauck SM, Kolevzon A, Lee I, Lei J, Lehtimäki T, Lin CF, Ma'ayan A, Marshall CR, McInnes AL, Neale B, Owen MJ, Ozaki N, Parellada M, Parr JR, Purcell S, Puura K, Rajagopalan D, Rehnström K, Reichenberg A, Sabo A, Sachse M, Sanders SJ, Schafer C, Schulte-Rüther M, Skuse D, Stevens C, Szatmari P, Tammimies K, Valladares O, Voran A, Wang LS, Weiss LA, Willsey AJ, Yu TW, Yuen RK, Cook EH, Freitag CM, Gill M, Hultman CM, Lehner T, Palotie A, Schellenberg GD, Sklar P, State MW, Sutcliffe JS, Walsh CA, Scherer SW, Zwick ME, Barrett JC, Cutler DJ, Roeder K, Devlin B, Daly MJ, Buxbaum JD (2014) Synaptic, transcriptional and chromatin genes disrupted in autism. *Nature* 515:209–215.

de Silva PN (2018) Do patterns of synaptic pruning underlie psychoses, autism and ADHD? *BJPsych Advances* 24:212–217.

Deciphering Developmental Disorders (2015) Large-scale discovery of novel genetic causes of developmental disorders. *Nature* 519:223–228.

Deciphering Developmental Disorders (2017) Prevalence and architecture of de novo mutations in developmental disorders. *Nature* 542:433–438.

Deng H, Xiao X, Wang Z (2016) Periaqueductal gray neuronal activities underlie different aspects of defensive behaviors. *Journal of Neuroscience* 36:7580–7588.

DeOca BM, DeCola JP, Maren S, Fanselow MS (1998) Distinct regions of the periaqueductal gray are involved in the acquisition and expression of defensive responses. *Journal of Neuroscience* 18:3426–3432.

Depaulis A, Keay KA, Bandler R (1992) Longitudinal neuronal organization of defensive reactions in the midbrain periaqueductal gray region of the rat. *Experimental Brain Research* 90:307–318.

Destexhe A, Contreras D, Steriade M (1999) Spatiotemporal analysis of local field potentials and unit discharges in cat cerebral cortex during natural wake and sleep states. *Journal of Neuroscience* 19:4595–4608.

Devlin B, Boone BE, Levy SE, Lihm J, Buxbaum JD, Wu Y, Lewis L, Han Y, Boerwinkle E, Gibbs RA, Fromer M, Shakir K, Fennell T, Garimella K, Banks E, Poplin R, Gabriel S, De Pristo M, Sunyaev S, Daly MJ (2012) Patterns and rates of exonic de novo mutations in autism spectrum disorders. *Nature* 485:242–246.

Di Scala G, Mana MJ, Jacobs WJ, Phillips AG (1987) Evidence of Pavlovian conditioned fear following electrical stimulation of the periaqueductal grey in the rat. *Physiology and Behavior* 40:55–63.

Diehl MM, Bravo-Rivera C, Rodriguez-Romaguera J, Pagan-Rivera PA, Burgos-Robles A, Roman-Ortiz C, Quirk GJ (2018) Active avoidance requires inhibitory signaling in the rodent prelimbic prefrontal cortex. *eLife* 7:1–19.

Dobrunz LE, Stevens CF (1997) Heterogeneity of release probability, facilitation, and depletion at central synapses. *Neuron* 18:995–1008.

Dudek SM, Bear MF (1992) Homosynaptic long-term depression in area CA1 of hippocampus and effects of N-methyl-D-aspartate receptor blockade. *Proceedings of the National Academy of Sciences of the United States of America* 89:4363–7.

Duong L, Klitten LL, Møller RS, Ingason A, Jakobsen KD, Skjødt C, Didriksen M, Hjalgrim H, Werge T, Tommerup N (2012) Mutations in NRXN1 in a family multiply affected with brain disorders: NRXN1 mutations and brain disorders. *American Journal of Medical Genetics, Part B: Neuropsychiatric Genetics* 159 B:354–358.

Ellenbroek B, Youn J (2016) Rodent models in neuroscience research: Is it a rat race? *DMM Disease Models and Mechanisms* 9:1079–1087.

Ernst TM, Brol AE, Gratz M, Ritter C, Bingel U, Schlamann M, Maderwald S, Quick HH, Josef Merz C, Timmann D, Michael Ernst T, Evelina Brol A, Gratz M, Ritter C, Bingel U, Schlamann M, Maderwald S, Quick HH, Josef Merz C, Timmann D (2019) The cerebellum is involved in processing of predictions and prediction errors in a fear conditioning paradigm. *eLife* 8:1–26.

Esclapez M, Campistron G, Trottier S (1987) Immunocytochemical localization and morphology of GABA-containing neurons in the prefrontal and frontoparietal cortex of the rat. *Neuroscience Letters* 77:131–136.

Esclassan F, Francois J, Phillips KG, Loomis S, Gilmour G (2015) Phenotypic characterization of nonsocial behavioral impairment in neurexin 1α knockout rats. *Behavioral Neuroscience* 129:74–85.

Etherton M, Földy C, Sharma M, Tabuchi K, Liu X, Shamloo M (2011) Autism-linked neuroligin-3 R451C mutation differentially Alters Hippocampal and Cortical Synaptic Function. *PNAS* 103:13764–13769.

Etherton MR, Blaiss Ca, Powell CM, Südhof TC (2009) Mouse neurexin-1alpha deletion causes correlated electrophysiological and behavioral changes consistent with cognitive impairments. *Proceedings of the National Academy of Sciences of the United States of America* 106:17998–18003.

Evans DA, Stempel AV, Vale R, Ruehle S, Lefler Y, Branco T (2018) A synaptic threshold mechanism for computing escape decisions. *Nature* 558:590–594.

Faber DS, Korn H (1991) Applicability of the coefficient of variation method for analyzing synaptic plasticity. *Biophysical Journal* 60:1288–1294.

Fadok JP, Krabbe S, Markovic M, Courtin J, Xu C, Massi L, Botta P, Bylund K, Müller C, Kovacevic A, Tovote P, Lüthi A (2017) A competitive inhibitory circuit for selection of active and passive fear responses. *Nature* 542:96–99.

Fan YT, Chen C, Chen SC, Decety J, Cheng Y (2014) Empathic arousal and social understanding in individuals with autism: Evidence from fMRI and ERP measurements. *Social Cognitive and Affective Neuroscience* 9:1203–1213.

Fan Y, Fricker D, Brager DH, Chen X, Lu HC, Chitwood RA, Johnston D (2005) Activity-dependent decrease of excitability in rat hippocampal neurons through increases in Ih. *Nature Neuroscience* 8:1542–1551.

Fanselow MS (1991) The Midbrain Periaqueductal Gray as a Coordinator of Action in Response to Fear and Anxiety. *The Midbrain Periaqueductal Gray Matter* pp. 151–173.

Fanselow MS, Decola JP, DeOca BM, Landeira Fernandez J (1995) Ventral and dorsolateral regions of the midbrain periaqueductal gray PAG control different stages of defensive behavior. *Aggressive Behav.* 21:63–77.

Faull OK, Subramanian HH, Ezra M, Pattinson KT (2019) The midbrain periaqueductal gray as an integrative and interoceptive neural structure for breathing. *Neuroscience and Biobehavioral Reviews* 98:135–144.

Fidzinski P, Shor O, Behr J (2008) Target-cell-specific bidirectional synaptic plasticity at hippocampal output synapses. *European Journal of Neuroscience* 27:1111–1118.

Fiebig E (1988) Connections of the Corpus Cerebelli in the Thornback Guitarfish , Plutyrhinoidis triseriata (Elasmobranchii): A Study With WGA-HRP and Extracellular Granule Cell Recording. *The Journal of Comparative Neurology* 583:567–583.

Fitzjohn SM, Kingston AE, Lodge D, Collingridge GL (1999) DHPG-induced LTD in area CA1 of juvenile rat hippocampus; characterisation and sensitivity to novel mGlu receptor antagonists. *Neuropharmacology* 38:1577–1583.

Floyd NS, Price JL, Ferry AT, Keay KA, Bandler R (2000) Orbitomedial Prefrontal Cortical Projections to Distinct Longitudinal Columns of the Periaqueductal Gray in the Rat. *Journal of Comparative Neurology* 578:556–578.

Földy C, Malenka R, Südhof T (2013) Autism-Associated Neuroligin-3 Mutations Commonly Disrupt Tonic Endocannabinoid Signaling. *Neuron* 78:498–509.

Fragale JE, Khariv V, Gregor DM, Smith IM, Jiao X, Elkabes S, Servatius RJ, Pang KC, Beck KD (2016) Dysfunction in amygdala-prefrontal plasticity and extinction-resistant avoidance: A model for anxiety disorder vulnerability. *Experimental Neurology* 275:59–68.

Frey U, Morris RGM (1997) Synaptic tagging and LTP. *Nature* 385:533–536.

Friedman JM, Baross A, Delaney AD, Ally A, Arbour L, Armstrong L, Asano J, Bailey DK, Barber S, Birch P, Brown-John M, Cao M, Chan S, Charest DL, Farnoud N, Fernandes N, Flibotte S, Go A, Gibson WT, Holt Ra, Jones SJM, Kennedy GC, Krzywinski M, Langlois S, Li HI, McGillivray BC, Nayar T, Pugh TJ, Rajcan-Separovic E, Schein JE, Schnerch A, Siddiqui A, Van Allen MI, Wilson G, Yong SL, Zahir F, Eydoux P, Marra Ma (2006) Oligonucleotide microarray analysis of genomic imbalance in children with mental retardation. *American journal of human genetics* 79:500–13.

Fu Z, Washbourne P, Ortinski P, Vicini S (2003) Functional Excitatory Synapses in HEK293 Cells Expressing Neuroligin and Glutamate Receptors. *Journal of Neurophysiology* 90:3950–3957.

Futai K, Doty CD, Baek B, Ryu J, Sheng M (2013) Specific Trans-synaptic interaction with inhibitory interneuronal neurexin underlies differential ability of neuroligins to induce functional inhibitory synapses. *Journal of Neuroscience* 33:3612–3623.

Gadow KD, Devincent CJ, Pomeroy J, Azizian A (2005) Comparison of DSM-IV symptoms in elementary school-age children with PDD versus clinic and community samples. *Autism* 9:392–415.

Gauthier J, Bonnel A, St-Onge J, Karemera L, Laurent S, Mottron L, Fombonne É, Joober R, Rouleau GA (2005) NLGN3/NLGN4 gene mutations are not responsible for autism in the Quebec population. *American Journal of Medical Genetics - Neuropsychiatric Genetics* 132 B:74–75.

Gauthier J, Siddiqui TJ, Huashan P, Yokomaku D, Hamdan FF, Champagne N, Lapointe M, Spiegelman D, Noreau A, Lafreniére F, Fathalli F, Joober R, Krebs MO, DeLisi LE, Mottron L, Fombonne É, Michaud JL, Drapeau P, Carbonetto S, Craig AM, Rouleau GA (2011) Truncating mutations in NRXN2 and NRXN1 in autism spectrum disorders and schizophrenia. *Human Genetics* 130:563–573.

Getahun D, Fassett MJ, Peltier MR, Wing DA, Xiang AH, Chiu V, Jacobsen SJ (2017) Association of Perinatal Risk Factors with Autism Spectrum Disorder. *American Journal of Perinatology* 34:295–304.

Gibbs RA, Metzker ML, Muzny DM, Sodergren EJ, Scherer S, Scott G, Steffen D, Worley KC, Burch PE (2004) Genome sequence of the Brown Norway rat yields insights into mammalian evolution. *Nature* 428:493–521.

Gibson JR, Huber KM, Südhof TC (2009) Neuroligin-2 deletion selectively decreases inhibitory synaptic transmission originating from fast-spiking but not from somatostatin-positive interneurons. *Journal of Neuroscience* 29:13883–13897.

Giese KP, Aziz W, Kraev I, Stewart MG (2015) Generation of multi-innervated dendritic spines as a novel mechanism of long-term memory formation. *Neurobiology of Learning and Memory* 124:48–51.

Gilbert M, Smith J, Roskams Aj (2001) Neuroligin 3 Is a Vertebrate Gliotactin Expressed in the Olfactory Ensheathing Glia , a Growth- Promoting Class of Macroglia. *Glia* 164:151–164.

Gioia M, Tredici G, Bianchi R (1985) A golgi study of the periaqueductal gray matter in the cat. Neuronal types and their distribution. *Experimental Brain Research* 58:318–332.

Girirajan S, Dennis MY, Baker C, Malig M, Coe BP, Campbell CD, Mark K, Vu TH, Alkan C, Cheng Z, Biesecker LG, Bernier R, Eichler EE (2013) Refinement and discovery of new hotspots of copy-number variation associated with autism spectrum disorder. *American Journal of Human Genetics* 92:221–237.

Gkogkas CG, Khoutorsky A, Ran I, Rampakakis E, Nevarko T, Weatherill DB, Vasuta C, Yee S, Truitt M, Dallaire P, Major F, Lasko P, Ruggero D, Nader K, Lacaille JC, Sonenberg N (2013) Autism-related deficits via dysregulated eIF4E-dependent translational control. *Nature* 493:371–377.

Glessner JT, Wang K, Cai G, Korvatska O, Kim CE, Wood S, Zhang H, Estes A, Brune CW, Bradfield JP, Imielinski M, Frackelton EC, Reichert J, Crawford EL, Munson J, Sleiman PM, Chiavacci R, Annaiah K, Thomas K, Hou C, Glaberson W, Flory J, Otieno F, Garris M, Soorya L, Klei L, Piven J, Meyer KJ, Anagnostou E, Sakurai T, Game RM, Rudd DS, Zurawiecki D, McDougle CJ, Davis LK, Miller J, Posey DJ, Michaels S, Kolevzon A, Silverman JM, Bernier R, Levy SE, Schultz RT, Dawson G, Owley T, McMahon WM, Wassink TH, Sweeney JA, Nurnberger JI, Coon H, Sutcliffe JS, Minshew NJ, Grant SF, Bucan M, Cook EH, Buxbaum JD, Devlin B, Schellenberg GD, Hakonarson H (2009) Autism genome-wide copy number variation reveals ubiquitin and neuronal genes. *Nature* 459:569–572.

Goosens KA, Maren S (2004) NMDA receptors are essential for the acquisition, but not expression, of conditional fear and associative spike firing in the lateral amygdala. *European Journal of Neuroscience* 20:537–548.

Górecki DC, Szklarczyk A, Lukasiuk K, Kaczmarek L, Simons JP (1999) Differential seizure-induced and developmental changes of neurexin expression. *Molecular and Cellular Neurosciences* 13:218–227.

Goutianos G, Tzioura A, Kyparos A, Paschalis V, Margaritelis NV, Veskoukis AS, Zafeiridis A, Dipla K, Nikolaidis MG, Vrabas IS (2015) The rat adequately reflects human responses to exercise in blood biochemical profile: A comparative study. *Physiological Reports* 3:1–9.

Graf ER, Zhang X, Jin SX, Linhoff MW, Craig AM (2004) Neurexins induce differentiation of GABA and glutamate postsynaptic specializations via neuroligins. *Cell* 119:1013–1026.

Greene JR, Totterdell S (1997) Morphology and distribution of electrophysiologically defined classes of pyramidal and nonpyramidal neurons in rat ventral subiculum in vitro. *Journal of Comparative Neurology* 380:395–408.

Gross CT, Canteras NS (2012) The many paths to fear. *Nature Reviews Neuroscience* 13:651–658.

Grover LM, Teyler TJ (1990) Two components of long-term potentiation induced by different patterns of afferent activation. *Nature* 347:477–479.

Gu N, Vervaeke K, Hu H, Storm JF (2005) Kv7/KCNQ/M and HCN/h, but not KCa2/SK channels, contribute to the somatic medium after-hyperpolarization and excitability control in CA1 hippocampal pyramidal cells. *Journal of Physiology* 566:689–715.

Gulledge AT, Dasari S, Onoue K, Stephens EK, Hasse JM, Avesar D (2013) A Sodium-Pump-Mediated Afterhyperpolarization in Pyramidal Neurons. *Journal of Neuroscience* 33:13025–13041.

Gullone E (2000) The Development of Normal Fear: A Century of Research. *Clinical Psychology Review* 20:429–451.

Guttmann-Steinmetz S, Gadow KD, Devincent CJ, Crowell J (2010) Anxiety symptoms in boys with autism spectrum disorder, attention-deficit hyperactivity disorder, or chronic multiple tic disorder and community controls. *Journal of Autism and Developmental Disorders* 40:1006–1016.

Guy J, Gan J, Selfridge J, Cobb S, Bird A (2007) Reversal of Neurological Defects in a Mouse Model of Rett Syndrome. *Science* 315:1143–1148.

Guzman SJ, Schlögl A, Schmidt-Hieber C (2014) Stimfit: quantifying electrophysiological data with Python. *Frontiers in Neuroinformatics* 8.

Haider B, Schulz DPP, Häusser M, Carandini M (2016) Millisecond Coupling of Local Field Potentials to Synaptic Currents in the Awake Visual Cortex. *Neuron* 90:35–42.

Halladay LR, Blair HT (2015) Distinct ensembles of medial prefrontal cortex neurons are activated by threatening stimuli that elicit excitation vs. inhibition of movement. *Journal of Neurophysiology* 114:793–807.

Hallmayer J, Cleveland S, Torres A, Phillips J, Cohen B, Torigoe T, Miller J, Fedele A, Collins J, Smith K, Lotspeich L, Croen LA, Ozonoff S, Lajonchere C, Grether JK, Risch N (2011) Genetic heritability and shared environmental factors among twin pairs with autism. *Archives of General Psychiatry* 68:1095–1102.

Hamilton BL (1973) Projections of the nuclei of the periaqueductal gray matter in the cat. *Journal of Comparative Neurology* 152:45–57.

Hamilton BL, Skultety FM (1970) Efferent connections of the periaqueductal gray matter in the cat. *Journal of Comparative Neurology* 139:105–114.

Hamilton SM, Green JR, Veeraragavan S, Yuva L, McCoy A, Wu Y, Warren J, Little L, Ji D, Cui X, Weinstein E, Paylor R (2014) Fmr1 and Nlgn3 knockout rats: novel tools for investigating autism spectrum disorders. *Behavioral neuroscience* 128:103–9.

Harkin LF, Lindsay SJ, Xu Y, Alzu'Bi A, Ferrara A, Gullon EA, James OG, Clowry GJ (2017) Neurexins 1-3 each have a distinct pattern of expression in the early developing human cerebral cortex. *Cerebral Cortex* 27:216–232.

Harrison V, Connell L, Hayesmoore J, McParland J, Pike MG, Blair E (2011) Compound heterozygous deletion of NRXN1 causing severe developmental delay with early onset epilepsy in two sisters. *American Journal of Medical Genetics, Part A* 155:2826–2831.

Harvey CD, Svoboda K (2007) Locally dynamic synaptic learning rules in pyramidal neuron dendrites. *Nature* 450:1195–1200.

Hata Y, Butz S, Südhof TC (1996) CASK: A novel dlg/PSD95 homolog with an N-terminal calmodulin-dependent protein kinase domain identified by interaction with neurexins. *Journal of Neuroscience* 16:2488–2494.

Hata Y, Davletov B, Petrenko AG, Jahn R, Südhof TC (1993) Interaction of synaptotagmin with the cytoplasmic domains of neurexins. *Neuron* 10:307–315.

Hebb DO (1949) *The organization of behavior: A neuropsychological theory.* John Wiley and Sons, Inc.

Heine M, Groc L, Frischknecht R, Beiquem JC, Lounis B, Bumbaugh G, Huganair RL, Cognet L, Choquet D (2002) Surface Mobility of Postsynaptic AMPARs Tunes Synaptic Transmission. *Science* 297:5–9.

Heinisch S, Palma J, Kirby LG (2011) Interactions between chemokine and mu-opioid receptors: Anatomical findings and electrophysiological studies in the rat periaqueductal grey. *Brain, Behavior, and Immunity* 25:360–372.

Herreras O (2016) Local field potentials: Myths and misunderstandings. *Frontiers in Neural Circuits* 10:1–16.

Herry C, Ciocchi S, Senn V, Demmou L, Müller C, Lüthi A (2008) Switching on and off fear by distinct neuronal circuits. *Nature* 454:600–606.

Herry C, Trifilieff P, Micheau J, Lüthi A, Mons N (2006) Extinction of auditory fear conditioning requires MAPK/ERK activation in the basolateral amygdala. *European Journal of Neuroscience* 24:261–269.

Ho YC, Cheng JK, Chiou LC (2013) Hypofunction of glutamatergic neurotransmission in the periaqueductal gray contributes to nerve-injury-induced neuropathic pain. *Journal of Neuroscience* 33:7825–7836.

Ho YC, Lin TB, Hsieh MC, Lai CY, Chou D, Chau YP, Chen GD, Peng HY (2018) Periaqueductal gray glutamatergic transmission governs chronic stress-induced depression. *Neuropsychopharmacology* 43:302–312.

Hobin JA, Ji J, Maren S (2006) Ventral hippocampal muscimol disrupts context-specific fear memory retrieval after extinction in rats. *Hippocampus* 16:174–182.

Hoffman RC, Jennings LL, Tsigelny I, Comoletti D, Flynn RE, Sudhof TC, Taylor P (2004) Structural Characterization of Recombinant Soluble Rat Neuroligin 1: Mapping of Secondary Structure and Glycosylation by Mass Spectrometry. *Biochemistry* 43:1496–1506.

Hollmann M, Heinemann S (1994) Cloned Glutamate Receptors. *Annual Review of Neuroscience* 17:31–108.

Hosie S, Malone DT, Liu S, Glass M, Adlard PA, Hannan AJ, Hill-Yardin EL (2018) Altered amygdala excitation and CB1 receptor modulation of aggressive behavior in the neuroligin-3R451C mouse model of autism. *Frontiers in Cellular Neuroscience* 12:1–10.

Hu J, Wang Z, Guo YY, Zhang XN, Xu ZH, Liu SB, Guo HJ, Yang Q, Zhang FX, Sun XL, Zhao MG (2009) A role of periaqueductal grey NR2B-containing NMDA receptor in mediating persistent inflammatory pain. *Molecular Pain* 5:1–10.

Huang Cc, Lee Cc, Hsu Ks (1999) An investigation into signal transduction mechanisms involved in DHPG-induced LTD in the CA1 region of the hippocampus. *Neuropharmacology* 38:1585–1596.

Huang EP, Stevens CF (1997) Estimating the distribution of synaptic reliabilities. *Journal of Neurophysiology* 78:2870–2880.

Huang H, Trussell LO (2011) KCNQ5 channels control resting properties and release probability of a synapse. *Nature Neuroscience* 14:840–847.

Huang YY, Simpson E, Kellendonk C, Kandel ER (2004) Genetic evidence for the bidirectional modulation of synaptic plasticity in the prefrontal cortex by D1 receptors. *Proceedings of the National Academy of Sciences* 101:3236–3241.

Hubel DH, Wiesel TN (1970) The period of susceptibility to the physiological effects of unilateral eye closure in kittens. *The Journal of Physiology* 206:419–436.

Huber KM, Gallagher SM, Warren ST, Bear MF (2002) Altered synaptic plasticity in a mouse model of fragile X mental retardation. *Proceedings of the National Academy of Sciences of the United States of America* 99:7746–7750.

Huber KM, Kayser MS, Bear MF (2000) Role for rapid dendritic protein synthesis in hippocampal mGluR- dependent long-term depression. *Science* 288:1254–1256.

hui Jiang Y, Armstrong D, Albrecht U, Atkins CM, Noebels JL, Eichele G, Sweatt JD, Beaudet AL (1998) Mutation of the Angelman ubiquitin ligase in mice causes increased cytoplasmic p53 and deficits of contextual learning and long-term potentiation. *Neuron* 21:799–811.

Huttenlocher PR (1979) Synaptic Density in Human Frontal Cortex- Developmental Changes and Effects of Aging. *Brain Research* 163:195–205.

Ichtchenko K, Hata Y, Nguyen T, Ullrich B, Missler, M. Moomaw C, T.C. S (1996) Neuroligin 1: A Splice Site-Specific Ligand for I -Neurexins. *Journal of Biological Chemistry* 271:2676–2682.

Ichtchenko K, Hata Y, Nguyen T, Ullrich B, Missler M, Moomaw C, Südhof TC (1995) Neuroligin 1: A splice site-specific ligand for β-neurexins. *Cell* 81:435–443.

Iossifov I, O'Roak BJ, Sanders SJ, Ronemus M, Krumm N, Levy D, Stessman HA, Witherspoon KT, Vives L, Patterson KE, Smith JD, Paeper B, Nickerson DA, Dea J, Dong S, Gonzalez LE, Mandell JD, Mane SM, Murtha MT, Sullivan CA, Walker MF, Waqar Z, Wei L, Willsey AJ, Yamrom B, Lee YH, Grabowska E, Dalkic E, Wang Z, Marks S, Andrews P, Leotta A, Kendall J, Hakker I, Rosenbaum J, Ma B, Rodgers L, Troge J, Narzisi G, Yoon S, Schatz MC, Ye K, McCombie WR, Shendure J, Eichler EE, State MW, Wigler M (2014) The contribution of de novo coding mutations to autism spectrum disorder. *Nature* 515:216–221.

Iossifov I, Ronemus M, Levy D, Wang Z, Hakker I, Rosenbaum J, Yamrom B, ha Lee Y, Narzisi G, Leotta A, Kendall J, Grabowska E, Ma B, Marks S, Rodgers L, Stepansky

A, Troge J, Andrews P, Bekritsky M, Pradhan K, Ghiban E, Kramer M, Parla J, Demeter R, Fulton LL, Fulton RS, Magrini VJ, Ye K, Darnell JC, Darnell RB, Mardis ER, Wilson RK, Schatz MC, McCombie RW, Wigler M (2012) De Novo Gene Disruptions in Children on the Autistic Spectrum. *Neuron* 74:285–299.

Irie M, Hata Y, Takeuchi M, Ichtchenko K, Toyoda A, Hirao K, Takai Y, Rosahl TW, Su TC (1997) Binding of Neuroligins to PSD-95. *Science* 277:1511–1516.

Ishikawa A, Nakamura S (2006) Ventral hippocampal neurons project axons simultaneously to the medial prefrontal cortex and amygdala in the rat. *Journal of Neurophysiology* 96:2134–2138.

Jamain S, Quach H, Betancur C, Råstam M, Colineaux C, Gillberg IC, Soderstrom H, Giros B, Leboyer M, Gillberg C, Bourgeron T (2003) Mutations of the X-linked genes encoding neuroligins NLGN3 and NLGN4 are associated with autism. *Nature genetics* 34:27–9.

Janak PH, Tye KM (2015) From circuits to behaviour in the amygdala. *Nature* 517:284–292.

Jaramillo TC, Escamilla CO, Liu S, Peca L, Birnbaum SG, Powell CM (2018) Genetic Background Effects in Neuroligin-3 Mutant Mice : Minimal Behavioral Abnormalities on C57 Background. *Autism Research* 11:234–244.

Jaramillo TC, Liu S, Pettersen A, Birnbaum SG, Powell CM (2014) Autism-Related Neuroligin-3 Mutation Alters Social Behavior and Spatial Learning. *Autism Research* 7:264–272.

Jiang M, Polepalli J, Chen LY, Zhang B, Südhof TC, Malenka RC (2017) Conditional ablation of neuroligin-1 in CA1 pyramidal neurons blocks LTP by a cell-autonomous NMDA receptor-independent mechanism. *Molecular Psychiatry* 22:375–383.

Johansen JP, Tarpley JW, Ledoux JE, Blair HT (2010) Neural substrates for expectation-modulated fear learning in the amygdala and periaqueductal gray. *Nature Publishing Group* 13:979–986.

Johnston D, Wu S (1994) *Foundations of cellular neurophysiology* Bradford Books.

Johnstone VP, Raymond CR (2013) Postsynaptic protein synthesis is required for presynaptic enhancement in persistent forms of long-term potentiation. *Frontiers in Synaptic Neuroscience* 5:1–10.

Kajikawa Y, Schroeder CE (2011) How local is the local field potential? *Neuron* 72:847–858.

Kang H, Schuman EM (1996) A requirement for local protein synthesis in neurotrophin-induced hippocampal synaptic plasticity. *Science* 273:1402–1406.

Kang J, Huguenard JR, Prince DA (2000) Voltage-gated potassium channels activated during action potentials in layer V neocortical pyramidal neurons. *Journal of Neurophysiology* 83:70–80.

Kang S, Cox CL, Gulley JM (2018) High frequency stimulation-induced plasticity in the prelimbic cortex of rats emerges during adolescent development and is associated with an increase in dopamine receptor function. *Neuropharmacology* 141:158–166.

Karalis N, Dejean C, Chaudun F, Khoder S, R Rozeske R, Wurtz H, Bagur S, Benchenane K, Sirota A, Courtin J, Herry C (2016) 4-Hz oscillations synchronize prefrontal-amygdala circuits during fear behavior. *Nature Neuroscience* 19.

Katzner S, Nauhaus I, Benucci A, Bonin V, Ringach DL, Carandini M (2009) Local Origin of Field Potentials in Visual Cortex. *Neuron* 61:35–41.

Kawahara H, Drew GM, Christie MJ, Vaughan CW (2011) Inhibition of fatty acid amide hydrolase unmasks CB 1 receptor and TRPV1 channel-mediated modulation of glutamatergic synaptic transmission in midbrain periaqueductal grey. *British Journal of Pharmacology* 163:1214–1222.

Keay KA, Bandler R (2001) Parallel circuits mediating distinct emotional coping reactions to different types of stress. *Neuroscience and Biobehavioral Reviews* 25:669–678.

Keay KA, Bandler R (2004) *Chapter 10 The Periaqueductal Gray* Elsevier, Inc., third edit edition.

Keay KA, Crowfoot LJ, Floyd NS, Henderson LA, Christie MJ, Bandler R (1997) Cardiovascular effects of microinjections of opioid agonists into the 'Depressor Region' of the ventrolateral periaqueductal gray region. *Brain Research* 762:61–71.

Kenny EM, Cormican P, Furlong S, Heron E, Kenny G, Fahey C, Kelleher E, Ennis S, Tropea D, Anney R, Corvin AP, Donohoe G, Gallagher L, Gill M, Morris DW (2014) Excess of rare novel loss-of-function variants in synaptic genes in schizophrenia and autism spectrum disorders. *Molecular Psychiatry* 19:872–879.

Kerkhofs A, Canas PM, Timmerman AJ, Heistek TS, Real JI, Xavier C, Cunha RA, Mansvelder HD, Ferreira SG (2018) Adenosine A2A receptors control glutamatergic synaptic plasticity in fast spiking interneurons of the prefrontal cortex. *Frontiers in Pharmacology* 9:1–12.

Kerns C, Kendall P (2014) Chapter 6- Autism and Anxiety: Overlap, Similarities, and Differences In *The Handbook of Autism and Anxiety*, pp. 75–89. Springer US.

Kim EJ, Horovitz O, Pellman BA, Tan LM, Li Q, Richter-Levin G, Kim JJ (2013) Dorsal periaqueductal gray-amygdala pathway conveys both innate and learned fear responses in rats. *Proceedings of the National Academy of Sciences* 110:14795–14800.

Kim E, Sheng M (2004) PDZ domain proteins of synapses. *Nature Reviews Neuroscience* 5:771–781.

Kim HG, Kishikawa S, Higgins AW, Seong IS, Donovan DJ, Shen Y, Lally E, Weiss LA, Najm J, Kutsche K, Descartes M, Holt L, Braddock S, Troxell R, Kaplan L, Volkmar F, Klin A, Tsatsanis K, Harris D, Noens I, Pauls D, Daly MJ, Macdonald ME, Morton CC, Quade BJ, Gusella JF (2008) Disruption of neurexin 1 associated with autism spectrum disorder. *The American Journal of Human Genetics* 82:199–207.

Kim HH, Lee KH, Lee D, Han YE, Lee SH, Sohn JW, Ho WK (2015) Costimulation of AMPA and metabotropic glutamate receptors underlies phospholipase C activation by glutamate in hippocampus. *Journal of Neuroscience* 35:6401–6412.

Kim JJ, Rison RA, Fanselow MS (1993) Effects of amygdala, hippocampus, and periaqueductal gray lesions on short- and long-term contextual fear. *Behavioral Neuroscience* 107:1093–1098.

Kim JJ, DeCola JP, Landeira-Fernandez J, Fanselow MS (1991) N-Methyl-D-Aspartate Receptor Antagonist APV Blocks Acquisition but Not Expression of Fear Conditioning. *Behavioral Neuroscience* 105:126–133.

Kim JJ, Jung MW (2006) Neural circuits and mechanisms involved in Pavlovian fear conditioning: A critical review. *Neuroscience and Biobehavioral Reviews* 30:188–202.

Kingsbury MA, Kelly AM, Schrock SE, Goodson JL (2011) Mammal-Like Organization of the Avian Midbrain Central Gray and a Reappraisal of the Intercollicular Nucleus. *PLoS ONE* 6:1–13.

Kirischuk S, Clements JD, Grantyn R (2002) Presynaptic and postsynaptic mechanisms underlie paired pulse depression at single GABAergic boutons in rat collicular cultures. *Journal of Physiology* 543:99–116.

Kittelberger JM, Land BR, Bass AH (2006) The Midbrain Periaqueductal Gray and Vocal Patterning in a Teleost Fish . *Journal of neurophysiology* 96:71–85.

Koekkoek SK, Yamaguchi K, Milojkovic BA, Dortland BR, Ruigrok TJ, Maex R, De Graaf W, Smit AE, VanderWerf F, Bakker CE, Willemsen R, Ikeda T, Kakizawa S, Onodera K, Nelson DL, Mientjes E, Joosten M, De Schutter E, Oostra BA, Ito M, De Zeeuw CI (2005) Deletion of FMR1 in purkinje cells enhances parallel fiber LTD, enlarges spines, and attenuates cerebellar eyelid conditioning in fragile X syndrome. *Neuron* .

Kolb B, Mychasiuk R, Muhammad A, Li Y, Frost DO, Gibb R (2012) Experience and the developing prefrontal cortex. *Proceedings of the National Academy of Sciences of the United States of America* 109:17186–17196.

Kolomiets B, Marzo A, Caboche J, Vanhoutte P, Otani S (2009) Background dopamine concentration dependently facilitates long-term potentiation in rat prefrontal cortex through postsynaptic activation of extracellular signal-regulated kinases. *Cerebral Cortex* 19:2708–2718.

Komiyama NH, Watabe AM, Carlisle HJ, Porter K, Charlesworth P, Monti J, Strathdee DJC, O'Carroll CM, Martin SJ, Morris RGM, O'Dell TJ, Grant SGN (2002) SynGAP regulates ERK/MAPK signaling, synaptic plasticity, and learning in the complex with postsynaptic density 95 and NMDA receptor. *The Journal of neuroscience : the official journal of the Society for Neuroscience* 22:9721–9732.

Kotekar N, Shenkar A, Nagaraj R (2018) Postoperative cognitive dysfunction – current preventive strategies. *Clinical Interventions in Aging* 13:2267–2273.

Krug M, Lössner B, Ott T (1984) Anisomycin blocks the late phase of long-term potentiation in the dentate gyrus of freely moving rats. *Brain Research Bulletin* 13:39–42.

Krumm N, O'Roak BJ, Karakoc E, Mohajeri K, Nelson B, Vives L, Jacquemont S, Munson J, Bernier R, Eichler EE (2013) Transmission disequilibrium of small CNVs in simplex autism. *American Journal of Human Genetics* 93:595–606.

Krumm N, Roak BJO, Shendure J, Eichler EE (2014) A de novo convergence of autism genetics and molecular neuroscience. *Trends in Neurosciences* 37:95–105.

Kummer KK, Hofhansel L, Barwitz CM, Schardl A, Prast JM, Salti A, El Rawas R, Zernig G (2014) Differences in social interaction- vs. cocaine reward in mouse vs. rat. *Frontiers in Behavioral Neuroscience* 8:1–7.

Kurshan PT, Merrill SA, Dong Y, Ding C, Hammarlund M, Bai J, Jorgensen EM, Shen K (2018) γ-Neurexin and Frizzled Mediate Parallel Synapse Assembly Pathways Antagonized by Receptor Endocytosis. *Neuron* 100:150–166.e4.

Kurt S, Moeller CK, Jeschke M, Schulze H (2008) Differential effects of iontophoretic application of the GABAA-antagonists bicuculline and gabazine on tone-evoked local field potentials in primary auditory cortex: Interaction with ketamine anesthesia. *Brain Research* 1220:58–69.

Kwon JT, Nakajima R, Kim HS, Jeong Y, Augustine GJ, Han JH (2014) Optogenetic activation of presynaptic inputs in lateral amygdala forms associative fear memory. *Learning and Memory* 21:627–633.

Langston RF, Wood ER (2010) Associative recognition and the hippocampus: Differential effects of hippocampal lesions on object-place, object-context and object-place-context memory. *Hippocampus* 20:1139–1153.

Larkin A, Chen MY, Kirszenblat L, Reinhard J, van Swinderen B, Claudianos C (2015) Neurexin-1 regulates sleep and synaptic plasticity in Drosophila melanogaster. *European Journal of Neuroscience* 42:2455–2466.

Lau BK, Karim S, Goodchild AK, Vaughan CW, Drew GM (2014) Menthol enhances phasic and tonic GABAA receptor-mediated currents in midbrain periaqueductal grey neurons. *British Journal of Pharmacology* 171:2803–2813.

Laurent V, Westbrook RF (2009) Inactivation of the infralimbic but not the prelimbic cortex impairs consolidation and retrieval of fear extinction. *Learning and Memory* 16:520–529.

Leblond CS, Cliquet F, Carton C, Huguet G, Mathieu A, Kergrohen T, Buratti J, Lemière N, Cuisset L, Bienvenu T, Boland A, Deleuze JF, Stora T, Biskupstoe R, Halling J, Andorsdóttir G, Billstedt E, Gillberg C, Bourgeron T (2019) Both rare and common genetic variants contribute to autism in the Faroe Islands. *npj Genomic Medicine* 4.

LeDoux E, Cicchetti P, Reis DJ (1988) Different Projections of the Central Amygdaloid Nucleus Mediate Autonomic and Behavioral Correlates of Conditioned Fear. *Journal of Neuroscience* 8:2517–2529.

Lee SH, Hjerling-Leffler J, Zagha E, Fishell G, Rudy B (2010) The largest group of superficial neocortical GABAergic interneurons expresses ionotropic serotonin receptors. *Journal of Neuroscience* 30:16796–16808.

Lerche C, Scherer CR, Seebohm G, Derst C, Wei AD, Busch AE, Steinmeyer K (2000) Molecular cloning and functional expression of KCNQ5, a potassium channel subunit that may contribute to neuronal M-current diversity. *Journal of Biological Chemistry* 275:22395–22400.

Lesburguères E, Sparks FT, O'Reilly KC, Fenton AA (2016) Active place avoidance is no more stressful than unreinforced exploration of a familiar environment. *Hippocampus* 26:1481–1485.

Levinsoni JN, Chéry N, Huang K, Wong TP, Gerrow K, Kang R, Prange O, Wang YT, El-Husseini A (2005) Neuroligins mediate excitatory and inhibitory synapse formation: Involvement of PSD-95 and neueexin-1β in neuroligin-induced synaptic specificity. *Journal of Biological Chemistry* 280:17312–17319.

Levy D, Ronemus M, Yamrom B, ha Lee Y, Leotta A, Kendall J, Marks S, Lakshmi B, Pai D, Ye K, Buja A, Krieger A, Yoon S, Troge J, Rodgers L, Iossifov I, Wigler M (2011) Rare De Novo and Transmitted Copy-Number Variation in Autistic Spectrum Disorders. *Neuron* 70:886–897.

Lewis AS, Vaidya SP, Blaiss CA, Liu Z, Stoub TR, Brager DH, Chen X, Bender RA, Estep CM, Popov AB, Kang CE, van Veldhoven PP, Bayliss DA, Nicholson DA, Powell CM, Johnston D, Chetkovich DM (2011) Deletion of the hyperpolarization-activated cyclic nucleotide-gated channel auxiliary subunit TRIP8b impairs hippocampal Ih localization and function and promotes antidepressant behavior in mice. *Journal of Neuroscience* 31:7424–7440.

Leyfer OT, Folstein SE, Bacalman S, Davis NO, Dinh E, Morgan J, Tager-Flusberg H, Lainhart JE (2006) Comorbid psychiatric disorders in children with autism: Interview development and rates of disorders. *Journal of Autism and Developmental Disorders* 36:849–861.

Li H, Penzo MA, Taniguchi H, Kopec CD, Huang ZJ, Li B (2013) Experience-dependent modification of a central amygdala fear circuit. *Nature Neuroscience* 16:332–339.

Li T, Tian Y, Li Q, Chen H, Lv H, Xie W, Han J (2015) The neurexin/N-ethylmaleimide-sensitive factor (NSF) interaction regulates short term synaptic depression. *Journal of Biological Chemistry* 290:17656–17667.

Li XF, Armony JL, Ledoux JE (1996) GABA(A) and GABA(B) receptors differentially regulate synaptic transmission in the auditory thalamo-amygdala pathway: An in vivo microiontophoretic study and a model. *Synapse* 24:115–124.

Lisé MF, El-Husseini A (2006) The neuroligin and neurexin families: From structure to function at the synapse. *Cellular and Molecular Life Sciences* 63:1833–1849.

Liu H, Chandler S, Beitz AJ, Shipley MT, Behbehani MM (1994) Characterization of the effect of cholecystokinin (CCK) on neurons in the periaqueductal gray of the rat: immunocytochemical and in vivo and in vitro electrophysiological studies. *Brain Research* 642:83–94.

Liu RP, Hamilton BL (1980) Neurons of the periaqueductal gray matter as revealed by Golgi study. *Journal of Comparative Neurology* 189:403–418.

Liu X, Ramirez S, Pang PT, Puryear CB, Govindarajan A, Deisseroth K, Tonegawa S (2012a) Optogenetic stimulation of a hippocampal engram activates fear memory recall. *Nature* 484:381–385.

Liu Y, Hu Z, Xun G, Peng Y, Lu L, Xu X, Xiong Z, Xia L, Liu D, Li W, Zhao J, Xia K (2012b) Mutation analysis of the NRXN1 gene in a Chinese autism cohort. *Journal of Psychiatric Research* 46:630–634.

Liu Y, Du Y, Liu W, Yang C, Liu Y, Wang H, Gong X (2013) Lack of Association between NLGN3, NLGN4, SHANK2 and SHANK3 Gene Variants and Autism Spectrum Disorder in a Chinese Population. *PLoS ONE* 8:1–6.

Lledo PM, Zhang X, Südhof TC, Malenka RC, Nicoll RA (1998) Postsynaptic membrane fusion and long-term potentiation. *Science* 279:399–403.

Louros SR, Osterweil EK (2016) Perturbed proteostasis in autism spectrum disorders. *Journal of Neurochemistry* 139:1081–1092.

Lovick TA, Stezhka VV (1999) Neurones in the dorsolateral periaqueductal grey matter in coronal slices of rat midbrain: Electrophysiological and morphological characteristics. *Experimental Brain Research* 124:53–58.

Lowther C, Speevak M, Armour CM, Goh ES, Graham GE, Li C, Zeesman S, Nowaczyk MJ, Schultz LA, Morra A, Nicolson R, Bikangaga P, Samdup D, Zaazou M, Boyd K, Jung JH, Siu V, Rajguru M, Goobie S, Tarnopolsky MA, Prasad C, Dick PT, Hussain AS, Walinga M, Reijenga RG, Gazzellone M, Lionel AC, Marshall CR, Scherer SW, Stavropoulos DJ, Mccready E, Bassett AS (2017) Molecular characterization of NRXN1 deletions from 19,263 clinical microarray cases identifies exons important for neurodevelopmental disease expression. *Genetics in Medicine* 19:53–61.

Luján R, Nusser Z, Roberts JDB, Shigemoto R, Somogyi P (1996) Perisynaptic location of metabotropic glutamate receptors mGluR1 and mGluR5 on dendrites and dendritic spines in the rat hippocampus. *European Journal of Neuroscience* 8:1488–1500.

Lüscher C, Malenka RC (2012) NMDA Receptor-Dependent Long-Term Potentiation and Long-Term Depression (LTP/LTD). *Cold Spring Harbor perspectives in biology* 4:1–16.

Magoun H, Atlas D, Ingersoll E, Ranson S (1937) Associated facial, vocal and respiratory components of emotional expression: an experimental study. *Journal of neurology and psychopathology* 17:241–255.

Malenka RC (1994) Synaptic plasticity in the hippocampus: LTP and LTD. *Cell* 78:535–538.

Man HY, Lin JW, Ju WH, Ahmadian G, Liu L, Becker LE, Sheng M, Wang YT (2000) Regulation of AMPA receptor-mediated synaptic transmission by clathrin-dependent receptor internalization. *Neuron* 25:649–662.

Mantyh PW (1982) The Midbrain Periaqueductal Gray in the Rat , Cat , and Monkey : A Nissl , Weil , and Golgi Analysis. *Journal of Comparative Neurology* 363:349–363.

Maren S, Quirk GJ (2004) Neuronal signalling of fear memory. *Nature Reviews Neuroscience* 5:844–852.

Markus EJ, Petit TL (1987) Neocortical synaptogenesis, aging, and behavior: Lifespan development in the motor-sensory system of the rat. *Experimental Neurology* 96:262–278.

Mason J, Scior K (2004) 'Diagnostic overshadowing' amongst clinicians working with people with intellectual disabilities in the UK. *Journal of Applied Research in Intellectual Disabilities* 17:85–90.

Massey PV, Johnson BE, Moult PR, Auberson YP, Brown MW, Molnar E, Collingridge GL, Bashir ZI (2004) Differential roles of NR2A and NR2B-containing NMDA receptors in cortical long-term potentiation and long-term depression. *Journal of Neuroscience* .

Matovic S, Ichiyama A, Igarashi H, Salter E, Wang X, Henry M, Verneouz N, Tremblay M, Inoue W (2019) Stress-induced neuronal hypertrophy decreases the intrinsic excitability in stress habituation. *bioRxiv preprint* pp. 1–32.

Matsuda Y, Marzo A, Otani S (2006) The presence of background dopamine signal converts long-term synaptic depression to potentiation in rat prefrontal cortex. *Journal of Neuroscience* 26:4803–4810.

Matsuzaki M, Honkura N, Ellis-Davies GCR, Kasai H (2004) Structural basis of long-term potentiation in single dendritic spines. *Nature* 429:761–766.

Mayer ML, Westbrookt GL, Guthriet PB (1984) Responses in Spinal Cord Neurones. *Nature* 309:261–263.

McDonald AJ, Mascagni F, Guo L (1996) Projections of the medial and lateral prefrontal cortices to the amygdala: a Phaseolus vulgaris leucoagglutinin study in the rat. *Neuroscience* 71:55–75.

McKay BM, Matthews EA, Oliveira FA, Disterhoft JF (2009) Intrinsic neuronal excitability is reversibly altered by a single experience in fear conditioning. *Journal of Neurophysiology* 102:2763–2770.

Meijer MK, Sommer R, Spruijt BM, Van Zutphen LF, Baumans V (2007) Influence of environmental enrichment and handling on the acute stress response in individually housed mice. *Laboratory Animals* 41:161–173.

Meller ST, Dennis BJ (1986) Afferent projections to the periaqueductal gray in the rabbit. *Neuroscience* 19:927–964.

Meller ST, Dennis BJ (1990) A multiple golgi analysis of the periaqueductal gray in the rabbit. *Journal of Comparative Neurology* 302:66–86.

Meyer D, Bonhoeffer T, Scheuss V (2014) Balance and stability of synaptic structures during synaptic plasticity. *Neuron* 82:430–443.

Meyer G, Varoqueaux F, Neeb A, Oschlies M, Brose N (2004) The complexity of PDZ domain-mediated interactions at glutamatergic synapses: A case study on neuroligin. *Neuropharmacology* 47:724–733.

Mikhailov A, Fennell A, Plong-On O, Sripo T, Hansakunachai T, Roongpraiwan R, Sombuntham T, Ruangdaraganon N, Vincent JB, Limprasert P (2014) Screening of NLGN3 and NLGN4X genes in Thai children with autism spectrum disorder. *Psychiatric Genetics* 24:42–43.

Milad R, Quirk G (2002) Neuronsinmedialprefrontalcortex signal memory for fear extinction. *Nature* 420:68–70.

Miserendino MJ, Sananes CB, Melia KR, Davis M (1990) Blocking of acquisition but not expression of conditioned fear-potentiated startle by NMDA antagonists in the amygdala. *Nature* 345:716–718.

Missler M, Zhang W, Rohlmann A, Kattenstroth G, Hammer RE, Gottmann K, Südhof TC (2003) Alpha-neurexins couple Ca2+ channels to synaptic vesicle exocytosis. *Nature* 423:939–948.

Modi B, Pimpinella D, Pazienti A, Zacchi P, Cherubini E, Griguoli M (2019) Possible Implication of the CA2 Hippocampal Circuit in Social Cognition Deficits Observed in the Neuroligin 3 Knock-Out Mouse, a Non-Syndromic Animal Model of Autism. *Frontiers in Psychiatry* 10:1–16.

Monyer H, Burnashev N, Laurie DJ, Sakmann B, Seeburg PH (1994) Developmental and regional expression in the rat brain and functional properties of four NMDA receptors. *Neuron* 12:529–540.

Morishita W, Lu W, Smith GB, Nicoll RA, Bear MF, Malenka RC (2007) Activation of NR2B-containing NMDA receptors is not required for NMDA receptor-dependent long-term depression. *Neuropharmacology* 52:71–76.

Morrow EM, Yoo SY, Flavell S, Kim TK, Lin Y, Hill RS, Mukaddes NM, Balkhy S, Gascon GG, Hashmi A, Al-Saad S, Ware J, Joseph RM, Greenblatt R, Gleason D, Ertelt JA, Apse KA, Bodell A, Partlow JN, Barry B, Yao H, Markianos K, Ferland RJ, Greenberg ME, Walsh CA (2008) Identifying Autism Loci and Genes Here, we show that homozygosity mapping can be useful for identifying loci and genes in ASDs by Tracing Recent Shared Ancestry. *2Science* 321:218–321.

Moult PR, Gladding CM, Sanderson TM, Fitzjohn SM, Bashir ZI, Molnar E, Collingridge GL (2006) Tyrosine phosphatases regulate AMPA receptor trafficking during metabotropic glutamate receptor-mediated long-term depression. *Journal of Neuroscience* 26:2544–2554.

Mulkey RM, Malenka RC (1992) Mechanisms underlying induction of homosynaptic long-term depression in area CA1 of the hippocampus. *Neuron* 9:967–975.

Nägerl UV, Eberhorn N, Cambridge SB, Bonhoeffer T (2004) Bidirectional activity-dependent morphological plasticity in hippocampal neurons. *Neuron* 44:759–767.

Nam CI, Chen L (2005) Postsynaptic assembly induced by neurexin-neuroligin interaction and neurotransmitter. *Proceedings of the National Academy of Sciences of the United States of America* 102:6137–6142.

Ness TV, Remme MW, Einevoll GT (2016) Active subthreshold dendritic conductances shape the local field potential. *Journal of Physiology* 594:3809–3825.

Ness TV, Remme MW, Einevoll GT (2018) H-type membrane current shapes the local field potential from populations of pyramidal neurons. *Journal of Neuroscience* 38:6011–6024.

Netto MB, de Oliveira Junior AN, Goldim M, Mathias K, Fileti ME, da Rosa N, Laurentino AO, de Farias BX, Costa AB, Rezin GT, Fortunato JJ, Giustina AD, Barichello T, Dal-Pizzol F, Petronilho F (2018) Oxidative stress and mitochondrial dysfunction contributes to postoperative cognitive dysfunction in elderly rats. *Brain, Behavior, and Immunity* 73:661–669.

Nguyen T, Südhof TC (1997) Binding properties of neuroligin 1 and neurexin 1β reveal function as heterophilic cell adhesion molecules. *Journal of Biological Chemistry* 272:26032–26039.

Nicholson AA, Friston KJ, Zeidman P, Harricharan S, McKinnon MC, Densmore M, Neufeld RW, Théberge J, Corrigan F, Jetly R, Spiegel D, Lanius RA (2017) Dynamic causal modeling in PTSD and its dissociative subtype: Bottom–up versus top–down processing within fear and emotion regulation circuitry. *Human Brain Mapping* 38:5551–5561.

Nolan MF, Malleret G, Lee KH, Gibbs E, Dudman JT, Santoro B, Yin D, Thompson RF, Siegelbaum SA, Kandel ER, Morozov A (2003) The Hyperpolarization-Activated HCN1 Channel Is Important for Motor Learning and Neuronal Integration by Cerebellar Purkinje Cells. *Cell* 115:551–564.

Norris RH, Churilov L, Hannan AJ, Nithianantharajah J (2019) Mutations in neuroligin-3 in male mice impact behavioural flexibility but not relational memory in a touchscreen test of visual transitive inference. *Molecular Autism* 10:1–21.

Nosyreva ED, Huber KM (2005) Developmental switch in synaptic mechanisms of hippocampal metabotropic glutamate receptor-dependent long-term depression. *Journal of Neuroscience* 25:2992–3001.

Nosyreva ED, Huber KM (2006) Metabotropic receptor-dependent long-term depression persists in the absence of protein synthesis in the mouse model of fragile X syndrome. *Journal of Neurophysiology* 95:3291–3295.

O ' Roak BJ, Vives L, Girirajan S, Karakoc E, Krumm N, Coe BP, Levy R, Ko A, Lee C, Smith JD, Turner EH, Stanaway IB, Vernot B, Malig M, Baker C, Akey JM, Borenstein E, Rieder MJ, Nickerson DA, Bernier R, Shendure J, Eichler EE (2012) Sporadic autism exomes reveal a highly interconnected protein network of de novo mutations. *Nature* 485:246–250.

Oka T, Tsumori T, Yokota S, Yasui Y (2008) Neuroanatomical and neurochemical organization of projections from the central amygdaloid nucleus to the nucleus retroambiguus via the periaqueductal gray in the rat. *Neuroscience Research* 62:286–298.

Oliet SH, Malenka RC, Nicoll RA (1997) Two distinct forms of long-term depression coexist in CA1 hippocampal pyramidal cells. *Neuron* 18:969–982.

Ollendick T, Davis T, Muris P (2004) Chapter 12- Treatment of Specific Phobia in Children and Adolescents In *Handbook of Interventions that Work with Children and Adolescents*, pp. 273–299. John Wiley & Sons Ltd.

Onay H, Kacamak D, Kavasoglu AN, Akgun B, Yalcinli M, Kose S, Ozbaran B (2016) Mutation analysis of the NRXN1 gene in autism spectrum disorders. *Balkan Journal of Medical Genetics* 19:17–22.

Opazo P, Choquet D (2011) A three-step model for the synaptic recruitment of AMPA receptors. *Molecular and Cellular Neuroscience* 46:1–8.

O'Roak BJ, Stessman HA, Boyle EA, Witherspoon KT, Martin B, Lee C, Vives L, Baker C, Hiatt JB, Nickerson DA, Bernier R, Shendure J, Eichler EE (2014) Recurrent de novo mutations implicate novel genes underlying simplex autism risk. *Nature Communications* 5:1–6.

Osborne PB, Vaughan CW, Wilson HI, Christie MJ (1996) Opioid inhibition of rat periaqueductal grey neurones with identified projections to rostral ventromedial medulla in vitro. *Journal of Physiology* 490:383–389.

Osterweil EK, Krueger DD, Reinhold K, Bear MF (2010) Hypersensitivity to mGluR5 and ERK1/2 leads to excessive protein synthesis in the hippocampus of a mouse model of fragile X syndrome. *Journal of Neuroscience* 30:15616–15627.

Oswald MJ, Oorschot DE, Schulz JM, Lipski J, Reynolds JN (2009) IH current generates the afterhyperpolarisation following activation of subthreshold cortical synaptic inputs to striatal cholinergic interneurons. *Journal of Physiology* 587:5879–5897.

Overstreet LS, Pasternak JF, Colley PA, Slater NT, Trommer BL (1997) Metabotropic glutamate receptor mediated long-term depression in developing hippocampus. *Neuropharmacology* 36:831–844.

Pak CH, Danko T, Zhang Y, Aoto J, Anderson G, Maxeiner S, Yi F, Wernig M, Südhof TC (2015) Human Neuropsychiatric Disease Modeling using Conditional Deletion Reveals Synaptic Transmission Defects Caused by Heterozygous Mutations in NRXN1. *Cell Stem Cell* 17:316–328.

Palmer MJ, Irving AJ, Seabrook GR, Jane DE, Collingridge GL (1997) The group I mGlu receptor agonist DHPG induces a novel form of LTD in the CA1 region of the hippocampus. *Neuropharmacology* 36:1517–1532.

Pampanos A, Volaki K, Kanavakis E, Papandreou O, Youroukos S, Thomaidis L, Karkelis S, Tzetis M, Kitsiou-Tzeli S (2009) A substitution involving the NLGN4 gene associated with autistic behavior in the Greek population. *Genetic testing and molecular biomarkers* 13:611–615.

Panju S, Brian J, Dupuis A, Anagnostou E, Kushki A (2015) Atypical sympathetic arousal in children with autism spectrum disorder and its association with anxiety symptomatology. *Molecular Autism* 6:1–10.

Paré D, Smith Y, Paré JF (1995) Intra-amygdaloid projections of the basolateral and basomedial nuclei in the cat: Phaseolus Vulgaris-Leucoagglutinin anterograde tracing at the light and electron microscopic level. *Neuroscience* 69:567–583.

Park C, Kim JH, Yoon BE, Choi EJ, Lee CJ, Shin HS (2010) T-type channels control the opioidergic descending analgesia at the low threshold-spiking GABAergic neurons in the periaqueductal gray. *Proceedings of the National Academy of Sciences of the United States of America* 107:14857–14862.

Park J, Moghaddam B (2017) Impact of anxiety on prefrontal cortex encoding of cognitive flexibility. *Neuroscience* 345:193–202.

Park S, Park JM, Kim S, Kim JA, Shepherd JD, Smith-Hicks CL, Chowdhury S, Kaufmann W, Kuhl D, Ryazanov AG, Huganir RL, Linden DJ, Worley PF (2008) Elongation Factor 2 and Fragile X Mental Retardation Protein Control the Dynamic Translation of Arc/Arg3.1 Essential for mGluR-LTD. *Neuron* 59:70–83.

Paxinos G, Watson C (2007) *The Rat Brain in Stereotaxic Coordinates* Elsevier Academic Press.

Pelkey KA, Chittajallu R, Craig MT, Tricoire L, Wester JC, McBain CJ (2017) Hippocampal gabaergic inhibitory interneurons. *Physiological Reviews* 97:1619–1747.

Petanjek Z, Judaš M, Šimić G, Rašin MR, Uylings HB, Rakic P, Kostović I (2011) Extraordinary neoteny of synaptic spines in the human prefrontal cortex. *Proceedings of the National Academy of Sciences of the United States of America* 108:13281–13286.

Peters HC, Hu H, Pongs O, Storm JF, Isbrandt D (2005) Conditional transgenic suppression of M channels in mouse brain reveals functions in neuronal excitability, resonance and behavior. *Nature Neuroscience* 8:51–60.

Petrovic MM, Nowacki J, Olivo V, Tsaneva-Atanasova K, Randall AD, Mellor JR (2012) Inhibition of post-synaptic Kv7/KCNQ/M channels facilitates long-term potentiation in the hippocampus. *PLoS ONE* 7:1–10.

Pezalla PD (1983) Morphine-Induced Analgesia and Explosive Motor Behavior in an Amphibian Nociceptive testing. *Brain research* 273:297–305.

Philibert RA, Winfield SL, Sandhu HK, Martin BM, Ginns EI (2000) The structure and expression of the human neuroligin-3 gene. *Gene* 236:303–310.

Phillips RG, LeDoux JE (1992) Differential Contribution of Amygdala and Hippocampus to Cued and Contextual Fear Conditioning. *Behavioral Neuroscience* 106:274–285.

Pibiri F, Nelson M, Guidotti A, Costa E, Pinna G (2008) Decreased corticolimbic allopregnanolone expression during social isolation enhances contextual fear: A model relevant for posttraumatic stress disorder. *Proceedings of the National Academy of Sciences of the United States of America* 105:5567–5572.

Pinto D, Delaby E, Merico D, Barbosa M, Merikangas A, Klei L, Thiruvahindrapuram B, Xu X, Ziman R, Wang Z, Vorstman JAS, Thompson A, Regan R, Pilorge M, Pellecchia G, Marshall CR, Magalhaes TR, Pagnamenta AT, Lowe JK, Howe JL, Griswold AJ, Gilbert J, Duketis E, Dombroski BA, Jonge MVD, Cuccaro M, Crawford EL, Conceic C, Casey JP, Cai G, Cabrol C, Bolshakova N, Bacchelli E, Anney R, Gallinger S, Cotterchio M, Casey G, Zwaigenbaum L, Wittemeyer K, Wing K, Wallace S, Engeland HV, Tryfon A, Roberts W, Poustka F, Thomson S, Soorya L, Roge B, Mouga S, Minshew N, Mcinnes LA, Mcgrew SG, Lord C, Bernier R, Baird G, Bailey AJ, Anagnostou E, Almeida J, Wijsman EM, Vieland VJ, Maestrini E, Klauck SM, Hakonarson H, Haines JL, Geschwind DH, Freitag CM, Folstein SE, Ennis S, Coon H, Battaglia A, Szatmari P, Sutcliffe JS, Hallmayer J, Gill M, Cook EH, Buxbaum JD, Devlin B, Gallagher L (2014) Convergence of Genes and Cellular Pathways Dysregulated in Autism Spectrum Disorders. *The American Journal of Human Genetics* 94:677–694.

Pinto D, Pagnamenta AT, Klei L, Anney R, Merico D, Regan R, Conroy J, Magalhaes TR, Correia C, Abrahams BS, Almeida J, Bacchelli E, Bader GD, Bailey AJ, Baird G, Battaglia A, Berney T, Bolshakova N, Bölte S, Bolton PF, Bourgeron T, Brennan S, Brian J, Bryson SE, Carson AR, Casallo G, Casey J, Chung BH, Cochrane L, Corsello C, Crawford EL, Crossett A, Cytrynbaum C, Dawson G, De Jonge M, Delorme R, Drmic I, Duketis E, Duque F, Estes A, Farrar P, Fernandez BA, Folstein SE, Fombonne E, Freitag CM, Gilbert J, Gillberg C, Glessner JT, Goldberg J, Green A, Green J, Guter SJ, Hakonarson H, Heron EA, Hill M, Holt R, Howe JL, Hughes G, Hus V, Igliozzi R, Kim C, Klauck SM, Kolevzon A, Korvatska O, Kustanovich V, Lajonchere CM, Lamb JA, Laskawiec M, Leboyer M, Le Couteur A, Leventhal BL, Lionel AC, Liu XQ, Lord C, Lotspeich L, Lund SC, Maestrini E, Mahoney W,

Mantoulan C, Marshall CR, McConachie H, McDougle CJ, McGrath J, McMahon WM, Merikangas A, Migita O, Minshew NJ, Mirza GK, Munson J, Nelson SF, Noakes C, Noor A, Nygren G, Oliveira G, Papanikolaou K, Parr JR, Parrini B, Paton T, Pickles A, Pilorge M, Piven J, Ponting CP, Posey DJ, Poustka A, Poustka F, Prasad A, Ragoussis J, Renshaw K, Rickaby J, Roberts W, Roeder K, Roge B, Rutter ML, Bierut LJ, Rice JP, Salt J, Sansom K, Sato D, Segurado R, Sequeira AF, Senman L, Shah N, Sheffield VC, Soorya L, Sousa I, Stein O, Sykes N, Stoppioni V, Strawbridge C, Tancredi R, Tansey K, Thiruvahindrapduram B, Thompson AP, Thomson S, Tryfon A, Tsiantis J, Van Engeland H, Vincent JB, Volkmar F, Wallace S, Wang K, Wang Z, Wassink TH, Webber C, Weksberg R, Wing K, Wittemeyer K, Wood S, Wu J, Yaspan BL, Zurawiecki D, Zwaigenbaum L, Buxbaum JD, Cantor RM, Cook EH, Coon H, Cuccaro ML, Devlin B, Ennis S, Gallagher L, Geschwind DH, Gill M, Haines JL, Hallmayer J, Miller J, Monaco AP, Nurnberger JI, Paterson AD, Pericak-Vance MA, Schellenberg GD, Szatmari P, Vicente AM, Vieland VJ, Wijsman EM, Scherer SW, Sutcliffe JS, Betancur C (2010) Functional impact of global rare copy number variation in autism spectrum disorders. *Nature* 466:368–372.

Pizzarelli R, Cherubini E (2013) Developmental regulation of GABAergic signalling in the hippocampus of neuroligin 3 R451C knock-in mice: an animal model of Autism. *Frontiers in cellular neuroscience* 7:85.

Platkiewicz J, Brette R (2010) A threshold equation for action potential initiation. *PLoS Computational Biology* 6:25.

Polepalli JS, Sullivan RK, Yanagawa Y, Sah P (2010) A specific class of interneuron mediates inhibitory plasticity in the lateral amygdala. *Journal of Neuroscience* 30:14619–14629.

Polepalli JS, Wu H, Goswami D, Halpern CH, Thomas C, Malenka RC, Sciences B, Physiology C, Südhof TC, Malenka RC (2017) Modulation of excitation on parvalbumin interneurons by neuroligin-3 regulates the hippocampal network. *Nature Neuroscience* 20:219–229.

Poolos NP, Johnston D (1999) Calcium-activated potassium conductances contribute to action potential repolarization at the soma but not the dendrites of hippocampal CA1 pyramidal neurons. *Journal of Neuroscience* 19:5205–5212.

Poultney CS, Goldberg AP, Drapeau E, Kou Y, Harony-Nicolas H, Kajiwara Y, De Rubeis S, Durand S, Stevens C, Rehnström K, Palotie A, Daly MJ, Ma'Ayan A, Fromer M, Buxbaum JD (2013) Identification of small exonic CNV from whole-exome sequence data and application to autism spectrum disorder. *American Journal of Human Genetics* 93:607–619.

Prasad A, Merico D, Thiruvahindrapuram B, Wei J, Lionel AC, Sato D, Rickaby J, Lu C, Szatmari P, Roberts W, Fernandez BA, Marshall CR, Hatchwell E, Eis PS, Scherer SW (2012) A Discovery resource of rare copy number variations in individuals with autism spectrum disorder. *G3: Genes, Genomes, Genetics* 2:1665–1685.

Price JL, Amaral DG (1981) An autoradiographic study of the projections of the central nucleus of the monkey amygdala. *Journal of Neuroscience* .

Prieto GA, Trieu BH, Dang CT, Bilousova T, Gylys KH, Berchtold NC, Lynch G, Cotman CW (2017) Pharmacological rescue of long-term potentiation in alzheimer diseased synapses. *Journal of Neuroscience* 37:1197–1212.

Quartier A, Courraud J, Thi Ha T, McGillivray G, Isidor B, Rose K, Drouot N, Savidan MA, Feger C, Jagline H, Chelly J, Shaw M, Laumonnier F, Gecz J, Mandel JL, Piton A (2019) Novel mutations in NLGN3 causing autism spectrum disorder and cognitive impairment. *Human Mutation* 40:2021–2032.

Quirk GJ (2002) Memory for extinction of conditioned fear is long-lasting and persists following spontaneous recovery. *Learning and Memory* 9:402–407.

Quirk GJ, Likhtik E, Pelletier JG, Paré D (2003) Stimulation of Medial Prefrontal Cortex Decreases the Responsiveness of Central Amygdala Output Neurons. *Journal of Neuroscience* 23:8800–8807.

Quirk GJ, Repa JC, LeDoux JE (1995) Fear conditioning enhances short-latency auditory responses of lateral amygdala neurons: Parallel recordings in the freely behaving rat. *Neuron* 15:1029–1039.

Radyushkin K, Hammerschmidt K, Boretius S, Varoqueaux F, El-Kordi A, Ronnenberg A, Winter D, Frahm J, Fischer J, Brose N, Ehrenreich H (2009) Neuroligin-3-deficient mice: Model of a monogenic heritable form of autism with an olfactory deficit. *Genes, Brain and Behavior* 8:416–425.

Rao A, Kim E, Sheng M, Craig AM (1998) Heterogeneity in the molecular composition of excitatory postsynaptic sites during development of hippocampal neurons in culture. *Journal of Neuroscience* 18:1217–1229.

Redgrave P, Dean P, Mitchell IJ, Odekunle A, Clark A (1988) The projection from superior colliculus to cuneiform area in the rat - I. Anatomical studies. *Experimental Brain Research* 72:626–639.

Redin C, Gérard B, Lauer J, Herenger Y, Muller J, Quartier A, Masurel-Paulet A, Willems M, Lesca G, El-Chehadeh S, Gras SL, Vicaire S, Philipps M, Dumas M, Geoffroy V, Feger C, Haumesser N, Alembik Y, Barth M, Bonneau D, Colin E, Dollfus H, Doray B, Delrue MA, Drouin-Garraud V, Flori E, Fradin M, Francannet C, Goldenberg A, Lumbroso S, Mathieu-Dramard M, Martin-Coignard D, Lacombe D, Morin G, Polge A, Sukno S, Thauvin-Robinet C, Thevenon J, Doco-Fenzy M, Genevieve D, Sarda P, Edery P, Isidor B, Jost B, Olivier-Faivre L, Mandel JL, Piton A (2014) Efficient strategy for the molecular diagnosis of intellectual disability using targeted high-throughput sequencing. *Journal of Medical Genetics* 51:724–736.

Regehr WG, Delaney KR, Tank DW (1994) The role of presynaptic calcium in short-term enhancement at the hippocampal mossy fiber synapse. *Journal of Neuroscience* 14:523–537.

Reimann MW, Anastassiou CA, Perin R, Hill SL, Markram H, Koch C (2013) A Biophysically Detailed Model of Neocortical Local Field Potentials Predicts the Critical Role of Active Membrane Currents. *Neuron* 79:375–390.

Rizvi TA, Ennis MMHEWMMHEW, Behbehani MM, Shipley MT (1991) Connections between the central nucleus of the amygdala and the midbrain periaqueductal gray: Topography and reciprocity. *Journal of Comparative Neurology* 303:121–131.

Robertson CE, Baron-Cohen S (2017) Sensory perception in autism. *Nature Reviews Neuroscience* 18:671–684.

Rogan MT, Staubli UV, Ledoux JE (1997) Fear conditioning induces associative long-term potentiation in the amygdala. *Nature* 390:604–607.

Romanò N, Yip SH, Hodson DJ, Guillou A, Parnaudeau S, Kirk S, Tronche F, Bonnefont X, Le Tissier P, Bunn SJ, Grattan DR, Mollard P, Martin AO (2013) Plasticity of hypothalamic dopamine neurons during lactation results in dissociation of electrical activity and release. *Journal of Neuroscience* 33:4424–4433.

Rosahl TW, Geppert M, Spillane D, Herz J, Hammer RE, Malenka RC, Südhof TC (1993) Short-term synaptic plasticity is altered in mice lacking synapsin I. *Cell* 75:661–670.

Rosas-Vidal LE, Do-Monte FH, Sotres-Bayon F, Quirk GJ (2014) Hippocampal-prefrontal BDNF and memory for fear extinction. *Neuropsychopharmacology* 39:2161–2169.

Rothwell PE, Fuccillo MV, Maxeiner S, Hayton SJ, Gokce O, Lim BK, Fowler SC, Malenka RC, Su TC (2014) Autism-Associated Neuroligin-3 Mutations Commonly Impair Striatal Circuits to Boost Repetitive Behaviors. *Cell* 158:198–212.

Rowen L, Young J, Birditt B, Kaur A, Madan A, Philipps DL, Qin S, Minx P, Wilson RK, Hood L, Graveley BR (2002) Analysis of the human neurexin genes: alternative splicing and the generation of protein diversity. *Genomics* 79:587–597.

Rozeske RR, Jercog D, Karalis N, Chaudun F, Khoder S, Girard D, Winke N, Herry C (2018) Prefrontal-Periaqueductal Gray-Projecting Neurons Mediate Context Fear Discrimination. *Neuron* 97:898–910.e6.

Saar D, Grossman Y, Barkai E (1998) Reduced after-hyperpolarization in rat piriform cortex pyramidal neurons is associated with increased learning capability during operant conditioning. *European Journal of Neuroscience* 10:1518–1523.

Sah P, Faber ES, De Armentia ML, Power J (2003) The amygdaloid complex: Anatomy and physiology. *Physiological Reviews* 83:803–834.

Sailer CA, Kaufmann WA, Kogler M, Chen L, Sausbier U, Ottersen OP, Ruth P, Shipston MJ, Knaus HG (2006) Immunolocalization of BK channels in hippocampal pyramidal neurons. *European Journal of Neuroscience* 24:442–454.

Sánchez D, Ganfornina MD, Ribas J (1988) Periaqueductal gray neurons' activity in a mesencephalic slice preparation. *Brain Research* 455:166–169.

Sánchez D, Ribas J (1991) Properties and ionic basis of the action potentials in the periaqueductal grey neurones of the guinea-pig. *The Journal of Physiology* 440:167–187.

Sandin S, Lichtenstein P, Kuja-Halkola R, Hultman C, Larsson H, Reichenberg A (2017) The Heritability of Autism Spectrum Disorder. *Journal of the American Medical Association* 318:1182–1184.

Sandner G, Dessort D, Schmitt P, Karli P (1981) Distribution of GABA in the periaqueductal gray matter. Effects of medial hypothalamic lesions. *Brain Research* 224:279–290.

Sangha S, Robinson PD, Greba Q, Davies DA, Howland JG (2014) Alterations in reward, fear and safety cue discrimination after inactivation of the rat prelimbic and infralimbic cortices. *Neuropsychopharmacology* 39:2405–2413.

Santini E, Quirk GJ, Porter JT (2008) Fear conditioning and extinction differentially modify the intrinsic excitability of infralimbic neurons. *Journal of Neuroscience* 28:4028–4036.

Schaaf CP, Boone PM, Sampath S, Williams C, Bader PI, Mueller JM, Shchelochkov OA, Brown CW, Crawford HP, Phalen JA, Tartaglia NR, Evans P, Campbell WM, Chun-Hui Tsai A, Parsley L, Grayson SW, Scheuerle A, Luzzi CD, Thomas SK, Eng PA, Kang SHL, Patel A, Stankiewicz P, Cheung SW (2012) Phenotypic spectrum and genotype-phenotype correlations of NRXN1 exon deletions. *European Journal of Human Genetics* 20:1240–1247.

Scheiffele P, Fan J, Choih J, Fetter R, Serafini T (2000) Neuroligin Expressed in Nonneuronal Cells Triggers Presynaptic Development in Contacting Axons. *Cell* 101:657–669.

Schenberg LC, Costa MB, Borges PC, Castro MF (1990) Logistic analysis of the defense reaction induced by electrical stimulation of the rat mesencephalic tectum. *Neuroscience and Biobehavioral Reviews* 14:473–479.

Schneider K, Regenbogen C, Pauly KD, Gossen A, Schneider DA, Mevissen L, Michel TM, Gur RC, Habel U, Schneider F (2013) Evidence for gender-specific endophenotypes in high-functioning autism spectrum disorder during empathy. *Autism Research* 6:506–521.

Schoepp DD, Conn P (1993) Metabotropic glutamate receptors in brain function and pathology. *Trends in Pharmacological Sciences* 14:13–20.

Selyanko AA, Hadley JK, Wood IC, Abogadie FC, Delmas P, Buckley NJ, London B, Brown DA (1999) Two types of K+ channel subunit, Erg1 and KCNQ2/3, contribute to the M- like current in a mammalian neuronal cell. *Journal of Neuroscience* 19:7742–7756.

Semenenko EM, Lumb BM (1992) Projections of anterior hypothalamic neurones to the dorsal and ventral periaqueductal grey in the rat. *Brain Research* 582:237–245.

Senn V, Wolff SB, Herry C, Grenier F, Ehrlich I, Gründemann J, Fadok JP, Müller C, Letzkus JJ, Lüthi A (2014) Long-range connectivity defines behavioral specificity of amygdala neurons. *Neuron* 81:428–437.

Shaban H, Humeau Y, Herry C, Cassasus G, Shigemoto R, Ciocchi S, Barbieri S, Van Der Putten H, Kaupmann K, Bettler B, Lüthi A (2006) Generalization of amygdala LTP and conditioned fear in the absence of presynaptic inhibition. *Nature Neuroscience* 9:1028–1035.

Shah AK, Tioleco NM, Nolan K, Locker J, Groh K, Villa C, Stopkova P, Pedrosa E, Lachman HM (2010) Rare NRXN1 promoter variants in patients with schizophrenia. *Neuroscience Letters* 475:80–84.

Shah MM, Mistry M, Marsh SJ, Brown DA, Delmas P (2002) Molecular correlates of the M-current in cultured rat hippocampal neurons. *Journal of Physiology* 544:29–37.

Short PJ, McRae JF, Gallone G, Sifrim A, Won H, Geschwind DH, Wright CF, Firth HV, Fitzpatrick DR, Barrett JC, Hurles ME (2018) De novo mutations in regulatory elements in neurodevelopmental disorders. *Nature* 555:611–616.

Sierra-Mercado D, Padilla-Coreano N, Quirk GJ (2011) Dissociable roles of prelimbic and infralimbic cortices, ventral hippocampus, and basolateral amygdala in the expression and extinction of conditioned fear. *Neuropsychopharmacology* 36:529–538.

Silva BA, Mattucci C, Krzywkowski P, Murana E, Illarionova A, Grinevich V, Canteras NS, Ragozzino D, Gross CT (2013) Independent hypothalamic circuits for social and predator fear. *Nature Neuroscience* 16:1731–1733.

Sinha P, Kjelgaard MM, Gandhi TK, Tsourides K, Cardinaux AL, Pantazis D, Diamond SP, Held RM (2014) Autism as a disorder of prediction. *Proceedings of the National Academy of Sciences of the United States of America* 111:15220–15225.

Song JY, Ichtchenko K, Südhof TC, Brose N (1999) Neuroligin 1 is a postsynaptic cell-adhesion molecule of excitatory synapses. *Proceedings of the National Academy of Sciences of the United States of America* 96:1100–1105.

Sotres-Bayon F, Bush DE, LeDoux JE (2007) Acquisition of fear extinction requires activation of NR2B-containing NMDA receptors in the lateral amygdala. *Neuropsychopharmacology* 32:1929–1940.

Springer SJ, Burkett BJ, Schrader LA (2015) Modulation of BK channels contributes to activity-dependent increase of excitability through MTORC1 activity in CA1 pyramidal cells of mouse hippocampus. *Frontiers in Cellular Neuroscience* 8:1–12.

Srivastava AK, Schwartz CE (2014) Intellectual disability and autism spectrum disorders: Causal genes and molecular mechanisms. *Neuroscience and Biobehavioral Reviews* 46:161–174.

Stanton PK, Sarvey JM (1984) Blockade of long-term potentiation in rat hippocampal CA1 region by inhibitors of protein synthesis. *Journal of Neuroscience* 4:3080–3088.

Steffenburg S, Gillberg C, Hellgren L, Andersson L, Gillberg IC, Jakobsson G, Bohman M (1989) A Twin Study of Autism in Denmark, Finland, Iceland, Norway and Sweden. *Journal of Child Psychology and Psychiatry* 30:405–416.

Steinberg KM, Ramachandran D, Patel VC, Shetty AC, Cutler DJ, Zwick ME (2012) Identification of rare X-linked neuroligin variants by massively parallel sequencing in males with autism spectrum disorder. *Molecular Autism* 3:1.

Stent GS (1973) A physiological mechanism for Hebb's postulate of learning. *Proceedings of the National Academy of Sciences of the United States of America* 70:997–1001.

Sterky FH, Trotter JH, Lee Sj, Recktenwald CV, Du X, Zhou B, Zhou P, Schwenk JM, Fakler B, Sudhof TC (2017) Correction: Carbonic anhydrase-related protein CA10 is an evolutionarily conserved pan-neurexin ligand (Proceedings of the National Academy of Sciences of the United States of America (2017) 114 (E1253-E1262) DOI: 10.1073/pnas.1621321114). *Proceedings of the National Academy of Sciences of the United States of America* 114:E2984.

Stessman HA, Xiong B, Coe BP, Wang T, Hoekzema K, Fenckova M, Kvarnung M, Gerdts J, Trinh S, Cosemans N, Vives L, Lin J, Turner TN, Santen G, Ruivenkamp C, Kriek M, Van Haeringen A, Aten E, Friend K, Liebelt J, Barnett C, Haan E, Shaw M, Gecz J, Anderlid BM, Nordgren A, Lindstrand A, Schwartz C, Kooy RF, Vandeweyer G, Helsmoortel C, Romano C, Alberti A, Vinci M, Avola E, Giusto S, Courchesne E, Pramparo T, Pierce K, Nalabolu S, Amaral DG, Scheffer IE, Delatycki MB, Lockhart PJ, Hormozdiari F, Harich B, Castells-Nobau A, Xia K, Peeters H, Nordenskjöld M, Schenck A, Bernier RA, Eichler EE (2017) Targeted sequencing identifies 91 neurodevelopmental-disorder risk genes with autism and developmental-disability biases. *Nature Genetics* 49:515–526.

Storm BYJF (1989) After-hyperpolarization of medium duration. *Journal of Physiology* 409:171–190.

Sutton MA, Ito HT, Cressy P, Kempf C, Woo JC, Schuman EM (2006) Miniature Neurotransmission Stabilizes Synaptic Function via Tonic Suppression of Local Dendritic Protein Synthesis. *Cell* 125:785–799.

Sutton RS, Barto AG (1981) Toward a modern theory of adaptive networks: Expectation and prediction. *Psychological Review* 88:135–170.

Swanwick CC, Murthy NR, Mtchedlishvili Z, Sieghart W, Kapur J (2006) Development of γ-aminobutyric acidergic synapses in cultured hippocampal neurons. *Journal of Comparative Neurology* 495:497–510.

Szatmari P, Paterson AD, Zwaigenbaum L, Roberts W, Brian J, Liu XQ, Vincent JB, Skaug JL, Thompson AP, Senman L, Feuk L, Qian C, Bryson SE, Jones MB, Marshall CR, Scherer SW, Vieland VJ, Bartlett C, Mangin LV, Goedken R, Segre A, Pericak-Vance MA, Cuccaro ML, Gilbert JR, Wright HH, Abramson RK, Betancur C, Bourgeron T, Gillberg C, Leboyer M, Buxbaum JD, Davis KL, Hollander E, Silverman JM, Hallmayer J, Lotspeich L, Sutcliffe JS, Haines JL, Folstein SE, Piven J, Wassink TH, Sheffield V, Geschwind DH, Bucan M, Brown WT, Cantor RM, Constantino JN, Gilliam TC, Herbert M, LaJonchere C, Ledbetter DH, Lese-Martin C, Miller J, Nelson S, Samango-Sprouse CA, Spence S, State M, Tanzi RE, Coon H, Dawson G, Devlin B, Estes A, Flodman P, Klei L, McMahon WM, Minshew N, Munson J, Korvatska E, Rodier PM, Schellenberg GD, Smith M, Spence MA, Stodgell C, Tepper PG, Wijsman EM, Yu CE, Rogé B, Mantoulan C, Wittemeyer K, Poustka A, Felder B, Klauck SM, Schuster C, Poustka F, Bölte S, Feineis-Matthews S, Herbrecht E, Schmötzer G, Tsiantis J, Papanikolaou K, Maestrini E, Bacchelli E, Blasi F, Carone S, Toma C, Van Engeland H, De Jonge M, Kemner C, Koop F, Langemeijer M, Hijimans C, Staal WG, Baird G, Bolton PF, Rutter ML, Weisblatt E, Green J, Aldred C, Wilkinson JA, Pickles A, Le Couteur A, Berney T, McConachie H, Bailey AJ, Francis K, Honeyman G, Hutchinson A, Parr JR, Wallace S, Monaco AP, Barnby G, Kobayashi K, Lamb JA, Sousa I, Sykes N, Cook EH, Guter SJ, Leventhal BL, Salt J, Lord C, Corsello C, Hus V, Weeks DE, Volkmar F, Tauber M, Fombonne E, Shih A (2007) Mapping autism risk loci using genetic linkage and chromosomal rearrangements. *Nature Genetics* 39:319–328.

Szinyei C, Narayanan RT, Pape HC (2007) Plasticity of inhibitory synaptic network interactions in the lateral amygdala upon fear conditioning in mice. *European Journal of Neuroscience* 25:1205–1211.

Tabuchi K, Blundell J, Etherton MR, Hammer RE, Liu X, Powell CM, Südhof TC, Liu X, Powell CM, Südhof TC (2007) A neuroligin-3 mutation implicated in autism increases inhibitory synaptic transmission in mice. *Science (New York, N.Y.)* 318:71–6.

Talebizadeh Z, Lam DY, Theodoro MF, Bittel DC, Lushington GH, Butler MG (2006) Novel splice isoforms for NLGN3 and NLGN4 with possible implications in autism. *Journal of medical genetics* 43:1–7.

Tang J, Wagner S, Schachner M, Dityatev A, Wotjak CT (2003) Potentiation of amygdaloid and hippocampal auditory-evoked potentials in a discriminatory fear-conditioning task in mice as a function of tone pattern and context. *European Journal of Neuroscience* 18:639–650.

Taylor GT (1981) Fear and affiliation in domesticated male rats. *Journal of Comparative and Physiological Psychology* 95:685–693.

Thomas AM, Schwartz MD, Saxe MD, Kilduff TS (2017) Sleep/wake physiology and quantitative electroencephalogram analysis of the neuroligin-3 knockout rat model of autism spectrum disorder. *Sleep* 40.

Thorsell A, Slawecki CJ, El Khoury A, Mathe AA, Ehlers CL (2006) The effects of social isolation on neuropeptide Y levels, exploratory and anxiety-related behaviors in rats. *Pharmacology Biochemistry and Behavior* 83:28–34.

Till SM, Asiminas A, Jackson AD, Katsanevaki D, Barnes SA, Osterweil EK, Bear MF, Chattarji S, Wood ER, Wyllie DJA, Kind PC (2015) Conserved hippocampal cellular pathophysiology but distinct behavioural deficits in a new rat model of FXS. *Human Molecular Genetics* 24:5977–5984.

Toft AK (2019) The impact of two autism related genes on amygdala physiology Ph.D. diss., The University of Edinburgh.

Tomaz C, Brandão M, Bagri A, Carrive P, Schmitt P (1988) Flight behavior induced by microinjection of GABA antagonists into periventricular structures in detelencephalated rats. *Pharmacology, Biochemistry and Behavior* 30:337–342.

Toni N, Buchs PA, Nikonenko I, Bron CR, Muller D (1999) LTP promotes formation of multiple spine synapses between a single axon terminal and a dendrite. *Nature* 402:421–425.

Toni N, Buchs PA, Nikonenko I, Povilaitite P, Parisi L, Muller D (2001) Remodeling of synaptic membranes after induction of long-term potentiation. *Journal of Neuroscience* 21:6245–6251.

Torres-García ME, Medina AC, Quirarte GL, Prado-Alcalá RA (2017) Differential effects of inactivation of discrete regions of medial prefrontal cortex on memory consolidation of moderate and intense inhibitory avoidance training. *Frontiers in Pharmacology* 8:1–10.

Tovote P, Esposito MS, Botta P, Chaudun F, Jonathan P (2016) Midbrain circuits for defensive behaviour. *Nature* 534:206–212.

Tovote P, Fadok JP, Lüthi A (2015) Neuronal circuits for fear and anxiety. *Nature Reviews Neuroscience* 16:317–331.

Trouche S, Sasaki JM, Tu T, Reijmers LG (2013) Fear Extinction Causes Target-Specific Remodeling of Perisomatic Inhibitory Synapses. *Neuron* 80:1054–1065.

Turrigiano GG, Nelson SB (2004) Homeostatic plasticity in the developing nervous system. *Nature Reviews Neuroscience* 5:97–107.

Twining RC, Vantrease JE, Love S, Padival M, Rosenkranz JA (2017) An intra-amygdala circuit specifically regulates social fear learning. *Nature Neuroscience* 20:459–469.

Tzingounis AV, Heidenreich M, Kharkovets T, Spitzmaul G, Jensen HS, Nicoll RA, Jentsch TJ (2010) The KCNQ5 potassium channel mediates a component of the afterhyperpolarization current in mouse hippocampus. *Proceedings of the National Academy of Sciences of the United States of America* 107:10232–10237.

Uchigashima M, Leung M, Watanabe T, Cheung A, Watanabe M, Kawasawa YI, Futai K (2020) Neuroligin3 Splice Isoforms Shape Mouse Hippocampal Inhibitory Synaptic Function. *bioRxiv preprint* January.

Uematsu M, Hirai Y, Karube F, Ebihara S, Kato M, Abe K, Obata K, Yoshida S, Hirabayashi M, Yanagawa Y, Kawaguchi Y (2008) Quantitative chemical composition of cortical GABAergic neurons revealed in transgenic venus-expressing rats. *Cerebral Cortex* 18:315–330.

Uhlén M, Fagerberg L, Hallström BM, Lindskog C, Oksvold P, Mardinoglu A, Sivertsson Å, Kampf C, Sjöstedt E, Asplund A, Olsson IM, Edlund K, Lundberg E, Navani S, Szigyarto CAK, Odeberg J, Djureinovic D, Takanen JO, Hober S, Alm T, Edqvist PH, Berling H, Tegel H, Mulder J, Rockberg J, Nilsson P, Schwenk JM, Hamsten M, Von Feilitzen K, Forsberg M, Persson L, Johansson F, Zwahlen M, Von Heijne G, Nielsen J, Pontén F (2015) Tissue-based map of the human proteome. *Science* 347:http://www.proteinatlas.org.

Ullrich B, Ushkaryov YA, Südhof TC (1995) Cartography of neurexins: More than 1000 isoforms generated by alternative splicing and expressed in distinct subsets of neurons. *Neuron* 14:497–507.

Ultanir SK, Kim JE, Hall BJ, Deerinck T, Ellisman M, Ghosh A (2007) Regulation of spine morphology and spine density by NMDA receptor signaling in vivo. *Proceedings of the National Academy of Sciences of the United States of America* 104:19553–19558.

Urban KR, Valentino RJ (2017) Age- and Sex-Dependent Impact of Repeated Social Stress on Intrinsic and Synaptic Excitability of the Rat Prefrontal Cortex. *Cerebral cortex (New York, N.Y. : 1991)* 27:244–253.

Uribe-Mario A, Francisco A, Castiblanco-Urbina MA, Twardowschy A, Salgado-Rohner CJ, Crippa JAS, Hallak JEC, Zuardi AW, Coimbra NC (2012) Anti-aversive effects of cannabidiol on innate fear-induced behaviors evoked by an ethological model of panic attacks based on a prey vs the wild snake epicrates cenchria crassus confrontation paradigm. *Neuropsychopharmacology* 37:412–421.

Ushkaryov Ya, Petrenko aG, Geppert M, Südhof TC (1992) Neurexins: synaptic cell surface proteins related to the alpha-latrotoxin receptor and laminin. *Science (New York, N.Y.)* 257:50–56.

van Bockstaele EJ, Aston-Jones G, Pieribone VA, Ennis M, Shipley MT (1991) Subregions of the periaqueductal gray topographically innervate the rostral ventral medulla in the rat. *Journal of Comparative Neurology* 309:305–327.

van Steensel FJ, Bögels SM, Dirksen CD (2012) Anxiety and Quality of Life: Clinically Anxious Children With and Without Autism Spectrum Disorders Compared. *Journal of Clinical Child and Adolescent Psychology* 41:731–738.

Varela JA, Sen K, Gibson J, Fost J, Abbott LF, Nelson SB (1997) A quantitative description of short-term plasticity at excitatory synapses in layer 2/3 of rat primary visual cortex. *Journal of Neuroscience* 17:7926–7940.

Varela JA, Wang J, Christianson JP, Maier SF, Cooper DC (2012) Control over Stress , But Not Stress Per Se Increases Prefrontal Cortical Pyramidal Neuron Excitability. *Journal of Neuroscience* 32:12848–12853.

Varoqueaux F, Aramuni G, Rawson RL, Mohrmann R, Missler M, Gottmann K, Zhang W, Südhof TC, Brose N (2006) Neuroligins Determine Synapse Maturation and Function. *Neuron* 51:741–754.

Varoqueaux F, Jamain S, Brose N (2004) Neuroligin 2 is exclusively localized to inhibitory synapses. *European journal of cell biology* 83:449–456.

Veening J, Buma P, Ter Horst GJ, Roeling TAP, Luiten PGM, Nieuwenhuys R (1991) Hypothalamic Projections to the PAG in the Rat: Topographical, Immuno-Electronmicroscopical and Functional Aspects In *The Midbrain Periaqueductal Gray Matter*, pp. 387–415. Springer US.

Veening JG, Lie ST, Posthuma P, Geeraedts LM, Nieuwenhuys R (1987) A topographical analysis of the origin of some efferent projections from the lateral hypothalamic area in the rat. *Neuroscience* 22:537–551.

Vianna DM, Brandão ML (2003) Anatomical connections of the periaqueductal gray: Specific neural substrates for different kinds of fear. *Brazilian Journal of Medical and Biological Research* 36:557–566.

Vianna DM, Graeff FG, Landeira-Fernandez J, Brandão ML (2001) Lesion of the ventral periaqueductal gray reduces conditioned fear but does not change freezing induced by stimulation of the dorsal periaqueductal gray. *Learning and Memory* 8:164–169.

Vincent JB, Kolozsvari D, Roberts WS, Bolton PF, Gurling HM, Scherer SW (2004) Mutation screening of X-chromosomal neuroligin genes: No mutations in 196 autism probands. *American Journal of Medical Genetics* 129B:82–84.

Volaki K, Pampanos A, Kitsiou-Tzeli S, Vrettou C, Oikonomakis V, Sofocleous C, Kanavakis E (2013) Mutation screening in the Greek population and evaluation of NLGN3 and NLGN4X genes causal factors for autism. *Psychiatric Genetics* 23:198–203.

Volk LJ, Daly CA, Huber KM (2006) Differential roles for group 1 mGluR subtypes in induction and expression of chemically induced hippocampal long-term depression. *Journal of Neurophysiology* 95:2427–2438.

Walkup WG, Mastro TL, Schenker LT, Vielmetter J, Hu R, Iancu A, Reghunathan M, Bannon BD, Kennedy MB (2016) A model for regulation by SynGAP-a1 of binding of synaptic proteins to PDZ-domain 'Slots' in the postsynaptic density. *eLife* 5:1–31.

Wan Y, Xu J, Ma D, Zeng Y, Cibelli M, Maze M (2007) Postoperative Impairment of Cognitive Function in Rats. *Anesthesiology* 106:436–443.

Wang HS, Pan Z, Shi W, Brown BS, Wymore RS, Cohen IS, Dixon JE, McKinnon D (1998) KCNQ2 and KCNQ3 potassium channel subunits: Molecular correlates of the M-channel. *Science* 282:1890–1893.

Wang L, Chen IZ, Lin D (2015) Collateral Pathways from the Ventromedial Hypothalamus Mediate Defensive Behaviors. *Neuron* 85:1344–1358.

Wang T, Guo H, Xiong B, Stessman HA, Wu H, Coe BP, Turner TN, Liu Y, Zhao W, Hoekzema K, Vives L, Xia L, Tang M, Ou J, Chen B, Shen Y, Xun G, Long M, Lin J, Kronenberg ZN, Peng Y, Bai T, Li H, Ke X, Hu Z, Zhao J, Zou X, Xia K, Eichler EE (2016) De novo genic mutations among a Chinese autism spectrum disorder cohort. *Nature Communications* 7:1–10.

Watson TC, Cerminara NL, Lumb BM, Apps R (2016) Neural correlates of fear in the periaqueductal gray. *Journal of Neuroscience* 36:12707–12719.

Wermter AK, Kamp-Becker I, Strauch K, Schulte-Körne G, Remschmidt H (2008) No evidence for involvement of genetic variants in the x-linked neuroligin genes NLGN3 and NLGN4X in probands with autism spectrum disorder on high functioning level. *American Journal of Medical Genetics, Part B: Neuropsychiatric Genetics* 147:535–537.

Whishaw I, Tomie Ja (1996) Department of Psychology and NeuroDetective Inc., University of Lethbridge, Lethbridge, Alberta, TIK 3M4 Canada. *Physiology & behavior* 60:1191–1197.

White SW, Oswald D, Ollendick T, Scahill L (2009) Anxiety in children and adolescents with autism spectrum disorders. *Clinical Psychology Review* 29:216–229.

Wijetunge LS, Angibaud J, Frick A, Kind PC, Nägerl UV (2014) Stimulated emission depletion (STED) microscopy reveals nanoscale defects in the developmental trajectory of dendritic spine morphogenesis in a mouse model of fragile X syndrome. *Journal of Neuroscience* 34:6405–6412.

Willsey J, Yamrom B, Lee Yh, Grabowska E, Dalkic E, Rosenbaum J, Ma B, Rodgers L, Troge J (2014) The contribution of de novo coding mutations to autism spectrum disorder. *Nature* 13:216–221.

Wiśniowiecka-Kowalnik B, Nesteruk M, Peters SU, Xia Z, Cooper ML, Savage S, Amato RS, Bader P, Browning MF, Haun CL, Duda AW, Cheung SW, Stankiewicz P (2010) Intragenic rearrangements in NRXN1 in three families with autism spectrum disorder, developmental delay, and speech delay. *American Journal of Medical Genetics, Part B: Neuropsychiatric Genetics* 153:983–993.

Wolff SB, Gründemann J, Tovote P, Krabbe S, Jacobson GA, Müller C, Herry C, Ehrlich I, Friedrich RW, Letzkus JJ, Lüthi A (2014) Amygdala interneuron subtypes control fear learning through disinhibition. *Nature* 509:453–458.

Woodbury-Smith M, Nicolson R, Zarrei M, Yuen RK, Walker S, Howe J, Uddin M, Hoang N, Buchanan JA, Chrysler C, Thompson A, Szatmari P, Scherer SW (2017) Variable phenotype expression in a family segregating microdeletions of the NRXN1 and MBD5 autism spectrum disorder susceptibility genes. *npj Genomic Medicine* 2:1–7.

Wuri G, Wang DX, Zhou Y, Zhu SN (2011) Effects of surgical stress on long-term memory function in mice of different ages. *Acta Anaesthesiologica Scandinavica* 55:474–485.

Xing D, Yeh CI, Shapley RM (2009) Spatial spread of the local field potential and its laminar variation in visual cortex. *Journal of Neuroscience* 29:11540–11549.

Xu J, Kang N, Jiang L, Nedergaard M, Kang J (2005) Activity-dependent long-term potentiation of intrinsic excitability in hippocampal CA1 pyramidal neurons. *Journal of Neuroscience* 25:1750–1760.

Xu X, Xiong Z, Zhang L, Liu Y, Lu L, Peng Y, Guo H, Zhao J, Xia K, Hu Z (2014) Variations analysis of NLGN3 and NLGN4X gene in Chinese autism patients. *Molecular Biology Reports* 41:4133–4140.

Yan J, Oliveira G, Coutinho A, Yang C, Feng J, Katz C, Sram J, Bockholt A, Jones IR, Craddock N, Cook EH, Vicente A, Sommer SS (2005) Analysis of the neuroligin 3 and 4 genes in autism and other neuropsychiatric patients [1]. *Molecular Psychiatry* 10:329–332.

Yan J, Noltner K, Feng J, Li W, Schroer R, Skinner C, Zeng W, Schwartz CE, Sommer SS (2008) Neurexin 1α structural variants associated with autism. *Neuroscience Letters* 438:368–370.

Yan Q, Weyn-Vanhentenryck SM, Wu J, Sloan SA, Zhang Y, Chen K, Wu JQ, Barres BA, Zhang C (2015) Systematic discovery of regulated and conserved alternative exons in the mammalian brain reveals NMD modulating chromatin regulators. *Proceedings of the National Academy of Sciences of the United States of America* 112:3445–3450.

Yanagi K, Kaname T, Wakui K, Hashimoto O, Fukushima Y, Naritomi K (2012) Identification of Four Novel Synonymous Substitutions in the X-Linked Genes Neuroligin 3 and Neuroligin 4X in Japanese Patients with Autistic Spectrum Disorder. *Autism Research and Treatment* 2012:1–5.

Yang CH, Huang CC, Hsu KS (2011) Generalization of fear inhibition by disrupting hippocampal protein synthesis-dependent reconsolidation process. *Neuropsychopharmacology* 36:1992–2008.

Yang Y, Calakos N (2013) Presynaptic long-term plasticity. *Frontiers in Synaptic Neuroscience* 5:1–22.

Ye X, Kapeller-Libermann D, Travaglia A, Inda MC, Alberini CM (2017) Direct dorsal hippocampal-prelimbic cortex connections strengthen fear memories. *Nature Neuroscience* 20:52–61.

Ylisaukko-oja T, Rehnström K, Auranen M, Vanhala R, Alen R, Kempas E, Ellonen P, Turunen Ja, Makkonen I, Riikonen R, Nieminen-von Wendt T, von Wendt L, Peltonen L, Järvelä I (2005) Analysis of four neuroligin genes as candidates for autism. *European Journal of Human Genetics* 13:1285–92.

Yu J, He X, Yao D, Li Z, Li H, Zhao Z (2011) A sex-specific association of common variants of neuroligin genes (NLGN3 and NLGN4X) with autism spectrum disorders in a Chinese Han cohort. *Behavioral and Brain Functions* 7:13.

Yu TW, Chahrour MH, Coulter ME, Jiralerspong S, Okamura-Ikeda K, Ataman B, Schmitz-Abe K, Harmin DA, Adli M, Malik AN, D'Gama AM, Lim ET, Sanders SJ, Mochida GH, Partlow JN, Sunu CM, Felie JM, Rodriguez J, Nasir RH, Ware J, Joseph RM, Hill RS, Kwan BY, Al-Saffar M, Mukaddes NM, Hashmi A, Balkhy S, Gascon GG, Hisama FM, LeClair E, Poduri A, Oner O, Al-Saad S, Al-Awadi SA, Bastaki L, Ben-Omran T, Teebi AS, Al-Gazali L, Eapen V, Stevens CR, Rappaport L, Gabriel SB, Markianos K, State MW, Greenberg ME, Taniguchi H, Braverman NE, Morrow EM, Walsh CA (2013) Using Whole-Exome Sequencing to Identify Inherited Causes of Autism. *Neuron* 77:259–273.

Yue C (2004) KCNQ/M Channels Control Spike Afterdepolarization and Burst Generation in Hippocampal Neurons. *Journal of Neuroscience* 24:4614–4624.

Yuen RK, Merico D, Bookman M, L Howe J, Thiruvahindrapuram B, Patel RV, Whitney J, Deflaux N, Bingham J, Wang Z, Pellecchia G, Buchanan JA, Walker S, Marshall CR, Uddin M, Zarrei M, Deneault E, D'Abate L, Chan AJS, Koyanagi S, Paton T, Pereira SL, Hoang N, Engchuan W, Higginbotham EJ, Ho K, Lamoureux S, Li W, MacDonald JR, Nalpathamkalam T, Sung WWL, Tsoi FJ, Wei J, Xu L, Tasse AM, Kirby E, Van Etten W, Twigger S, Roberts W, Drmic I, Jilderda S, Modi BM, Kellam B, Szego M, Cytrynbaum C, Weksberg R, Zwaigenbaum L, Woodbury-Smith M, Brian J, Senman L, Iaboni A, Doyle-Thomas K, Thompson A, Chrysler C, Leef J, Savion-Lemieux T, Smith IM, Liu X, Nicolson R, Seifer V, Fedele A, Cook EH, Dager S, Estes A, Gallagher L, Malow BA, Parr JR, Spence SJ, Vorstman J, Frey BJ, Robinson JT, Strug LJ, Fernandez BA, Elsabbagh M, Carter MT, Hallmayer J, Knoppers BM, Anagnostou E, Szatmari P, Ring RH, Glazer D, Pletcher MT, Scherer SW (2017) Whole genome sequencing resource identifies 18 new candidate genes for autism spectrum disorder. *Nature Neuroscience* 20:602–611.

Zerbo O, Qian Y, Yoshida C, Grether J, Water JVD, Croen LA (2016) Maternal Infection during Pregnancy and Autism Spectrum Disorders Ousseny. *Journal of Autism and Developmental Disorders* 45:4015–4025.

Zhang B, Seigneur E, Wei P, Gokce O, Morgan J, Südhof TC (2017) Developmental plasticity shapes synaptic phenotypes of autism-associated neuroligin-3 mutations in the calyx of held. *Molecular Psychiatry* 22:1483–1491.

Zhang SP, Bandler R, Carrive P (1990) Flight and immobility evoked by excitatory amino acid microinjection within distinct parts of the subtentorial midbrain periaqueductal gray of the cat. *Brain Research* 520:73–82.

Zhang W (2005) Extracellular Domains of -Neurexins Participate in Regulating Synaptic Transmission by Selectively Affecting N- and P/Q-Type Ca2+ Channels. *Journal of Neuroscience* 25:4330–4342.

Zhou Q, Homma KJ, Poo MM (2004) Shrinkage of dendritic spines associated with long-term depression of hippocampal synapses. *Neuron* 44:749–757.

Zhou Y, Takahashi E, Li W, Halt A, Wiltgen B, Ehninger D, Li GD, Hell JW, Kennedy MB, Silva AJ (2007) Interactions between the NR2B receptor and CaMKII modulate synaptic plasticity and spatial learning. *Journal of Neuroscience* 27:13843–13853.

Zucker RS (1989) Short-term synaptic plasticity. *Annual Review of Neuroscience* 12:13–31.